Alexander A. Stotsky

Automotive Engines

CONTROL, ESTIMATION, STATISTICAL DETECTION

Springer

Automotive Engines

Alexander A. Stotsky

Automotive Engines

Control, Estimation, Statistical Detection

Springer

Professor Dr. Alexander A. Stotsky
Department of Computer Science and Engineering
Aalborg University
Niels Bohrs Vej 8
6700 Esbjerg
Denmark
astotsky@aaue.dk
stotskya@mail.ru

ISBN 978-3-642-00163-5 e-ISBN 978-3-642-00164-2
DOI 10.1007/978-3-642-00164-2
Springer Dordrecht Heidelberg London New York

Library of Congress Control Number: 2009921493

Cover design: Kirchner, Erich

Printed on acid-free paper

Springer is part of Springer Science+Business Media (www.springer.com)

Preface

Increasing requirements for a fuel economy, exhaust emissions and the output performance and also the complexity of the automotive engines necessitate the development of a new generation of the engine control functionality. This book offers the solutions of a number of the engine control and estimation problems and consists of ten Chapters grouped in four Parts. Idle speed control and cylinder flow estimation techniques are presented in the first Part of the book; engine torque and friction estimation methods are presented in the second Part; engine misfire and Cam Profile Switching diagnostic methods are presented in the third Part; and engine knock detection and control algorithms are discussed in the fourth Part of the book. The algorithms presented in the first Part of the book use a mean value engine model and the techniques described in the rest of the book are based on the cylinder individual engine model. The book provides a sufficiently wide coverage of the engine functionality.

The book also offers a tool-kit of new techniques developed by the author which was used for the problems described above. The techniques can be listed as follows: input estimation, composite adaptation, spline and trigonometric interpolations, a look-up table adaptation and a threshold detection adaptation. These methods can successfully be used for other engine control and estimation applications. These methods are listed in Table 0.1 and Table 0.2 which contain a brief description of the methods, application areas and references providing a reader with the overview and a guidance through the book.

One of the key techniques used in this book is the statistical techniques. A periodic nature of the engine rotational dynamics and a cycle-to-cycle variability allows the presentation of the engine signals as statistical signals utilizing such statistical variables as mean values and standard deviations. The detection of the engine events such as misfire events, knock events and others can be associated with the statistical hypotheses. The statistical hypotheses can in turn be tested via decision making procedures, described in Table 0.3 for example. Two basic types of errors can be made in the statistical tests of the

Technique	Purpose	References
Input Estimation	Estimation of Unmeasured Input of a Dynamic System from the Output Measurements	[5], [48], [49], [85],[95], [99], [100]
Composite Adaptation	Parameter Estimation Technique Driven by both Tracking and Prediction Error with Improved Convergence Rate	[96], [97], [100]
Recursive Spline Interpolation	A Polynomial Fitting of Measured Signal in the Least-Squares Sense and Analytical Calculation of the Derivatives with a High Accuracy.	[90], [93], [102]
Trigonometric Interpolation	Calculation of the Frequency Contents of the Oscillating Signal in a Moving Window	[86], [87], [88],[105]
Look-Up Table Adaptation	Adaptation of the Engine Look-up Tables with Meager New Data Representation	[89],[90], [107], [108]
Detection Threshold Adaptation	Event Misdetection Avoidance via Adaptation of the Detection Threshold of the Signal Using a Confidence Interval Method	[91], [92]

Table 0.1. Techniques

Technique	Described in Chapter	Application	Applied in Chapter
Input Estimation	2.2.1	Idle speed control, Cylinder Flow Estimation	1, 2
Composite Adaptation	2.3.1	Cylinder Flow Estimation	2
Recursive Spline Interpolation	3	Engine Acceleration Estimation	3,4
Trigonometric Interpolation	4.3, 7.2	Torque Estimation, Misfire Diagnostic, Knock Detection	4, 7, 9
Look-Up Table Adaptation	5.5, 6.3	Adaptation of the Engine Friction Look-Up Table	5,6
Detection Threshold Adaptation	10.5	Adaptation of the Engine Knock Detection Threshold	10

Table 0.2. Application of Different Techniques

hypotheses called α-risk and β-risk specified by the engineer. The detection performance of the engine events such as misfire events, knock events and others can in turn be associated with these errors, for example with α-risk. The same detection performance (with the same α-risk) can be achieved if the parameters of the signal such as a mean value and a standard deviation involved in the detection of the engine events change due to aging of the engine components, for example. Many types of the engine event detection problems can be formulated as hypothesis-testing problems aiming to a robust detec-

tion providing the same detection performance for new and aged engines.
A great potential for a robust engine control system design is in a combination of statistical hypotheses and a feedback principle. A control aim can also be associated with the statistical hypothesis and the feedback can be used for either rejection or not rejection of a null hypothesis. A tracking error which is driven to zero via a proper choice of a feedback loop could be presented as a difference between the value of the statistic associated with a hypothesis test and a desired value of the statistic. A desirable hypothesis achieved by a feedback when the tracking error converges to zero, in turn determines desired statistical properties of the closed loop system. For example, the rejection of a null hypothesis in favor of the alternative hypothesis achieved by the engine knock feedback described in Chapter 10 offers a desired statistical separation between a mean value of the maximum amplitude of the knock sensor signal at a given frequency and the threshold value. This in turn, allows the design of a robust engine knock control system with desired α-risk and probability of the knock occurrence.
These statistical methods are not only used widely in the book in Chapters 6-10, but also collected and described in Appendix as the most future prospective methods for a new generation of a robust engine functionality. The statistical methods are also listed in Table 0.3 providing references to the description of the method and application areas. This book is one of the first steps towards a statistical robustification of the engine control functionality.

The major part of the book is devoted to the real-time algorithms, and Chapter 9 is devoted to the statistical automatic calibration of the engine knock detection algorithm. Rising number of the engine calibration parameters and a time and cost associated with the engine calibration necessitate the development of a software for automatic calibration of the engine functionality. Automatic engine calibration is a rapidly growing area and Chapter 9 of the book shows an example for the statistical automatic calibration of the engine knock frequency.

Practising automotive engineers should find this book useful when they need the solutions of engine control and estimation problems described in this book, or when they are working on a new engine control or estimation problem and want to use the techniques described in this book. Black Belts working in automotive industry should also find the book useful due to the comprehensive collection of the statistical techniques and their applications to the automotive engines. Engine functionality forms the part of the Automotive Engineering Courses at Universities. This book should also be useful for lecturers, researchers and students since it provides a sufficiently wide coverage of the engine control and estimation problems, detailed descriptions of the techniques useful in automotive applications, and also describes future trends and challenges in the engine functionality.

The author is grateful to his colleagues from Chalmers University, Ford Motor Company and Volvo Car Corporation for interesting discussions. The

Statistical Method	Described in Chapter	Application	Applied in Chapter
One Sample t-Test	14.1.1	Misfire Detection, Knock control	7,10
Two Sample t-Test	14.1.2	Knock detection	9
Test For Equal Variances	14.1.3	Look-up tables adaptation	6
Outlier Detection Test	14.1.6	Knock Control	10
Confidence Intervals as Thresholds	14.1.6	Knock Control	10
Markov Inequality	10.3.2	Knock Control	10
Random Number Generators	10.2.1	Knock Modeling & Control	10

Table 0.3. Application of the Statistical Methods

statistical part of this work was carried out within the Volvo Six Sigma Programme.

Contents

1

Idle Speed Control with Estimation of Unmeasurable Disturbances

A new controller for throttle and spark advance to control the engine speed at idle under *unknown time varying* disturbances is described in this Chapter. By using measurements of the engine speed the disturbance estimator is designed to reconstruct a disturbance torque. The controller is formulated so that the throttle is used as much as possible as a main tool to produce a torque and a spark advance is used to compensate intake to torque production delay. The stability of the system is proved via Lyapunov function method.

1.1 Introduction

The main source of the performance deterioration of the idle speed control (ISC) systems is disturbances such as rapid external load changes and slow varying changes in operating conditions. External load changes are the result of loading due to the air conditioning, battery charging etc.. Very often such disturbances are measurable and feedforward compensation is used to improve the performance. However, the loads applied to the engine may change in time and more power consuming equipment may be installed in a vehicle after it leaves the factory. In this case one must consider the ISC problem under unmeasurable disturbances.

Although ISC is a well studied topic, see for example the comprehensive survey [35] and references there in, many works ignore intake to torque production delay, which is essential in this case [36] or based on linearized engine model, which is valid locally only.

This Chapter describes a new approach to the ISC problem based on a second order nonlinear engine model, which takes into account intake to torque production delay and unmeasurable time varying disturbances.

Two inputs may be used to control the engine speed at idle: throttle and spark advance. Throttle provides large variations of torque without increasing exhaust emissions, however, the main problem of using throttle as a control is intake to torque production delay. Spark advance can be seen as a fast control,

A.A. Stotsky, *Automotive Engines*, DOI 10.1007/978-3-642-00164-2_1,

however, it produces limited torque and increases both emissions and fuel consumption. In this Chapter an innovative solution for ISC is proposed. The solution utilizes advantages and compensates disadvantages of both controls. A similar combined spark/throttle control law was proposed in [24] (see also [11]), however, the stability proof is based on the assumption that the spark influence is constant when deriving the throttle control law. In other words two controls are treated independently and it is not practical in many cases.

The key idea of our control law is the following. First, a high gain disturbance estimator for estimation of unknown disturbances, such that the upper bound of the estimation error can be made arbitrarily small (this error is compensated by spark advance) is designed. A control law is designed such that the throttle is used as a main tool to produce the torque, while spark is used both for compensation of throttle to torque delay and for variable structure feedback that compensates the disturbance estimation error. Since the retarded spark increases the exhaust emissions, our control law drives spark advance to MBT (minimum spark advance for the best torque), if the engine speed is close to the desired engine speed and there is no need for fast control. It is worth remarking that similar disturbance estimation technique was proposed in [22],[42] for discrete time case and in [5],[85] for continuous time adaptive control.

1.2 Engine Model

In this Section the engine model which is based on the results described in [10] and [40] is developed.

The first equation is obtained by considering the conservation of mass

$$\dot{m}_a = \dot{m}_{maf} - \dot{m}_{cyl} \tag{1.1}$$

where m_a is the mass of air in the intake manifold, $\dot{m}_{maf}$ is the mass rate of air entering the manifold and $\dot{m}_{cyl}$ is the mass rate of air leaving the manifold and entering the combustion chamber. The mass rate of air entering the manifold is modeled as

$$\dot{m}_{maf} = a_1 u_1 p_r \tag{1.2}$$

where $a_1 = 0.3861 \frac{kg}{s}$ for the engine of interest, u_1 is normalized throttle characteristic $[0:1]$, p_r is normalized pressure influence

$$p_r = \begin{cases} \sqrt{(\frac{p}{p_0})^{1.428} - (\frac{p}{p_0})^{1.714}} & \text{if } \frac{p}{p_0} > 0.528 \\ 0.259 & \text{otherwise} \end{cases}$$

where p is the pressure in the intake manifold, p_0 is atmospheric pressure ($p_0 = 1$ Bar).

Pressure p in the intake manifold changes according to the following equation,

which comes from the differentiation of the ideal gas law under the assumption that the intake manifold temperature is constant,

$$\dot{p} = k_m(\dot{m}_{maf} - \dot{m}_{cyl}) \tag{1.3}$$

where

$$k_m = \frac{RT}{V_m} \tag{1.4}$$

where $R = 287.9 \ \ Nm/Kg/K$ is a gas constant, T is the intake manifold temperature,$T = 318°K$ $(45°C)$, $V_m = 5 \cdot 10^{-3}\ m^3$ is intake manifold volume. It is convenient to use the pressure ratio $(\frac{p}{p_0})$ as a state variable. The pressure ratio $(\frac{p}{p_0})$ in the intake manifold changes according to the following equation

$$\frac{\dot{p}}{p_0} = k_1(\dot{m}_{maf} - \dot{m}_{cyl}) \tag{1.5}$$

where

$$k_1 = \frac{T}{V_m T_0 \rho_0} \tag{1.6}$$

where ρ_0 is the atmospheric density and T_0 is the corresponding atmospheric temperature. In our case $\rho_0 = 1.2\frac{kg}{m^3}$ and $T_0 = 288°K$ $(15°C)$.
The mass flow rate entering the combustion chamber satisfies the following equation which comes from the speed density calculation [10], [40]

$$\dot{m}_{cyl} = k\omega\frac{p}{p_0} \tag{1.7}$$

where

$$k = \frac{\rho_0 T_0 V_{cyl}\eta}{4\pi T} \tag{1.8}$$

where ω is the engine speed $(\frac{rad}{s})$, η is a volumetric efficiency (for simplicity the constant value of efficiency is taken i.e., $\eta = 0.8$), $V_{cyl} = 2.5 \cdot 10^{-3}\ m^3$ is the volume of five cylinders of the engine, $\pi = 3.1416$.

The rotational dynamics of the engine is modeled as

$$J_e\dot{\omega} = T_{ind} - T_f - T_d - T_p \tag{1.9}$$

where T_{ind} is indicated torque, T_f is friction torque, T_p is pump torque and T_d is disturbance torque, $J_e = 0.255kgm^2$ is the inertia moment of the engine.

Indicated Engine Torque is the following

$$T_{ind} = a_2 \ \ \frac{\dot{m}_{cyl}(t - t_d)}{\omega(t - t_d)} \ \ a_{fi}(t - t_d) \ \ f_s(t - t_s) \tag{1.10}$$

where $a_2 = 8.51 \cdot 10^5 Nm/kg/rad$ represents the maximum torque capacity, $a_{fi}(t - t_d)$ is normalized air to fuel influence (in this Chapter it is assumed

that air to fuel ratio is under control and $a_{fi}(t-t_d)=1$), $f_s(t-t_s)$ is a function of spark influence.
Substituting (1.7) in (1.10) one gets the following expression for indicated torque:

$$T_{ind}=a_2 \quad k \quad \frac{p(t-t_d)}{p_0} \quad f_s(t-t_s) \tag{1.11}$$

At low engine speeds MBT (minimum spark advance for the best torque) is about 20 degrees before top dead center and it is possible to retard spark up to 10 degrees after top dead center. This means that the total range for spark advance/retard is 30 degrees or ±15 if spark is retarded by 15 degrees from MBT.
The following curve may be used for the spark influence [10]:

$$f_s=(cos(-b+u_2))^{2.875} \tag{1.12}$$

where b is the position of OY axis from MBT (see Figure 1.1), measured in radians, and u_2 is our control. Notice, that the distance b can be fixed or adjusted within the interval $[0,15^\circ]$, thereby control action u_2 varies within the interval $[-b,b]$. If b is fixed and $u_2=0$ then spark is retarded still from MBT. Unfortunately, retarding spark increases emissions, coefficient of variation of engine torque and hence partial burns and misfires. Moreover, retarding spark affects negatively the fuel economy. On the other hand when the engine speed is close enough to the desired engine speed there is no need for spark as a control and it should be kept at MBT whenever possible. By adjusting the distance b it is possible to drive the spark advance to MBT when engine speed is close to the desired engine speed. On the other hand, if the engine speed mismatch is big enough b should be kept at 15° so that to provide the largest range for control.

Since the engine torque production is a discrete process, but modeled in the continuous time domain the following delays are introduced [10] :

$$t_d=\frac{5.48}{\omega} \tag{1.13}$$

$$t_s=\frac{1.3}{\omega} \tag{1.14}$$

where t_d is intake to torque production delay, and t_s is spark to torque production delay. As can be seen from (1.13) and (1.14) intake to torque production delay is more than four times larger than spark to torque delay. As it is observed by simulations spark to torque delay can be neglected,see also [60].

Engine Friction Torque can be modeled as

$$T_f=(a_{1f}+a_{2f}\omega+a_{3f}\omega^2)\frac{V_{1cyl} \quad 1000 \quad z}{4\pi} \tag{1.15}$$

where $a_{1f}=97\frac{N}{m^2}$, $a_{2f}=0.1432\frac{N}{m^2}\frac{s}{rad}$, $a_{3f}=2.74\cdot 10^{-4}\frac{N}{m^2}\frac{s^2}{rad^2}$, $V_{1cyl}=0.5\cdot 10^{-3}m^3$ is the volume of one cylinder, $z=5$ is the number of cylinders.

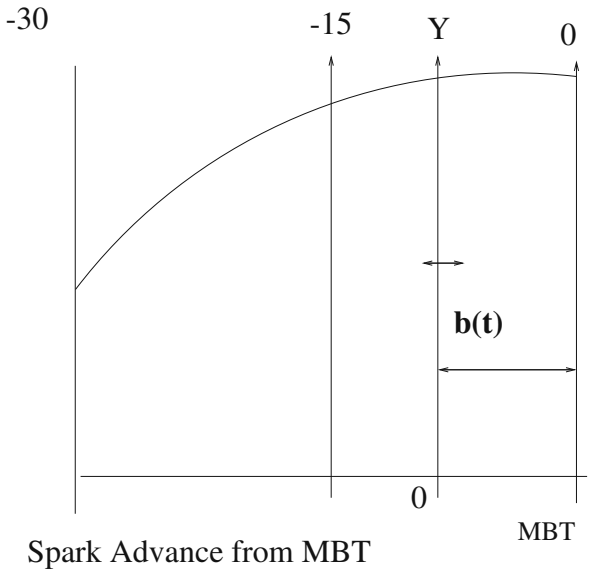

Fig. 1.1. Spark advance

Engine Pump Torque can be modeled as

$$T_p = (p_0 - p) \quad \frac{V_{1cyl} \quad z}{4\pi} \tag{1.16}$$

Engine Disturbance Torque T_d can be presented, for idle control problem, by a class of bounded functions with bounded derivatives, i.e.,

$$|T_d(t)| \leq c, \qquad |\dot{T}_d(t)| \leq c_1 \tag{1.17}$$

where c and c_1 are positive constants. Typical value for c is $20Nm$.

Finally the engine model can be written as follows:

$$J_e\dot{\omega} = a_2 \quad k \quad \frac{p(t-t_d)}{p_0} \quad (cos(-b+u_2))^{2.875} - T_f - T_d - T_p \tag{1.18}$$

$$\dot{m}_{cyl} = \quad k \quad \omega \quad \frac{p}{p_0} \tag{1.19}$$

$$\frac{\dot{p}}{p_0} = k_1(a_{1s}u_1 - \dot{m}_{cyl}) \tag{1.20}$$

where T_f and T_p are given by (1.15) and (1.16), k and k_1 are given by (1.8) and (1.6), $a_{1s} = a_1 p_r$.

The next step is to present the problem statement.

1.3 Problem Statement

It is well known that the engine at idle is very sensitive to the disturbance torques, and very often disturbances are unmeasurable so that feedforward compensation can not be applied.
Our problem is to find controls u_1 and u_2 (throttle and spark advance) so that, to achieve the following control aim:

$$\lim_{t\to\infty} \mid \omega(t) - \omega_d \mid = 0 \tag{1.21}$$

where $\omega_d = 100\frac{rad}{s}$ is the idle speed, under unknown time varying disturbances $T_d(t)$. Engine speed ω and the intake manifold pressure p are measured. Friction torque and pump torque can be computed as well using measurements of the engine speed and pressure, see (1.15) and (1.16). Modeling errors in pump and friction torques can be considered as a disturbance torque as well. Engine parameters are assumed to be known. The disturbance torque is unknown and unmeasurable, but it is assumed that it is bounded with bounded derivative.

1.4 Control Design

1.4.1 Observer Design for Disturbance Torque $T_d(t)$

Define the following estimation error

$$e = \alpha_0 J_e \omega - \varepsilon + T_d(t) \tag{1.22}$$

where $\alpha_0 > 0$ and $\varepsilon(t)$ is the solution of the following differential equation

$$\begin{aligned}\dot{\varepsilon} = &-\alpha_0\varepsilon + \alpha_0 a_2 \;\; k \;\; \frac{p(t-t_d)}{p_0} \quad (cos(-b+u_2))^{2.875} \\ &-\alpha_0 T_f - \alpha_0 T_p + \alpha_0^2 J_e \omega\end{aligned} \tag{1.23}$$

Our next aim is to show that the upperbound of the error $|e(t)|$ can be made arbitrarily small. Choosing the following Lyapunov like function

$$V = \frac{1}{2}e^2 \tag{1.24}$$

its derivative is evaluated along the solutions of the system (1.18), (1.22), (1.23):

$$\dot{V} = -\alpha_0 e^2 + e\dot{T}_d \leq -\alpha_0 V + \frac{c_1^2}{2\alpha_0} \tag{1.25}$$

and the following bound for the estimation error is true:

$$|e(t)| \leq \sqrt{e^2(0)e^{-\alpha_0 t} + \frac{c_1^2}{\alpha_0^2}} \tag{1.26}$$

The bound (1.26) guarantees that the estimation error can be made arbitrarily small by amplifying the design parameter α_0. The estimate of the disturbance torque follows from (1.22)

$$T_d(t) = -\alpha_0 J_e \omega + \varepsilon + e(t) \tag{1.27}$$

where $e(t)$ can be made arbitrarily small. Notice that $e(t) \to 0$ if $T_d = const$. Notice, that the way of the estimation of unknown disturbances presented above is equivalent to the estimation of $\dot{\omega}$ via a " dirty differentiator". In this case T_d can be computed via (1.18).
Substituting (1.27) in (1.18) one gets the following:

$$\begin{aligned} J_e\dot{\omega} = {} & a_2 \;\; k \;\; \frac{p(t-t_d)}{p_0} \;\; (cos(-b+u_2))^{2.875} \\ & - T_f - T_p + \alpha_0 J_e \omega - \varepsilon - e(t) \end{aligned} \tag{1.28}$$

$$\dot{m}_{cyl} = \;\; k \;\; \omega \;\; \frac{p}{p_0} \tag{1.29}$$

$$\frac{\dot{p}}{p_0} = k_1(a_{1s}u_1 - \dot{m}_{cyl}) \tag{1.30}$$

1.4.2 Control Law Design for a Spark Advance

Define the spark advance, u_2, as a solution of the following algebraic equation:

$$p(t-t_d)(cos(-b+u_2))^{2.875} = p(t)(cos(-b+u_{2b}))^{2.875} - \gamma_s sign(\omega - \omega_d) \tag{1.31}$$

where $u_{2b} = 0$ corresponds to the case where spark advance is not controlled, $\gamma_s > 0$. The physical meaning of the spark advance control gets clear by substituting (1.31) into (1.28). Then,

$$J_e\dot{\omega} = \;\; \frac{a_2 \;\; k \;\; p(t) \;\; c_a}{p_0} - \frac{a_2 k \gamma_s}{p_0} sign(\omega - \omega_d) - T_f - T_p + \alpha_0 J_e \omega - \varepsilon - e(t) \tag{1.32}$$

where $c_a = cos(-b+u_{2b}))^{2.875}$. It is clear that the first term in the right hand side of (1.31) compensates the time delay t_d for $p(t-t_d)$, and the second term gives a relevant variable structure feedback which drives ω to ω_d. Unfortunately, the spark influence on the torque production is limited and γ_s should be chosen sufficiently small.
Resolving (1.31) with respect to the control one gets

$$u_2 = b - acos(\{\frac{p(t)}{p(t-t_d)}c_a - \frac{\gamma_s}{p(t-t_d)} sign(\omega - \omega_d)\}^{\frac{1}{2.875}}) \tag{1.33}$$

Notice that, if there is no time delay $t_d = 0$, and $\omega = \omega_d$ then $u_2 = u_{2b}$ and spark is retarded on b radians from MBT.

Remark As was already mentioned the distance b from MBT to OY axis (see Figure 1), can be fixed or adjusted. Below the following adjustment law for the moving axis is proposed:

$$\dot{b} = -\frac{1}{\tau}(b - 0.2618 sat(\omega - \omega_d)), \qquad b(0) = 0 \tag{1.34}$$

where $\tau > 0$, b is measured in *radians* and $sat(\omega - \omega_d)$ is the following saturation function

$$sat(\omega - \omega_d) = \begin{cases} \frac{1}{\lambda_0}|\omega - \omega_d| & \text{if } |\omega - \omega_d| < \lambda_0 \\ 1 & \text{otherwise} \end{cases}$$

where $\lambda_0 > 0$ is the size of the boundary layer. Finally, the spark advance is limited by taking into account the adjustable offset. Redenoting u_2 defined in (1.33) as u_{20}, the bounded spark control law is the following:

$$u_{20} = b - acos(\{\frac{p(t)}{p(t-t_d)}c_a - \frac{\gamma_s}{p(t-t_d)} sign(\omega - \omega_d)\}^{\frac{1}{2.875}}) \tag{1.35}$$

and

$$u_2 = \begin{cases} b & \text{if } u_{20} \geq b \\ u_{20} & \text{if } -b \leq u_{20} \leq b \\ -b & \text{if } u_{20} \leq -b \end{cases}$$

The physical meaning of the adjustable axis is the following. If $(\omega - \omega_d)$ is out of the boundary layer λ_0, then the axis moves to the 15 degrees ($0.2618[radians]$) from MBT, exponentially, according to the differential equation (1.34) with the rate $\frac{1}{\tau}$. The position of the axis at 15° corresponds to the maximal control power. If $(\omega - \omega_d)$ is within the boundary layer λ_0 then b is adjusted as follows

$$\dot{b} = -\frac{1}{\tau}(b - \frac{0.2618}{\lambda_0}|\omega - \omega_d|) \tag{1.36}$$

and as soon as $(\omega(t) - \omega_d) \to 0$ then b and u_2 tend to zero, and spark advance tends to MBT. Notice that, *only the sum* $(-b + u_2)$ defines the position of the spark advance from MBT (if $-b + u_2 = 0$ then the spark advance is at MBT). ♢ ♢

Due to the choice of the spark advance the system (1.28), (1.30) can be written in the following form:

$$J_e\dot{\omega} = \frac{a_2 \;\; k \;\; p(t) \;\; c_a}{p_0} - \frac{a_2 k \gamma_s}{p_0} sign(\omega - \omega_d) - T_f - T_p + \alpha_0 J_e \omega - \varepsilon - e(t) \tag{1.37}$$

$$\dot{m}_{cyl} = k \;\; \omega \;\; \frac{p}{p_0} \tag{1.38}$$

$$\frac{\dot{p}}{p_0} = k_1(a_{1s}u_1 - \dot{m}_{cyl}) \tag{1.39}$$

1.4.3 Control Law Design for Throttle

First, the desired pressure ratio $(\frac{p}{p_0})_d$ is defined,

$$(\frac{p}{p_0})_d = \frac{1}{c_a a_2 k}\{-\alpha_1\tilde{\omega} + T_f + T_p + \varepsilon - \alpha_0 J_e\omega\} \tag{1.40}$$

where $\tilde{\omega}(t) = \omega - \omega_d$, $\alpha_1 > 0$. The physical meaning of the desired pressure ratio $(\frac{p}{p_0})_d$ gets clear if $\frac{p}{p_0} = (\frac{p}{p_0})_d$, then substituting (1.40) into (1.37), one gets,

$$J_e\dot{\omega} = \quad -\alpha_1\tilde{\omega} - \frac{a_2 k\gamma_s}{p_0} sign\tilde{\omega} - e(t) \tag{1.41}$$

Notice, that the upper bound of the estimation error $e(t)$ can be made arbitrarily small, so that even small γ_s is able to compensate the estimation error.
Now the aim is to choose the throttle position so as to drive the pressure ratio to the desired one. Substituting (1.38) in (1.39) one gets the following equation for the pressure evolution:

$$\frac{\dot{p}}{p_0} = k_1 a_{1s} u_1 - k_1 k\omega\frac{p}{p_0} \tag{1.42}$$

Choosing the throttle position as follows

$$u_1 = \frac{1}{a_{1s}} k\omega\frac{p}{p_0} + \frac{1}{a_{1s}k_1}(-\alpha_2(\frac{p}{p_0} - (\frac{p}{p_0})_d) + (\frac{\dot{p}}{p_0})_d) \tag{1.43}$$

one gets

$$\frac{\dot{p}}{p_0} - (\frac{\dot{p}}{p_0})_d = -\alpha_2(\frac{p}{p_0} - (\frac{p}{p_0})_d) \tag{1.44}$$

where $\alpha_2 > 0$.

Notice, that the implementation of (1.43) requires measurements of $(\frac{\dot{p}}{p_0})_d$. The derivative can be estimated via a sliding mode observer which guarantees the convergence of the estimation error in a finite time, see [19] and [94] for details, or via a spline interpolation method described in Chapter 3.

1.5 Stability Analysis of the System

Finally the error model of the system can be written in the following form:

$$J_e\dot{\tilde{\omega}} = \quad -\alpha_1\tilde{\omega} - \frac{a_2 k\gamma_s}{p_0} sign\tilde{\omega} + c_a a_2 e_p - e(t) \tag{1.45}$$

$$\dot{e}_p = -\alpha_2 e_p \tag{1.46}$$

where $e_p = \frac{p}{p_0} - (\frac{p}{p_0})_d$. In order to study the stability of the system (1.45), (1.46) the following Lyapunov function candidate is evaluated

$$V = \frac{J_e}{2}\tilde{\omega}^2 + \frac{1}{2}e_p^2 \tag{1.47}$$

Differentiating (1.47) along the solutions of (1.45), (1.46) one gets

$$\begin{aligned}\dot{V} \leq -\alpha_1\tilde{\omega}^2 + |\tilde{\omega}|(-\frac{a_2 k\gamma_s}{p_0} + |e|)\\ + |\tilde{\omega}||e_p|a_2 - \alpha_2 e_p^2\end{aligned} \tag{1.48}$$

Now it is clear how to choose γ_s. Substituting the bound (1.26) in the derivative of the Lyapunov function γ_s is chosen as

$$\gamma_s = \frac{p_0}{a_2 k}\sqrt{e^2(0)e^{-\alpha_0 t} + \frac{c_1^2}{\alpha_0^2}} \tag{1.49}$$

Notice that, the power of the spark advance as a control is limited and γ_s should be chosen sufficiently small so as not to force the spark advance into saturation. This can be achieved by choosing sufficiently large α_0, or in other words for any sufficiently small γ_s there exists α_0 satisfying (1.49). Notice also that, the estimation error (1.26) gets smaller via amplifying the design parameter α_0.
Substituting (1.49) in (1.48) one gets

$$\dot{V} \leq \tilde{\omega}^2(-\alpha_1 + \frac{a_2}{2}) + e_p^2(-\alpha_2 + \frac{a_2}{2}) \tag{1.50}$$

If the algorithm parameters are chosen in order to satisfy the following inequalities

$$\begin{aligned}\alpha_1 &> \frac{a_2}{2} + \kappa\frac{J_e}{2}\\ \alpha_2 &> \frac{a_2}{2} + \frac{\kappa}{2}\end{aligned} \tag{1.51}$$

where $\kappa > 0$, then the following inequality holds

$$\dot{V} \leq -\kappa V \tag{1.52}$$

and our control aim (1.21) is reached.

1.6 Simulation Results

The system (1.18) - (1.20) is simulated with the throttle control (1.43) and the spark advance control (1.33),(1.34). The algorithm is tested under the following disturbances:

$$T_d(t) = \begin{cases} 0 & \text{if } t < 2.5[sec] \\ 20 & \text{otherwise} \end{cases}$$

Simulation results are presented in Figure 1.2 and Figure 1.3.

Figure 1.2 demonstrates the performance of the disturbance estimation. Idle speed control performance together with the control variables, throttle and spark advance, are demonstrated in Figure 1.3. It is worth remarking that the separation between b and u_2 in our spark control loop is artificial, and despite the fact that it plays an important role in our control design procedure, only the sum $-b + u_2$ gives information about the position of spark advance from MBT (if $-b + u_2 = 0$ then the spark advance is at MBT).

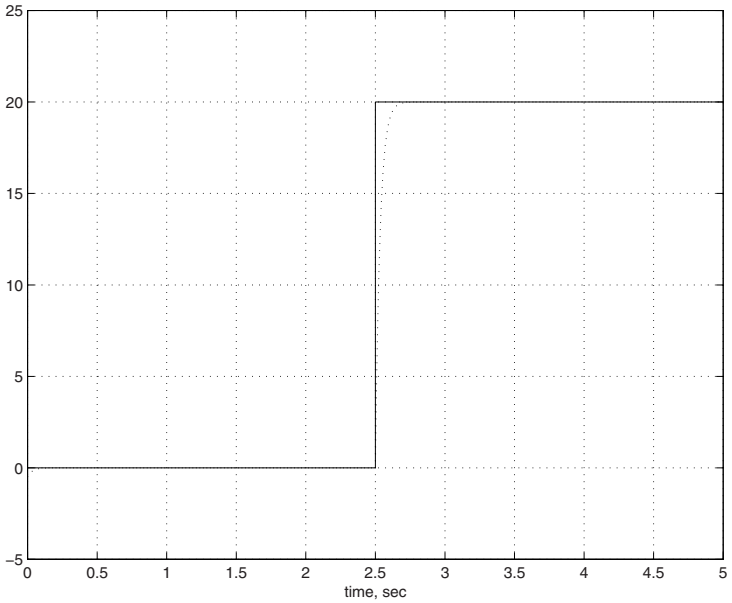

Fig. 1.2. Disturbance (Nm): solid line. Disturbance estimate (Nm): dotted line

1.7 Conclusion

In this Chapter a new solution for the ISC problem under unknown time varying disturbances is proposed. The solution is based on explicit identification of the unknown disturbance and uses advantages and compensates disadvantages of throttle and spark advance as controls. The result allows to improve the performance of ISC systems.

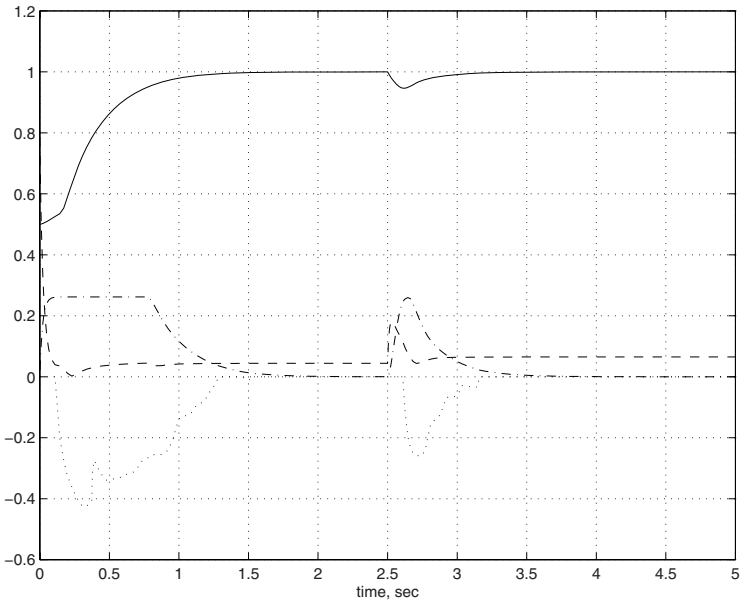

Fig. 1.3. Engine Speed $\frac{\omega}{100}(\frac{rad}{sec})$: solid line. Throttle position: dashed line. $-b+u_2$ (rad) : dotted line. Position of the axis b (rad): dashdotted line.

2

Cylinder Flow Estimation

The performance of air charge estimation algorithms in spark ignition automotive engines can be significantly enhanced using advanced estimation techniques available in the controls literature. This Chapter illustrates two approaches of this kind, that can improve the engine cylinder flow estimation. The first approach is based on an input observer while the second approach relies on an adaptive estimation. Assuming that the cylinder flow is nominally estimated via a *speed-density* calculation, and that the uncertainty is additive to the volumetric efficiency, the straightforward application of an input observer provides an easy-to-implement algorithm that corrects the nominal air flow estimate. The experimental results presented in this Chapter point to a sufficiently good transient behavior of the estimator. The signal quality may be deteriorating, however, for extremely fast transients. This motivates the development of an adaptive estimator that relies mostly on the feedforward speed-density calculation during transients while during engine operation close to steady-state conditions, it relies mostly on the adaptation. In our derivation of the adaptive estimator the uncertainty is modeled as an unknown parameter multiplying the intake manifold temperature. The tracking error between the measured and modeled intake manifold pressure together with an appropriately defined *prediction error estimate* are used in the adaptation algorithm with the improved identifiability and convergence rate. A robustness enhancement, via a σ-modification with the σ-factor depending on the prediction error estimate, ensures that in transients the parameter estimate converges to a pre-determined *a priori* value. In close to steady-state conditions, the σ- modification is rendered essentially inactive and the evolution of the parameter estimate is determined by both tracking error and prediction error estimate. Further enhancements are made by incorporating a functional dependence of the a priori value on the intake manifold pressure. The coefficients of this function can be *learned* in the process of engine operation from the values to which the parameter estimate happens to converge in close to steady-state conditions. This feedforward learning functionality improves

A.A. Stotsky, *Automotive Engines*, DOI 10.1007/978-3-642-00164-2_2,

transient estimation accuracy and reduces the convergence time of the parameter estimate.

2.1 Introduction

The accuracy of engine air charge determination has a direct impact on the quality of the air-to-fuel ratio control, on the torque estimation and hence on the engine output performance. Good air charge estimation accuracy is therefore necessary to meet ever more aggressive emission and drivability targets. Inaccurate air charge estimation may also negatively affect a fuel economy if the spark timing is not set to the best efficiency at given engine operating conditions. With the introduction of new technologies such as variable valve timing, continuously variable valve lift, cam profile switching, variable geometry intake manifold, cylinder deactivation, boost on demand, variable geometry turbocharging, etc., a renewed interest is now paid to improving charge estimation algorithms to enable them to handle significant variations in volumetric efficiency and intake manifold temperature that may occur during transient operation of advanced engines. Of particular importance is also the ability of the algorithms to correct on-line for calibration inaccuracy that may be caused by part-to-part hardware variability, late in the development process hardware changes, aging, shortened development times.

The engine configuration considered in this work is shown schematically in Figure 2.1. Note that the engine has no external exhaust gas recirculation (EGR): Three-Way Catalyst and internal exhaust gas recirculation via, for example, an optimized valve timing schedule are assumed to sufficiently reduce feedgas emissions of nitric oxides. On the intake side, the engine is equipped with the mass air flow (MAF) sensor and with the intake manifold pressure (MAP) sensor. The temperature of air in the intake manifold is either measured or estimated.

Based on the intake manifold pressure measurement, the cylinder air flow can be estimated using the so called *speed-density* equation:

$$m_{cyl} = \eta_v \frac{n_e}{2} V_d \frac{p}{RT}, \tag{2.1}$$

where m_{cyl} is the mean-value of the flow into the engine cylinders (g/s), n_e is the engine speed (rev/s), p is the intake manifold pressure (kPa), T is the intake manifold temperature (deg K), R is the difference of specific heats (kJ/kg/K), η_v is the volumetric efficiency, and V_d is the displacement volume, i.e., the volume displaced by the engine cylinders during one engine cycle. The air charge per cylinder for a four stroke engine is estimated as

$$M_{cyl} = m_{cyl} \frac{2}{n_e n_{cyl}},$$

where n_{cyl} is the number of running engine cylinders. From the idealized thermodynamic analysis [110], the volumetric efficiency is determined by the following expression

$$\eta_v = 1 - \frac{1}{\gamma(CR-1)}(\frac{p_e}{p} - 1), \tag{2.2}$$

where $\gamma \approx 1.4$ is the ratio of specific heats for the air, CR is the engine compression ratio, and p_e is the engine exhaust pressure but this tends to give large errors on the real engines and does not reflect other key dependencies such as on valve timing, intake and exhaust temperatures, etc. Hence, in practice, the volumetric efficiency is correlated to key engine operating parameters such as n_e, p, T, intake and exhaust valve opening and closing timing, etc., based on the regressions of the data collected from the engine in the process of engine mapping. See, for example, [28], [69], [78].

The filling and emptying of the intake manifold can be modelled by a mean-value isothermal model that immediately follows from the ideal gas law and mass balance under the assumption of constant temperature,

$$\dot{p} = \frac{RT}{V_{IM}}(m_{th} - m_{cyl}) \tag{2.3}$$

where R is the gas constant, V_{IM} is the intake manifold volume, and m_{th} is the actual flow through the throttle. The isothermal assumption used in deriving the model (2.3) from the ideal gas law is only valid when the intake manifold temperature changes slowly. It turns out that the filling and emptying process observed on the real engine is in-between isothermal and adiabatic [9],[65], the latter is characterized by zero heat transfer from the intake manifold. It is possible to achieve a close match with the real measurements in transients with a more complex model, but significant time and efforts are required to accurately identify the heat transfer parameters; these parameters are also sensitive to ambient conditions. In practice, a simple approximation (2.3) is frequently utilized on non-boosted engines but V_{IM} may be treated as an adjustable parameter tuned to the best match of measured data.

Sensors for both flow through the throttle and intake manifold pressure are installed in modern engines to improve the robustness of engine air charge estimation and provide additional opportunities for diagnostics, see Figure 2.1. In steady-state conditions, the MAF sensor accurately predicts the flow into the engine cylinders, since by mass conservation, $m_{th} = m_{cyl}$. Errors in the model (2.1) caused by calibration inaccuracies, aging, or incorrect estimation of the key engine operating variables such as intake temperature may render (2.1) less accurate in steady-state conditions than the direct MAF sensor reading. Because of the filling and emptying dynamics, the MAF sensor, located upstream of the intake manifold, is not an accurate predictor for the cylinder flow in transients. In transients conditions, the reading of the MAP sensor (which measures p) and the speed-density calculation (2.1) provide a

more accurate estimate of m_{cyl}. It is, therefore, clear that an air charge estimation algorithm must provide an estimate that matches more closely MAF sensor in conditions close to steady-state but matches more closely the speed-density calculation in transient conditions, and, if necessary, corrects it for inaccuracies or long-term aging effects.

In this Chapter two techniques from the theory of input observers and adaptive estimation are used to develop two estimation algorithms. Both algorithms ensure a seamless transition between an estimate which is closer to (2.1) in transients and an estimate which is closer to MAF sensor reading in conditions close to steady-state operation and, in addition, correct for inaccuracies. The algorithms can be further enhanced with the steady-state feedforward *learning* functionality.

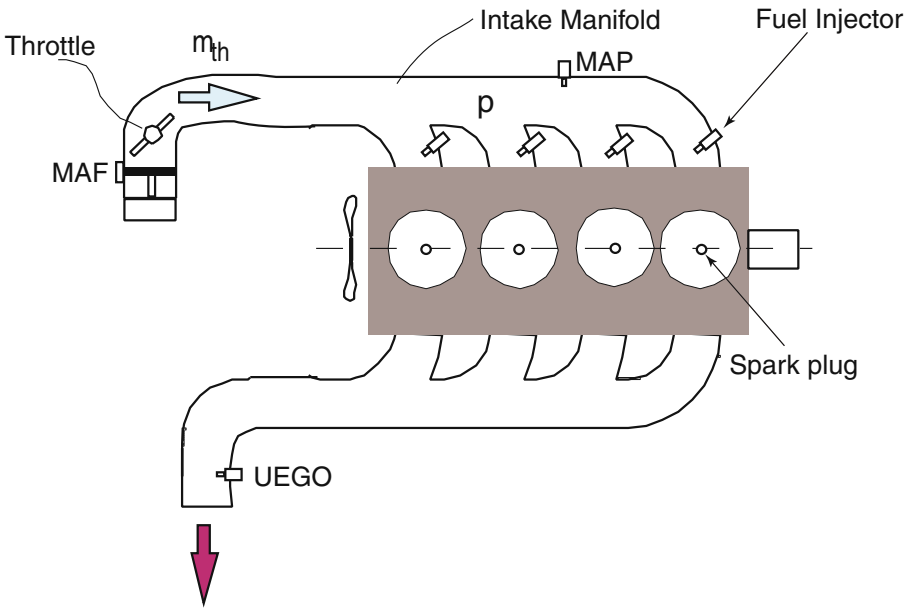

Fig. 2.1. Schematic diagram of a spark-ignition engine.

In recent years a number of observer-based and adaptive techniques have been already proposed for engine air charge estimation (see, for example, recent papers [43], [44], [45], [46], [84], [99],[111], [98] and references therein). Two algorithms described in this Chapter follow from two distinct approaches and two different assumptions about the nature of the uncertainty. Specifically, the first algorithm is based on an input observer that estimates an additive error in volumetric efficiency as in [99]. The second algorithm is based on the use of an adaptive estimator to determine an unknown factor multiplicative to the intake manifold temperature. A preliminary version of

the adaptive estimation work appeared as a conference paper [98] and as a journal paper [100]. This application of adaptation for air charge estimation goes well beyond the prior literature due to several enhancements. These include fast composite adaptation driven by both tracking error and by the prediction error estimate, robustification with a *special* σ-modification, and learning in close to steady-state operation to improve the feedforward part of the algorithm. The adaptive estimator that finally emerges can outperform an input-observer based algorithm in fast transients. The input observer-based algorithm is detailed in Section 2.2 while the adaptive estimator is described in Section 2.3.

The degree to which the improved air charge estimates can influence the overall system performance depends on the engine configuration. For direct injection (DI) engines, the spark timing and the injected fuel quantity can be set more accurately using the improved estimates. In port-fuel injection (PFI) engines the ignition system benefits the same way but the fuel injection system may not be able to take full advantage of the improved estimates during extremely fast transients because of the delay between the fuel injection and cylinder induction. In advanced PFI engines, if the air charge is rapidly increasing the fueling system may be able to compensate by adding fuel via an open valve post-injection; but still the fuel *cannot* be taken out of the intake manifold once injected so the fuel injection system of PFI engines may not be able to react to rapidly decreasing air charge. The detrimental effect of the delay in PFI engines can be mitigated by predicting air charge several events into the future. This prediction functionality is briefly discussed in Section 2.4. Concluding remarks are made in the end of this Chapter.

2.2 Air Charge Determination Using Input Observer

Input observers estimate an unknown input to a dynamic system using state or output measurements. Input observer enhances the performance of a charge estimation algorithm according to implementation results presented in this Section. A number of input estimation algorithms is reviewed, and one is chosen for application to the problem at hand.

2.2.1 Input Estimation Algorithms: General Case

The purpose of this Section is to review several algorithms for input estimation, point out similarities and differences between them. The collection of input estimation algorithms presented in this Section is a useful tool-kit in automotive applications where the input and the state are frequently related by the first order differential equation. A comparison of different input estimation techniques is also given in [99].

Problem Statement

Consider a first order dynamic system

$$\dot{z} = y + x, \tag{2.4}$$

where x is the unknown time-varying input (disturbance) which has to be estimated on-line using measured signals z and y. This type of problems appears frequently in automotive applications i.e, flow rate estimation from the pressure measurements described in Section 2.2.2, engine torque estimation from the engine speed measurements described in Chapter 1 and others. A number of different techniques which solve the problem stated above are reviewed below.

High Gain Observer

The input high gain observer is described first. It is also shown that the estimation algorithm is robust with respect to a sensor noise.

The input observer is defined in terms of the auxiliary variables v and ε, where

$$v = \gamma z - \varepsilon - x, \tag{2.5}$$

and ε satisfies

$$\dot{\varepsilon} = -\gamma\varepsilon + \gamma y + \gamma^2 z. \tag{2.6}$$

Here γ is a positive observer gain. Evaluating the derivative of v along the solutions of the system (2.5) one obtains

$$\dot{v} = -\gamma v - \dot{x}. \tag{2.7}$$

Assume now that $\dot{x}$ is bounded, i.e., that there exists a positive constant b_1 such that $\sup_t |\dot{x}(t)| \leq b_1$. Then the following transient bound for the estimation error is valid

$$|v(t)| \leq \sqrt{v(0)^2 e^{-\gamma t} + \frac{b_1^2}{\gamma^2}}. \tag{2.8}$$

Transient bound (2.8) implies that the upper bound on the estimation error for any $t > 0$ can be made arbitrarily small by increasing the design parameter $\gamma > 0$. Then, the estimate of x can be found from (2.5) as

$$\hat{x} = \gamma z - \varepsilon. \tag{2.9}$$

Note that if one defines $\hat{z} = \frac{\varepsilon}{\gamma}$, then equation (2.6) reduces to $\dot{\hat{z}} = -\gamma(\hat{z} - z) + y$. Thus $\hat{z}$ can be viewed as an estimate of z, provided that $\gamma > 0$ is sufficiently large.

The same result can be obtained by filtering both sides of equation (2.4) with a low pass filter. Indeed, from (2.4) it follows that

$$x = \dot{z} - y, \tag{2.10}$$

and by filtering both sides of equation (2.10) with a low pass filter one obtains

$$\frac{1}{\tau s + 1} x = \frac{1}{\tau s + 1}(sz - y), \tag{2.11}$$

where $\tau > 0$ is the filter time time constant and $s = j\omega$ is the Laplace variable. Then the following holds:

$$\frac{1}{\tau s + 1} x = \frac{1}{\tau s + 1}(sz - y) = \frac{z}{\tau} - \frac{1}{\tau s + 1}(\frac{z}{\tau} + y). \tag{2.12}$$

Denoting

$$\varepsilon = \frac{1}{\tau s + 1}(\frac{z}{\tau} + y), \tag{2.13}$$

it follows that the estimate of x can be found as

$$\hat{x} = \frac{1}{\tau} z - \varepsilon, \tag{2.14}$$

which is the same as (2.9) with $\gamma = \frac{1}{\tau}$. To summarize, equation (2.13) is realized as (2.6) with $\gamma = \dfrac{1}{\tau}$.

Suppose now that the sensor noises w_1 and w_2 affect y and z variables, respectively, so that the observer equations become

$$\dot{\varepsilon} = -\gamma\varepsilon + \gamma(y + w_1) + \gamma^2(z + w_2),$$

$$\hat{x} = \gamma(z + w_2) - \varepsilon.$$

Assume that $\sup_t |\dot{w}_2(t) - w_1(t)| \leq b_w$ for some $b_w > 0$. Then, the following upper bound on the estimation error $v = \hat{x} - x$ can be derived:

$$|v(t)| \leq \sqrt{v(0)^2 e^{-\gamma t} + \frac{(b_1 + \gamma b_w)^2}{\gamma^2}}. \tag{2.15}$$

This estimate implies that for large γ the asymptotic estimation error may be of the order of the above noise bound b_w.

Dirty Differentiation Observer

The unknown variable x can also be estimated by evaluating the so called "dirty derivative" of z , i.e.,

$$\hat{x} = \frac{sz}{\tau s + 1} - y = \frac{z}{\tau} - \frac{z}{\tau(\tau s + 1)} - y. \tag{2.16}$$

One difference between (2.9) and (2.16) is that the known variable y is filtered by a low-pass filter in (2.9), but there is a direct coupling between $\hat{x}$ and

y in (2.16). Experimental results show that (2.9) provides a smoother estimate than (2.16). Moreover, by evaluating the estimation error of the algorithm (2.16) it follows that the upper bound of the estimation error depends on the upper bound on the second derivative of z, $\ddot{z}$, i.e.,

$$|x(t) - \hat{x}(t)| \leq \sqrt{(x(0) - \hat{x}(0))^2 e^{-\gamma t} + \tau^2 b_2^2}, \tag{2.17}$$

where $\sup_t |\ddot{z}(t)| \leq b_2$, $b_2 > 0$. On the contrary, the upper bound (2.8) on the estimation error for the algorithm (2.9) depends only on the upper bound on $|\dot{x}|$.

Sliding Mode Observer

The sliding mode observer is based on the following variable structure filter,

$$\dot{\hat{z}} = y + \gamma sign(v_1), \tag{2.18}$$

where $\gamma > 0$, $v_1 = z - \hat{z}$, and $v_1 = 0$ defines the sliding surface. The error model can be written as follows

$$\dot{v}_1 = x - \gamma sign(v_1). \tag{2.19}$$

Then for any $t \geq t_*$, where $t_* = \frac{2}{\gamma_0}|v_1(0)|$, the system is in the sliding mode on the surface $v_1 = 0$, if $\gamma > b_0 + \frac{\gamma_0}{2}$, $\sup_t |x(t)| \leq b_0$. The following equivalence hold in a sliding mode:

$$x = (\gamma sign(v_1))_{eq} \tag{2.20}$$

defining an estimate of the input x as $\gamma sign(0)$. Equivalence (2.20) means that the average of $\gamma sign(v_1)$ is equal to the input x and hence an estimate of x, $\hat{x}$, can be extracted using a low-pass filter [112]:

$$\dot{\hat{x}} = \frac{1}{\tau}(-\hat{x} + \gamma sign(v_1)), \tag{2.21}$$

where $\tau > 0$. The following bound can be obtained for the estimation error

$$|x(t) - \hat{x}(t)| \leq \sqrt{(x(0) - \hat{x}(0))^2 e^{-\gamma t} + \tau^2 b_1^2}, \tag{2.22}$$

where $\sup_t |\dot{x}(t)| \leq b_1$, $b_1 > 0$. Assuming that $\tau = \frac{1}{\gamma}$, it can be confirmed that the upper bounds of estimation errors for the high gain observer and the sliding mode observer are the same. The implementation of the sliding mode observer, however, requires two filters whereas only one filter is required for implementing the high gain observer.

A differentiator that is based on the second order sliding mode can also be applied for estimation of $\dot{z}$ [54]. However, two filters are also required for implementation of the second order sliding mode differentiator.

Spline Interpolation

A spline interpolation method described in Chapter 3 is based on on-line least-squares polynomial fitting over the moving in time window of a given size. The advantage of this method over the dirty differentiation described above is its good transient behavior. The idea for the spline interpolation method is to fit a polynomial of a certain order as a function of time in the least squares sense and take the derivatives analytically. Thus the derivative $\dot{z}$ in (2.4) can be estimated via analytical calculation of the derivative of a polynomial approximation of z. This method is recommended for applications where the signal z is noisy. A polynomial of a certain order fitted in the least-squares sense in the moving window filters a measurement noise. Moreover, the order of the polynomial can also be chosen via evaluation of the residuals. The order of the polynomial is increased until the variance of the residual is approximately equal to the variance of the measurement noise that provides the best polynomial fitting in each step of the moving window. That in turn provides optimal attenuation of the measurement noise. A computational complexity can be mentioned as a disadvantage of the spline interpolation method.

2.2.2 Input Observer Application to Charge Estimation

The starting point for the derivation of an input observer for the cylinder flow is to represent the volumetric efficiency, η_v, as a sum of two terms. The first term is known (e.g., our initial calibration that determines the volumetric efficiency as a function of engine speed, intake manifold pressure, valve timing, etc.) while the second term needs to be estimated:

$$\eta_v = \eta_{vk} + \Delta\eta_v, \tag{2.23}$$

where η_{vk} is the known term and $\Delta\eta_v$ needs to be estimated. The values of the volumetric efficiency are normally calibrated on the engine dynamometer under steady-state running conditions and "room temperature" ambient conditions. Various uncertainty sources come into play when transferring the calibration to the actual vehicle and using it during transient operation of the engine; these uncertainties can be modelled as $\Delta\eta_v$, an additive volumetric efficiency error. Additionally, $\Delta\eta_v \neq 0$ may reflect long term aging effects (such as soot deposits in the intake ports) or engine-to-engine hardware variability.

The "speed-density" calculation (2.1) can be rewritten as follows

$$m_{cyl} = \eta_{vk}\frac{n_e}{2}V_d\frac{p}{RT} + \Delta\eta_v\frac{n_e}{2}V_d\frac{p}{RT}. \tag{2.24}$$

From (2.3) it follows that

$$\dot{p} = -\eta_{vk}\frac{n_e}{2}V_d\frac{p}{V_{IM}} - \Delta\eta_v\frac{n_e}{2}V_d\frac{p}{V_{IM}} + \frac{RT}{V_{IM}}m_{th}. \tag{2.25}$$

Thus the following input estimation problem results: by measuring p, $\eta_{vk}\frac{n_e}{2}V_d\frac{p}{V_{IM}}$ and $\frac{RT}{V_{IM}}m_{th}$, one has to estimate $\Delta\eta_v\frac{n_e}{2}V_d\frac{p}{V_{IM}}$. It is very easy to see that this problem is exactly the input estimation problem discussed in Subsection 2.2.1 with $z = p$, $y = -\eta_{vk}\frac{n_e}{2}V_d\frac{p}{V_{IM}} + \frac{RT}{V_{IM}}m_{th}$, $x = -\Delta\eta_v\frac{n_e}{2}V_d\frac{p}{V_{IM}}$. Hence, the flow into the engine can be estimated as

$$\hat{m}_{cyl} = \eta_{vk}\frac{n_e}{2}V_d\frac{p}{RT} + (\varepsilon - \gamma p)\frac{V_{IM}}{RT}, \tag{2.26}$$

where ε is adjusted as follows

$$\begin{aligned}\dot{\varepsilon} &= -\gamma\varepsilon - \gamma\eta_{vk}\frac{n_e}{2}V_d\frac{p}{V_{IM}} + \gamma\frac{RT}{V_{IM}}m_{th} + \gamma^2 p \\ &= -\gamma\frac{RT}{V_{IM}}(\hat{m}_{cyl} - m_{th}).\end{aligned} \tag{2.27}$$

Note that equation (2.26) estimates the flow into the engine cylinders as a sum of the nominal "speed-density" estimate and a correction term that depends on ε defined in equation (2.27).

The observer has several properties that are very desirable in the actual engine application. Equations (2.26), (2.27) imply that in steady-state $\hat{m}_{cyl} = m_{th}$. Thus the observer estimate agrees with the throttle flow measurement by MAF sensor in steady-state (as it should based on the mass balance). Note that the estimate of the cylinder flow on the basis of the nominal "speed-density" equation alone may not match m_{th} in steady-state, if there is a sizable discrepancy between η_v and η_{vk}. The observer also corrects the nominal speed-density estimate in transients. It turns out that due to the presence of the feedforward term, η_{vk}, in (2.26), the observer gain γ need not be very high to obtain accurate estimates of the cylinder flow in transients. This property was confirmed during the experimental evaluation of the observer. The observer gain would have to be much higher if the feed-forward term was not used.

If

$$V = \frac{1}{2}(m_{cyl} - \hat{m}_{cyl})^2,$$

then for any $c > 0$,

$$\dot{V} \le (-2\gamma + c)\cdot V + \frac{\sup_t |\dot{A}|^2}{2c},$$

where

$$A = \Delta\eta_v\frac{n_e}{2}V_d\frac{p}{RT}.$$

Thus the accuracy of the estimate may deteriorate during very fast transients, when $|\dot{A}|$ is large compared to γ. Note that γ cannot be made arbitrarily large in practice due, for example, to constraints imposed by the sample data implementation.

To implement the observer (2.26), (2.27), it is necessary to additionally process the measurements, m_{th} and p so that to compensate for a phase lag introduced by MAF sensor dynamics and to filter out periodic oscillations in the intake manifold pressure measurements without introducing an excessive phase lag. The periodic oscillations in the intake manifold pressure measurement are primarily caused by the cyclic nature of engine induction process. Specifically, an input observer can be applied to a model of MAF sensor dynamics to estimate the actual throttle flow based on the measured throttle flow signal. This observer serves a similar purpose as a "lead" filter introduced in [12],[25]. The intake manifold pressure measurement can be filtered using a state observer of the form

$$\dot{\hat{p}} = \frac{RT}{V_{IM}}(\hat{m}_{th} - \hat{m}_{cyl}) - \gamma_p(\hat{p} - p),$$

where $\gamma_p > 0$ and $\hat{m}_{th}$ is the actual throttle flow estimated with an input observer. The observer essentially combines an intake manifold pressure model and a low pass filter. The estimate, $\hat{p}$, can replace p in (2.26), (2.27). The theoretical analysis of the estimation accuracy of the algorithm with the additional observers is reported in [99]. The feedforward, η_{vk}, can be improved on-line using values to which $\Delta\eta_v$ converges in steady-state at various engine operating conditions. This functionality can be provided by a *learning* algorithm similar the one described in Section 2.3.3.

2.2.3 Experimental Evaluation

The scheme has been evaluated experimentally on a vehicle. The estimate of the air flow into the engine (normalized by the engine speed) obtained by the input observer algorithm is compared to the one obtained by the conventional speed-density calculation (equation (2.1)) in Figure 2.2. The equivalence ratio (air-to-fuel ratio divided by the stoichiometric value) measured by a UEGO sensor is shown in Figure 2.3. Note that since the actual flow into the engine cannot be measured, the quality of the estimate can only be judged from the air-to-fuel ratio trace. These plots represent a response to an aggressive throttle opening ("tip-in"). Note that the undesirable upward excursion of the air-to-fuel ratio (the so-called "lean spike") would be much higher if our fuel quantity calculation was based on the conventional "speed-density" cylinder flow estimate. Note also that in steady-state the estimate of the cylinder flow provided by our observer matches the measurement of the throttle flow provided by the MAF sensor, as it should, based on the mass balance.

2.3 Composite Adaptive Engine Air Charge Estimation

In the derivation of the adaptive air change estimation algorithm it is assumed that the uncertainty has an impact on the intake manifold temperature measurement. The algorithm can be analogously formulated for the case of either

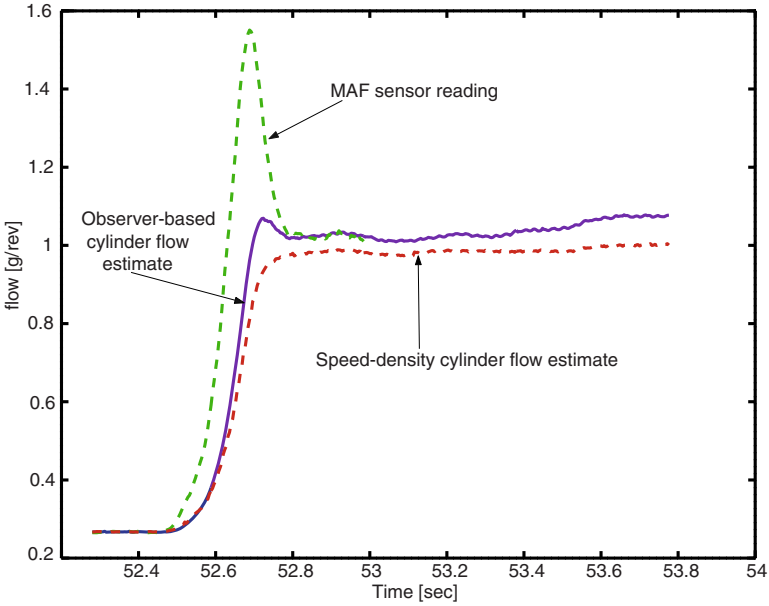

Fig. 2.2. Experimental results for a different operating condition. Observer-based and conventional estimates of flow (normalized by engine speed, i.e., in g/rev) into the engine and MAF sensor readings in response to a "tip-in".

additive or multiplicative uncertainty in volumetric efficiency. For example, is some engines, the temperature sensor is combined with the MAF sensor located upstream of the intake manifold and intake runners. In this case, the actual intake manifold temperature may then be modelled as the upstream temperature multiplied by an unknown parameter. While the input observer provides a simple solution to the air charge estimation problem, the accuracy of the estimation deteriorates in very fast transients. In this Section the theoretical results available in the adaptive control literature are used to develop an adaptive air charge estimator with various enhancements. In particular, the prediction error estimate is introduced into the adaptation law in order to improve the convergence rate of the estimated parameters. Because the resulting adaptation law is driven by both the tracking error and by the prediction error estimate, it is referred to as *composite* adaptive law. Nevertheless, the composite adaptation alone cannot cope with very fast transients and further enhancements are needed. Specifically, to find a compromise between the speed of adaptation and the quality of the estimation signal the *a priori* value of the estimated parameter is used during transients and to enable composite adaptation under close to steady-state conditions. This idea is realized by introduction of a σ- modification [37] which depends on a prediction error estimate. Then under the transient conditions the estimated parameter converges to its a priori value, but under steady-state conditions the σ -

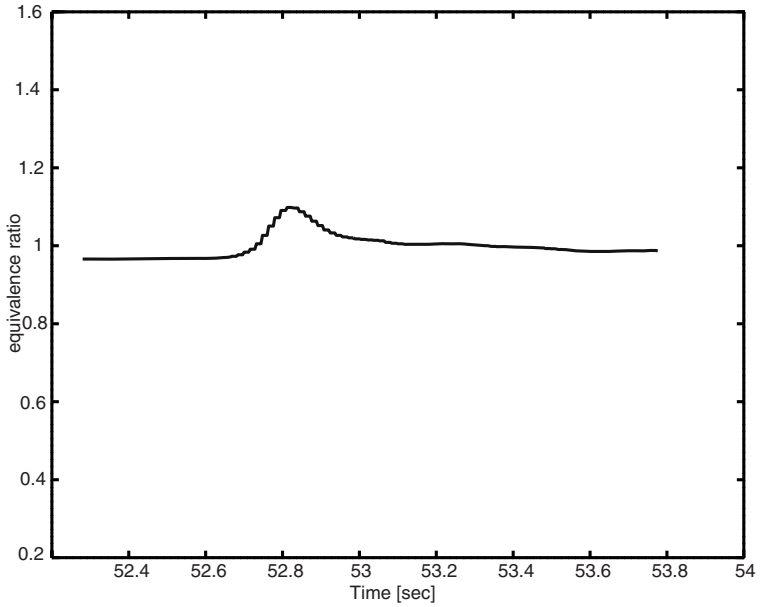

Fig. 2.3. Experimental results for a different operating condition. Equivalence ratio (air-to-fuel ratio divided by the stoichiometric value) with the observer-based cylinder flow estimate. Lean spike would be higher if the nominal "speed-density" estimate alone was used.

modification is not active and the adjustment law is driven by the tracking error and by the prediction error estimate. Further improvements are made by adapting the feedforward part. Specifically, due to modelling errors the estimated parameter may converge to different values depending on engine operating point. Therefore the *a priori* value is additionally represented as a linear function of the intake manifold pressure and update (or learn) the two coefficients of this function using the values to which the estimated parameter converges under close to steady-sate conditions. In transients, the updated feedforward provides an improved nominal estimate thereby improving the transient estimation accuracy of the overall algorithm and also shortens time for the convergence of the composite adaptation.

2.3.1 Composite Adaptive Algorithms: General Case

Consider a first order *error* system,

$$\dot{e} = -\alpha_0 e + \zeta^{\mathrm{T}} \tilde{\theta}, \tag{2.28}$$

where e denotes the tracking error (e.g., the difference between the measured and estimated state of the system), $\zeta \in \mathbf{R}^p$ is a regressor, $\tilde{\theta} = \theta - \theta_*$ is the

parameter error i.e., the error between the estimated and true parameters (unknown), $\theta, \theta_* \in \mathbf{R}^p$. The control objective is to drive the tracking error e to zero by choosing $\theta(t)$ appropriately. Composite adaptation defined as an adaptation driven by both tracking error e and prediction error which is defined as an error directly related to the parameter error $\tilde{\theta}$ is described in this Section. Two types of composite adaptation which use different techniques for prediction error estimation are described. The prediction error estimation technique which offers an exponential convergence of the prediction error estimate to its true value and the prediction error estimation technique on sliding modes which offers the convergence of the prediction error estimate in a finite time are described in the next two Sections. Moreover, a simultaneous disturbance and parameter estimation technique is described in the third Section.

Composite Adaptation with Exponentially Fast Prediction Error Estimation

The composite adaptation law [94], [96] can be defined as follows

$$\dot{\theta} = -\Gamma(t)[\zeta e + \alpha_0 \phi(e - \epsilon) + \kappa \alpha_0 sign(e - \epsilon)], \quad \kappa, \alpha_0 > 0 \tag{2.29}$$

$$\dot{\phi} = -\alpha_0 \phi + \zeta \tag{2.30}$$

$$\dot{\epsilon} = -\alpha_0 \epsilon - \phi^{\mathrm{T}} \dot{\theta} + \kappa \alpha_0 sign(e - \epsilon) \tag{2.31}$$

$$\dot{\Gamma} = -\alpha_0 \Gamma \phi \phi^{\mathrm{T}} \Gamma + \alpha_0 \lambda(t) \Gamma, \quad \|\Gamma(0)\| \leq k_0 \tag{2.32}$$

$$\lambda(t) = \lambda_0 (1 - ||\Gamma||/k_0), \quad \lambda_0 > 0, \ k_0 > 0 \tag{2.33}$$

where equation (2.29) is the equation of the adjustable parameter $\theta(t)$, equation (2.30) is the lowpass filter for the regressor ζ, equation (2.31) is the prediction error estimate, equation (2.32) is the least-squares gain update with a variable forgetting factor (2.33) [81].

Remark 1. The following least-squares gain update with the properties similar to the properties of (2.32),(2.33) can also be used [4].:

$$\dot{\Gamma} = -\alpha_0 \Gamma \phi \phi^{\mathrm{T}} \Gamma + \alpha_0 (\Gamma + \Gamma^{\mathrm{T}} \Gamma / k_0), \tag{2.34}$$

where $0 < \Gamma(0) \leq k_0 I_p$, I_p is $p \times p$ unity matrix, $k_0 > 0$ being an upper bound of the gain matrix Γ.

A prediction error is defined as an error which is directly related to the parameter error $\tilde{\theta}$. The tracking error e is not directly related to the parameter error $\tilde{\theta}$ and a dynamical system between the tracking error e and the parameter error $\tilde{\theta}$ reduces the convergence rate of the estimated parameters to their true values. The parameter error $\tilde{\theta}$ is estimated via $e - \epsilon$.

Defining, $e_1 = e - \epsilon - \phi^{\mathrm{T}} \tilde{\theta}$, it is straightforward to show that $\dot{e}_1 = -\alpha_0 e_1$, with $\kappa = 0$ and therefore $e - \epsilon$ is an estimate of the prediction error $\phi^{\mathrm{T}} \tilde{\theta}$ that contains the information about the parameter error $\tilde{\theta}$.

Thus equation (2.29) is the adaptation law driven by both tracking error, e, and by the prediction error estimate, $e - \epsilon$. One can expect that the convergence speed is improved due to a feedback of $\tilde{\theta}$ into the adaptation law

through $e-\epsilon$. An additional relay term driven by $e-\epsilon$ in (2.29) is beneficial to deal with the additive unmeasurable disturbances [96].

Remark 2. Algorithm (2.29),(2.30),(2.31),(2.32) can be initialized as follows $\epsilon(0)=e(0)$ and $\phi(0)=0$. Thus $e(t)-\epsilon(t)=\phi^{\mathrm{T}}(t)\tilde{\theta}(t)$ for $\forall t\geq 0$, with $\kappa=0$.

Remark 3. The prediction error can also be estimated as follows. First, equations (2.28),(2.30),(2.31) with $\kappa=0$ are written as follows:

$$e=\frac{\zeta^{\mathrm{T}}\tilde{\theta}}{s+\alpha_0},\quad \phi=\frac{\zeta}{s+\alpha_0},\quad \epsilon=-\frac{\phi^{\mathrm{T}}[s\theta]}{s+\alpha_0}, \tag{2.35}$$

where $s=j\omega$ is a Laplace variable.
Evaluation of $\phi^{\mathrm{T}}\tilde{\theta}$ with ϕ given by (2.35) yields to the prediction error estimate:

$$\begin{aligned}\phi^{\mathrm{T}}\tilde{\theta}&=\frac{(s+\alpha_0)\phi^{\mathrm{T}}\tilde{\theta}}{s+\alpha_0}=\frac{s[\phi^{\mathrm{T}}\tilde{\theta}]+\alpha_0\phi^{\mathrm{T}}\tilde{\theta}}{s+\alpha_0}\\&=\frac{[(s+\alpha_0)\phi^{\mathrm{T}}]\tilde{\theta}+\phi^{\mathrm{T}}[s\theta]+\alpha_0\phi^{\mathrm{T}}\tilde{\theta}-\alpha_0\phi^{\mathrm{T}}\tilde{\theta}}{s+\alpha_0}\\&=\frac{\zeta^{\mathrm{T}}\tilde{\theta}+\phi^{\mathrm{T}}[s\theta]}{s+\alpha_0}=\underbrace{\frac{\zeta^{\mathrm{T}}\tilde{\theta}}{s+\alpha_0}}_{e}-\underbrace{\Big(-\frac{\phi^{\mathrm{T}}[s\theta]}{s+\alpha_0}\Big)}_{\epsilon}\\&=(e-\epsilon).\end{aligned}$$

The convergence of the tracking error to zero for the system (2.28)-(2.32) can be established with the help of the following Lyapunov function [94], [96]:

$$V=\frac{1}{2}e^2+\frac{1}{2}(e-\epsilon-\phi^{\mathrm{T}}\tilde{\theta})^2+\frac{1}{2}\tilde{\theta}^{\mathrm{T}}\Gamma^{-1}\tilde{\theta} \tag{2.36}$$

The first term is the term which is responsible for the convergence of the tracking error. The derivative of this term along the solutions of (2.28) can be evaluated as follows:

$$\frac{d}{dt}(\frac{1}{2}e^2)=-\alpha_0e^2+e\zeta^{\mathrm{T}}\tilde{\theta} \tag{2.37}$$

The second term is the term which is responsible for the prediction error estimate. The derivative of this term along the solutions of (2.28),(2.29), (2.30) and (2.31) can be evaluated as follows:

$$\begin{aligned}&\frac{d}{dt}\frac{1}{2}(e-\epsilon-\phi^{\mathrm{T}}\tilde{\theta})^2=(e-\epsilon-\phi^{\mathrm{T}}\tilde{\theta})\\&(-\alpha_0e+\zeta^{\mathrm{T}}\tilde{\theta}+\alpha_0\epsilon+\phi^{\mathrm{T}}\dot{\theta}-\kappa\alpha_0 sign(e-\epsilon)-\dot{\phi}^{\mathrm{T}}\tilde{\theta}-\phi^{\mathrm{T}}\dot{\theta})\\=&(e-\epsilon-\phi^{\mathrm{T}}\tilde{\theta})(-\alpha_0(e-\epsilon-\phi^{\mathrm{T}}\tilde{\theta})-\kappa\alpha_0 sign(e-\epsilon))\end{aligned}$$

$$= -\alpha_0(e-\epsilon-\phi^{\mathrm{T}}\tilde{\theta})^2 - \kappa\alpha_0|e-\epsilon| + \tilde{\theta}^{\mathrm{T}}\phi\kappa\alpha_0 sign(e-\epsilon)$$
$$= -\frac{\alpha_0}{2}(e-\epsilon-\phi^{\mathrm{T}}\tilde{\theta})^2 - \frac{\alpha_0}{2}(e-\epsilon)^2 - \frac{\alpha_0}{2}\tilde{\theta}^{\mathrm{T}}\phi\phi^{\mathrm{T}}\tilde{\theta} - \kappa\alpha_0|e-\epsilon|$$
$$+ \tilde{\theta}^{\mathrm{T}}(\alpha_0\phi(e-\epsilon) + \phi\kappa\alpha_0 sign(e-\epsilon)) \tag{2.38}$$

The last term $\tilde{\theta}^{\mathrm{T}}(\alpha_0\phi(e-\epsilon) + \phi\kappa\alpha_0 sign(e-\epsilon))$ should be canceled in the derivative of the Lyapunov function due to (2.29). The negative term $-\kappa\alpha_0|e-\epsilon|$ is beneficial when dealing with additive bounded unmeasurable disturbances.

The third term is the term which is responsible for the parameter error convergence. The derivative of this term along the solutions of (2.29), (2.32) and (2.33) can be evaluated taking into account that $\dot{\Gamma}\Gamma^{-1} + \Gamma\dot{\Gamma}^{-1} = 0$ and $\dot{\Gamma}^{-1} = \alpha_0\phi\phi^{\mathrm{T}} - \alpha_0\lambda(t)\Gamma^{-1}$

$$\frac{d}{dt}\frac{1}{2}\tilde{\theta}^{\mathrm{T}}\Gamma^{-1}\tilde{\theta} = \tilde{\theta}^{\mathrm{T}}\Gamma^{-1}\dot{\theta} + \frac{1}{2}\tilde{\theta}^{\mathrm{T}}\dot{\Gamma}^{-1}\tilde{\theta}$$
$$= -\tilde{\theta}^{\mathrm{T}}(\zeta e + \alpha_0\phi(e-\epsilon) + \phi\kappa\alpha_0 sign(e-\epsilon))$$
$$+ \frac{\alpha_0}{2}\tilde{\theta}^{\mathrm{T}}\phi\phi^{\mathrm{T}}\tilde{\theta} - \frac{\alpha_0}{2}\lambda(t)\tilde{\theta}^{\mathrm{T}}\Gamma^{-1}\tilde{\theta} \tag{2.39}$$

Finally, the derivative of Lyapunov function candidate V along the solutions of the system is the following sum of (2.37), (2.38) and (2.39):

$$\dot{V} = -\alpha_0 e^2 - \frac{\alpha_0}{2}(e-\epsilon-\phi^{\mathrm{T}}\tilde{\theta})^2 - \frac{\alpha_0}{2}(e-\epsilon)^2 - \kappa\alpha_0|e-\epsilon| - \frac{\alpha_0}{2}\lambda(t)\tilde{\theta}^{\mathrm{T}}\Gamma^{-1}\tilde{\theta}$$

This implies that the tracking error, e, is bounded and square integrable. The convergence of the tracking error is established by proving boundness of $\dot{e}$ from (2.28) and using Barbalat's lemma. Convergence of $\tilde{\theta}$ to zero follows from the existence of the positive number λ_1 such that $\lambda(t) \geq \lambda_1 > 0$ if $\phi(t)$ is persistently exciting.

The Lyapunov function (2.36) allows

- the design of the filter (2.30), (2.31) for a prediction error estimate $e-\epsilon$ simultaneously with the adaptive algorithm (2.29) design,
- the connection of the filter parameter α_0 with the adaptive algorithm (2.29) parameters,
- inclusion of the relay term $\kappa\alpha_0 sign(e-\epsilon)$ driven by the prediction error estimate $e-\epsilon$ for a robustness with respect to unmeasurable disturbances,
- inclusion of the least-squares gain update (2.32) with a variable forgetting factor (2.33) which is a useful technique in dealing with time varying parameters.

Composite Adaptation with Prediction Error Estimation on a Sliding Mode

A prediction error $\zeta^{\mathrm{T}}\tilde{\theta}$ of the system (2.28) can also be estimated by using a sliding mode theory [112]. Introducing a filter for prediction error estimation

$$\dot{\epsilon} = -\alpha_0 \epsilon + \gamma sign(e - \epsilon), \quad \epsilon(0) = e(0), \tag{2.40}$$

where $\gamma = \|\zeta\|(\|\theta\| + \theta_b) + \frac{\kappa}{2}$, $\|\theta_*\| \leq \theta_b$, $\kappa > 0$, the derivative of the positive define function $V_1 = (e - \epsilon)^2$ is evaluated along the solutions of (2.28), (2.40) as follows

$$\begin{aligned}\dot{V}_1 &= 2(e - \epsilon)(-\alpha_0(e - \epsilon) + \zeta^{\mathrm{T}}\tilde{\theta} - \gamma sign(e - \epsilon)) \\ &\leq 2|e - \epsilon|(\|\zeta\|(\|\theta\| + \theta_b) - \gamma) \\ &\leq -\kappa\sqrt{V_1}\end{aligned}$$

Since the following inequality is valid

$$\sqrt{V_1} \leq \sqrt{V_1(0)} - \frac{\kappa}{2}t \tag{2.41}$$

for all $t \geq t_*$, where $t_* = \frac{2}{\kappa}\sqrt{V_1(0)}$ a sliding mode arises in the system and

$$\underbrace{\dot{e} - \dot{\epsilon}}_{=0} = -\alpha_0 \underbrace{(e - \epsilon)}_{=0} + \zeta^{\mathrm{T}}\tilde{\theta} + \gamma sign(e - \epsilon) \tag{2.42}$$

and the following equivalence hold

$$\gamma sign(e - \epsilon)|_{eq} = \zeta^{\mathrm{T}}\tilde{\theta} \tag{2.43}$$

which gives the prediction error $\zeta^{\mathrm{T}}\tilde{\theta}$.

The composite adaptive law can be defined as follows

$$\dot{\theta} = -\Gamma(t)[\zeta e + \frac{1}{2}\zeta\gamma sign(e - \epsilon)], \quad \kappa > 0 \tag{2.44}$$

$$\dot{\epsilon} = -\alpha_0 \epsilon + \gamma sign(e - \epsilon) \tag{2.45}$$

$$\dot{\Gamma} = -\Gamma\zeta\zeta^{\mathrm{T}}\Gamma + \lambda(t)\Gamma, \quad \|\Gamma(0)\| \leq k_0 \tag{2.46}$$

$$\lambda(t) = \lambda_0(1 - ||\Gamma||/k_0), \quad \lambda_0 > 0, \ k_0 > 0 \tag{2.47}$$

where equation (2.44) is the equation of the adjustable parameter $\theta(t)$ which can also be written by taking into account (2.43) as follows $\dot{\theta} = -\Gamma(t)[\zeta e + \frac{1}{2}\zeta\zeta^{\mathrm{T}}\tilde{\theta}]$, equation (2.45) is the filter for a prediction error estimate, and equation (2.46) is the least-squares gain update with a variable forgetting factor (2.47).

The stability of the system (2.28),(2.44),(2.45), (2.46) can be established using the following Lyapunov function

$$V_2 = \frac{1}{2}e^2 + \frac{1}{2}\tilde{\theta}^{\mathrm{T}}\Gamma^{-1}\tilde{\theta} \tag{2.48}$$

whose derivative along the solutions of the system is the following

$$\begin{aligned}\dot{V}_2 &= -\alpha_0 e^2 + e\zeta^{\mathrm{T}}\tilde{\theta} - \tilde{\theta}^{\mathrm{T}}(\zeta e + \frac{1}{2}\zeta\zeta^{\mathrm{T}}\tilde{\theta}) \\ &+ \frac{1}{2}\tilde{\theta}^{\mathrm{T}}\zeta\zeta^{\mathrm{T}}\tilde{\theta} - \frac{1}{2}\lambda(t)\tilde{\theta}^{\mathrm{T}}\Gamma^{-1}\tilde{\theta} \\ &= -\alpha_0 e^2 - \frac{1}{2}\lambda(t)\tilde{\theta}^{\mathrm{T}}\Gamma^{-1}\tilde{\theta} \end{aligned} \tag{2.49}$$

The convergence of the tracking and parameter errors can be established using similar arguments as in the previous case.

A comparison of composite algorithms (2.29),(2.30),(2.31), (2.32) and (2.44),(2.45), (2.46) shows that the algorithms are similar with the only difference that the regressor ζ is filtered in algorithm (2.29),(2.30),(2.31), (2.32) by a lowpass filter (see equation (2.30)). The relay term $sign(e-\epsilon)$ which is useful in dealing with unmeasurable disturbances in composite algorithm (2.29) is used for both prediction error estimation and disturbance rejection in algorithm (2.44) [5]. The term $\gamma sign(e-\epsilon)$ in algorithm (2.44) should be filtered via a lowpass filter in order to get an estimate of the prediction error $\zeta^{\mathrm{T}}\tilde{\theta}$ according to the *equivalent control method* [112]. In other words the equivalence (2.43) is a definition of $\gamma sign(0)$, and an average of $\gamma sign(e-\epsilon)$ is equal to the prediction error $\zeta^{\mathrm{T}}\tilde{\theta}$. Prediction error estimation by using *equivalent control method* is beneficial in adaptive algorithms since adaptation mechanism (2.44) takes a role of a filter that averages the input term $\gamma sign(e-\epsilon)$ and therefore this lowpass filter is omitted. Undesirable chattering of the adjustable parameters θ can be seen as a disadvantage of the algorithm (2.44).

Notice that the prediction error in the case of noisy tracking error measurements can also be estimated from (2.28) via estimation of the derivative of the tracking error $\dot{e}$ via a spline interpolation method, which is suitable for derivative estimation in the presence of a measurement noise. A recursive spline interpolation method for calculation of the derivatives of the signal is described in Chapter 3.

Composite adjustment law (2.29),(2.30),(2.31), (2.32) with $\Gamma(t) = \gamma I$, where I_p is $p \times p$ unity matrix, $\gamma > 0$ and $\kappa = 0$ is therefore chosen for air charge estimation in Section 2.3.2. Moreover, a σ-modification that depends on the prediction error estimate is introduced for separation of the transient and steady-state conditions.

Simultaneous Disturbance/Input and Parameter Estimation

The development of a simultaneous disturbance and parameter estimation technique is also motivated by the practical applications in the engine control area. An example of a simultaneous estimation of the exhaust flow via the EGR (Exhaust Gas Recirculation) valve which is treated as an unknown input (disturbance) and the volumetric efficiency parameters is considered in [47]. Another example described there is a simultaneous estimation of unknown

engine load torque which is treated as a disturbance, (see also Chapter 1) and the engine brake torque parameterized by an offset and a multiplier. The key idea of the simultaneous input and parameter estimation is a presentation of the estimate of unknown input in terms of unknown parameters or a parameter error. After that the problem is reduced to the parameter estimation problem. The convergence of the tracking error can be shown, but the estimate of the input does not converge to the *true* input, and unknown parameters do not converge to their true values. This technique is therefore recommended in the model reference adaptive control applications where the control aim is the minimization of the tracking error i.e., the error between the system state and the state of the reference model.

Consider a first order *error* system,

$$\dot{e} = -\alpha_0 e + \zeta^{\mathrm{T}}\tilde{\theta} + d + u_a, \tag{2.50}$$

where e denotes the tracking error, $\zeta \in \mathbf{R}^p$ is a regressor, $\tilde{\theta} = \theta - \theta_*$ is the parameter error, $d = d(t)$ is bounded unmeasurable time-varying disturbance, $|d(t)| \leq \bar{d}$, $|\dot{d}(t)| \leq \bar{d}_1$, and u_a is an additional control input. The problem of simultaneous disturbance and parameter estimation can be reduced to the problem of the design of an additional input u_a for a disturbance compensation. Notice that two unknown variables a prediction error $\zeta^{\mathrm{T}}\tilde{\theta}$ and a disturbance d can not be estimated using only one equation (2.50). Therefore the control aim is minimization of the tracking error e. The disturbance estimation objective can be stated as follows:

$$\overline{\lim_{t\to\infty}} \mid d(t) - \hat{d}(t) \mid = \Delta, \tag{2.51}$$

where $\hat{d}$ is the disturbance estimate and Δ is a small positive number. Consider the following disturbance estimate:

$$\hat{d} = \epsilon + \beta e + \varphi^T \tilde{\theta} \tag{2.52}$$

where $\beta > 0$, $\varepsilon \in R^1$ and $\varphi \in R^p$ are adjusted as follows

$$\dot{\epsilon} = -\beta\epsilon + \beta\alpha_0 e - \beta u_a - \varphi^T\dot{\theta} - \beta^2 e \tag{2.53}$$

$$\dot{\varphi} = -\beta\varphi - \beta\zeta, \quad \varphi(0) = 0, \tag{2.54}$$

where $\dot{\theta}$ is the derivative of the adjustable parameters specified below. Consider the following Lyapunov-like function candidate:

$$V = \frac{1}{2}(d - \hat{d})^2 = \frac{1}{2}(d - \epsilon - \beta e - \varphi^T\tilde{\theta})^2 \tag{2.55}$$

whose derivative along the solutions of (2.50),(2.52), (2.53), and (2.54) is

$$\begin{aligned} \dot{V} &\leq -\beta(d - \epsilon - \beta e - \varphi^T\tilde{\theta})^2 + \bar{d}_1 \mid d - \hat{d} \mid \\ &\leq -\frac{\beta}{2}(d - \hat{d})^2 + \frac{1}{2}\frac{\bar{d}_1^{\,2}}{\beta} \end{aligned} \tag{2.56}$$

and

$$(d(t) - \hat{d}(t))^2 \leq (d(0) - \hat{d}(0))^2 e^{-\beta t} + \frac{\bar{d}_1^{\,2}}{\beta^2} \tag{2.57}$$

Note, that the convergence of the disturbance estimate to its true value can be obtained with any pre-specified accuracy by amplifying the design parameter β, but the disturbance estimate (2.52) depends on unknown parameter mismatch $\tilde{\theta}$. The convergence of the estimate to its true value is exponential when $d(t) = d$.

Thus the compensation signal u_a can be chosen as follows: $u_a = -\varepsilon - \beta e$, and (2.53) can be simplified:

$$\dot{\epsilon} = \beta\alpha_0 e - \varphi^T \dot{\theta} \tag{2.58}$$

Finally, (2.50) can be written as follows

$$\dot{e} = -\alpha_0 e + [f + \varphi]^T \tilde{\theta} + (d - \hat{d}) \tag{2.59}$$

This, in turn, represents a stable dynamics driven by the input $[f+\varphi]^T\tilde{\theta}+(d-\hat{d})$ whereas the upper bound of $\mid d-\hat{d} \mid$ is known and can be made arbitrarily small. The problem of a simultaneous disturbance and parameter estimation was reduced to a well-known tracking error minimization problem. Composite adaptive algorithms modified with a σ-modification [96] and described in the previous Sections can now be applied for the reduction of the upper bound of the module of the tracking error to a arbitrarily small positive constant. This disturbance estimation technique was proposed in [5],[85]. The robustness with respect to a measurement noise is shown in [46], [47].

Notice that the problem of simultaneous disturbance and parameter estimation can also be solved by the expansion of the parameter vector i.e., via inclusion of the disturbance estimate into the parameter vector θ.

2.3.2 Derivation of Composite Adaptive Air Charge Estimator

The derivation of the adaptive air charge estimator starts with an ideal gas law for the intake manifold, where the intake manifold temperature is modified by an unknown constant multiplier, θ_*,

$$p = \frac{RT\theta_* M_{IM}}{V_{IM}}. \tag{2.60}$$

Here M_{IM} denotes the mass of air in the intake manifold.

Assuming that the intake manifold temperature is constant and differentiating (2.60) an equation similar to (2.3) is obtained:

$$\dot{p} = \frac{RT\theta_*}{V_{IM}}(m_{th} - m_{cyl}). \tag{2.61}$$

The flow into the engine is calculated on the basis (2.1) as

$$m_{cyl} = \eta_v \frac{n_e}{2} V_d \frac{p}{RT\theta_*} \tag{2.62}$$

Unfortunately, (2.62) is not directly implementable since the parameter θ_* is unknown. Our objective is, therefore, to define an adaptation law for the parameter estimate, $\theta(t)$, such that $\theta(t) \to \theta_*$.

The intake manifold pressure satisfies the following equation, which comes from (2.61) and (2.62):

$$\dot{p} = -\eta_v \frac{n_e}{2} \frac{V_d}{V_{IM}} p + \frac{RT}{V_{IM}} \theta_* m_{th}. \tag{2.63}$$

Consider the following adaptive observer for p,

$$\dot{\hat{p}} = -\eta_v \frac{n_e}{2} \frac{V_d}{V_{IM}} \hat{p} + \frac{RT}{V_{IM}} \theta m_{th} \tag{2.64}$$

where $\theta = \theta(t)$ is the parameter estimate. Notice that (2.64) has the same structure as (2.63) and, in particular, measured pressure would be used as an input to calculate volumetric efficiency, η_v, in both cases. The tracking error that should be driven to zero is defined as

$$e(t) = p(t) - \hat{p}(t). \tag{2.65}$$

From (2.63), (2.64) the following error model is obtained:

$$\dot{e} = -\eta_v \frac{n_e}{2} \frac{V_d}{V_{IM}} e - \frac{RT}{V_{IM}} m_{th} \tilde{\theta} \tag{2.66}$$

where $\tilde{\theta} = (\theta - \theta_*)$. From (2.66) one can define an adaptation law driven by the tracking error, e, as has been done, for example, in [45]. Here an adaptation law that is driven by both tracking and prediction errors is defined.

The prediction error (the error between the unknown parameter and its estimate multiplied by the regressor) is defined according to

$$e_p = \varphi \tilde{\theta} \tag{2.67}$$

and the prediction error estimate is defined according to

$$e_{es} = e - \varepsilon \tag{2.68}$$

where ε and φ are adjusted as follows

$$\dot{\varepsilon} = -\eta_v \frac{n_e}{2} \frac{V_d}{V_{IM}} \varepsilon + \alpha_0 (e - \varepsilon) - \varphi \dot{\theta} \tag{2.69}$$

$$\dot{\varphi} = -(\eta_v \frac{n_e}{2} \frac{V_d}{V_{IM}} + \alpha_0) \varphi - \frac{RT}{V_{IM}} m_{th}. \tag{2.70}$$

Here $\alpha_0 > 0$ is a gain, $\varphi(0) < 0$ and $\varepsilon(0)$ is arbitrary. The adaptation law that determines $\dot{\theta}$ will be defined in the sequel.

To show the convergence of the prediction error (2.67) to its estimate (2.68) we consider the following error

$$e_1 = e - \varepsilon - \varphi\tilde{\theta}. \tag{2.71}$$

Straightforward calculations show that e_1 satisfies the following equation

$$\dot{e}_1 = -(\eta_v \frac{n_e}{2}\frac{V_d}{V_{IM}} + \alpha_0)e_1 \tag{2.72}$$

and, therefore,

$$(e - \varepsilon) \to \varphi\tilde{\theta} \qquad as \quad t \to \infty. \tag{2.73}$$

Consider the following composite adaptation law [98] with the additional σ-modification:

$$\dot{\theta} = -\gamma(\alpha_0\varphi(e - \varepsilon) - \frac{RT}{V_{IM}}m_{th}e + \sigma \cdot (\theta - \overline{\theta})) \tag{2.74}$$

where $\overline{\theta}$ is an a priori estimate of θ_* and

$$\sigma = \beta(e - \varepsilon)^2, \qquad \beta > 0. \tag{2.75}$$

The adjustment law that determines $\theta(t)$ is driven by the tracking error e, the prediction error estimate $(e - \varepsilon)$ and by the adjustable σ-modification. In this Subsection the case when the a priori value is a constant, i.e., $\overline{\theta} = 1$ is analyzed in details. In the next Subsection the functional dependence of $\overline{\theta}$ on engine operating parameters and development of an algorithm to learn this functional dependence on-line will be considered.

Remark: In the actual engine implementation, it is preferable to use a calibratable lookup table with the prediction error estimate $(e - \varepsilon)$ as an input instead of (2.75). Such a table should have a dead-zone around 0 so that the σ-modification is disabled in conditions close to steady-state. As a result, during fast transients, the σ-modification dominates, and $\theta(t)$ converges to the a priori value θ_*; in conditions close to steady-state, the composite adaptive law dominates and the adaptation of $\theta(t)$ is driven by the tracking error and by the prediction error estimate. Instead of $(e - \varepsilon)$ one may also use an estimate of the time rate of change of intake manifold pressure as an input to σ-modification since the latter is indicative of whether the engine is in transients. The σ-modification can also be made asymmetric to differentiate between positive and negative transients.

Proposition: Consider the system (2.66), (2.70), (2.69), (2.74). Suppose the system parameter α_0 satisfies the constraint

$$\alpha_0 > 4\beta C^2, \tag{2.76}$$

where $|\theta_* - \overline{\theta}| \leq C$ and $\overline{\theta} = 1$. Then,

$$\lim_{t\to\infty} e(t) \to 0, \tag{2.77}$$

$$\lim_{t\to\infty} (e(t) - \varepsilon(t)) \to 0 \tag{2.78}$$

$$\lim_{t\to\infty} \varphi(t)\tilde{\theta}(t) \to 0, \tag{2.79}$$

$$\lim_{t\to\infty} \theta(t) \to \theta_* \tag{2.80}$$

and all signals remain bounded.

Proof: Consider the following Lyapunov function candidate

$$V(t) = \frac{1}{2}e^2 + \frac{1}{2}((e-\varepsilon) - \varphi\tilde{\theta})^2 + \frac{1}{2\gamma}\tilde{\theta}^2. \tag{2.81}$$

Evaluating its derivative along the solutions of the system yields:

$$\begin{aligned}\dot{V} = e(&-\eta_v \frac{n_e}{2}\frac{V_d}{V_{IM}}e - \frac{RT}{V_{IM}}m_{th}\tilde{\theta})\\ &- (\alpha_0 + \eta_v \frac{n_e}{2}\frac{V_d}{V_{IM}})((e-\varepsilon) - \varphi\tilde{\theta})^2\\ &- \tilde{\theta}(\alpha_0\varphi(e-\varepsilon) - \frac{RT}{V_{IM}}m_{th}e + \sigma(\theta - \bar{\theta})).\end{aligned} \tag{2.82}$$

Decomposing the third term and noting that

$$\tilde{\theta}(\theta - \bar{\theta}) = (\theta - \theta_*)(\theta - \bar{\theta}) = \tilde{\theta}^2 + \tilde{\theta}(\theta_* - \bar{\theta}),$$

yeilds

$$\begin{aligned}\dot{V} &= -\eta_v \frac{n_e}{2}\frac{V_d}{V_{IM}}e^2\\ &- \frac{\alpha_0}{2} + \eta_v \frac{n_e}{2}\frac{V_d}{V_{IM}})((e-\varepsilon) - \varphi\tilde{\theta})^2\\ &- \frac{\alpha_0}{2}((e-\varepsilon)^2 - \frac{\alpha_0}{2}(\varphi\tilde{\theta})^2\\ &- \tilde{\theta}\beta(e-\varepsilon)^2(\theta - \bar{\theta})\\ &\leq -\eta_v \frac{n_e}{2}\frac{V_d}{V_{IM}}e^2\\ &- (\frac{\alpha_0}{2} + \eta_v \frac{n_e}{2}\frac{V_d}{V_{IM}})((e-\varepsilon) - \varphi\tilde{\theta})^2\\ &- (\frac{\alpha_0}{2} + \beta|\tilde{\theta}|^2 - \frac{\beta}{2}|\tilde{\theta}|^2 - \beta C^2)(e-\varepsilon)^2 - \frac{\alpha_0}{2}(\varphi\tilde{\theta})^2.\end{aligned}$$

By taking into account (2.76) it follows that

$$\begin{aligned}\dot{V} \leq &-\eta_v \frac{n_e}{2}\frac{V_d}{V_{IM}}e^2\\ &- (\frac{\alpha_0}{2} + \eta_v \frac{n_e}{2}\frac{V_d}{V_{IM}})((e-\varepsilon) - \varphi\tilde{\theta})^2\\ &- \frac{\alpha_0}{4}(e-\varepsilon)^2 - \frac{\alpha_0}{2}(\varphi\tilde{\theta})^2.\end{aligned} \tag{2.83}$$

It is concluded now that e and $((e-\varepsilon)-\varphi\tilde{\theta})$ are bounded and square-integrable, $\tilde{\theta}$ is bounded, and $\varphi\tilde{\theta}$ and $(e-\varepsilon)$ are square-integrable. From (2.66) it is concluded that $\dot{e}$ is also bounded, and (2.77) is achieved. Using (2.69) one can show that $\dot{\varepsilon}$ and ε are also bounded. Then (2.78) and hence (2.79) are achieved. The convergence of the parameter (see (2.80)) can be proved by considering the following equation

$$\dot{\theta} = -\gamma(\alpha_0\varphi^2\tilde{\theta} - \frac{RT}{V_{IM}}m_{th}e + \sigma\cdot(\theta-\overline{\theta})), \tag{2.84}$$

which represents a stable time varying low-pass filter with a square-integrable and convergent input and by noting that there exists a positive constant C_ϕ such that $\varphi^2 \geq C_\phi$.

Then,

$$\eta_v\frac{n_e}{2}V_d\frac{p}{RT\theta(t)} \rightarrow \eta_v\frac{n_e}{2}V_d\frac{p}{RT\theta_*} \quad as \quad t\rightarrow\infty. \tag{2.85}$$

Therefore the cylinder air flow (2.62) can be estimated as follows

$$\hat{m}_{cyl} = \eta_v\frac{n_e}{2}V_d\frac{p}{RT\theta(t)}, \tag{2.86}$$

where $\theta(t)$ is adjusted according to (2.74), (2.70), (2.69).

For a later convenience all the equations for the composite adaptive cylinder flow estimation are listed:

$$\hat{m}_{cyl} = \eta_v\frac{n_e}{2}V_d\frac{p}{RT\theta(t)} \tag{2.87}$$

$$\dot{\hat{p}} = -\eta_v\frac{n_e}{2}\frac{V_d}{V_{IM}}\hat{p} + \frac{RT}{V_{IM}}\theta m_{th} \tag{2.88}$$

$$\dot{\varepsilon} = -\eta_v\frac{n_e}{2}\frac{V_d}{V_{IM}}\varepsilon + \alpha_0(p-\hat{p}-\varepsilon) - \varphi\dot{\theta} \tag{2.89}$$

$$\dot{\varphi} = -(\eta_v\frac{n_e}{2}\frac{V_d}{V_{IM}} + \alpha_0)\varphi - \frac{RT}{V_{IM}}m_{th} \tag{2.90}$$

$$\dot{\theta} = -\gamma(\alpha_0\varphi(e-\varepsilon) - \frac{RT}{V_{IM}}m_{th}e + \sigma\cdot(\theta-\overline{\theta})). \tag{2.91}$$

The algorithm guarantees that in steady-state conditions, $\hat{m}_{cyl} = m_{th}$. In transient conditions, the estimator follows (2.1) more closely.

2.3.3 Improving Feedforward via Learning

Due to other, unmodelled uncertainty sources, the parameter estimate, $\theta(t)$, produced by the adaptive estimator may converge to different values depending on the engine operating conditions. To address this issue, the a priori

value $\overline{\theta}$, that may be viewed as a feedforward part of the algorithm, can be additionally modelled as a static function of the intake manifold pressure, i.e., $\overline{\theta} = f(p)$. This functional dependence can be learned on-line from the values to which $\theta(t)$ converges.

Specifically, a linear parametrization of the following form is considered here:

$$\overline{\theta} = k_1 p + k_2, \tag{2.92}$$

where k_1 and k_2 are unknown parameters to be defined. The whole intake manifold pressure region is divided into two sub-regions corresponding to low and high pressures: $0 < p_{low} < p_{bl}$ and $p_{bu} < p_{high} < p_{amb}$, where p_{amb} is the ambient pressure, and $p_{bl} < p_{bu}$ are boundaries of the two sub-regions. Suppose that the values $\overline{\theta}_{low}$ and $\overline{\theta}_{high}$ to which $\theta(t)$ converges at a certain low pressure value, p_{low}, and at a certain high pressure, p_{high} are memorized. Then the coefficients k_1 and k_2 can be found as solutions of the following equations

$$\overline{\theta}_{high} = k_1 p_{high} + k_2, \tag{2.93}$$

$$\overline{\theta}_{low} = k_1 p_{low} + k_2. \tag{2.94}$$

Thus,

$$k_1(t) = \frac{\overline{\theta}_{high} - \overline{\theta}_{low}}{p_{high} - p_{low}} \tag{2.95}$$

$$k_2(t) = \overline{\theta}_{low} - k_1(t) p_{low}. \tag{2.96}$$

In practice, the updates of $k_1(t)$ and $k_2(t)$ can be enabled under close to steady-state engine operating conditions. In particular, $k_1(t)$ and $k_2(t)$ can be recursively updated each time new close to steady-state conditions are reached using, for example, a recursive least squares algorithm. Alternatively, to obtain a system functioning continuously in real-time one can adapt $\overline{\theta}_{low}$ for low pressure as:

$$\begin{aligned} &If \quad \sigma(t) < \Delta \quad and \quad 0 < p < p_{bl} \\ &\dot{\overline{\theta}}_{low} = -\gamma_\theta(\overline{\theta}_{low} - \theta), \quad \overline{\theta}_{low}(0) = 1 \qquad (2.97) \\ &\dot{p}_{low} = -\gamma_p(p_{low} - p), p_{low}(0) = p_{mp1} \qquad (2.98) \\ &else \\ &\dot{\overline{\theta}}_{low} = 0 \\ &\dot{p}_{low} = 0 \end{aligned}$$

and one can adapt $\overline{\theta}_{high}$ for high pressure as:

$$\begin{aligned} &If \quad \sigma(t) < \Delta \quad and \quad p_{bu} > p > p_b \\ &\dot{\overline{\theta}}_{high} = -\gamma_\theta(\overline{\theta}_{high} - \theta), \quad \overline{\theta}_{high}(0) = 1 \qquad (2.99) \end{aligned}$$

$$\dot{p}_{high} = -\gamma_p(p_{high} - p), p_{high}(0) = p_{mp2} \quad (2.100)$$
$$else$$
$$\dot{\overline{\theta}}_{high} = 0$$
$$\dot{p}_{high} = 0$$

where Δ,γ_θ, and γ_p are positive design parameters.

The learning process proceeds as follows. During steady-state conditions if the intake manifold pressure is low ($p < p_{bl}$), $\overline{\theta}_{low}$ is adapted according to (2.97) and $\overline{\theta}_{low}$ converges to the value of θ, while $\overline{\theta}_{high}$ remains constant. Note that in practice when σ-modification with a deadzone is used, θ does not depend on $\overline{\theta}$ under close to steady-state conditions since the term $\sigma(\theta - \overline{\theta})$ disappears from equation (2.91) and the adaptation law is driven by tracking and prediction errors only. Suppose that due to a positive transient the intake manifold pressure becomes high. Then, in conditions close to steady-state, $\overline{\theta}_{high}$ is adapted according to (2.99), while $\overline{\theta}_{low}$ is frozen. Now the mapping $\overline{\theta} = f(p)$ is based on two recently learned values $\overline{\theta}_{low}$ and $\overline{\theta}_{high}$. The gradual improvement of the feedforward part of the algorithm ensures better transient estimation accuracy (especially during fast transients) and speeds up the convergence of the estimated parameter to its true value.

2.3.4 Evaluation

The algorithm was implemented in Matlab. The inputs to the algorithm were based on the vehicle measurements of the intake manifold pressure, flow through the throttle and engine speed sampled at 10 msec.

First, the behavior of the adaptive estimator (2.87) - (2.91) without the feedforward learning functionality, i.e., with $\overline{\theta} \equiv 1$ is illustrated. Figure 2.5 compares the nominal speed-density estimate (2.1) with the response of the adaptive estimator with and without the σ-modification. The adaptive estimator and the nominal speed-density estimate converge to different values in steady-state. This is especially pronounced in the beginning part of the trace. Note that the adaptive estimator always agrees with the MAF sensor reading in steady-state conditions. Therefore the adaptive estimator is more accurate that the nominal speed-density estimate in steady-state conditions. Nevertheless in rapid transients, the prediction error estimate, $(e - \epsilon)$ is large and the σ-modification ensures that the adaptive estimator follows closely the nominal speed-density estimate. The nominal speed-density estimate is more accurate than MAF sensor reading in transients. Figure 2.5 confirms that this speeds up the parameter convergence. One may also observe from Figure 2.5 that $\theta(t)$ converges to different values at low intake manifold pressure and high intake manifold pressure. These values can be captured via the feedforward learning as described in Subsection 2.3.3.

Figure 2.4 illustrates a typical iteration of the feed-forward learning. Once operating conditions close to steady-state are reached, the values of $\overline{\theta}_{high}$

and $\overline{\theta}_{low}$ are adapted. At low intake manifold pressure conditions, $\overline{\theta}_{low}$ is adapted while $\overline{\theta}_{high}$ is frozen. At high intake manifold pressure conditions, $\overline{\theta}_{high}$ is adapted while $\overline{\theta}_{low}$ is frozen. As can be seen from Figure 2.4, $\overline{\theta}_{low}$ is rapidly adapted to a value less than 1 in low pressure conditions but a positive transient affects the system before the adaptation is completed. The $\overline{\theta}_{high}$ starts at 1 and adapts to a value slightly less than 1 at the end of the trace. Note that the speed-density calculation with the a priori value $\overline{\theta}(t)$ calculated according to (2.92) matches the output of the adaptive estimator at the end of the trace.

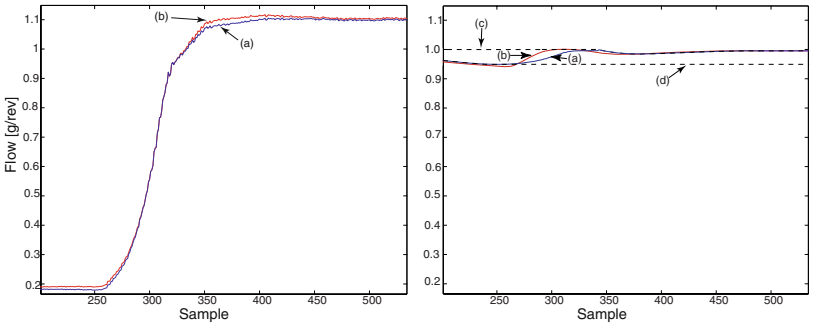

Fig. 2.4. Left: Normalized by engine speed cylinder flow estimate for (a) nominal speed-density; (b) adaptive estimator (2.87) - (2.91) with the feedforward calculated according to (2.92) and feedforward learning. Right: Parameter estimate for (a) $\overline{\theta}(t)$ calculated according to (2.92); (b) $\theta(t)$ for adaptive estimator with feedforward learning; (c) $\overline{\theta}_{high}$; (d) $\overline{\theta}_{low}$.

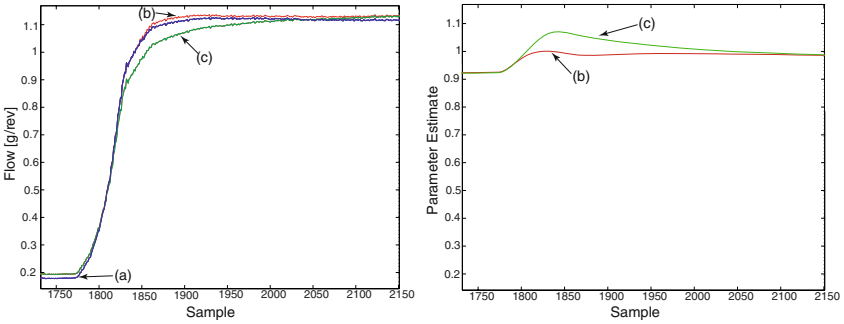

Fig. 2.5. Adaptive estimator responses without feedforward learning: (a) nominal speed-density estimate; (b) adaptive estimator with σ-modification; (c) adaptive estimator without σ-modification. Normalized flow (left) and estimated parameter, $\theta(t)$ (right).

2.4 Air Charge Prediction

Unlike for direct injection (DI) engines, for PFI engines the delay between fuel injection and actual induction may have a detrimental effect in very fast transients. Air charge prediction algorithms can be used to compensate for the effect of this delay [100]. The prediction algorithms encompass two distinct functionalities. Firstly, it predicts the throttle angle and the flow via the throttle plate thereby compensating for the delay and dynamics in the throttle system. Secondly, it uses the intake manifold dynamic equation (2.3) and the speed-density calculation (2.1) to predict the intake manifold pressure and cylinder air flow several events into the future. During very rapid transients, it is advantageous to use this prediction of the cylinder air flow to determine correctly the fuel amount to be injected. The estimated cylinder air flow can still be used to determine the fueling rate when transients are not very fast, and it can also be used directly by the ignition system to set correctly the spark timing. The prediction algorithm benefits from the improved feedforward (2.92) that is achieved with our learning algorithm. Figure 2.6 illustrates the experimental results of the prediction algorithm application in a vehicle.

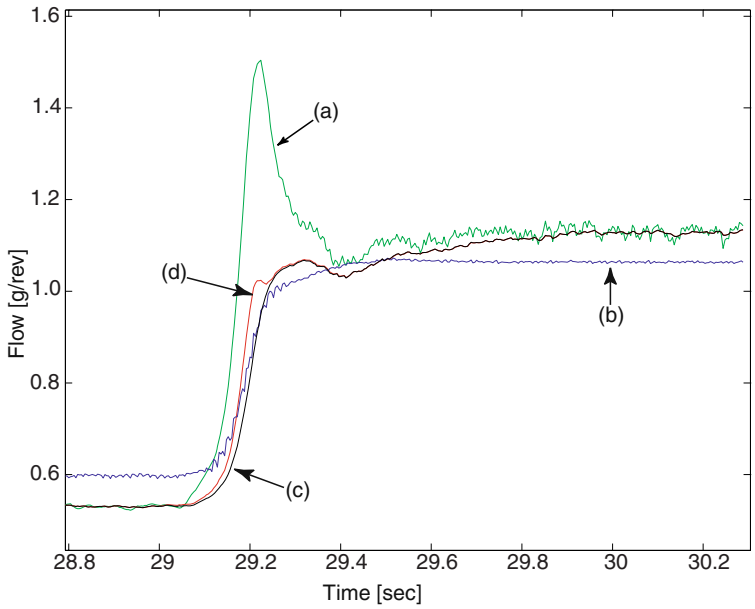

Fig. 2.6. Experimental results for the cylinder flow prediction algorithm: (*a*) MAF sensor signal; (*b*) nominal speed-density estimate of the cylinder flow; (*c*) cylinder flow estimated with an input observer based technique; (*d*) predicted cylinder flow signal (made to smoothly transition to estimated cylinder flow once transient subdue. Cylinder flow estimates are normalized by engine speeds.

2.5 Concluding Remarks

Two powerful techniques which significantly enhance the performance of the air charge estimation algorithms are presented in this Chapter. Both techniques are theoretically justified and verified on a real vehicle. Both techniques use the measured flow via the throttle under the steady state conditions and the speed-density flow or input estimator during transients. The simplicity of the input estimation technique makes the corresponding load signal very attractive for implementation. The engine load signal based on the adaptive estimation technique is more complicated, but can cope better with fast transients than the signal based on the input estimation technique due to the adjustable σ - modification. Adaptive estimation technique developed here employed methods known in the adaptive control literature such as composite adaptation and variable σ - modification to construct the sophisticated engine load estimator.

3

Recursive Spline Interpolation Method

In this Chapter new computationally efficient algorithms for spline interpolation method are explained. Theoretical comparative analysis of the spline interpolation method with combined high-gain observer and spline interpolation method is presented. New spline interpolation algorithms are implemented in a test vehicle for estimation of the engine angular acceleration from the crankshaft angle measurements.

3.1 Introduction

Numerical calculation of the derivatives of a signal is an old problem in numerical analysis and digital signal processing. The backward difference method gives one of the simplest numerical differentiators. Despite the fact that it is quite common in engineering applications the behavior of the derivative is very often accompanied with peaking phenomena. Spline interpolation method proposed in [18] is based on on-line least-squares polynomial fitting over the moving in time window of a size w. The advantage of this method over the backward difference method is its good transient behavior. The idea for the spline interpolation method is to fit a polynomial of a certain order as a function of time in least squares sense and take the derivatives analytically. Properties of this method are described in [14], [18]. However, several practical problems remain. A relatively large window size w requires more on-line computations and makes practical implementation of the method difficult. This necessitates the development of computationally efficient recursive algorithms. Moreover, in the papers [14], [18] only constant intersampling time is considered, which in many practical applications is not constant. For example, crankshaft angle measurements in automotive engines are based on the measurements of the crankwheel tooth number and therefore the elapsed time between two teeth passing a fixed point varies. This necessitates the development of recursive computationally efficient algorithms for variable discretization step.

The contributions of this Chapter are the following :

A.A. Stotsky, *Automotive Engines*, DOI 10.1007/978-3-642-00164-2_3,

• new computationally efficient recursive spline interpolation algorithms for variable discretization step,

• theoretical comparative analysis of the spline interpolation method and combined spline method with high gain observer,

• real-time implementation of the spline interpolation method for the crankshaft acceleration estimation.

3.2 The Estimation of the Derivatives of Signal via Spline Interpolation

The first step is to choose the interpolating polynomial as

$$\hat{\alpha} = c_0 + c_1 t + ... + c_n t^n \tag{3.1}$$

where $\hat{\alpha}$ is an estimate of the measured signal α, t is continuous time, c_i,$i = 0, ..., n$ are coefficients to be found. The estimates of the derivatives are obtained by differentiating (3.1) analytically.

Suppose that there is a measured window of data $\{\alpha_{k-(w-1)}, ..., \alpha_k\}$ of a size w, measured discretely with variable discretization step. It is convenient to place the origin at the point $k-(w-1)$, where k is the step number, then there is a window of data $\{\alpha_0, ..., \alpha_{w-1}\}$ measured at $\{0, ..., t_{w-1}\}$ respectively Variable discretization step is presented as $\Delta t_i = t_i - t_{i-1}$, $i = 1, ..., w-1$.

The sum to be minimized at every step is

$$S = \sum_{i=0}^{w-1} (\alpha_i - (c_0 + c_1 t_i + ... + c_n t_i^n))^2 \tag{3.2}$$

where t_i, $i = 0, ..., w-1$ is a discrete time which corresponds to the signal measurements α_i, $t_0 = 0$.

Minimum of S is achieved when equating to zero partial derivatives of S with respect to c_i, $i = 0, ..., n$, i.e.,

$$\frac{\partial S}{\partial c_i} = 0 \tag{3.3}$$

Equations (3.3) can be written as follows

$$c_0\, w + c_1 \sum_{i=0}^{w-1} t_i + ... + c_n \sum_{i=0}^{w-1} t_i^n = \sum_{i=0}^{w-1} \alpha_i \tag{3.4}$$

$$c_0 \sum_{i=0}^{w-1} t_i + c_1 \sum_{i=0}^{w-1} t_i^2 + ... + c_n \sum_{i=0}^{w-1} t_i^{n+1} = \sum_{i=0}^{w-1} \alpha_i t_i \tag{3.5}$$

$$\cdots \quad \cdots\cdots$$

$$c_0 \sum_{i=0}^{w-1} t_i^n + c_1 \sum_{i=0}^{w-1} t_i^{n+1} + ... + c_n \sum_{i=0}^{w-1} t_i^{2n} = \sum_{i=0}^{w-1} \alpha_i t_i^n \tag{3.6}$$

where equation (3.4) represents $\frac{\partial S}{\partial c_0} = 0$, equation (3.5) represents $\frac{\partial S}{\partial c_1} = 0$ and finally equation (3.6) represents $\frac{\partial S}{\partial c_n} = 0$.

The system (3.4) - (3.6) should be resolved at every step in order to find the coefficients c_i, $i = 0, ..., n$. It is clear that for a sufficiently large window size w, the calculation of sums in the system (3.4) - (3.6) requires a lot of computational power and the next step is to present recursive computationally efficient algorithms to compute these sums.

Let us consider one step of the moving window of a size w. Suppose that at step $k-1$ there is the following data $\{\alpha_0, ..., \alpha_{w-1}\}$ measured at $\{0, ..., t_{w-1}\}$, and at step k there is $\{\alpha_1, ..., \alpha_w\}$ measured at $\{0, ..., t_w\}$. The new value α_w measured at the time t_w enters the window (buffer) and the value α_0 leaves the window. The problem statement is to find computationally efficient recursive algorithms to compute the sums $S_{m_k} = \sum_{i=1}^{w} t_i^m$ via the sums at the previous step $S_{m_{k-1}} = \sum_{i=0}^{w-1} t_i^m$, where $m = 1, ...2n$.

Define the sum of order m at step k as follows

$$S_{m_k} = \sum_{i=1}^{w} t_i^m = \Delta t_2^m + (\Delta t_2 + \Delta t_3)^m + ... + (\Delta t_2 + \Delta t_3 + ... + \Delta t_w)^m \quad (3.7)$$

where $t_1 = 0$.
The sum (3.7) should be computed using the same sum at a previous step $k-1$ which can written as

$$S_{m_{k-1}} = \sum_{i=0}^{w-1} t_i^m = \Delta t_1^m + (\Delta t_1 + \Delta t_2)^m + ... + (\Delta t_1 + \Delta t_2 + ... + \Delta t_{w-1})^m \quad (3.8)$$

and the sums of lower order at step k which are defined as

$$S_{(m-j)k} = \sum_{i=1}^{w} t_i^{m-j} = \Delta t_2^{m-j} + (\Delta t_2 + \Delta t_3)^{m-j} + ... + (\Delta t_2 + \Delta t_3 + ... + \Delta t_w)^{m-j} \quad (3.9)$$

where $1 \leq j \leq (m-1)$, $m > 1$.

Starting with (3.8) and using the following identity

$$(x+y)^m = \sum_{j=0}^{m} C_j^m x^j y^{m-j}, \qquad C_j^m = \frac{m!}{j!(m-j)!} \quad (3.10)$$

where $m = 0, 1, 2, ...$, one gets

$$S_{m_{k-1}} = (w-1)\Delta t_1^m + \Delta t_2^m + (\Delta t_2 + \Delta t_3)^m + ...$$
$$+(\Delta t_2 + \Delta t_3 + ... + \Delta t_{w-1})^m$$
$$+ \sum_{j=1}^{m-1} C_j^m (\Delta t_1^j \Delta t_2^{m-j} + ... + \Delta t_1^j (\Delta t_2 + ... + \Delta t_{w-1})^{m-j}) \quad (3.11)$$

Notice that

$$\Delta t_2^m + (\Delta t_2 + \Delta t_3)^m + ... + (\Delta t_2 + \Delta t_3 + ... + \Delta t_{w-1})^m$$
$$= S_{mk} - (\Delta t_2 + \Delta t_3 + ... + \Delta t_w)^m \quad (3.12)$$

and

$$\sum_{j=1}^{m-1} C_j^m (\Delta t_1^j \Delta t_2^{m-j} + ... + \Delta t_1^j (\Delta t_2 + ... + \Delta t_{w-1})^{m-j})$$
$$= \sum_{j=1}^{m-1} C_j^m \Delta t^j (S_{(m-j)k} - (\Delta t_2 + ... + \Delta t_w)^{m-j}) \quad (3.13)$$

Substituting (3.12) and (3.13) in (3.11) one gets

$$S_{m_k} = S_{m_{k-1}} - (w-1)\Delta t_1^m - \sum_{j=1}^{m-1} C_j^m \Delta t^j (S_{(m-j)k} - (\Delta t_2 + ... + \Delta t_w)^{m-j})$$
$$+(\Delta t_2 + \Delta t_3 + ... + \Delta t_{w-1})^m \quad (3.14)$$

where $C_j^m = \frac{m!}{j!(m-j)!}$, $1 \le j \le (m-1)$, $m > 1$.

The next step is to calculate the sums on the right hand side of the equation (3.4) - (3.6). The sums $S_{\alpha m_k} = \sum_{i=1}^{w} \alpha_i t_i^m$ should be calculated via the sums at the previous step $S_{\alpha m_{k-1}} = \sum_{i=0}^{w-1} \alpha_i t_i^m$, where $m = 2, ...n$.

Using similar arguments one can show that

$$S_{\alpha m_k} = S_{\alpha m_{k-1}} - (\alpha_1 + \alpha_2 + ... + \alpha_{w-1})\Delta t_1^m -$$
$$\sum_{j=1}^{m-1} C_j^m \Delta t_1^j (S_{\alpha(m-j)k} - \alpha_w (\Delta t_2 + \Delta t_3 + ... + \Delta t_w)^{m-j})$$
$$+\alpha_w (\Delta t_2 + \Delta t_3 + ... + \Delta t_w)^m \quad (3.15)$$

where

$$S_{\alpha m_{k-1}} = \sum_{i=0}^{w-1} \alpha_i t_i^m = \alpha_1 \Delta t_1^m + \alpha_2 (\Delta t_1 + \Delta t_2)^m + ... \\ + \alpha_{w-1} (\Delta t_1 + \Delta t_2 + ... + \Delta t_{w-1})^m \tag{3.16}$$

is the sum on the step $(k-1)$, and

$$S_{\alpha(m-j)k} = \sum_{i=1}^{w} \alpha_i t_i^{m-j} = \alpha_2 \Delta t_2^{m-j} + \alpha_3 (\Delta t_2 + \Delta t_3)^{m-j} + \\ ... + \alpha_w (\Delta t_2 + \Delta t_3 + ... + \Delta t_w)^{m-j} \tag{3.17}$$

where $1 \leq j \leq (m-1)$, $m > 1$.

The order of the interpolating polynomial should be so selected to be as low as possible in order to reduce the computational burden and to filter out measurement noise.

In the next Section the detailed solution of the interpolation problem for the second order polynomial is presented. This example is used in Section 3.4 for the crankshaft acceleration estimation.

3.3 Second Order Example

3.3.1 Spline Interpolation Method

For the second order polynomial (3.1), where $n = 2$, equations (3.4) - (3.6) can be written as follows

$$c_0\, w + c_1 \sum_{i=0}^{w-1} t_i + c_2 \sum_{i=0}^{w-1} t_i^2 = \sum_{i=0}^{w-1} \alpha_i \tag{3.18}$$

$$c_0 \sum_{i=0}^{w-1} t_i + c_1 \sum_{i=0}^{w-1} t_i^2 + c_2 \sum_{i=0}^{w-1} t_i^3 = \sum_{i=0}^{w-1} \alpha_i t_i \tag{3.19}$$

$$c_0 \sum_{i=0}^{w-1} t_i^2 + c_1 \sum_{i=0}^{w-1} t_i^3 + c_2 \sum_{i=0}^{w-1} t_i^4 = \sum_{i=0}^{w-1} \alpha_i t_i^2 \tag{3.20}$$

The next step is to present recursive computations for all the sums in (3.18) - (3.20). Suppose that at the first step all the sums are computed. Then

$$S_{1_k} = \sum_{i=1}^{w} t_i = S_{1_{k-1}} - (w-1)\Delta t_1 + (\Delta t_2 + \Delta t_3 + ... + \Delta t_w) \tag{3.21}$$

Using (3.14) one gets

$$S_{2_k} = \sum_{i=1}^{w} t_i^2 = S_{2_{k-1}} - (w-1)\Delta t_1^2 - 2\Delta t_1(S_{1k} - (\Delta t_2 + ... + \Delta t_w))$$
$$+(\Delta t_2 + \Delta t_3 + ... + \Delta t_w)^2$$
$$S_{3_k} = \sum_{i=1}^{w} t_i^3 = S_{3_{k-1}} - (w-1)\Delta t_1^3 - 3\Delta t_1(S_{2k} - (\Delta t_2 + ... + \Delta t_w)^2)$$
$$-3\Delta t_1^2(S_{1k} - (\Delta t_2 + ... + \Delta t_w)) + (\Delta t_2 + \Delta t_3 + ... + \Delta t_w)^3$$
$$S_{4_k} = \sum_{i=1}^{w} t_i^4 = S_{4_{k-1}} - (w-1)\Delta t_1^4 - 4\Delta t_1(S_{3k} - (\Delta t_2 + ... + \Delta t_w)^3)$$
$$-6\Delta t_1^2(S_{2k} - (\Delta t_2 + ... + \Delta t_w)^2) - 4\Delta t_1^3(S_{1k} - (\Delta t_2 + ... + \Delta t_w))$$
$$+(\Delta t_2 + \Delta t_3 + ... + \Delta t_w)^4 \tag{3.22}$$

and

$$S_{\alpha k} = \sum_{i=1}^{w} \alpha_i = S_{\alpha(k-1)} + \alpha_w - \alpha_0 \tag{3.23}$$

$$S_{\alpha_{1k}} = \sum_{i=1}^{w} \alpha_i t_i = S_{\alpha_{1(k-1)}} - (\alpha_1 + \alpha_2 + ... + \alpha_{w-1})\Delta t_1$$
$$+\alpha_w(\Delta t_2 + \Delta t_3 + ... + \Delta t_w) \tag{3.24}$$

$$S_{\alpha_{2k}} = \sum_{i=1}^{w} \alpha_i t_i^2 = S_{\alpha_{2(k-1)}} - (\alpha_1 + \alpha_2 + ... + \alpha_{w-1})\Delta t_1^2$$
$$+\alpha_w(\Delta t_2 + \Delta t_3 + ... + \Delta t_w)^2$$
$$-2\Delta t_1(S_{\alpha_{1k}} - \alpha_w(\Delta t_2 + \Delta t_3 + ... + \Delta t_w)) \tag{3.25}$$

Presenting equations (3.18) - (3.20) in matrix form yields

$$Ac = b \tag{3.26}$$

where
$A = \begin{pmatrix} a_{11} & a_{12} & a_{13} \\ a_{21} & a_{22} & a_{23} \\ a_{31} & a_{32} & a_{33} \end{pmatrix}$, $c^T = (c_0, c_1, c_2)$, $b^T = (b_1, b_2, b_3)$. where

$$a_{11} = w, \quad a_{12} = S_{1k}, \quad a_{13} = S_{2k}$$
$$a_{21} = S_{1k}, \quad a_{22} = S_{2k}, \quad a_{23} = S_{3k}$$
$$a_{31} = S_{2k}, \quad a_{32} = S_{3k}, \quad a_{33} = S_{4k}$$
$$b_1 = S_{\alpha k}, \quad b_2 = S_{\alpha 1k}, \quad b_3 = S_{\alpha 2k}$$

Notice that, $a_{12} = a_{21}$ and $a_{22} = a_{31} = a_{13}$, $a_{23} = a_{32}$.

In order to find spline coefficients c_i, $i = 0, 1, 2$ the matrix equation (3.26) should be solved with respect to c_i at every step ($c = A^{-1}b$). To this end matrix A is inverted analytically.

Remark 1. This algorithm has only one parameter to be optimized, this being the size of the moving window w. If the derivative of the measured signal changes slowly it is advisable to have a relatively large window size to filter out measurement noise. If the derivative changes quickly, the window size should be sufficiently small to capture corresponding fast changes in the derivative. The disadvantage of a small window size is the noise in the estimated signal. Ideally, the window size should be adjustable so that it is small enough during transients to capture fast changes in the derivative of the signal, and large enough under steady-state conditions to filter out measurement and space-discretization noise.

Remark 2. For a constant discretization step the sums S_m do not change with time, matrix A is constant and computational burden is minimal.

Remark 3. The recursive computations presented above accumulate an approximation error, which increases with time. To avoid this error accumulation problem, repeatable initialization of the algorithms is required.

3.3.2 Combination of High Gain Observer and Spline Interpolation Method and Their Comparative Analysis

In papers [14], [18] it is mentioned that the spline interpolation method can be combined with high-gain observers. The combined scheme shows improved transient behavior. In this Section the comparative analysis of the spline interpolation method and combined method is presented.

The signal is estimated via the second order polynomial described above

$$\hat{\alpha}(t) = c_0 + c_1 t + c_2 t^2 \tag{3.27}$$

where $\hat{\alpha}(t)$ is the estimate of the signal α.

A combination of the spline interpolation algorithm with a simple high gain observer is presented as follows

$$y(t) = \frac{1}{\tau}\alpha + y_1(t) \tag{3.28}$$

$$\dot{y}_1(t) = -\frac{1}{\tau}y(t) + \hat{\ddot{\alpha}}, \qquad y_1(t_0) = \hat{\dot{\alpha}}(t_0) - \frac{1}{\tau}\alpha(t_0) \tag{3.29}$$

where $y(t)$ is the estimate of the $\dot{\alpha}$, $\tau > 0$ is the algorithm parameter, $\hat{\dot{\alpha}}(t_0)$ is the estimate of the derivative from spline interpolation method evaluated at time t_0, $\hat{\ddot{\alpha}}$ is spline estimate of the second derivative. The condition $y_1(t_0) = \hat{\dot{\alpha}}(t_0) - \frac{1}{\tau}\alpha(t_0)$ corresponds to the following initial value assignment $y(t_0) = \hat{\dot{\alpha}}(t_0)$. This means that high gain observer (3.28), (3.29) is initialized to the

spline estimate. Moreover, the second order derivative $\hat{\ddot{\alpha}}$ is used directly as an input to the high gain observer. Notice that, $\hat{\dot{\alpha}}(t_0) = c_1 + 2c_2t_0$ and $\hat{\ddot{\alpha}} = 2c_2$.

Remark 4. Equations (3.28) and (3.29) represent the following estimator of the derivative

$$y(p) = \frac{p}{\tau p + 1}\alpha(p) \tag{3.30}$$

if $\hat{\ddot{\alpha}} = 0$, where $p = jw$ is a Laplace variable. Estimates from the spline interpolation method are used as a feedforward part in the estimator (3.30).

Assuming a spline approximation error, then this error is expressed in terms of the error in spline coefficients and the true signal can be expressed as follows

$$\alpha(t) = c_{0*} + c_{1*}t + c_{2*}t^2 \tag{3.31}$$

where $\alpha(t)$ is the signal, c_{i*}, $i = 0, 1, 2$ are true coefficients.

Assuming a constant error in the coefficients w.r.t. time one gets

$$c_i = c_{i*} + \Delta c_i \tag{3.32}$$

where Δc_i, $i = 0, 1, 2$ are constant errors in spline coefficients.

Our task is to compare the following estimation errors

$$e_1(t_1) = \hat{\dot{\alpha}}(t_1) - \dot{\alpha}(t_1) \tag{3.33}$$

$$e_2(t_1) = y(t_1) - \dot{\alpha}(t_1) \tag{3.34}$$

where t_1 is a fixed time.

First we evaluate $e_1(t_1)$

$$e_1(t_1) = \Delta c_1 + 2\Delta c_2 t_1 \tag{3.35}$$

The next step is to evaluate $e_2(t_1)$. Differentiating (3.28) and taking into account that $\hat{\ddot{\alpha}} = \ddot{\alpha} + 2\Delta c_2$ one gets

$$\dot{y} - \ddot{\alpha} = -\frac{1}{\tau}(y - \dot{\alpha}) + 2\Delta c_2 \tag{3.36}$$

The solution of (3.36) is the following

$$y(t) - \dot{\alpha}(t) = (y(t_0) - \dot{\alpha}(t_0) - 2\Delta c_2\tau)e^{-\frac{t - t_0}{\tau}} + 2\Delta c_2\tau \tag{3.37}$$

Initialization of high gain observer gives the following: $y(t_0) = \hat{\dot{\alpha}}(t_0)$. Taking into account that $\hat{\dot{\alpha}}(t_0) - \dot{\alpha}(t_0) = \Delta c_1 + 2\Delta c_2 t_0$ one obtains

$$y(t) - \dot{\alpha}(t) = (\Delta c_1 + 2\Delta c_2 t_0 - 2\Delta c_2\tau)e^{-\frac{t - t_0}{\tau}} + 2\Delta c_2\tau \tag{3.38}$$

Evaluating $e_2(t_1)$ yields:

$$e_2(t_1) = (\Delta c_1 + 2\Delta c_2 t_0 - 2\Delta c_2 \tau) e^{-\frac{t_1 - t_0}{\tau}} + 2\Delta c_2 \tau \tag{3.39}$$

Comparing (3.39) and (3.35), it can be seen that $|e_2(t_1)|$ can always be made smaller than $|e_1(t_1)|$ by reducing the design parameter τ. However, in the presence of noise the reduction of τ leads to a deterioration of the signal quality. The advantages of this combined scheme can be shown if the parameter τ can be reduced to a sufficiently small value without any signal quality deterioration.

As the simulation results did not show any significant superiority of the combined method over the spline interpolation method and the latter is chosen for implementation.

3.4 Implementation Results: Crankshaft Acceleration Estimation

In this Section the implementation results are presented for a second order spline fitting method, as described in Section 3.1. A Volvo S80 passenger car equipped with a crankshaft angle sensor is used for experiments. The method described in Section 3.1 is used to estimate the crankshaft acceleration,which gives vital information about the quality of the combustion in the engine, from the crankshaft angle measurements.

The car is equipped with a special Engine Control Unit, which is called Volvo Rapid Prototyping System. This system consists of the PM (Power Module) and the AM (Application Module) connected together via a 1 Mbit/s CAN channel.

The PM provides information based on a number of engine sensor signals. The crankshaft wheel has 58 teeth spaced every 6 degrees and a gap corresponding to two " missing teeth ". Engine speed and cylinder position can be calculated from the resulting crankshaft sensor signal. The PM calculates the engine speed based on the measured time between the tooth events via the backward difference method. This engine speed is transmitted along with other measurements every 4th millisecond to the AM.

The 4 millisecond sampled crankshaft angle calculated from the tooth number signal is the input to the crankshaft acceleration estimation, which runs in the AM. The accuracy of the estimation is verified by comparing the engine speed, calculated by the spline interpolation method, with the engine speed calculated in the PM.

Implementation results are presented in Figure 3.1-Figure 3.3. Figure 3.1 and Figure 3.2 show engine speeds and Figure 3.3 crankshaft acceleration as a function of time. Figure 3.1 and Figure 3.2 illustrate verification process for spline interpolation method with the window size $w = 60$. The accuracy of the estimation is verified by comparing fast engine speed measured in the PM module (dotted line) and engine speed calculated via spline interpolation

method (solid line). Crankshaft acceleration which corresponds to the engine speeds plotted in Figure 3.2 is presented in Figure 3.3

Figure 3.1 shows that the spline interpolation method provides smoother engine speed than the speed computed in the PM. However, minor deviations between solid and dotted lines are present for the cases where the engine speed changes rapidly.This problem, caused by a relatively large window size, can be solved by introduction of the adjustable window size w (see Remark 1). Notice that the high frequency oscillations in the PM signal correspond to the combustion events of the engine and spline interpolation method with the large window size filters out the high frequency component of the signal. In the combustion state monitoring functions, however, the high frequency component of the engine speed signal is widely used, and therefore the window size w should be reduced when using spline interpolation method. In the next example the application of the spline interpolation method for the combustion state monitoring, namely misfire detection, is discussed.

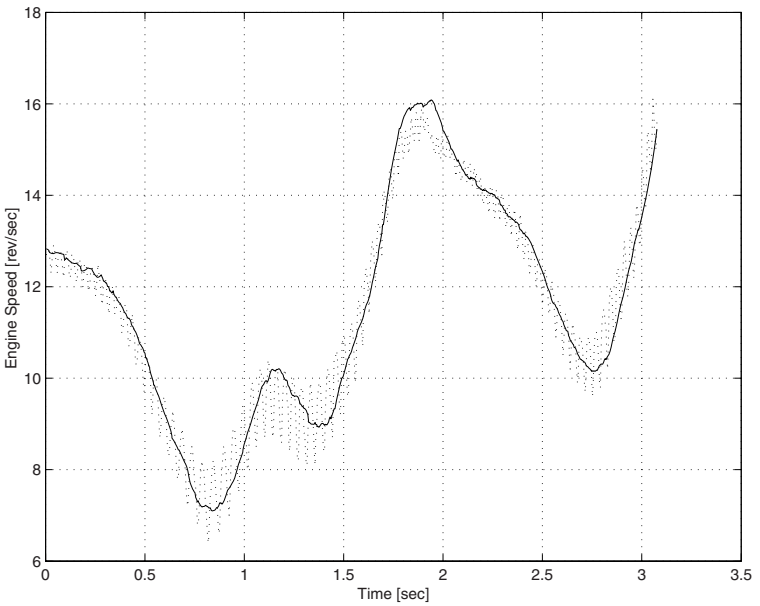

FIG 3.1. Experimental results. The comparison of two engine speeds as functions of time. Engine speed computed in PM is plotted with dotted line. Engine speed calculated with spline interpolation method is plotted with solid line.

Figure 5 shows an application of the proposed recursive spline interpolation method to the misfire diagnostics. In this Figure two engine cycles of a 5 cylinder engine are shown, and the misfire is generated on the second cycle of cylinder N 4. The tooth number signal is plotted with a dashdot line.

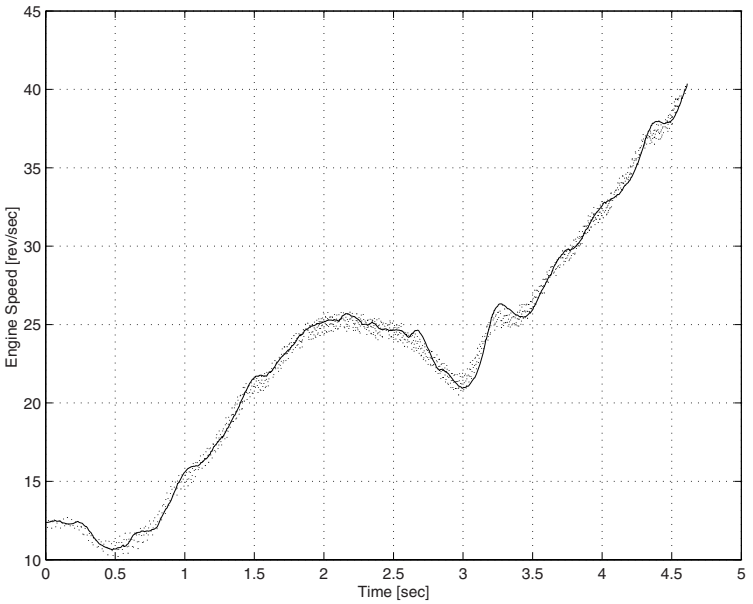

FIG 3.2. Experimental results. The comparison of two engine speeds as functions of time. Engine speed computed in PM is plotted with dotted line. Engine speed calculated with spline interpolation method is plotted with solid line.

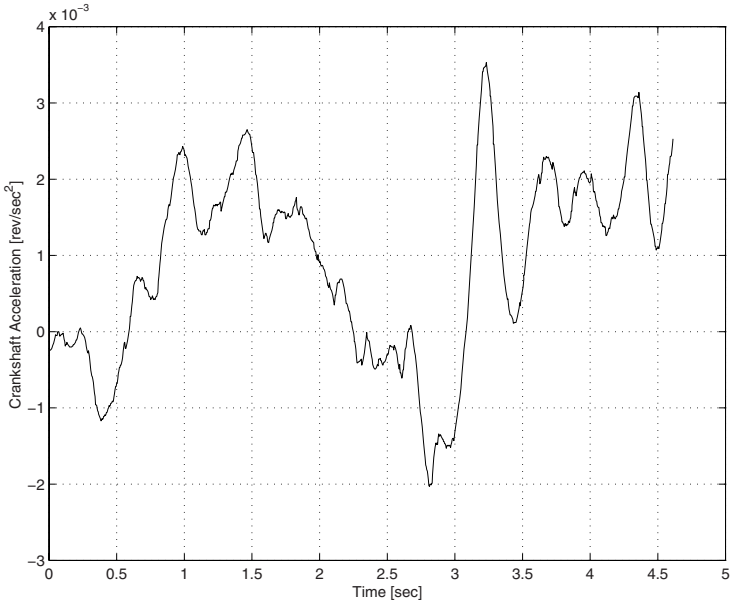

FIG 3.3. Experimental results. Engine crankshaft acceleration as a function of time. Crankshaft acceleration is computed with spline interpolation method.

Crankshaft acceleration estimated by the spline interpolation method is plotted with a solid line. In the event of a misfire, the crankshaft acceleration changes dramatically, which permits the cylinder individual misfire detection.

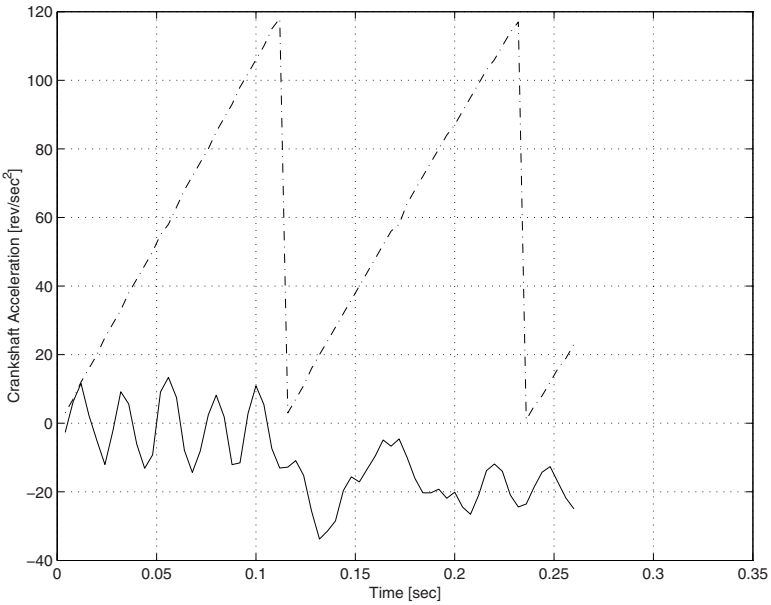

FIG 3.4. Experimental results. Two engine cycles of a five cylinder engine. The misfire is generated on the second cycle in the fourth cylinder. Tooth number signal is plotted with dashdot line. Crankshaft acceleration estimated by the spline interpolation method is plotted as a function of time with a solid line.

It is worth remarking that in production systems the time which is required to rotate 36 degrees on a crankshaft for 5 cylinder engines is available in the Electronic Control Unit. Discretization step w.r.t. crank angle is constant in this case while the time between the samples varies. In this case one could fit the following polynomial in the least squares sense to the measured data $\hat{t} = c_0 + c_1\alpha + c_2\alpha^2$, where $\hat{t}$ is the time estimate and α is the crank angle. This approach has reduced computational burden since the polynomial fitting is done with constant discretization step w.r.t. α (see Remark 2). Then $\dot{\alpha}$ is calculated as $\dot{\alpha} = \dfrac{1}{c_1 + 2c_2\alpha}$. It has a singular point $c_1 + 2c_2\alpha = 0$. The estimate of the derivative is not robust if $c_1 + 2c_2\alpha$ is close to zero. Moreover, the estimate of the derivative in this approach depends on the crank angle α, while the estimate of the derivative of the method described in Section 3.1 depends on the time t. The dependence of the derivative estimate on the crank angle makes the approach too sensitive to the missing teeth and, in turn, makes the approach difficult for implementation.

Further development of the crankshaft acceleration estimation method is possible if the time between the tooth events is available in the AM. The required discretization step w.r.t. the crankshaft angle is 6 degrees, or, in case of the missing teeth,18 degrees. This application requires higher computational power but in return, it gives the best estimation of the crankshaft speed and acceleration achievable by the spline interpolation method. The compromise is 36 degrees discretization step for 5 cylinders engine.

The crankshaft acceleration is widely used in many engine control and diagnostic functions such as crankshaft torque estimation, which is based on crankshaft acceleration. Crankshaft acceleration is used also in misfire diagnostics functions, for misfire detection and also in many combustion quality monitoring functions. The estimation accuracy of crankshaft acceleration improved by the spline interpolation method, in turn, improves the performance of these functions as well.

The method can also be used to estimate other signals and their derivatives. It has the greatest potential in diagnostics, when post processing of the signal is allowed and the derivatives of the signal can be taken in the middle of the moving window. That essentially improves the estimation accuracy and hence the performance of the on-board diagnostic functions.

3.5 Conclusion

Computationally efficient algorithms for spline interpolation method allowing a reduction in computational burden as well as the implementation of the spline interpolation method are presented. A further challenge is to improve the performance of these algorithms by adjusting the size of the moving window.

4

Engine Torque Estimation

Two new computationally efficient filtering algorithms for the reconstruction of the first harmonic of a periodic signal are presented. The first algorithm is based on the trigonometric interpolation method and the second one is based on the Kaczmarz projection method. The algorithms allow the recovery of the combustion quality information from the engine speed measurements which are noise contaminated. The algorithms are verified by using eight and six cylinder spark ignition engines in the torque estimation problem.

4.1 Introduction

Engine torque estimation function is an important function for an engine torque model, misfire diagnostics and dependability. The engine torque estimation function is based on monitoring of the cylinder individual fluctuations of the high resolution engine speed signal (see references [23],[71], [73]). The engine speed signal is based on the measurements of a passage time between two subsequent teeth on a crankwheel. The passage time decreases as the rotational speed increases thus the time interval errors increase. Moreover, low frequency oscillations from the powertrain and high frequency oscillations due to the crankshaft torsion, together with vibrations induced by the road, act as disturbances on the crankshaft [39]. These disturbances influence directly the performance of the engine speed signal and consequently the torque monitoring function. The problem described above is more important for six and eight cylinder engines than for five cylinder engines. This is due to a larger amount of combustion events which should be recognized in the presence of described disturbances.

A number of disturbance identification/rejection techniques, which is used in the misfire detection and torque estimation functions, is known in the literature.

A disturbance identification and compensation techniques for the misfire diagnostic function were proposed in [70] and [72]. The engine behaviour is

A.A. Stotsky, *Automotive Engines*, DOI 10.1007/978-3-642-00164-2_4,

learned during the fuel cut-off state and compensated when the engine is fueled. However, the changes in the engine speed due to the unpredictable stochastic external interference or even misfire may occur in the fuel cut-off state. If a misfire was learned during the learning process, then it would be compensated in the engine fueled behaviour and therefore would lead to the deterioration of the learning accuracy. Moreover, these compensation schemes do not cancel the crankshaft vibrations when the engine is fueled and require significant calibration efforts for different vehicle operating conditions.
A number of torque estimation techniques known in the literature (see for example, [72], [116], etc.) recognizes the crankshaft as a flexible body. Model inversion techniques (input observers) are employed for estimation of system inputs (torques acting on each crank throw) via system outputs (angular response measurements). In multicylinder engines, where the number of the cylinders is larger than the number of the angular response measurement locations, the number of unknown system inputs is larger than the number of known outputs. Pseudoinverse techniques applied to the case, do not give accurate solution for the cylinder individual torques. A number of misfire detection approaches known in the literature analyzes the engine firing frequency through Discrete Fourier Transform (DFT) (see for example, [23], [72], [73] and [116], etc.). The Fourier Series coefficients which represent continuous time integral functions, are approximated via discrete sums, provided that the sampling interval is properly chosen. Many misfire diagnostic functions utilize a low rate sampling of the engine crankshaft speed. Typically, the crankshaft speed is sampled once per cylinder firing event. At such a low rate sampling, the error between continuous time Fourier coefficients and their discrete time approximations could be sufficiently large. Moreover, high order harmonic components of the engine firing frequency, which often contain valuable misfire (combustion quality) information for higher engine speeds, are frequently folded back or aliased within the range of lower noise-related engine frequencies. These aliased signals may cause misinterpretation of the cylinder firing event data. In addition, the DFT approach is typically considered to be computationally complex in industry and therefore is not feasible for the on-board real-time estimation.

The engine speed can be approximated by a trigonometric polynomial due to the periodic nature of both engine rotational dynamics and combustion forces as functions of a crank angle. The first filtering technique proposed in this Chapter (see also [86]) uses the periodic signal at the combustion frequency and the amplitudes of the trigonometric functions are updated recursively according to the trigonometric interpolation method in the moving window of a certain size. The update law in the trigonometric interpolation method has a relatively simple form due to the orthogonality of the trigonometric polynomials on certain intervals. The orthogonality condition imposes the restrictions on the window size and limits the performance of the algorithm (too large window size implies relatively large estimation errors during the engine speed transients). The second approach proposed in this Chapter

is also based on the approximation of the engine speed via a trigonometric polynomial with known frequencies and unknown amplitudes. However, the estimated amplitudes are updated according to the Kaczmarz projection method, where the model matches the measured signal exactly at every discrete step. The convergence of the estimated parameters to their true values is ensured due to the richness (persistency of excitation) of the measured engine speed signal which is approximated by the trigonometric polynomial. This in turn implies faster convergence of the estimated parameters to their true values and better performance of the algorithm proposed in the this Chapter with respect to the trigonometric interpolation method [86]. The signal is completely reconstructed by the trigonometric polynomial and the filter uses a periodic signal at the firing frequency. The values of the trigonometric functions are computed recursively by using Chebyshev's three term recurrence relations for the trigonometric functions making the algorithm computationally efficient and implementable.

Notice, that the band-pass filter can also be used for filtering of the engine speed. Ideally, band-pass filter should reject all the frequencies outside the selected frequency (combustion frequency). In practice, the frequencies that are close to the selected one are attenuated, but not completely rejected. This deteriorates the performance of the filtering. The filtering approach proposed in this Chapter uses trigonometric functions with the combustion frequency in the explicit form that provides rejection of all the frequencies excepting the combustion one.

Volvo passenger cars equipped with eight and six cylinder prototype engines ware used in the experiments. Algorithms are implemented in Matlab[1] and applied to the measured data collected from the experimental vehicle.

4.2 Problem Statement

As a rule, a passage time between two teeth on a crankwheel is measured in production engines. The high resolution engine speed signal is then calculated as a ratio of the length of the angular segment on the crankwheel and the passage time for this segment.

The combustion state of the given cylinder is defined via the amplitude. The amplitude for the cylinder, whose power stroke occurs in the interval, in turn is defined as the difference between maximal and minimal values of the high resolution engine speed signal. The corresponding amplitude, which is the measure of the crankwheel speed perturbations induced by the periodic impulsive cylinder individual torque contributions, provides a method for estimation of the engine torque [41]. Here and below, a non-standard definition is used, and under the term 'amplitude' the difference between maximal and minimal values is understood.

[1] Matlab is a registered mark of the Mathworks, Inc of Natick, MA

Figure 4.1 shows the harmonics of the engine speed signal of a eight cylinder engine at 1800 rpm and 5400 rpm calculated by the Discrete Fourier Transform (DFT) method [58]. The input sequence was sampled with the step 30 CA (Crank Angle) degrees and the data was acquired over a 720 CA degree window. Amplitudes are plotted as a function of a harmonic number of a periodic signal with the period of 720 CA degrees. The harmonic number is defined as an integer which is equal to the ratio of two periods, $n_h = \frac{720^o}{T_h}$, where T_h is the period of the harmonic. Figure 4.1 shows that the engine speed signal at low rotational speeds has a dominant component which corresponds to the combustions events. The engine speed signal at high rotational speeds has fluctuations which occur as a consequence of the combustion process, low frequency oscillations from the powertrain as well as high frequency oscillations due to the crankshaft torsion. The high frequency oscillations due to the crankshaft twist and low frequency oscillations from the powertrain could be greater than the oscillations induced by the combustion events. Notice that, the input sequence was sampled with the step 30^o which is a relatively low rate sampling. At this rate the high order harmonic components could be aliased within the range of a lower frequency. Thus, the higher amplitudes at the lower harmonics ($n_h < 8$) showed in Figure 4.1, could be the superposition of low frequency torsional oscillations and the aliased high frequency oscillations.

Figure 4.2 shows the harmonics of the engine speed signal of a six cylinder engine at 1200 rpm and 5000 rpm calculated by the Discrete Fourier Transform (DFT) method. The engine speed was measured with 365C Angle Encoder which is a high precision optical sensor for angle related measurements. The angle mark resolution is 0.5 CA (Crank Angle) degrees. The data was acquired over a 720 CA degree window. Figure 4.2 shows that the engine speed signal at low rotational speeds has a dominating component which corresponds to the combustions events. The engine speed signal at high rotational speeds has fluctuations which occur as a consequence of the combustion events, low frequency oscillations from the powertrain as well as high frequency oscillations due to the crankshaft torsion. The high frequency oscillations due to the crankshaft twist and low frequency oscillations from the powertrain could be greater than the oscillations induced by the combustion events.

4.3 Recursive Trigonometric Interpolation Method

4.3.1 General Description

Suppose that there is a set of the Crank Angle synchronized data y_l, $l = 1, ..., w$ measured at the following points:

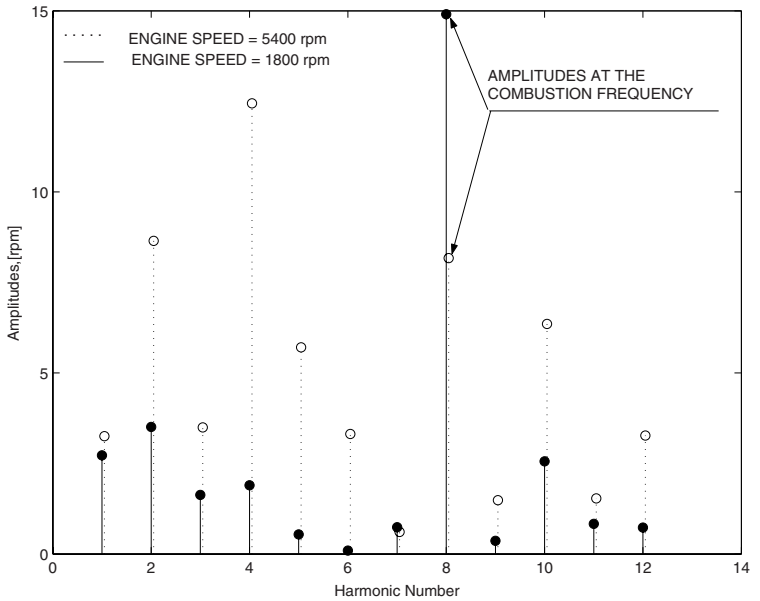

FIG 4.1. Harmonic contents of the engine speed signal at 1800 rpm and 5400 rpm computed via the DFT method. The input sequence is sampled with the step 30^o. The data is acquired over 720^o window. The measurements are made on the experimental vehicle on the chassis rolls. Amplitudes are plotted as a function of the harmonic number of the signal with the period of 720 CA degrees. The engine is operating at 50% load. Amplitudes at 1800 rpm are plotted with solid line and amplitudes at 5400 rpm are plotted with the dotted line.

$$x_1 = \Delta, \qquad x_2 = 2\Delta, \qquad .... \qquad x_w = w\Delta, \qquad \Delta = \frac{360^0}{w} \tag{4.1}$$

where Δ is the gear tooth angle. The high resolution engine speed signal is sampled on the basis of a Crank Angle (CA) at intervals Δ, namely,

$$\Delta = \frac{L_c}{n_p N} \tag{4.2}$$

where N is the number of the cylinders of the engine, n_p is the number of points measured for each combustion event ($n_p \geq 3$), L_c is the length of the engine cycle in CA degrees (as a rule, $L_c = 720^o$). Since an engine crankshaft is usually provided with 58 teeth and a gap corresponding to two missing teeth, the step Δ should be a multiple of 6^o. Notice that, according to the Shannon theorem, two points per each combustion event are required to recognize the signal of the combustion frequency. However, the phase of the signal changes due to the cycle-to-cycle variations, oscillations due to the crankshaft torsion and some other factors. In addition, in order to recognize

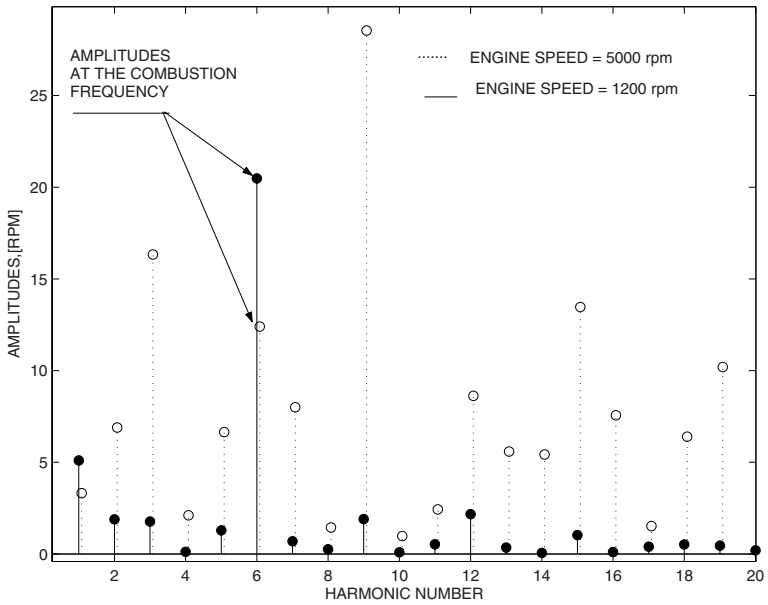

FIG 4.2. Harmonic contents of the engine speed signal at 1200 rpm and 5000 rpm computed via the DFT method. The input sequence is sampled with the step of 0.5^o. The data is acquired over 720^o window. The measurements are made on the experimental vehicle on the chassis rolls. Amplitudes are plotted as a function of the harmonic number of the signal with the period of 720 CA degrees. The engine is operating at full load. Amplitudes at 1200 rpm are plotted with solid line and amplitudes at 5000 rpm are plotted with the dotted line.

the high frequency disturbances acting on the crankshaft, it is necessary to measure more points per each combustion event.

Assume that the number of measurements w is greater than or equal to $(2n+1)$, where n is the number of the frequencies of the signal. Then there exists the trigonometric polynomial in the following form:

$$T_n(x) = a_0 + \sum_{q=1}^{n} (a_q cos(qx) + b_q sin(qx)), \tag{4.3}$$

which gives the best approximation of the measured data y_l at the points x_l in the least-squares sense. Notice, that the frequencies $q = 1, 2, ..., n$ defined in (4.3) should include the combustion frequency, as well as low powertrain frequencies and high frequencies due to the crankshaft torsion.

Measured data should be approximated by polynomial (4.3) in the least squares sense. The error to be minimized at every step is as follows:

$$E = \sum_{l=1}^{w}(y_l - (a_0 + \sum_{q=1}^{n}(a_q cos(qx_l) + b_q sin(qx_l))))^2. \quad (4.4)$$

Straightforward calculations show that the coefficients which minimize (4.4) are the following:

$$a_0 = \frac{1}{w}\sum_{l=1}^{w} y_l \quad (4.5)$$

$$a_q = \frac{2}{w}\sum_{l=1}^{w} y_l cos(qx_l) \quad (4.6)$$

$$b_q = \frac{2}{w}\sum_{l=1}^{w} y_l sin(qx_l) \quad (4.7)$$

The proof is given in Appendix A.

The expressions (4.3), (4.5) - (4.7) are known as the DFT method [38], [58]. The coefficients (4.5), (4.6), (4.7) of the DFT have such a simple form due to the property of the orthogonality of the trigonometric polynomials at the interval $[0 \div 360^o)$. It is interesting to note that the trigonometric polynomial can be fitted to the measured data at any interval (see Section 7.2). However, for computation of the coefficients a_0, a_q, b_q the matrix inversion is required, as it is usual for the least-squares fitting. Therefore the DFT method can be seen as a special case of the trigonometric interpolation method.

One of the main results of this Chapter is formulated below.

4.3.2 Computationally Efficient Filtering Algorithms

The amount of computation, when computing (4.5) - (4.7) can be reduced by the introduction of the local fixed coordinates, i.e. moving window of a size w. The same idea was proposed in the spline interpolation method described in [18] and is based on the on-line least-squares polynomial fitting over the window moving in time. The idea of the window moving in time is illustrated in Figure 4.3. The window is defined in the form of the local coordinates X_L, Y_L. Then, the least squares curve fitting problem is solved in local coordinates and the result is transformed into an original coordinate system. Moreover, at every step the coefficients (4.5) - (4.7) can be computed recursively using the information from the previous step. This makes the whole scheme computationally efficient and implementable.

Consider one step of the window moving in time. Assume that there is a set of measurements at step $(k-1)$, $\{y(1), y(2), y(3), ..., y(w)\}$, which is measured in the following local coordinate system based on the crank angle $\{0, \Delta, 2\Delta, ..., (w-1)\Delta\}$, where Δ is defined by (4.2).
At step k, new value $y(w+1)$ enters the window while $y(1)$ leaves the window. Whence, at step k there is a set of measurements $\{ y(2), y(3), y(4), ...,$

$y(w+1)\}$, measured in the same local coordinate system. One step of the moving window is shown in Figure 4.3, where the engine speed is measured for the $V8$ engine with the step $\Delta = 30^o$.

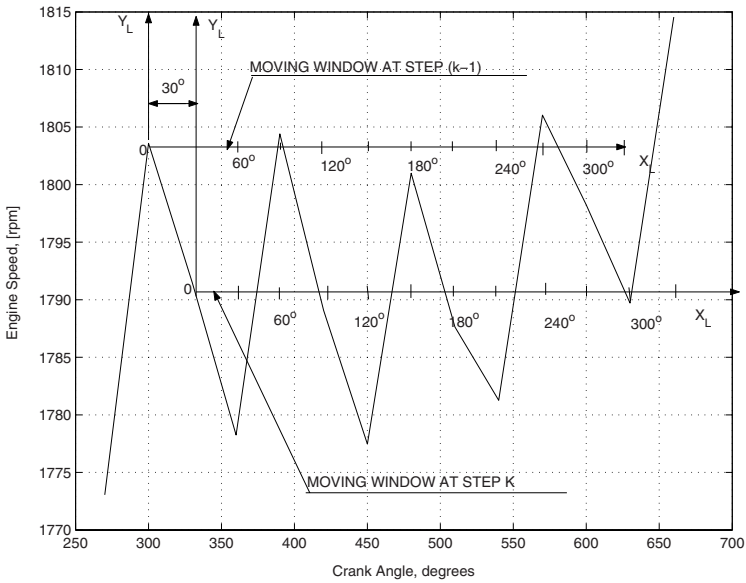

FIG 4.3. Measurements with the step 30 CA degrees on the V8 engine. The engine speed is plotted with the solid line. The engine is operating at full load. A window of the size $w = 12$ moving in time is defined in the form of local coordinates X_L, Y_L.

The coefficients (4.5) - (4.7) at step $(k-1)$ are defined as follows :

$$a_{0(k-1)} = \frac{1}{w}\sum_{i=1}^{w} y(i) \tag{4.8}$$

$$a_{q(k-1)} = \frac{2}{w}\sum_{i=1}^{w} y(i)cos((i-1)q\Delta) \tag{4.9}$$

$$b_{q(k-1)} = \frac{2}{w}\sum_{i=1}^{w} y(i)sin((i-1)q\Delta) \tag{4.10}$$

where q denotes the frequency. The coefficients (4.8) - (4.10) at step k are defined as follows:

$$a_{0k} = \frac{1}{w}\sum_{i=2}^{w+1} y(i) \tag{4.11}$$

$$a_{qk} = \frac{2}{w}\sum_{i=2}^{w+1} y(i)cos((i-2)q\Delta) \tag{4.12}$$

$$b_{qk} = \frac{2}{w}\sum_{i=2}^{w+1} y(i)sin((i-2)q\Delta) \tag{4.13}$$

The coefficients (4.11) - (4.13) are to be expressed via the coefficients (4.8) - (4.10).

Straightforward calculations give the expression for the first coefficient,

$$a_{0k} = a_{0(k-1)} + c_{q(k-1)}, \tag{4.14}$$

where $c_{q(k-1)} = \frac{1}{w}(y(w+1) - y(1))$, simply meaning that the value $y(w+1)$ enters the window, while the value $y(1)$ leaves the window.

Starting with a_{qk}, one gets,

$$\begin{aligned} a_{qk} &= \frac{2}{w}\sum_{i=2}^{w+1} y(i)cos((i-2)q\Delta) = \frac{2}{w}y(w+1)cos((w-1)q\Delta) \\ &+ \frac{2}{w}\sum_{i=2}^{w} y(i)cos((i-1)q\Delta - q\Delta) = \\ &\frac{2}{w}y(w+1)cos((w-1)q\Delta) + cos(q\Delta)(a_{q(k-1)} - \frac{2}{w}y(1)) \\ &+ sin(q\Delta)b_{q(k-1)} \\ &= b_{q(k-1)}sin(q\Delta) + d_{q(k-1)}cos(q\Delta) \end{aligned} \tag{4.15}$$

and

$$\begin{aligned} b_{qk} &= \frac{2}{w}\sum_{i=2}^{w+1} y(i)sin((i-2)q\Delta) = \frac{2}{w}y(w+1)sin((w-1)q\Delta) \\ &+ \frac{2}{w}\sum_{i=2}^{w} y(i)sin((i-1)q\Delta - q\Delta) = \\ &\frac{2}{w}y(w+1)sin((w-1)q\Delta) \\ &+ cos(q\Delta)(b_{q(k-1)} - \frac{2}{w}y(2)sin(q\Delta)) \\ &- sin(q\Delta)(a_{q(k-1)} - \frac{2}{w}(y(1) + y(2)cos(q\Delta)) \\ &= -d_{q(k-1)}sin(q\Delta) + b_{q(k-1)}cos(q\Delta) \end{aligned} \tag{4.16}$$

where $d_{q(k-1)} = a_{q(k-1)} + 2c_{q(k-1)}$. Notice that (4.15), (4.16) can be expressed in a single matrix equation

$$s_{qk} = A_{qk} z_q \tag{4.17}$$

where $s_{qk} = (a_{qk} \quad b_{qk})^T$,
$A_{qk} = \begin{pmatrix} b_{q(k-1)} & d_{q(k-1)} \\ -d_{q(k-1)} & a_{q(k-1)} \end{pmatrix}$
is a skew symmetric matrix and $z_q = (sin(q\Delta)cos(q\Delta))^T$ is a constant vector. Implementation of the algorithms (4.14) - (4.16) requires 5 multiplications and 7 additions only at a single frequency. The algorithms are suitable for implementation on a simple controller that has a multiply and add processor.

The number of the multiplications for the DFT computation is proportional to the number of the samples of the input sequence (the size of the moving window w) at a single frequency. The coefficients a_{0k}, a_{qk} and b_{qk} of the scheme proposed here are computed via (4.8) - (4.10) at the first step. Hence the number of the arithmetical operations which is required for implementation of the algorithms proposed here and the DFT algorithms is the same at the first step. However, the number of the arithmetical operations for recursive algorithms (4.14),(4.15) and (4.16) does not depend on the window size w at the subsequent steps. Then the advantage of the method proposed here with respect to the DFT method increases with the window size w.

The algorithms proposed above can also be used in the case of the engine speed transients, provided that a "slowly" varying trend of the engine speed is properly compensated. A simple compensation technique is described below. The measured engine speed signal ω_k is filtered by the following low pass filter:

$$\omega_{fk} = \omega_{f(k-1)} - \frac{\Delta t}{\tau_f(\omega_k, \dot{\omega}_k)}(\omega_{f(k-1)} - \omega_k) \tag{4.18}$$

where ω_{fk} is a filtered engine speed and $\tau_f(\omega_k, \dot{\omega}_k)$ is a "time constant" of the filter (4.18), Δt [sek] is the discretization step. The time constant is realized as a look-up table with engine speed ω_k and its derivative $\dot{\omega}_k$, which is estimated by the first difference method as two inputs. The look-up table is calibrated so that the time constant is reduced under the transients to capture fast changes in engine speed, and is increased under the steady-state conditions. The following difference,

$$y_k = \omega_k - \omega_{fk} \tag{4.19}$$

between measured engine speed signal w_k and filtered signal ω_{fk} represents the fluctuations which occur as a consequence of the combustion events, contaminated with errors. If this difference is approximated by the trigonometric interpolation method, then the engine speed is approximated via the sum of two components. The first one is the filtered engine speed ω_{fk} which approximates "slowly" varying trend of the engine speed. The second one is the approximation the combustion events.

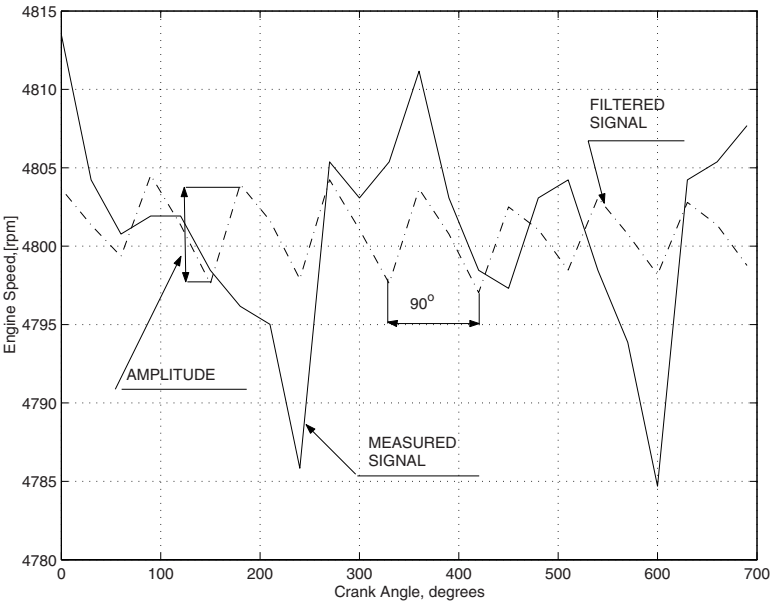

FIG 4.4. Measurements with the step 30 CA degrees on the V8 engine. A single engine cycle is plotted. The engine speed is plotted with the solid line. Relative load is 45%. Filtered signal corresponding to the firing frequency is plotted with dashdot line. The size of the moving window is equal to twelve ($w = 12$).

The variable y_k is approximated by $\hat{y}_k$ according to the following equation:

$$\hat{y}_k = a_{0k} + \sum_{q=1}^{n} (a_{qk} cos(q(w-1)\Delta) + b_{qk} sin(q(w-1)\Delta)) \tag{4.20}$$

where the coefficients are updated as follows:

$$a_{0k} = a_{0(k-1)} + c_{q(k-1)} \tag{4.21}$$
$$a_{qk} = b_{q(k-1)} sin(q\Delta) + d_{q(k-1)} cos(q\Delta) \tag{4.22}$$
$$b_{qk} = -d_{q(k-1)} sin(q\Delta) + b_{q(k-1)} cos(q\Delta) \tag{4.23}$$

where $d_{q(k-1)} = a_{q(k-1)} + 2c_{q(k-1)}$ and $c_{q(k-1)} = \frac{1}{w}(y(w+1) - y(1))$. The value of the interpolating polynomial $\hat{y}_k$ is taken at the end of the moving window $(w-1)\Delta$. Then the engine speed can be approximated as follows:

$$\hat{\omega}_k = \omega_{fk} + \hat{y}_k \tag{4.24}$$

where $\hat{y}_k$ is computed via (4.20) - (4.23).

Further in the Chapter, the trigonometric interpolation is used as a filter at the combustion frequency, i.e.,

$$\hat{y}_{ck} = a_{0k} + a_{q_c k} cos(q_c(w-1)\Delta) + b_{q_c k} sin(q_c(w-1)\Delta), \quad (4.25)$$

$$\hat{\omega}_{ck} = \omega_{fk} + \hat{y}_{ck} \quad (4.26)$$

where $q_c = \frac{N\pi}{360}$ is the combustion frequency, and N is the number of the engine cylinders. The combustion frequency is the frequency of the signal whose period is $\frac{720^o}{N}$. The coefficients a_{0k}, a_{qck}, b_{qck} are computed according to the recursive formulae (4.21) - (4.23).

Figure 4.4 shows the result of filtering. It can be seen that the fluctuations of the engine speed corresponding to the combustion events are recovered on the signal which is filtered by the filter (4.25), (4.26).

4.4 Filtering Technique Based on the Kaczmarz Projection Method

In Section 4.3 is shown that the measured signal ω_k can be approximated by the following trigonometric polynomial:

$$\hat{\omega}_k = a_{0k} + \sum_{q=1}^{n}(a_{qk}cos(qx_k) + b_{qk}sin(qx_k)), \tag{4.27}$$

where $q = 1, 2, ..., n$, $x_k = k\Delta$, $k = 1, 2, ...$ is updated in terms of the crank angle with the step (4.2). The equation (4.27) plays a role of a model, which has to match the measured data ω_k. Assume that the measured variable ω_k can be presented as follows:

$$\omega_k = a_{0*} + \sum_{q=1}^{n}(a_{q*}cos(qx_k) + b_{q*}sin(qx_k)), \tag{4.28}$$

where a_{0*}, a_{q*} b_{q*}, $q = 1, ..., n$ are constant unknown parameters. In other words, it is assumed that the measured signal ω_k can be approximated by the trigonometric polynomial with known frequencies and unknown amplitudes.

The equations (4.27) and (4.28) can be written in the following form:

$$\hat{\omega}_k = \varphi_k^T\theta_k, \tag{4.29}$$
$$\omega_k = \varphi_k^T\theta_*, \tag{4.30}$$

where θ_k is the vector of the adjustable parameters

$$\theta_k^T = [a_{0k} \quad a_{1k} \quad b_{1k} \quad a_{2k} \quad b_{2k}, ..., a_{nk} \quad b_{nk}], \tag{4.31}$$

θ_* is the vector of true parameters,

$$\theta_*^T = [a_{0*} \quad a_{1*} \quad b_{1*} \quad a_{2*} \quad b_{2*}, ..., a_{n*} \quad b_{n*}], \tag{4.32}$$

and

$$\varphi_k^T = [1 \quad cos(x_k) \quad sin(x_k) \quad cos(2x_k) \quad sin(2x_k), ..., cos(nx_k) \quad sin(nx_k)] \tag{4.33}$$

is the regressor. Notice, that the regressor φ includes n distinct frequencies and hence it is sufficiently rich for identification of $2n$ parameters of the signal (4.28).

Then, the estimation problem can be stated as follows: to find the update law θ_k, such that the following equality holds at every step

$$\omega_k = \hat{\omega}_k \tag{4.34}$$

and the vector of the adjustable parameters θ_k converges to the vector of true parameters θ_*. Then, the engine speed signal ω_k can fully be reconstructed by the polynomial (4.27). The components of the polynomial (4.27) which describe the combustion events can be used for the combustion state estimation.

Consider the following adjustment law

$$\theta_k = \theta_{k-1} + \frac{\varphi_k}{\varphi_k^T \varphi_k}(\omega_k - \theta_{k-1}^T \varphi_k) \tag{4.35}$$

By substituting (4.35) into the right hand side of the (4.29) it is easy to see that (4.34) is true. Notice, that $\varphi_k^T \varphi_k = n + 1$, where n is the number of frequencies involved and the adjustment law has a very simple form, namely,

$$\theta_k = \theta_{k-1} + \frac{\varphi_k}{(n+1)}(\omega_k - \theta_{k-1}^T \varphi_k) \tag{4.36}$$

Algorithm (4.36) guarantees the exact approximation of the measured data at every step, and the convergence of the parameters a_q, b_q, $q = 1, ..., n$ to their true values due to the sufficiently rich regressor φ which contains n distinct frequencies. Properties of the algorithm (4.36) are described in Appendix B.

Since the algorithm (4.36) guarantees exact approximation of the measured data at every step, the estimates obtained by using this algorithm might be noisy. It is necessary in this case to smooth the estimates by introducing the adjustable gain matrix. For example, by using the least squares gain update matrix Γ_k, the algorithm (4.36) can be modified as follows:

$$\theta_k = \theta_{k-1} + \frac{\Gamma_k \varphi_k}{(n+1)}(\omega_k - \theta_{k-1}^T \varphi_k) \tag{4.37}$$

$$\Gamma_k = \Gamma_{k-1} - \frac{\Gamma_{k-1}\varphi_k \varphi_k^T \Gamma_{k-1} - \lambda_0(\Gamma_k + \frac{\Gamma_k^T \Gamma_k}{k_0})}{1 + \varphi_k^T \Gamma_{k-1} \varphi_k}, \tag{4.38}$$

where $\Gamma(0) = \gamma I$, $\gamma > 0$, I is the unity matrix, λ_0, k_0 are the positive design parameters. Gain update (4.38) is a discrete-time analog of a continuous-time least-squares gain update (2.34).

Notice, that implementation of the algorithm (4.36) requires $3n$ multiplications and $2n$ additions, where n is the number of the frequencies. This number of arithmetical operations is larger than a number of operations which are required for implementation of the filtering DFT algorithm at a single frequency, described in [86]. Algorithm described in [86] has such a simple form due to the orthogonality condition, which in turn limits the approximation performance of the algorithm. The algorithm requires a computationally expensive matrix inversion as is usual for the least-squares fitting, if the orthogonality condition is violated [87].

The convergence of the estimated parameters to their true values and hence a reconstruction of the engine speed signal is ensured due to the condition of the persistency of excitation for the algorithm (4.36) (see Appendix B).

The condition of the persistency of excitation is valid since the engine speed is approximated using trigonometric polynomial. Engine speed can be approximated via a trigonometric polynomial due to the periodic nature of the engine rotational dynamics and combustion forces as functions of a crank angle. Therefore the algorithm (4.36) uses physical properties of the engine (such as periodicity of the rotational dynamics and combustion forces) for reconstruction of the frequency contents of the engine speed signal and hence does not require a computationally expensive matrix inversion [87].

Since the measured signal is completely reconstructed by the polynomial (4.27), the following filtered signal is used for the combustion state estimation:

$$\hat{\omega}_k = a_{0k} + a_{ck} cos(q_c x_k) + b_{ck} sin(q_c x_k) \tag{4.39}$$

where q_c is the combustion frequency, and a_{0k}, a_{ck}, b_{ck} are updated according to (4.36).

The trigonometric functions in the regressor (4.33) at step k are computed recursively by using the values of the regressor at step $k-1$. It is necessary to compute $sin(qk\Delta)$ and $cos(qk\Delta)$ which are the elements of the regressor φ_k at step k via the elements $sin(q(k-1)\Delta)$ and $cos(q(k-1)\Delta)$ of the regressor at the step $(k-1)$. First $sin(k\Delta)$ and $cos(k\Delta)$ $(q = 1)$ are computed via $sin((k-1)\Delta)$ and $cos((k-1)\Delta)$ and $cos(\Delta)$, $sin(\Delta)$. The remaining terms are computed via Chebyshev's three term recurrence relations (see Appendix B for details):

$$\begin{aligned} cos(qk\Delta) &= 2cos(k\Delta)cos((q-1)k\Delta) \\ &\quad - cos((q-2)k\Delta) \end{aligned} \tag{4.40}$$

$$\begin{aligned} sin(qk\Delta) &= 2cos(k\Delta)sin((q-1)k\Delta) \\ &\quad - sin((q-2)k\Delta) \end{aligned} \tag{4.41}$$

where $q = 2, ..., n$.

For computation of the elements of the regressor φ_k via algorithms (4.40), (4.41) 2 multiplications and 1 addition multiplied by $2(n-1)$ are required.

Figure 4.5 shows the result of the filtering. The engine speed signal is filtered by the filter (4.39). The engine is operating at 5000 rpm. It can be seen that the amplitude information is recovered on the signal which is filtered by the filter (4.39). Figure 4.6 shows the harmonics (calculated by the DFT method) of the original and filtered signals plotted in Figure 4.5. It can be seen that the amplitude corresponding to the combustion events becomes dominant after filtering.

At the end of the Section it is possible to make a comparative analysis of the Kacmarz approach to filtering of the engine speed data proposed above and the filtering approach based on the trigonometric interpolation method described in Section 4.3. The engine speed signal is approximated by the trigonometric polynomials with known frequencies and unknown amplitudes in both approaches. However, the estimated amplitudes are updated

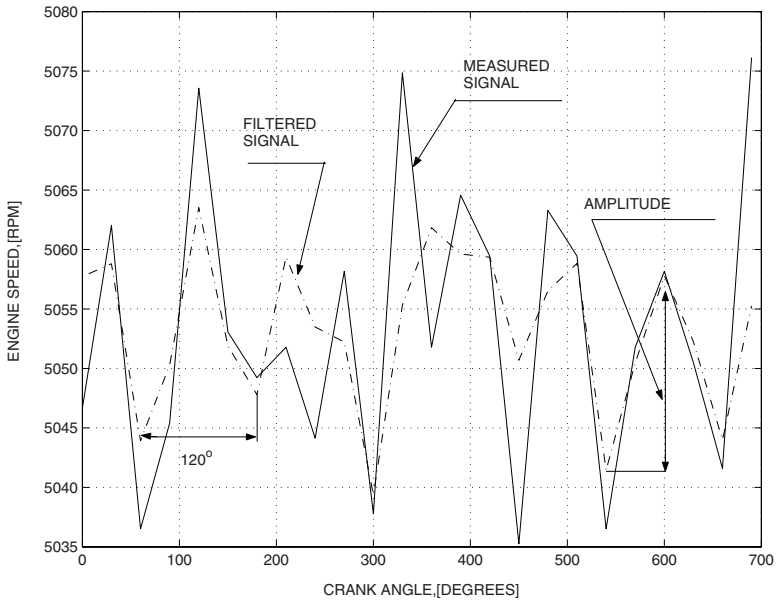

FIG 4.5. Measurements with the step of 30 CA degrees on the six cylinder prototype engine. A single engine cycle is plotted. The engine speed is plotted with the solid line. Relative load is 100%. Filtered signal corresponding to the firing frequency is plotted with dashdot line.

in different ways. In the trigonometric interpolation method the amplitudes are updated so that the error between the measured signal and its approximation is minimized in the least-squares sense in the moving window of a certain size. The amplitudes estimated by the Kacmarz approach are updated so that the model approximates the measured signal exactly at every discrete step. The trigonometric interpolation uses the orthogonality of the trigonometric polynomials to simplify the update law. The parameter convergence in the Kacmarz approach is ensured due to the richness (persistency of excitation) of the measured signal which is approximated by the trigonometric polynomial. In both approaches the estimated parameters converge to their true values, that in its turn, allows the complete reconstruction of the engine speed signal. The filters use the estimated amplitudes at the engine frequency in both cases. Main limitation of the trigonometric interpolation method is the restriction for the proper choice of the window size, which should satisfy the orthogonality equations. This limits the approximation performance of the trigonometric interpolation method. If the orthogonality condition is violated, then the implementation of the trigonometric interpolation method requires a matrix inversion, as it is usual for least-squares fitting, and this in turn, makes the method computationally expensive. Recursive and computationally efficient version of the trigonometric interpolation method is described in

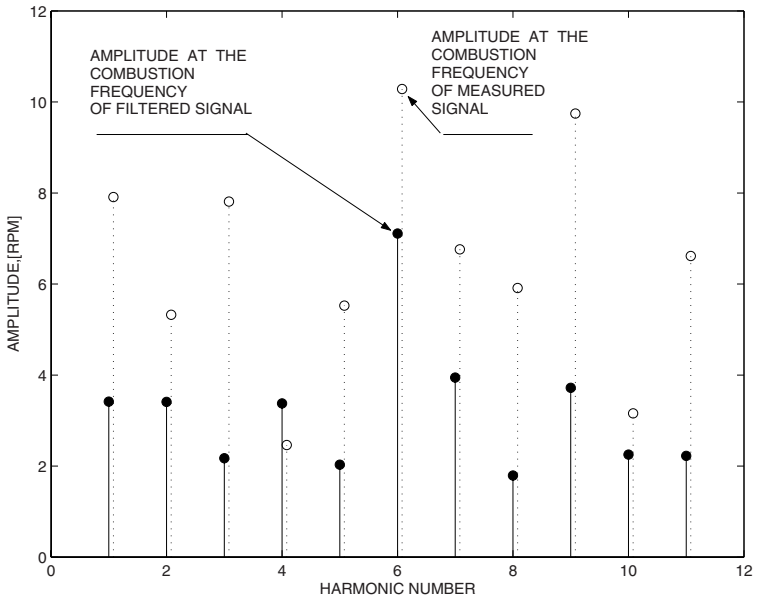

FIG 4.6. Harmonic contents of the engine speed signal at 5000 rpm computed via the DFT method. The input sequence is sampled with the step of 30^o. The data is acquired over 720^o window. Amplitudes are plotted as a function of the harmonic number of the signal with the period of 720 CA degrees. The engine is operating at 100% load. Amplitudes of the measured signal are plotted with the dotted line. Amplitudes of the signal filtered by the filter (4.39) are plotted with solid line.

Section 7.2 (see also [87]). The algorithms based on the Kacmarz approach are very simple, and do not depend on the window size selection. They have faster convergence, but could be more sensitive to the measurement noise. The Kacmarz algorithm can be combined with the trigonometric interpolation algorithm. The amplitudes estimated by the trigonometric interpolation algorithm can be used as a feedforward part to the Kacmarz approach. Introduction of the feedforward part in the Kacmarz algorithm might essentially reduce the convergence time of estimated parameters to their true values.

Algorithms (4.36)-(4.41) are presented in the vector form which is suitable for easy implementation of the algorithms both in Matlab and Simulink[2]. Algorithms were implemented in Matlab and Simulink and applied to the measured data collected from the experimental vehicle. Algorithms can easily be implemented in Engine Control Unit (ECU) using automatically generated code from the Simulink model.

[2] Simulink is an environment for multidomain simulation and model-based design for dynamic and embedded systems.

4.5 Estimation of the Engine Torque via Crankshaft Speed Fluctuations

The time rate change of the crankshaft angular velocity is proportional to the torque acting on the system. The engine rotational dynamics can be described as follows:

$$J\dot{\omega}(t) = T_e - T_l, \tag{4.42}$$

where ω is the speed of the engine, J is the crankshaft inertia moment, T_e is the engine brake torque, and T_l is the engine load torque. Notice that, the model (4.42) predicts neither low frequency oscillations of the driveline nor high frequency oscillations due to the crankshaft torsion. It is assumed here that the model (4.42) is valid at the combustion frequency only. Thus, the filtering problem of the engine speed and the problem of the estimation of the combustion state of a given cylinder via the amplitude are considered separately.

Equation (4.42) can be transformed into the crank angle domain using the chain rule of differentiation and employing the crank angle θ as an independent variable,

$$\omega J\frac{d\omega}{d\theta} = T_e - T_l. \tag{4.43}$$

Integrating over the crank angle interval $[\theta_s \quad \theta_f]$, where θ_s is the initial angle of the interval and θ_f is the final angle, when the engine speed gets minimal and maximal values respectively, yields,

$$\begin{aligned}
&\tfrac{1}{2}\,[\omega^2(\theta_f) - \omega^2(\theta_s)] \\
&= \frac{1}{2}[\omega(\theta_f) + \omega(\theta_s)][\omega(\theta_f) - \omega(\theta_s)] \\
&= \overline{\omega}[\omega(\theta_f) - \omega(\theta_s)] = \frac{1}{J}\int_{\theta_s}^{\theta_f}(T_e - T_l)d\vartheta.
\end{aligned} \tag{4.44}$$

where $\overline{\omega} = \frac{1}{2}[\omega(\theta_f) + \omega(\theta_s)]$ is the average speed in the interval.

If the torque is a continuous function at the interval $[\theta_s, \theta_f]$ then there exists $\theta_1 \in [\theta_s, \theta_f]$, such that the following holds:

$$\int_{\theta_s}^{\theta_f}(T_e - T_l)d\vartheta = (T_e(\theta_1) - T_l(\theta_1))(\theta_f - \theta_s). \tag{4.45}$$

due to the *first mean value theorem for integration* [50].
Substituting (4.45) into (4.44) the amplitude is defined as follows:

$$A = \omega(\theta_f) - \omega(\theta_s) = \frac{(\theta_f - \theta_s)}{J\overline{\omega}}(T_e(\theta_1) - T_l(\theta_1)), \tag{4.46}$$

where A is the crankshaft speed fluctuation at the crank angle interval $[\theta_s \quad \theta_f]$ for a certain cylinder. The amplitude can be seen as a measure of the difference between the engine brake torque and the load torque. Cylinder individual torque contributions are averaged by the engine crankshaft mechanism and the torque of each cylinder can be presented as a sum of two components, namely the mean value of the torque and the torque fluctuations. Torque fluctuations is the rest part of the cylinder individual torque contributions remaining after averaging. The magnitude of the torque fluctuations, as a rest part of the cylinder individual torque contributions is proportional to the magnitude of the average value of the torque. Mean value of the engine brake torque is equal to the load torque during a steady-state engine operation. Thus the amplitude is proportional to the engine brake torque fluctuations. Engine brake torque fluctuations are in turn, proportional to the average value of the engine brake torque. Therefore the mean value of the engine brake torque can be correlated to the amplitude. Since measured values of the amplitudes are noise contaminated due to the engine and driveline mechanical vibrations, variations in the combustion pressure, and some other factors, the amplitudes are averaged over a certain number of combustion events, typically for $8 \div 15$ events. The engine torque is estimated via the average fluctuation which is defined as follows $\overline{A}_k = \frac{1}{w} \sum_{i=k-(w-1)}^{i=k} A_i$, where w is the window size ($w = 8 \div 15$). The engine brake torque as a function of the average engine speed and the average amplitude $\overline{A}$ is plotted in Figure 4.7 for six cylinder engine.

The amplitude (4.46) may also be suitable for estimation of the engine brake torque in transient conditions provided that the load torque is known. The load torque may be estimated by using measurements of the speed of the wheel. Unfortunately, the load torque depends on the vehicle mass and the road gradient which are unknown parameters (see [114] for challenges and methods to simultaneously estimate of the vehicle mass and the road gradient). Another approach to engine torque estimation during transients is a compensation of the transient component of the engine speed signal. The difference between the engine brake torque and the load torque during transients results in the transients of the engine speed. Engine brake torque can also be estimated via the amplitude during transients provided that the transient component of the engine speed is properly compensated. A simple compensation technique of the 'slowly' varying trend of the engine speed is described in Section 4.3.2 (see also [86]). The performance of the engine torque estimation in the transient conditions is limited by the performance of this compensation technique.

Another limitation of the performance of the transient torque estimation is the measurement noise. The amplitude signal is averaged over a certain window of a size w for attenuation of the measurement noise. The larger the window size w, the more information is acquired over the window that in turn allows significant attenuation of the measurement noise. Large window size has a

direct impact on the performance of the transient torque estimation. Therefore, the selection of the window size w is a trade-off between the performance of the transient torque estimation and the performance of the measurement noise attenuation/rejection.

The engine brake torque as a function of the average engine speed and the average amplitude $\overline{A}$ is plotted in Figure 4.7 for a six cylinder engine.

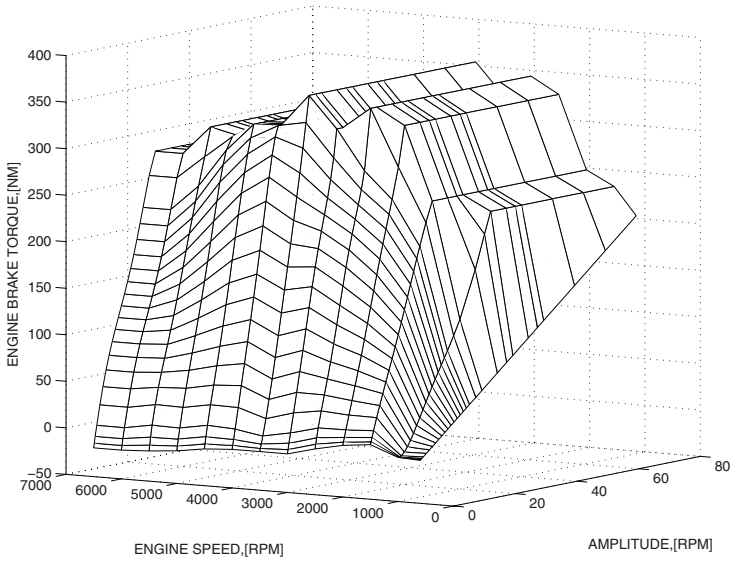

FIG 4.7. The engine brake torque as a function of the engine speed and average amplitude.

Since the passage time is available for measurements it is often convenient to use the index which is proportional to the amplitude A:

$$L_k = \frac{T_{k-d} - T_k}{T_k^2 T_{k-d}} \tag{4.47}$$

where T_k is the rotational time for the segment k, which corresponds to the maximum value of the engine speed $\omega(\theta_f)$, T_{k-d} is the rotational time for the segment $k-d$, which in turn corresponds to the minimum value of the engine speed $\omega(\theta_s)$, d is the step number. The length of the segment is Δ CA degrees. The index (4.47) is similar to the misfire detection index for monitoring of the derivative of the rotational energy introduced in [52] and [68]. Then the engine brake torque is estimated on-board by using the measurements of the average fluctuations $\overline{L}_k$ and the engine speed $\overline{\omega}$. The engine brake torque as a function

average engine speed and index L (4.47) for eight cylinder engine is plotted in Figure 4.8.

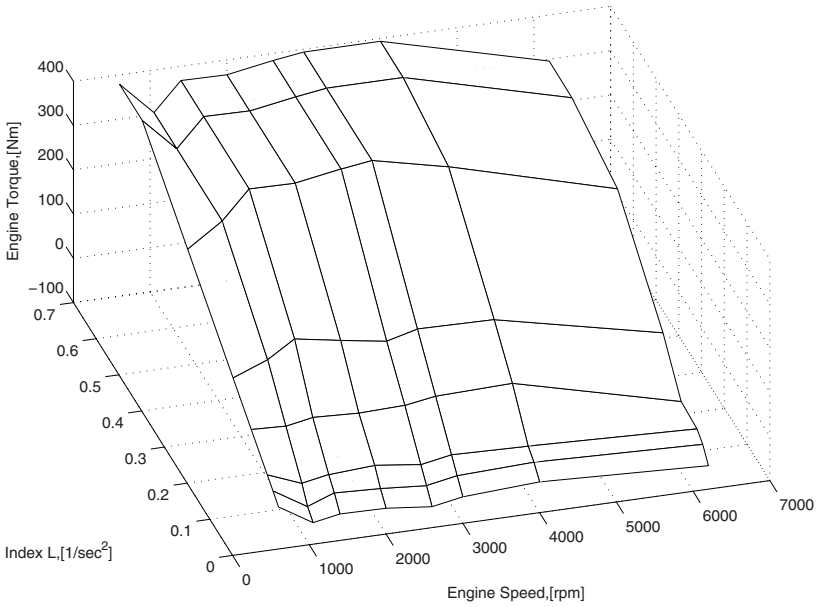

FIG 4.8. The engine brake torque for V8 engine as a function of engine speed and index 4.47.

It is worth remarking that according to (4.46) the engine torque depends not only on the engine speed fluctuations, but also on the inertia J, which in turn, is gear dependent. Measurements of the engine torque for different gears show that the gear dependence can be neglected in the torque estimation technique proposed above, due to the elasticity of the driveline.

Figure 4.9 illustrates the verification of the proposed algorithms for V8 engine. The torque measured on a rig (chassis rolls) is plotted with the solid line and the estimated torque obtained by using the technique proposed above, and the filtered signal (4.25), (4.26) is plotted with a dotted line. Figure 4.9 shows a strong correlation between measured and estimated torques.

Figure 4.10 illustrates the verification of the proposed algorithms for six cylinder engine. The torque measured via a traction force on the chassis rolls is plotted with the solid line and the estimated torque obtained by using the technique proposed above, and the filtered signal (4.39) is plotted with a dotted line. Figure 4.10 shows a strong correlation between measured and estimated torques.

Torque estimation algorithms described above were extensively tested in the engine rig, on a vehicle running both on chassis rolls and different roads.

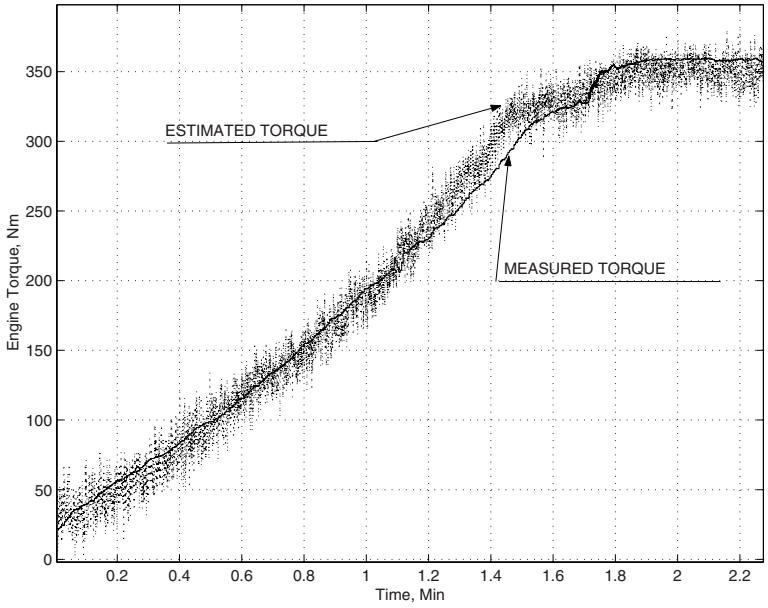

FIG 4.9. Measurements on the experimental vehicle equipped with the V8 engine. The measurements were made on chassis rolls. The engine speed is 4800 rpm. Measured engine torque is plotted with solid line. Estimated torque is plotted with dotted line.

The tests showed a satisfactory performance of both steady-state and transient torque estimation. Estimation accuracy deteriorated, unfortunately on rough road surfaces.

4.6 Conclusion

It has been shown that the torque estimation technique benefits from the availability of the combustion quality information provided by the filtering algorithms described in this Chapter. Fast and computationally efficient algorithms which provide filtering at the engine firing frequency were designed and verified for six and eight cylinder engines.

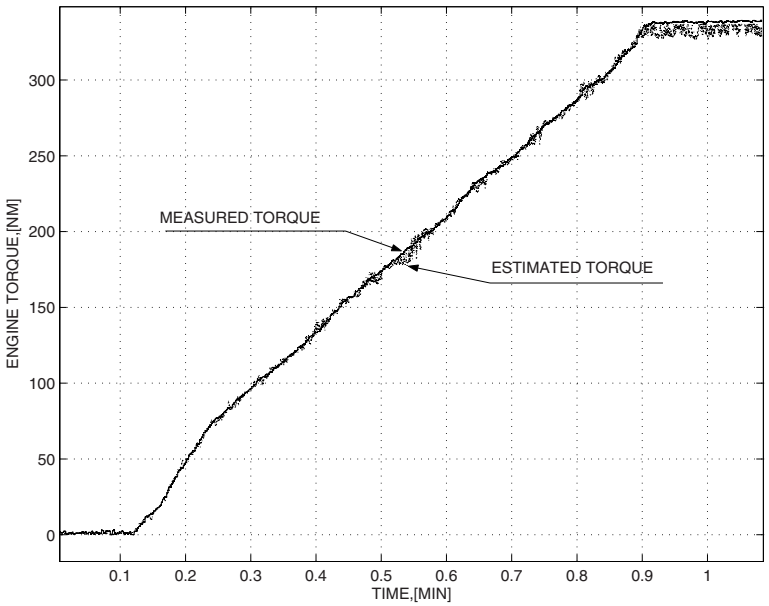

FIG 4.10. Measurements on the experimental vehicle equipped with six cylinder prototype engine. The measurements were made on chassis rolls. The engine speed is 5000 rpm. Measured engine torque is plotted with the solid line. Estimated torque is plotted with dotted line.

5

Engine Friction Estimation at Start

Errors in an estimate of friction torque in modern spark ignition automotive engines have a direct impact on driveability performance of a vehicle and necessitate a development of real-time algorithms for adaptation of the friction torque. The friction torque in the engine control unit is presented as a look-up table with two input variables (engine speed and indicated engine torque). Algorithms proposed in this Chapter estimate the friction torque during engine start and idle. Newton's second law for rotational dynamics is used as a reference model during engine start. The friction torque is estimated via a deviation from the reference model. The values of the friction torque at the nodes of the look-up table are updated, if new measured data of the friction torque is available. New recursive and computationally efficient algorithms are developed for adaptation of the nodes of the look-up tables. The algorithms are tested on a Volvo vehicle equipped with a six cylinder prototype engine.

5.1 Introduction

The performance of an engine control system depends on the accuracy of the engine torque model. One of the important parts of the torque model is the friction losses. The values of the engine friction torque, which is pre-calibrated, are memorized in a look-up table (static map) residing in the memory of an engine controller. Friction torque is mainly a function of engine speed, load (engine indicated torque) and engine oil temperature. Piece-to-piece variations of the engine components, changes of the engine components over time together with changes in the external environment, i.e. temperature variations, may result in variations in the engine friction torque. These variations causing errors in the estimate of the friction torque, lead to deterioration of driveability performance. Errors in the estimate of engine friction torque have a direct impact on the behaviour of the engine speed during negative transients (where the driver releases the accelerator pedal and switches to a neutral gear). Error in the engine friction estimate results in the error in

A.A. Stotsky, *Automotive Engines*, DOI 10.1007/978-3-642-00164-2_5,

actual indicated engine torque. The actual indicated engine torque (which is negative during a negative transient) is higher than it would be if the losses were estimated correctly. Therefore, the engine speed decays slowly. Moreover, overestimation of the friction torque can lead not only to slow negative transients of the engine speed, but also to a constant offset in the steady-state engine speed with respect to a target idle speed. The steady-state offset, due to the errors in friction estimation, could result in a jerk behaviour of the vehicle if a driver engages a low gear. Errors in the estimation of the friction losses thus can lead directly to deterioration of driveability performance.
Despite the fact that engine friction modeling is a well studied field (see for example [76] and references therein), very little attention has been paid to real-time friction estimation. The facts presented above necessitate the development of real-time adaptation algorithms to improve the accuracy of the engine friction model. The most promising opportunity for estimating friction is during engine idle when the engine is decoupled from the driveline [7]. The idle state however, could give an estimate of the friction torque only at idle speed and low indicated torque. Another opportunity for obtaining an accurate estimate of the friction torque is the period following engine start. At engine start, the engine speed increases to a relatively high (compared with the idle speed) level, and then slowly decreases, converging to the desired idle speed. This period when the engine speed decreases gives an opportunity to estimate engine friction torque. Warm starts only are considered in the present Chapter. Newton's law for rotational dynamics can be used as a reference model. The difference between the derivative of the engine speed multiplied by the inertia moment and the engine brake torque can be seen as a deviation from the reference model. The derivative of the engine speed is estimated by using the recursive spline interpolation method described in Chapter 3, (see also [93]). If a deviation from the reference model is detected, then the friction look-up table is updated so that the deviation is minimized. Notice that simple compensation techniques such as input observers can also be applied for correction of the friction torque model [95] at engine idle. The values of the correction parameter are not memorized in this case in the look-up table and a certain time for correction is required after every transient. Adaptation algorithms for look-up tables proposed in this Chapter overcome these difficulties. Adaptation of look-up tables (static maps) is widely used in the engine control functionality for robustness improvement [113]. However, adaptation algorithms described in [113] do not allow a prediction of the values of the operating parameter in the regions with meager new data representation.
In this Chapter the look-up table defines a surface for engine friction torque in three dimensional space with engine speed and indicated torque as independent variables. The shape of the surface reflects physical dependencies of the friction torque as a function of speed and indicated torque. If new data is available only in a certain operating region, then the part of the surface parameters are adapted (for example the offset and the gradient in the engine

speed direction). Adaptation of the look-up table is associated with a motion of the surface in three dimensional space. The position and the orientation of the surface in three dimensional space change only after adaptation, which in turn, allows for a prediction of the friction torque for a wide range of speeds and indicated torques. This prediction is possible with few measured points by taking into account physical dependencies, which are present in the shape of the surface. An adaptation algorithm is constructed so that only the nodes (sites) of the look-up table are adapted, thereby the values of engine friction torque between the nodes are computed using linear interpolation. In order to reduce the computational burden of the processor, recursive and computationally efficient algorithms for adaptation of the nodes in the look-up table are developed. The contributions of this Chapter are the following:

- new recursive algorithms for adaptation of the nodes of the look-up tables
- new algorithms for estimation of the engine friction torque at start.

A Volvo vehicle equipped with six cylinder prototype engine was used in the experiments.

5.2 Impact on Drivability

Errors in the estimate of engine friction torque have a direct impact on the behaviour of the engine speed during negative transients (where the driver releases the accelerator pedal and switches to a neutral gear). The engine speed during negative transients is governed by the torque model. Requested indicated engine torque is calculated from the requested engine brake torque by adding the torque losses (friction and pump losses). The requested engine brake torque is calculated as a function of accelerator pedal position and engine speed. The requested indicated engine torque in the negative transient of the engine speed with overestimated friction losses (real losses are less than estimated), is higher than it would be if friction losses were to be correctly estimated. The desired engine load is calculated from the desired indicated torque. The feedback load control system regulates the engine load to the desired load, which implies that the actual indicated torque converges to the desired indicated torque. The actual indicated engine torque (which is negative during a negative transient) is higher than it would be if the losses were estimated correctly. Therefore, the engine speed decays slowly. Moreover, overestimation of the friction torque leads not only to slow negative transients of the engine speed, but also to a constant offset in the steady-state engine speed with respect to a target idle speed. Errors in the estimation of the friction losses thus can lead directly to deterioration of driveability performance.

5.3 Problem Statement

The errors in the estimated friction losses have an effect on the behaviour of the engine torque at start and idle. Newton's law

$$J\dot{\omega} = T_{brake} - T_{acs} \tag{5.1}$$

can be seen as a reference model at the interval $[t_i \quad t_f]$, where t_i is the time when the engine speed nears a maximum value at start, t_f is the time when the engine speed reaches the desired idle speed, ω is the engine speed, J is the inertia moment of the engine, T_{brake} is the engine brake torque, T_{acs} is the torque corresponding to accessory loads. The engine brake torque is the difference between the engine indicated torque and the torque corresponding to the losses, i.e., $T_{brake} = T_{ind} - T_{loss}$, where T_{ind} is the indicated engine torque, $T_{loss} = T_f + T_p$, T_{loss} is the torque corresponding to the losses, which in turn is the sum of the friction T_f and the pump losses T_p.

Let us introduce the following error

$$e(t) = J\dot{\omega} - (T_{brake} - T_{acs}) \tag{5.2}$$

If the torque model is well calibrated, then the error $|e(t)|$ is close to zero at the interval of interest. Any deviation from the reference model is assumed to be related to the friction losses, since aging of the engine components mainly affects the friction losses. The friction torque is a function of engine speed and indicated engine torque, $T_f = f(\omega, T_{ind})$. The friction torque is presented as a look-up table with two inputs ω and T_{ind}. The nodes of the look-up table should be updated so that the absolute values of the error $e(t)$ are reduced after each start event. The control aim can be formulated as follows. It is necessary to find an adaptation mechanism for adaptation of the nodes of the engine friction look-up table such that the following control aim is reached:

$$\overline{\lim_{k\to\infty}}|e(t)| \leq \Delta \tag{5.3}$$

where k is the number of the start events, $\Delta > 0$ is a small positive constant, $t \in [t_i \quad t_f]$. The system as described can be seen as a model reference adaptive system driven by the engine start events.

5.4 Estimation of the Friction Torque at Start

The problem stated above can be solved in two steps. In the first step, the deviation from the engine friction torque, which is pre-calibrated in the rig, is calculated for each start event by a comparison of $J\dot{\omega}$ and $T_{brake} - T_{acs}$ at a certain interval. If $J\dot{\omega}$ significantly deviates from $T_{brake} - T_{acs}$, then the estimates of the engine friction torque are computed. These estimates of the engine friction torque as a function of speed and indicated torque is the input to the second step. In the second step, the nodes of the friction torque look-up table are adapted so that the deviation between $J\dot{\omega}$ and $T_{brake} - T_{acs}$ is reduced for the next start event.

Assume that the engine friction torque can be presented as a sum of two

components $T_{fc} + \Delta T_f$, where T_{fc} is the engine torque pre-calibrated in the rig, and ΔT_f is the deviation from the pre-calibrated torque. The deviation ΔT_f is calculated by using an error $e(t)$ which is evaluated at certain discrete points t_p, $(p = 1, 2, ...)$, on a time scale, i.e.,

$$\begin{aligned}\Delta T_f(w(t_p), T(t_p)_{ind}) = e(t_p) - J\dot{\omega}(t_p) + T(t_p)_{ind} \\ -T_{fc}(t_p) - T_p(t_p) - T_{acs}(t_p)\end{aligned} \tag{5.4}$$

where $t_p \in [t_i \quad t_f]$. The points t_p should be well separated from each other on the time scale, providing information about ΔT_f for different values of engine speed and indicated torque. From two to four measured points can be obtained during a negative transient. One point is obtained at idle. The deviation from the calibrated engine friction torque at idle $\Delta T_f(w_{id}, T_{ind_{id}})$, where w_{id} is the engine idle speed, $T_{ind_{id}}$ is the indicated torque at idle, is calculated as follows:

$$\Delta T_f(w_{id}, T_{ind_{id}}) = T_{ind_{id}} - T_{fc_{id}} - T_{p_{id}} - T_{acs_{id}} \tag{5.5}$$

where $T_{fc_{id}}$, $T_{p_{id}}$, $T_{acs_{id}}$ are the values of the friction torque, pump torque and the torque corresponding to the accessory loads, respectively. If the engine is idling for a relatively long period, the deviation ΔT_f is averaged over certain number of steps, providing a consistent estimate for the deviation $\Delta T_f(w_{id}, T_{ind_{id}})$.

For calculation of $\Delta T_f(w(t_p), T(t_p)_{ind})$ according to (5.4) during engine start event, the estimate of the derivative of the engine speed is required. The backward difference method, which is widely used for calculation of the derivative of the signal, often gives noisy estimates. For the improvement of the quality of the estimate of the derivative of the engine speed signal, a spline interpolation method described in Chapter 3 (see also [18], [93]) is used. A spline interpolation method is based on on-line least-squares polynomial fitting over a moving-in-time window of a certain size [27]. Since the nodes of the friction look-up table are adapted after the start events, a post-processing of the signals is allowed, i.e., the signals are memorized and processed 'offline'. The spline interpolation method gives an accurate estimate of the derivative of the engine speed in the post-processing, since the derivative of the engine speed is computed in the middle of a moving window. This technique improves essentially the quality of the engine speed derivative signal. Other signals in (5.4) should also be delayed. Figure 5.1 shows the behaviour of the engine speed together with its derivative and engine brake torque during engine start event where the friction losses are correctly estimated. Figure 5.2 and Figure 5.3 show the behaviour of the system where the friction losses are overestimated, i.e., $\Delta T_f = 10[Nm]$. As can be seen from the Figure 5.2 and Figure 5.3, two points are available for adaptation of the friction losses. The third point for calculation ΔT_f is available when engine is idling. Adaptation algorithms for look-up tables are presented in the next Section.

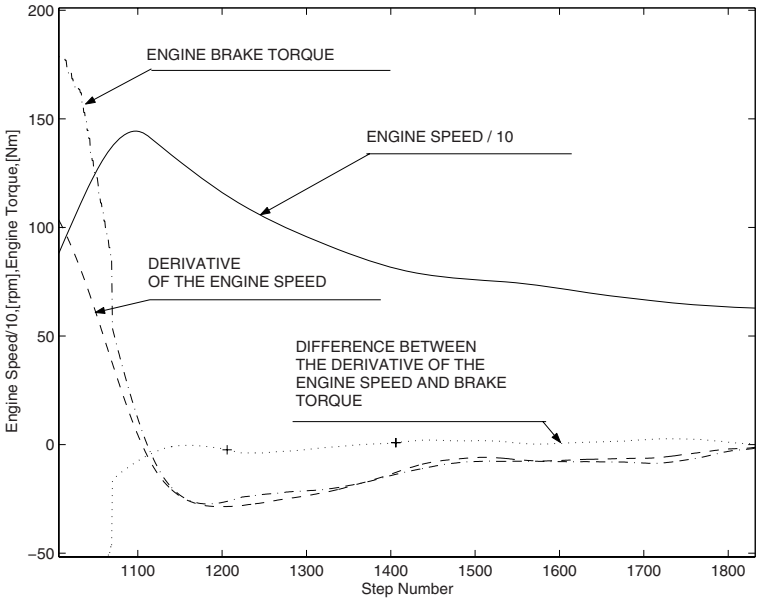

FIG 5.1. Measurements with the step of 4 ms on the prototype engine. The friction losses are correctly estimated. Engine speed during a start is plotted with solid line. The values of the engine speed are divided by ten. Engine brake torque is plotted with dashdot line. The derivative of the engine speed multiplied by the inertia moment $J\dot{\omega}$ is plotted with dashed line. The difference $e(t) = J\dot{\omega} - T_{brake}$ is plotted with dotted line. The points where $e(t_p)$ is evaluated are indicated with plus signs.

5.5 Adaptation Algorithms for Look-up Tables

5.5.1 Problem Statement

In Figure 5.4, engine friction torque is plotted as a function of engine speed and indicated torque. The friction torque is overestimated by $10[Nm]$. Two points representing the estimated friction torque from the start are plotted with plus signs. The point that represents the estimated friction torque at idle is plotted with round and plus signs. The problem statement is the following. It is necessary to design adaptation algorithms for the nodes of the look-up table by using three measured points of the actual friction torque. Estimation of the engine friction torque at engine start provides less consistent estimates than estimates of the friction torque at engine idle. Therefore, the measurements of the friction torque at idle and at start should be treated differently by assigning different weighting factors in the adaptation algorithms.

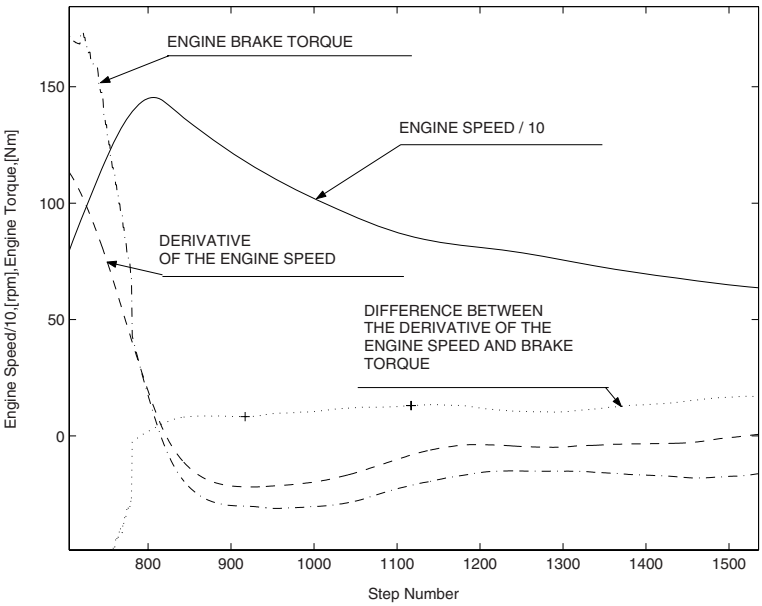

FIG 5.2. Measurements with the step of 4 ms on the prototype engine. The friction losses are overestimated by $10[Nm]$. Engine speed during a start is plotted with solid line. The values of the engine speed are divided by ten. Engine brake torque is plotted with dashdot line. The derivative of the engine speed multiplied by the inertia moment $J\dot{\omega}$ is plotted with dashed line. The difference $e(t) = J\dot{\omega} - T_{brake}$ is plotted with dotted line. The points where $e(t_p)$ is evaluated are indicated with plus signs.

5.5.2 General Adaptation Algorithms for Look-Up Tables

The algorithm of the adaptation of the nodes of two dimensional tables can be divided into three steps. In the first step, the output of the look-up table is approximated by a polynomial of two independent variables in the least-squares sense. In the second step, a recursive procedure is designed for adaptation of the part of the coefficients of the polynomial when new data is added. In the third step of the algorithm, the approximation error is reduced. Namely, the differences between the polynomial approximation of original table and the polynomial approximation after adaptation are evaluated at every node and added to the nodes of the original look-up table. This allows a reduction of the approximation error and usage of low order polynomials, which are more robust with respect to the measurement errors. Only the nodes of the look-up table are adapted as a result of the application of the algorithm described above. The values of the friction torque between the nodes are obtained by linear interpolation.

Suppose that there is a look-up table describing the variable z as a function of two variables x and y. The look-up table is presented as a number of nodes

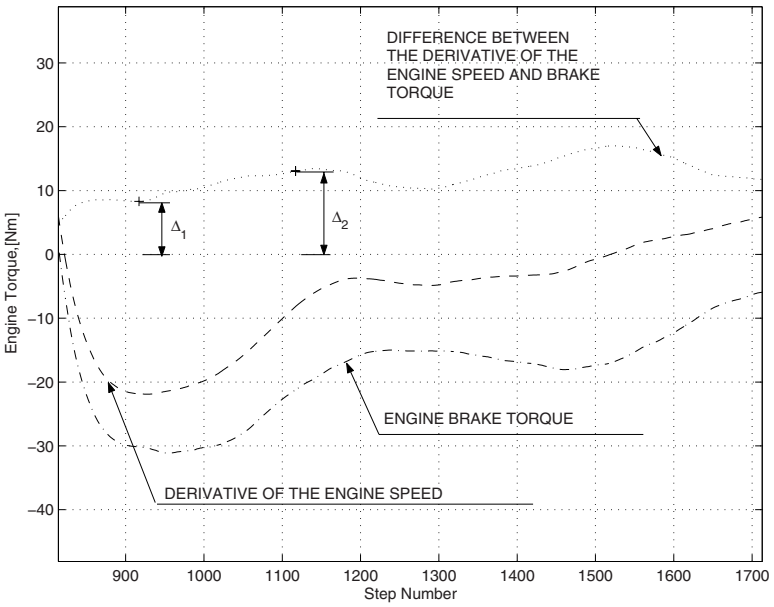

FIG 5.3. Measurements with the step of 4 ms on the prototype engine (the same as Figure 5.2). The friction losses are overestimated by $10[Nm]$. Engine brake torque is plotted with dashdot line. The derivative of the engine speed multiplied by the inertia moment $J\dot{\omega}$ is plotted with dashed line. The difference $e(t) = J\dot{\omega} - T_{brake}$ is plotted with dotted line. The points where $e(t_p)$ is evaluated are indicated with plus signs. The left point is evaluated at $\omega = 1180[rpm]$,$T_{ind} = 23[Nm]$, and the right point is evaluated at $\omega = 860[rpm]$,$T_{ind} = 43[Nm]$. The friction torque at idle is evaluated at $\omega = 650[rpm]$, $T_{ind} = 34[Nm]$.

(x_h, y_p) , $h = 1, ...D$, $p = 1, ..., G$, where the output variable $z_{h,p}$ is defined. The values of the variable z between the nodes are computed via a linear interpolation. The problem of the adaptation of a look-up table is reduced to the adaptation of $z_{h,p}$.

As it was mentioned above, the problem can be solved in three steps as follows.

Step 1. Polynomial Approximation.

In this step, the look-up table is approximated by the following polynomial:

$$\hat{z} = \sum_{i=0}^{n} \sum_{j=0}^{n} a_{i,j} x^i y^j \tag{5.6}$$

where n is the order of the polynomial, $a_{i,j}$ are the coefficients of the polynomial. The polynomial model (5.6) can be written in the following vector form:

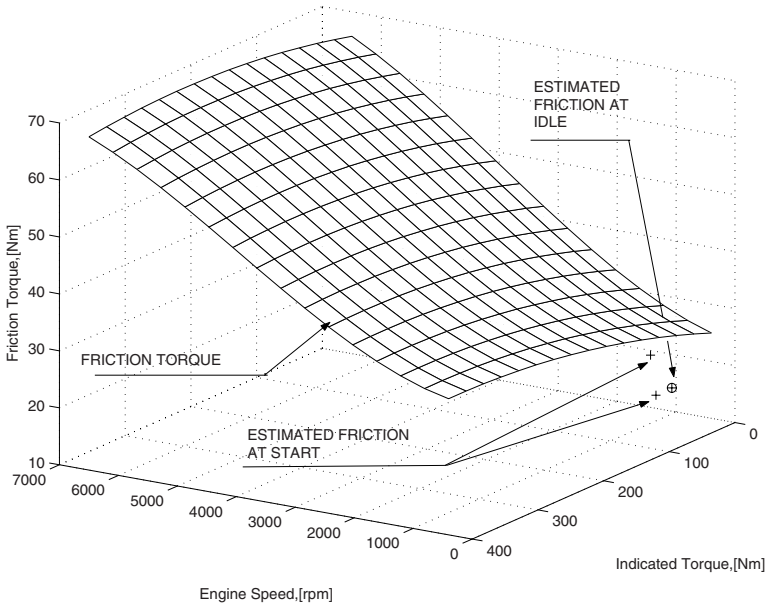

FIG 5.4. Engine friction torque is plotted as a function of engine speed and indicated engine torque. The friction torque is overestimated by $10[Nm]$. Two points which represent the estimated friction torque at start (see Figure 5.2 and Figure 5.3) are plotted with plus signs. The point which represents the estimated friction torque at idle is plotted with round and plus signs.

$$\hat{z} = \varphi^T \theta \tag{5.7}$$

where

$$\begin{aligned} \varphi &= [1, y, y^2, ..., y^n, x, xy, xy^2, ..., xy^n, ..., \\ &\quad x^n, x^n y, x^n y^2, ..., x^n y^n]^T \\ \theta &= [a_{00}, a_{01}, a_{02}, ..., a_{0n}, a_{10}, a_{11}, a_{12}, ..., a_{1n}, ..., \\ &\quad a_{n0}, a_{n1}, a_{n2}, ..., a_{nn}]^T \end{aligned} \tag{5.8}$$

The performance index to be minimized is the following:

$$S = \sum_{l=1}^{N} (z_l - \hat{z}_l)^2 w_l \tag{5.9}$$

where N is the number of the nodes (sites) of the look-up table, $l = 1, ..., N$,$N = D \times G$, w_l is the weighting factor at every node of the table. The parameter θ, which minimizes index (5.9) is computed as follows:

$$\theta = [\sum_{l=1}^{N} (\varphi_l \varphi_l^T w_l)]^{-1} \sum_{l=1}^{N} z_l \varphi_l w_l \tag{5.10}$$

Assuming, the parameter vector θ has been computed according to the formula (5.10) and memorized in the memory of the electronic control unit, the problem of the adaptation of the look-up table can be stated as the problem of the adaptation of the parameter vector θ for new measured data. The values $\hat{z}_{(h,p)}$ at the nodes (x_h, y_p) are computed according to (5.7).

Step 2. Adaptation of the coefficients. In this step of the algorithm, the vector θ is adapted for new data. Assuming, new measured data x_m, y_m, z_m with the weighting factor w_m is added to the data set, the parameter vector $\theta \in R^{(n+1)^2}$ is divided into two parts: the first part $\theta_c \in R^{(n+1)^2-q}$ remains unchanged from the previous step, and the second part $\theta_a \in R^q$ which should be adapted, where q is the number of the parameters to be adapted. Then,

$$\theta = [\theta_c \quad \theta_a]^T \tag{5.11}$$

$$\varphi = [\varphi_c \quad \varphi_a]^T \tag{5.12}$$

where φ_c is the part of the regressor, which corresponds to the parameter vector θ_c, and φ_a is the part of the regressor corresponding to the parameter vector, θ_a. New measured data x_m,y_m,z_m is added to the data set. The performance index to be minimized is the following:

$$S_1 = \sum_{l=1}^{N}(z_l - \hat{z}_l)^2 w_l + (z_m - \varphi_m^T\theta)^2 w_m \tag{5.13}$$

where

$$\begin{aligned}\varphi_m = [&1, y_m, y_m^2, ..., y_m^n, x_m, x_m y_m, x_m y_m^2, ...,\\ &x_m y_m^n, ..., x_m^n, x_m^n y_m, x_m^n y_m^2, ..., x_m^n y_m^n]^T\end{aligned} \tag{5.14}$$

$$\varphi_m = [\varphi_{cm} \quad \varphi_{am}]^T \tag{5.15}$$

The adaptive parameter θ_a is computed according to the following equation $\frac{\partial S_1}{\partial \theta_a} = 0$, i.e.,

$$\theta_a = [\sum_{l=1}^{N}(\varphi_{al}\varphi_{al}^T)w_l + \varphi_{am}\varphi_{am}^T w_m]^{-1}$$

$$\sum_{l=1}^{N}(z_l - \varphi_{cl}^T\theta_c)\varphi_{al}^T w_l + (z_m - \varphi_{cm}^T\theta_c\varphi_{am}^T)w_m \tag{5.16}$$

In order to reduce the computational burden on the engine controller, the adjustable parameter is computed recursively. The vector of the adjustable parameters is computed according to the following formula at step $(k-1)$

$$\theta_{a(k-1)} = [\sum_{l=1}^{N}(\varphi_{al}\varphi_{al}^T w_l)]^{-1} \sum_{l=1}^{N}(z_l - \varphi_{cl}^T\theta_c)\varphi_{al}^T w_l \tag{5.17}$$

and the adjustable parameter θ_{ak} at step k should be updated recursively via $\theta_{a(k-1)}$ as soon as new data z_m, φ_m with the weighting factor w_m are available. Applying the matrix inversion relation to (5.16) and taking into account (5.17) one gets the following adjustment law for the parameter θ_{ak} at step k:

$$\theta_{ak} = [I - \frac{\Gamma_{k-1} w_m \varphi_{am}\varphi_{am}^T}{(1 + w_m\varphi_{am}^T\Gamma_{k-1}\varphi_{am})}](\theta_{a(k-1)} + \Gamma_{k-1}(z_m - \varphi_{cm}^T\theta_c)w_m\varphi_{am}^T), \tag{5.18}$$

$$\Gamma_k = \Gamma_{k-1} - \frac{w_m\Gamma_{k-1}\varphi_{am}\varphi_{am}^T\Gamma_{k-1}}{(1 + w_m\varphi_{am}^T\Gamma_{k-1}\varphi_{am})}, \tag{5.19}$$

where $\Gamma_{k-1} = [\sum_{l=1}^{N}(\varphi_{al}\varphi_{al}^T w_l)]^{-1}$, I is $q \times q$ identity matrix, and the following condition for convergence of the algorithm imposes restrictions on the weighting factors:

$$-\Gamma_{k-1} < \Gamma_{k-1} - \frac{w_m\Gamma_{k-1}\varphi_{am}\varphi_{am}^T\Gamma_{k-1}}{(1 + w_m\varphi_{am}^T\Gamma_{k-1}\varphi_{am})} < \Gamma_{k-1}. \tag{5.20}$$

Algorithm (5.18), (5.19) is easily implementable since the dimension of the vector θ_a is low. As a rule, only the offset and the slope in one of the directions are updated; i.e., $q = 2$.
The values $\hat{z}_{a(h,p)}$ at the nodes (x_h, y_p) are computed according to the following formula $\hat{z}_{ak} = \varphi_{ck}^T\theta_c + \varphi_{ak}^T\theta_{ak}$. The vector θ_c is not updated. That, in turn, allows the shape of the surface to be maintained.

Notice, that the weighting factors w_m are assigned according to the accuracy of measured values of the operating parameter. Usually, the weighing factors are inversely proportional to the variances of the measurement noise [57], [59]. If the values of the operating parameter are measured with the same accuracy and averaged over a certain sample size the weighting factors could be chosen proportionally to the sample size. For example, the estimate of the engine friction torque at idle is averaged over a certain number of steps, providing more accurate estimate than the engine start events. Therefore, the weighting factor for the friction torque estimate at idle should be chosen higher than the weighting factor for the friction torque estimate at engine start events.

Step 3. Reducing the approximation error. Low order polynomials (5.6) is advisable to use for approximation of look-up tables. Low order polynomials are robust with respect to the measurement noise compared with the polynomials of a high order. However, approximation of a look-up table using low order polynomials could also give a relatively large approximation

error. In order to reduce the approximation error, the following differences $\hat{z}_{a(h,p)} - \hat{z}_{(h,p)}$ between the polynomial approximation of the adapted table and the polynomial approximation of the original table are computed at every node $h = 1, ...D$, $p = 1, ..., G$ and added to the values $z_{(h,p)}$ of the original look-up table. Namely, the values of variable z at the nodes of the look-up table are updated as follows:

$$z_{f(h,p)} = z_{(h,p)} + (\hat{z}_{a(h,p)} - \hat{z}_{(h,p)}) \tag{5.21}$$

In other words the approximation error which is present in the $\hat{z}_{a(h,p)}$ and $\hat{z}_{(h,p)}$, is reduced since only the difference $(\hat{z}_{a(h,p)} - \hat{z}_{(h,p)})$ (not the absolute values) is used for adaptation of the nodes of the look-up table. In the next subsection the algorithm proposed above is applied to the adaptation of the friction torque look-up table.

5.5.3 Adaptation Algorithms of the Engine Friction Torque Look-up Table

Suppose that the engine friction torque is overestimated with an offset of $10[Nm]$. Actual values (two values) of the engine friction torque as a function of speed and indicated torque were obtained during an engine start (see Figure 5.2 and Figure 5.3). A third value of the friction torque was obtained at idle by averaging the values of the friction torque over a certain interval. Weighting factors were assigned to all the values of the measured engine friction torque. The algorithm described above was applied for adaptation of the friction look-up table. The order of the approximating polynomial is two. Only the offset parameter a_{00} was adapted. The result is plotted in Figure 5.5. The friction torques before and after adaptation were plotted as white surfaces, and actual friction torque is plotted as black surface. The difference between actual friction torque and the friction torque after the adaptation is $0.77[Nm]$.

Notice that new values of the estimated engine friction torque are closely located to each other in the area of low speeds and torques only. Therefore adaptation of the offset only is chosen in this example. In order to make adaptation of the gradient in the engine speed direction more operational points are required at high rotational speeds.

The look-up table for the friction torque was updated in the engine electronic control unit (ECU) and the measurements of the engine speed and brake torque at the next start are plotted in Figure 5.6. The behavior of the engine speed and torque before adaptation is plotted in Figure 5.2. A comparison of Figure 5.2 and Figure 5.6 shows that the error $e(t) = J\dot{\omega} - T_{brake}$ is reduced and the control aim (5.3) is reached with a sufficiently small Δ.

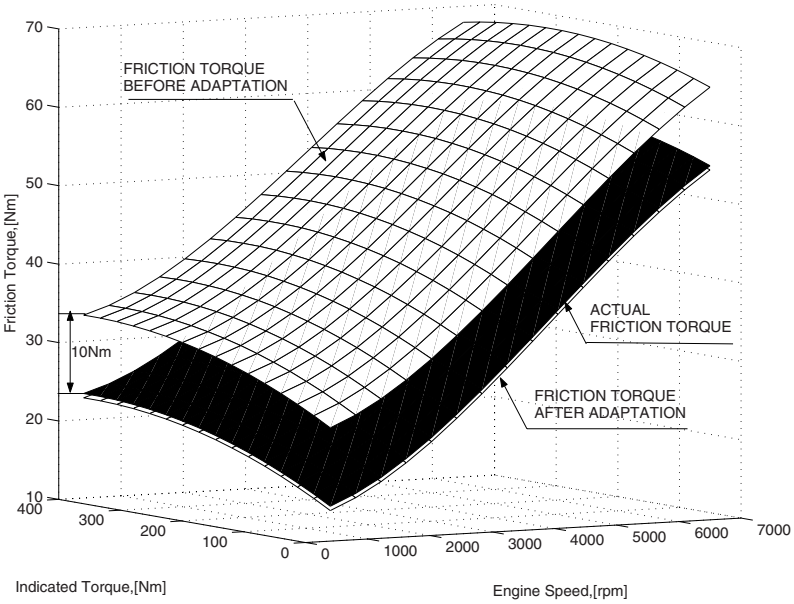

FIG 5.5. The friction torque is plotted as a function of engine speed and indicated engine torque. The friction torque before the adaptation and after adaptation are plotted as white surfaces. Actual friction torque is plotted as black surface.

5.6 Conclusions

New algorithms for real-time estimation of the engine friction torque are developed. Engine friction torque is estimated at start and at engine idle. Recursive and computationally efficient algorithms allow prediction of friction torque for a wide range of speeds and loads even with few new measured points by taking into account physical dependencies used for adaptation of the nodes of the look-up tables. The algorithms make it possible to avoid driveability problems that could result from errors in estimating engine friction torque.

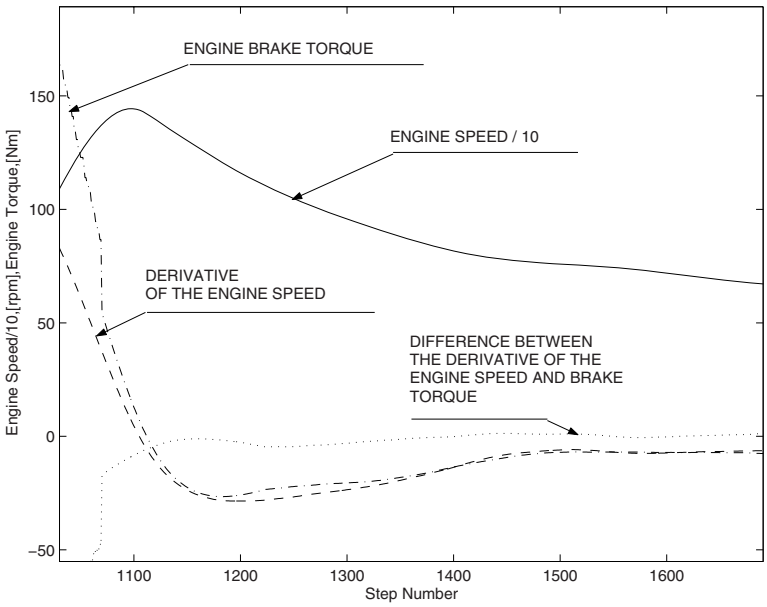

FIG 5.6. Measurements with the step of 4 ms on the prototype engine. The friction losses have been adapted. Engine speed during a start is plotted with solid line. The values of the engine speed are divided by ten. Engine brake torque is plotted with dashdot line. The derivative of the engine speed multiplied by the inertia moment $J\dot{\omega}$ is plotted with dashed line. The difference $e(t) = J\dot{\omega} - T_{brake}$ is plotted with dotted line.

6

Data-Driven Algorithms for Engine Friction Estimation

The engine friction estimation algorithms described in this Chapter estimate the engine friction torque via the crankshaft speed fluctuations at the fuel cut off state and at idle. A computationally efficient filtering algorithm for reconstruction of the first harmonic of a periodic signal is used to recover an amplitude which corresponds to engine events from the noise contaminated engine speed measurements at the fuel cut off state. The values of the friction torque at the nodes of the look-up table are updated, when new measured data of the friction torque are available. New data-driven algorithms which are based on a step-wise regression method are developed for adaptation of look-up tables. Algorithms are verified by using a spark ignition six cylinder prototype engine.

6.1 Introduction

The most promising opportunity for estimating friction is during engine idle when the engine is decoupled from the driveline [7] and at engine start (see Chapter 5). These methods however, could give an estimate of the friction torque only at the low speeds and low indicated torques. Better accuracy of the engine torque estimation can be achieved if more measurements of the friction torque are available at high rotational speeds.
Friction losses increase with speed and up to two thirds of engine friction can occur in the piston and rings (see [83], page 459). The friction force on the piston assembly has a direct impact on the piston acceleration and hence on the crankshaft speed variations. Wearing of the engine components has impact on the friction losses and, in turn, on the crankshaft speed variations. The amplitude of the crankshaft speed variations, which are induced by the periodic cylinder individual compression/expansion events, depends on a compression pressure, a friction force and the viscosity of a lubricating oil and only provides a method for estimation of the engine friction torque and pump torque when

A.A. Stotsky, *Automotive Engines*, DOI 10.1007/978-3-642-00164-2_6,

the engine is not fueled. The same amplitude provides a method for estimation of the engine brake torque, when the engine is fueled (see Chapter 4). A fuel cut off functionality which is used to enhance a fuel economy, is activated when the throttle valve is completely closed and the engine speed is higher than a predetermined value (usually this threshold value of the engine speed is around 3000 rpm). This fuel cut off operation gives an opportunity to provide new measured data of the friction torque at high rotational speeds. The engine friction look-up table is adapted if new data of the engine friction torque at high rotational speeds are available. However, crankshaft torsional vibrations at high rotational speeds, inertia torque due to reciprocating masses, piston mass imbalance, and other mechanically induced vibrations affect the behavior of the high resolution engine speed when the engine is not fueled. Therefore the high resolution engine speed signal should be filtered in order to recover an amplitude corresponding to engine events from a noise contaminated data. The engine speed signal is approximated by a trigonometric polynomial with known frequencies and unknown amplitudes (see Chapter 4). The convergence of the estimated parameters to their true values is ensured due to the richness (persistency of excitation) of the measured periodic engine speed signal which is approximated by the trigonometric polynomial. The signal is completely reconstructed by the trigonometric polynomial and the filter uses a periodic signal at the engine frequency. The algorithm described in this Chapter is divided in two parts. The first part is the engine friction estimation at the fuel cut off state and idle, and the second part is the adaptation of the friction look-up table.

Adaptation of look-up tables (static maps) is widely used in order to improve the robustness of the engine control functionality [113], [117]. However, adaptation algorithms described in [113] and [117] do not allow a prediction of the values of the operating parameter in the regions with meager new data representation. A new approach, described in Chapter 5 allows for a prediction of the friction torque for a wide range of speeds and indicated torques, even with few new measured points, by taking into account physical dependencies. However, in this approach the parameters to be adapted (coefficients of a polynomial) are chosen beforehand and are not coupled to the parameters of a new data set. Accuracy of adaptation however, depends on the accuracy, consistency and a sample size of new data of the operating parameter (friction torque). Different driving cycles and conditions give different sets of data of new measured friction torque. The parameters (coefficients of a polynomial) which should be selected for adaptation depend on the parameters of new data sets. For example, for some data sets the offset of the friction torque look-up table should be updated only, whereas for other data sets the offset and the gradient in the engine speed direction are updated. The adaptation algorithm proposed in this Chapter is based on the statistical step-wise least-squares method, and represents a flexible approach where the parameters to be adapted are chosen in every step. Step-wise regression method described in [20],[21],[57] examines new terms incorporated in the model at every stage

of the regression. After each new term is selected, its contribution is reviewed to ensure it remains statistically significant. The decision about inclusion of a new term in the model is based on the *Test for Equal Variances* (the name is carried over from [67]), where variances of the approximation errors in the current and previous steps are compared. The *Test for Equal Variances* is a hypothesis test where the hypothesis that two variances are equal is taken as a null hypothesis. In oder to reject the null hypothesis the difference between two compared variances with certain degrees of freedom and a level of significance should be significant. A probability of rejecting null hypothesis when it is true is called a level of significance or α risk. The null hypothesis can be tested provided that the approximation errors are normally distributed in each step of the regression. F-distribution is used for hypothesis testing of equal variances. The process is stopped if a corresponding variance and a variance of measurement noise are approximately the same or all the terms are used up.
Step-wise regression is defined as a data-driven automatic variable selection scheme, which is efficient for processing of small data sets isolated from each other. Moreover, recursive algorithm developed in this Chapter allows calculation of a parameter vector using values of the parameters in the previous step, making the method computationally efficient and implementable.

The contributions of this Chapter are the following: 1) New algorithms for real-time estimation of the engine friction torque. Engine friction torque is estimated at the fuel cut off state and at engine idle, 2) New recursive and computationally efficient data-driven algorithms for adaptation of look-up tables.

A Volvo passenger car equipped with a six cylinder prototype engine was used in the experiments. Algorithms are implemented in MATLAB and applied to the measured data collected from the experimental vehicle.

6.2 Estimation of Engine Losses During Fuel Cut Off State

6.2.1 Problem Statement

In general, the elapsed time between two teeth on a crankwheel is measured in production engines. The high resolution engine speed signal is then calculated as a ratio of the length of the angular segment on the crankwheel and the passage time for this segment.

The combustion state of the given cylinder is defined via the amplitude of the engine speed signal. The amplitude which is associated with the cylinder, whose power stroke occurs in the corresponding time interval, in turn is defined as the difference between maximal and minimal values of the high resolution engine speed signal. Here and below, a non-standard definition is used, and under the term 'amplitude' the difference between maximal and minimal

values is understood. This amplitude, which is the measure of the crankwheel speed perturbations induced by the periodic impulsive cylinder individual torque contributions, provides a method for estimation of the engine torque [23], [72], [86]. The same amplitude for the cylinder whose expansion stroke occurs in the interval depends on a compression pressure, a friction force and the viscosity of a lubricating oil only when the engine is not fueled, providing a method for estimation of the engine losses. Notice that the accuracy of the estimation of the engine losses via the amplitude when the engine is not fueled is better than the accuracy of the torque estimation via the same amplitude when the engine is fueled. This is due to the fact that the expansion stroke of the given cylinder is driven by the compression pressure only when the engine is not fueled, and the variations of the amplitude do not depend on the variations of the combustion pressure.

Figure 6.1 shows the harmonics of the engine speed signal, when the engine is not fueled, at 2000 rpm and 3500 rpm calculated by the Discrete Fourier Transform (DFT) method. Figure 6.1 shows that the engine speed signal at low rotational speeds has a dominating component which corresponds to the engine frequency (the sixth harmonic). The engine speed signal at high rotational speeds has fluctuations which occur as a consequence of the engine events (expansion events driven by the compression pressure), low frequency oscillations from the powertrain as well as high frequency oscillations due to the crankshaft torsion. The high frequency oscillations due to the crankshaft twist and low frequency oscillations from the powertrain could be greater than the oscillations induced by the engine events. Notice that the input sequence was sampled with the step of 30^o CA (Crank Angle) which is a relative low rate sampling. At this rate the high order harmonic components could be aliased within a lower frequency range. However, the fluctuations which correspond to engine events can still be recovered from the noise contaminated measurements even with such a relatively low sampling rate.
Computationally efficient algorithms which recover the engine speed fluctuations corresponding to engine events from the noise contaminated measurements of the engine speed, when the engine is not fueled, are described below.

6.2.2 Filtering Technique

Assuming that there is a set of the Crank Angle (CA) synchronized engine speed data ω_k, $k = 1, 2...$, measured at the following points $x_k = k\Delta$ where Δ is a step size. The measured signal ω_k can be approximated by the following trigonometric polynomial:

$$\hat{\omega}_k = a_{0k} + \sum_{q=1}^{n} (a_{qk} cos(qx_k) + b_{qk} sin(qx_k)), \tag{6.1}$$

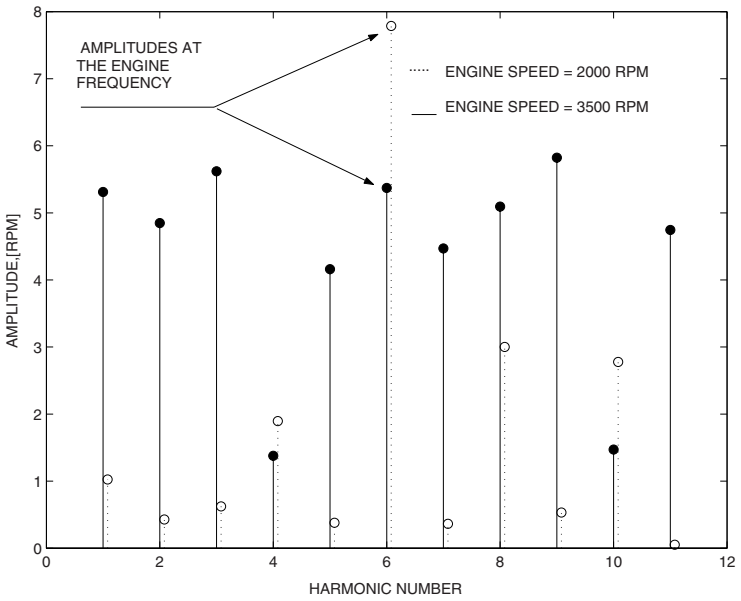

FIG 6.1. Harmonic contents of the engine speed signal at 2000 rpm and 3500 rpm are computed via the DFT method. The input sequence is sampled with the step of 30^o. The data is acquired over 720^o window. The engine is not fueled. The measurements are made on the experimental vehicle on the chassis rolls. Amplitudes are plotted as a function of the harmonic number of the signal with the period of 720 CA degrees. The harmonic number is defined as an integer which is equal to the ratio of two periods, $n_h = \frac{720^o}{T_h}$, where T_h is the period of the harmonic. The engine is operating at full load. Amplitudes at 2000 rpm are plotted with dotted line and amplitudes at 3500 rpm are plotted with solid line.

where $q = 1, 2, ..., n$ is the frequency. Equation (6.1) plays a role of a model, which has to match the measured data ω_k. Assume that the measured variable ω_k can be presented as follows:

$$\omega_k = a_{0*} + \sum_{q=1}^{n} (a_{q*} cos(qx_k) + b_{q*} sin(qx_k)), \tag{6.2}$$

where a_{0*}, a_{q*} b_{q*} are constant unknown parameters. In other words, it is assumed that the measured signal ω_k can be approximated by the trigonometric polynomial with known frequencies and unknown amplitudes.

The equations (6.1) and (6.2) can be written in the following form:

$$\hat{\omega}_k = \psi_k^T \vartheta_k, \tag{6.3}$$

$$\omega_k = \psi_k^T \vartheta_*, \tag{6.4}$$

where ϑ_k and ϑ_* are the vectors of the adjustable and true parameters respectively:

$$\vartheta_k^T = [a_{0k} \quad a_{1k} \quad b_{1k} \quad a_{2k} \quad b_{2k}, ..., a_{nk} \quad b_{nk}], \tag{6.5}$$
$$\vartheta_*^T = [a_{0*} \quad a_{1*} \quad b_{1*} \quad a_{2*} \quad b_{2*}, ..., a_{n*} \quad b_{n*}], \tag{6.6}$$

and

$$\psi_k^T = [1 \quad cos(x_k) \quad sin(x_k) \quad cos(2x_k) \\ sin(2x_k), ..., cos(nx_k) \quad sin(nx_k)] \tag{6.7}$$

is the regressor. Notice, that the regressor ψ includes n distinct frequencies and hence it is sufficiently rich for identification of $2n$ parameters of the signal (6.2).
The estimation problem can be stated as follows: *to find the update law ϑ_k, such that the following equality holds at each step*

$$\omega_k = \hat{\omega}_k \tag{6.8}$$

and the vector of the adjustable parameters ϑ_k converges to the vector of true parameters ϑ_*. Then, the engine speed signal ω_k can fully be reconstructed by the polynomial (6.1). The components of the polynomial (6.1) which describe engine events can be used for the engine losses estimation.

This problem is solved using a Kacmarz projection algorithm described in Section 4.4.

Figure 6.2 shows the result of the filtering on a engine event frequency. The engine speed signal is filtered by the filter (4.39) described in Section 4.4. The engine is operating at 5500 rpm. It can be seen that the amplitude information is recovered on the signal which is filtered by the filter (4.39).

The amplitude of the high resolution engine speed signal filtered at the engine firing frequency is correlated to engine losses (friction and pump losses). Wearing of the engine components over time affects the amplitude of the engine speed variations via friction forces on the piston assembly and piston acceleration, providing a method for a friction torque sensing. Amplitude of the engine speed variations is averaged over a certain number of engine events with the purpose of improvement of the signal quality, and correlated to the engine losses at every rotational speed (see Figure 6.3). Figure 6.4 shows engine losses as a function of average amplitude and rotational speed.

Notice that a fuel cut-off results in de-acceleration that is a transient of the engine speed to the idle speed. A transient component of the engine speed should be removed (see for example a compensation technique described in Section 4.3.2) when estimating a friction torque via the crankshaft speed fluctuations.

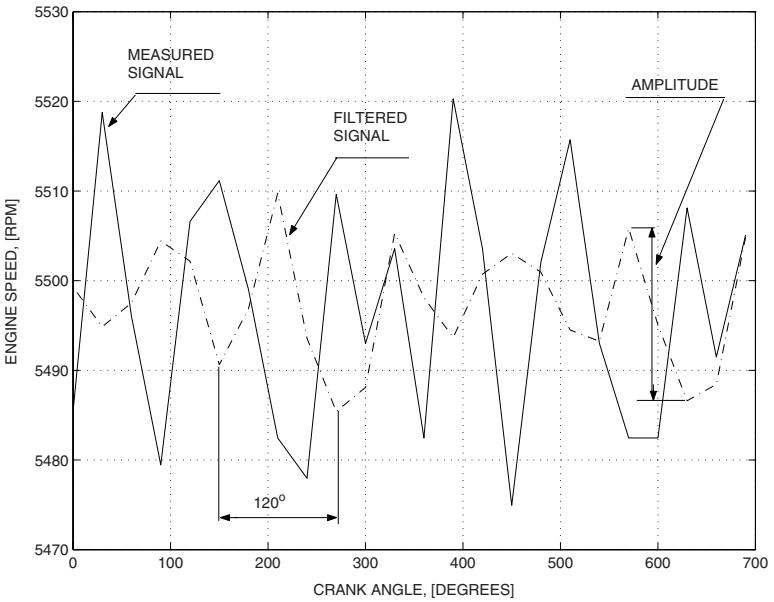

FIG 6.2. Measurements with the step of 30 CA degrees on the six cylinder prototype engine. A single engine cycle is plotted. The engine speed is plotted with the solid line. Relative load is 100%. The engine is not fueled. Filtered signal corresponding to the engine (firing) frequency is plotted with dashdot line.

6.3 Adaptation of the Friction Torque Look-up Table

6.3.1 Description of Adaptation Algorithm for Look-up Tables

Suppose that there is a look-up table describing a variable z as a function of two variables x and y. The look-up table is presented as a number of nodes (x_h, y_l) , $h = 1, ...D$, $l = 1, ..., G$, where the output variable $z_{h,l}$ is defined. The values of the variable z between the nodes are computed via a linear interpolation. The problem of adaptation of the look-up table is reduced to calculation of an additive compensation term which is based on a polynomial approximation of the difference between new measured values of the operating parameter and values of the parameter calculated from the look-up table. As soon as this compensation term is calculated it is resided in the memory of the control unit in the form of the coefficients of the polynomial or added to the nodes $z_{h,l}$ of the look-up table.

Assuming, new measured data x_{im}, y_{im}, z_{im} with the weighting factor w_{im} is available, where $i = 1, ..., N$. The difference between a value of the parameter z_i calculated via a look-up table and new measured value of the parameter z_{im} is $\varepsilon_i = z_i - z_{im}$. Assume that ε can be approximated with a linear (with respect to parameters) function of two variables, i.e.,

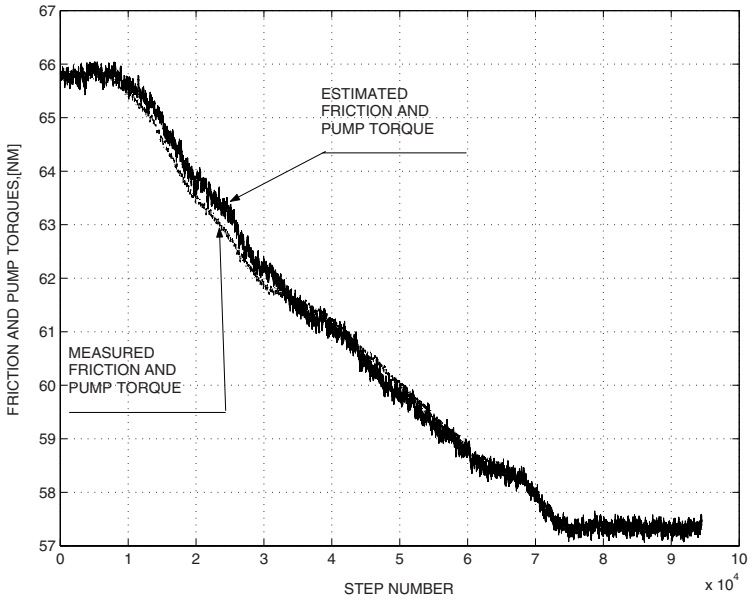

FIG 6.3. Estimated friction and pump torque and measured friction and pump torque are plotted as functions of a step number. Each step is 30 CA degrees. Engine speed is 5500 [rpm]. The engine is not fueled. Measured engine friction and pump torque is plotted with dash dotted line. Estimated torque is plotted with solid line.

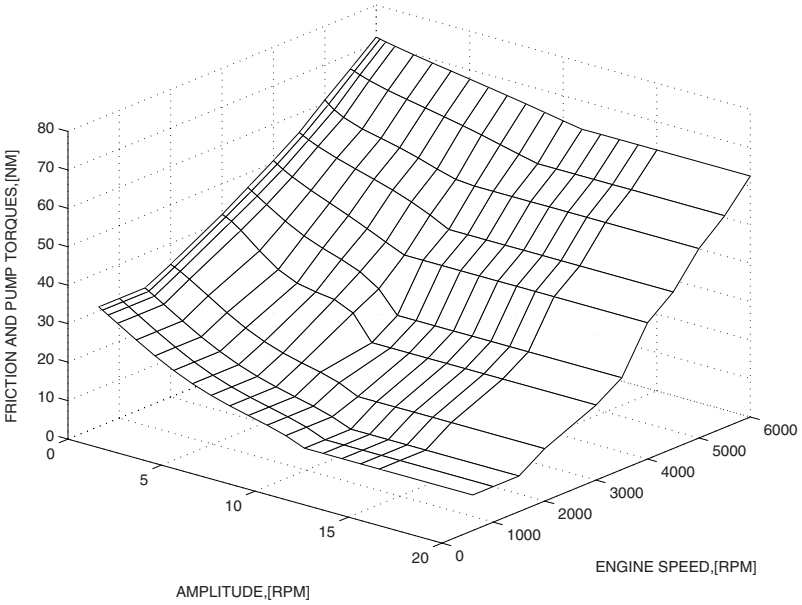

FIG 6.4. Engine losses as a function of average amplitude and rotational speed.

$$\hat{\varepsilon} = \varphi^T \theta \tag{6.9}$$

where

$$\begin{aligned} \varphi &= [1 \;\; y \;\; x \;\; y^2 \;\; y^3 \;\; ...]^T \\ \theta &= [a_0 \;\; a_1 \;\; a_2 \;\; ...]^T \end{aligned} \tag{6.10}$$

where $\hat{\varepsilon}$ is an estimate of ε. Step-wise regression examines the following sequence of new terms which are added in the model in each step: θ_1, $\varphi_2^T\theta_2, ...$ where $\theta_1 = a_0$, $\varphi_2^T = [1 \;\; y]$ and $\theta_2 = [a_0 \;\; a_1]^T$. The parameters θ_k, $k = 1, ...,$ are calculated by using a least-squares algorithm minimizing the difference between ε and $\hat{\varepsilon}$ in each step . Suppose that the term $\varphi_k^T\theta_k$, $k = 2, ...$ is examined as a candidate for inclusion in the model. The contribution of this term is determined by calculating the following variances in steps $k-1$ and k:

$$\begin{aligned} V_k = \frac{1}{(N-k)} \sum_{i=1}^{N} (\varepsilon_i - (\theta_1 + \varphi_{2i}^T\theta_2 + ... \\ + \varphi_{ki}^T\theta_k))^2 w_{im} \end{aligned} \tag{6.11}$$

$$\begin{aligned} V_{k-1} = \frac{1}{(N-(k-1))} \sum_{i=1}^{N} (\varepsilon_i - (\theta_1 + \varphi_{2i}^T\theta_2 + ... \\ + \varphi_{(k-1)i}^T\theta_{k-1}))^2 w_{im} \end{aligned} \tag{6.12}$$

The decision is based on a comparison of variances V_{k-1} and V_k. In order to include new term $\varphi_k^T\theta_k$, the variance V_k should be significantly less than the variance V_{k-1}. The *Test for Equal Variances* is a hypothesis test where the hypothesis that two variances V_{k-1} and V_k are equal is taken as a null hypothesis ($H_0 : V_{k-1} = V_k$). In order to reject the null hypothesis H_0 the difference between V_{k-1} and V_k with degrees of freedom $f_{k-1} = N-(k-1)$ and $f_k = N-k$, and a level of significance α should be significant. Reduction of the variance is statistically significant if the following inequality is valid:

$$\frac{V_{k-1}}{V_k} > F_{\alpha, f_{k-1}, f_k} \tag{6.13}$$

where a number F_{α, f_{k-1}, f_k} is taken from 'F-distribution' look-up table ([64], pages 716-720) for degrees of freedom $f_{k-1} = N-(k-1)$ and $f_k = N-k$, and a significance level α, which is chosen beforehand. If inequality (6.13) is valid, then the term $\varphi_k^T\theta_k$ is included in the model.
The method described above is able to reject a certain term, however, instead of this term, another term might significantly reduce an approximation error. The process is stopped if a corresponding variance and a variance of a measurement noise are approximately the same or all the variables are used up.

The order of the variables in φ plays an important role, since it decides the test sequence of new candidate terms which should be included in the model. Correct sequence of candidates minimizes a computational burden. If a number of measured points is sufficiently large, then the number of constraints (the number of constraints is equal to a number of coefficients in model (6.9)) is negligible. In real-time applications, where the number of measured points is not large each additional constraint has a significant impact on a variance. Therefore, it is advisable to reduce the number of the coefficients of approximating polynomial by taking into account physical dependencies via re-parametrization.

A parameter vector θ_k can be calculated recursively via a parameter vector θ_{k-1}. The parameter vector θ_k which is calculated according to the least-squares algorithm is the following:

$$\theta_k = [\sum_{i=1}^{N}(\varphi_{ki}\varphi_{ki}^T w_{im})]^{-1}\sum_{i=1}^{N}(\varepsilon_i - (\theta_1 + \varphi_{2i}^T\theta_2 + ... \\ +\varphi_{(k-1)i}^T\theta_{k-1}))\varphi_{ki}w_{im} \tag{6.14}$$

where $\varphi_k = [\varphi_{k-1}\varphi(k)]^T$, $\theta_k = [\theta_{k-1}\theta(k)]^T$, φ_{k-1} ,$\theta_{k-1} \in R^{k-1}$, $\varphi(k)$, $\theta(k) \in R^1$. Algorithm (6.14) minimizes the following performance index:

$$S_k = \sum_{i=1}^{N}(\varepsilon_i - (\theta_1 + \varphi_{2i}^T\theta_2 + ... \\ + \varphi_{ki}^T\theta_k))^2 w_{im} \tag{6.15}$$

where S_k is the sum of the squares of the residuals.

Parameter vector θ_{k-1} is defined as follows:

$$\theta_{k-1} = [\sum_{i=1}^{N}(\varphi_{(k-1)i}\varphi_{(k-1)i}^T w_{im})]^{-1}\sum_{i=1}^{N}(\varepsilon_i - (\theta_1 + ... \\ +\varphi_{(k-2)i}^T\theta_{k-2}))\varphi_{(k-1)i}w_{im} \tag{6.16}$$

Straightforward calculations show that θ_k is calculated via θ_{k-1} as follows:

$$\theta_k = \begin{bmatrix} \theta_{k-1} + \dfrac{A_{k-1}^{-1}vv^T\theta_{k-1}}{\beta} \\ -\dfrac{v^T}{\beta}\theta_{k-1} - \dfrac{v^T A_{k-1}^{-1}\delta b}{\beta} \end{bmatrix} + \\ + \begin{bmatrix} [A_{k-1}^{-1} + \dfrac{A_{k-1}^{-1}vv^T A_{k-1}^{-1}}{\beta}]\delta b - \dfrac{A_{k-1}^{-1}vb_1}{\beta} \\ \dfrac{b_1}{\beta} \end{bmatrix}$$

where A_{k-1}^{-1} is $(k-1) \times (k-1)$ matrix, $v \in R^{k-1}$,$\delta b \in R^{k-1}$, $\beta \in R^1$, $b_1 \in R^1$ are defined as follows:

$$A_{k-1} = \sum_{i=1}^{N} [\varphi_{k-1}\varphi_{k-1}^T] w_{im}, \quad v = \sum_{i=1}^{N} \varphi_{k-1}\varphi(k) w_{im}$$

$$a = \sum_{i=1}^{N} \varphi^2(k) w_{im}$$

$$b_1 = \sum_{i=1}^{N} (\varepsilon_i - (\theta_1 + \varphi_2^T\theta_2 + ... + \varphi_{k-2}^T\theta_{k-2} + \varphi_{k-1}^T\theta_{k-1})\varphi(k) w_{im}$$

$$\delta b = -\sum_{i=1}^{N} (\varphi_{k-1}^T\theta_{k-1}\varphi_{k-1}) w_{im}, \beta = a - v^T A_{k-1}^{-1} v$$

Matrix A_k^{-1} is computed via A_{k-1}^{-1} according to the following formula:

$$A_k^{-1} = \begin{bmatrix} A_{k-1}^{-1} + \dfrac{A_{k-1}^{-1} v v^T A_{k-1}^{-1}}{\beta} & -\dfrac{A_{k-1}^{-1} v}{\beta} \\ -\dfrac{v^T}{\beta} A_{k-1} & \dfrac{1}{\beta} \end{bmatrix}$$

6.3.2 Adaptation Algorithm for Engine Friction Look-up Table

Problem Statement

Suppose that there is a set of measurements of the engine friction torque obtained during engine fuel cut off state and during engine idle. Figure 6.5 shows pre-calibrated engine friction torque as a function of engine speed and indicated engine torque. Measured values of the engine friction torque during fuel cut-off state are shown with plus signs. The value of the engine friction torque obtained during idle is shown with a circle sign added.

Adaptation algorithms described above are applied for adaptation of the engine friction look-up table. In this case an operating parameter z is engine friction torque which is a function of two variables; i.e., engine speed y, and indicated engine torque x. As can be seen from Figure 6.5, new values of estimated engine friction torque obtained during fuel cut off state are available at high rotational speeds (the fuel cut off is usually activated at high speeds only) and zero indicated torque. Estimation of the friction torque at idle gives new measured value of the friction torque at low speed and indicated torque. Therefore, an offset and gradient in the engine speed direction can be estimated by using new measured values of the engine friction torque. Adaptation algorithms are divided in two steps. In a first step, the offset

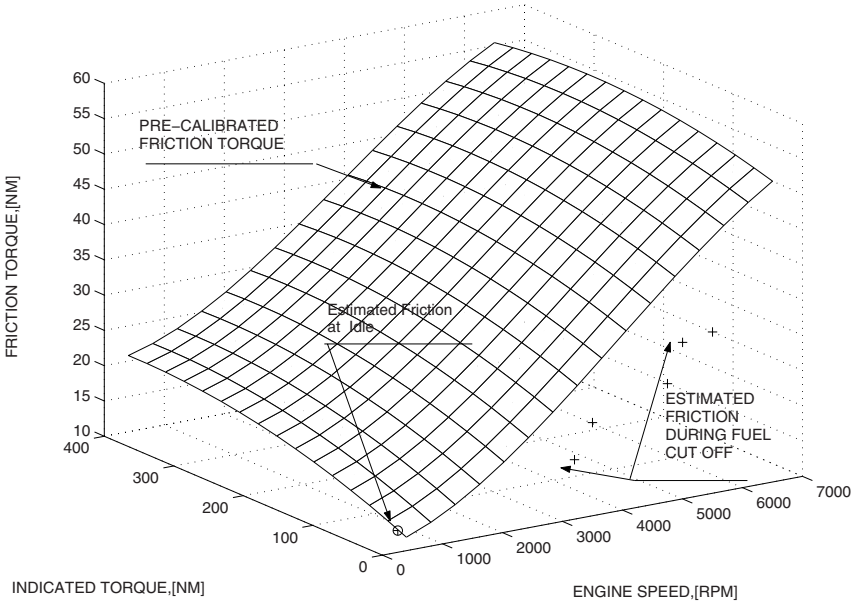

FIG 6.5. Pre-calibrated engine friction torque as a function of engine speed and indicated engine torque. Measured values of the engine friction torque during fuel cut off state are shown with plus signs. The value of the engine friction torque obtained during idle is shown with a circle sign added.

parameter θ_1 is computed by using a least-squares algorithm $\theta_1 = -9.9 \ [Nm]$. A corresponding variance is $V_1 = 16.65 \ \ [Nm]^2$. In a second step the term $a_1 y$ is tested as a candidate term for inclusion in the model (6.9). Parameter vector is defined as follows $\theta_2 = [a_0 \ \ a_1]^T$ and $\varphi_2 = [1 \ \ y]^T$. Parameter vector θ_2 is computed according to (6.14). Then $a_0 = 7.98 \ \ [Nm]$ and $a_1 = -2.12 \ \ [\frac{Nm}{rpm}]$. Variance V_2 is the following $V_2 = 3.27 \ \ \ [Nm]^2$. Ratio $\frac{V_1}{V_2} = 5.09$ should be compared with the F - value, which is equal to 4.05 for degrees of freedom $f_1 = 5$ and $f_2 = 4$, and significance level $\alpha = 0.1$ (see [64], page 717). Since the following inequality is valid $\frac{V_1}{V_2} > F_{\alpha, f_{k-1}, f_k}$, the term $\varphi_2^T \theta_2$ is included in the model. In this step the process should be stopped since the variance $V_2 = 3.27 \ \ \ [Nm]^2$ is close to the variance of the measurement noise $\sigma^2 = 2.37$ $[Nm]^2$. The closeness of two variances V_2 and σ^2 can again be verified via the *Test for Equal Variances* for a certain significance level and degrees of freedom $f_2 = 4$ and $f_{\sigma^2} = \infty$, where it is assumed that the variance of the measurement noise σ^2 is known from a relatively large number of previous observations and the degrees of freedom of the variance of the measurement noise f_{σ^2} is infinity.

Finally, the model has the following form $\hat{\varepsilon} = \theta_1 + \varphi_2^T \theta_2 = -9.9 + (7.98 - 2.12y)$. The result of adaptation is shown in Figure 6.6.

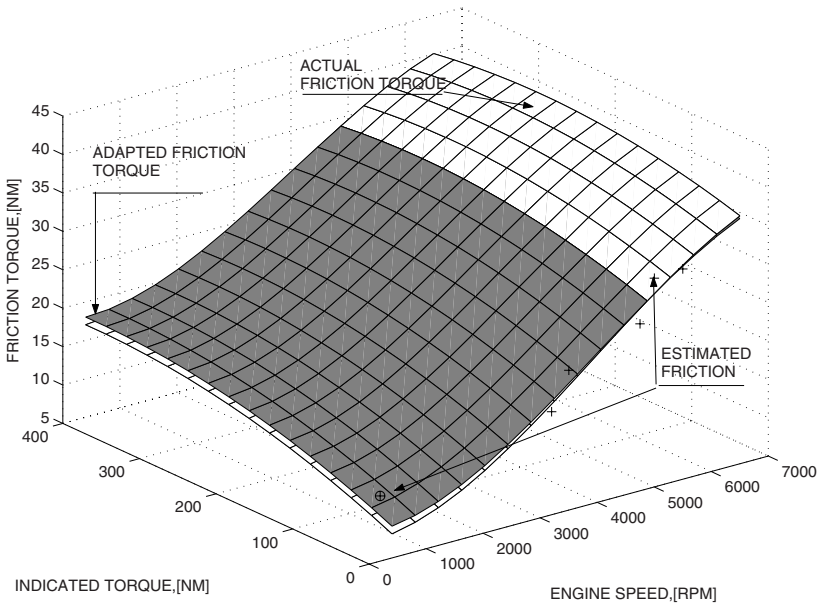

FIG 6.6. Actual engine friction torque as a function of engine speed and indicated engine torque is plotted as white surface. Adapted friction torque is plotted as gray surface. Measured values of the engine friction torque obtained during fuel cut off state are shown with plus signs. The value of the engine friction torque obtained during idle is shown with a circle sign added.

6.4 Conclusion

New algorithms for real-time estimation of the engine friction torque are developed. Engine friction torque is estimated at the fuel cut off state and at engine idle. New recursive and computationally efficient data-driven algorithms are developed for adaptation of the look-up tables. The algorithms make it possible to avoid driveability problems that could result from errors in estimating engine friction torque.

7

Statistical Engine Misfire Detection

New recursive filtering algorithms for misfire detection based on the trigonometric interpolation method are proposed for spark ignition automotive engines. The technique improves the performance of the filtering algorithms allowing a flexible choice of the size of the moving window. Correction algorithms are introduced for the recursive trigonometric interpolation method that ensure the robustness with respect to round-off errors which are present in the finite precision implementation environment. New real-time statistical algorithms based on a hypothesis testing for a misfire detection are proposed. Statistical decision making mechanism allows to make a misfire detection with a certain significance level with automatically selected sample size depending on the signal quality that in turn improves the robustness of the misfire detection functionality.

7.1 Introduction

Misfire is the state of an engine where the combustion does not occur due to the errors in fueling or ignition. As a consequence, such misfires affect long term performance of the exhaust emission control system. The misfiries cause changes in the crankshaft rate of rotation, because the misfired cylinder is not able to provide the torque. Engine misfire diagnostic functions are based on monitoring of the cylinder individual fluctuations of the high resolution engine speed signal or a passage time between subsequent teeth on a crankwheel. The high resolution engine speed signal is calculated as a ratio of the length of the angular segment on the crankwheel and the passage time for this segment (see Chapter 4). The passage time becomes less as the rotational speed rises, thereby time interval errors rise. Moreover, low frequency oscillations from the powertrain and high frequency oscillations due to the crankshaft torsion, together with vibrations induced by the road, act as disturbances on the crankshaft. These disturbances influence directly the performance of the

A.A. Stotsky, *Automotive Engines*, DOI 10.1007/978-3-642-00164-2_7,

engine speed signal and consequently the torque monitoring and misfire diagnostic functions. Recursive DFT (Discrete Fourier Transformation) method in the window of a certain size w moving in time can be used for filtering at the engine firing frequency [73],[86]. However, the orthogonality condition for the trigonometric polynomials in certain interval is the main restriction to the approximation performance and hence to the application of the DFT method. This is turn imposes restrictions on the window size w. If the orthogonality condition is violated, then the implementation of the DFT method (in this case a better name is a trigonometric interpolation method) requires a matrix inversion, as it is usual for least-squares fitting, and this in turn, makes the method computationally expensive. Algorithms described in this Chapter allow to make a trigonometric interpolation of the engine speed data for any window size. This is turn allows to improve the performance of the misfire diagnostic function. Recursive and computationally efficient version of the trigonometric interpolation method is developed.

Limited precision effects might severely deteriorate the performance of the recursive trigonometric interpolation method. The accumulation of round-off errors in a finite precision engine control implementation environment limits the trigonometric interpolation and hence the misfire detection performance. In this Chapter the correction algorithms are proposed for correction of the estimates obtained by the recursive trigonometric interpolation method.

The misfire detection approach proposed in this Chapter is based on a monitoring of the amplitudes at two frequencies. The first one is the engine firing frequency. The second amplitude is the amplitude of the component of the engine speed with a period of 720^o. Since the misfiring cylinder is active every 720^o of the crankshaft rotation a torque drop associated with the misfire occurs every 720^o generating a component of the engine speed with a period of 720^o. A torque behaviour associated with the misfire occurs once every two cycles of crankshaft rotation or one-half cycles per crankshaft revolution. This is typically referred as a half-order behaviour and the component of the engine speed with the period of 720^o is referred as a half engine order component. The location of the minimum of this component on the engine cycle shows which cylinder is misfiring. For example, the firing sequence of the six cylinder prototype engine is the following 1-5-3-6-2-4. Figure 7.1 shows two misfires instead of two neighboring combustions, i.e., in the first and fifth cylinders. Here and below a single misfire is introduced by cutting a fuel continuously to one of the engine cylinders. This situation corresponds to persistent errors in the fuel injection or ignition system. Figure 7.1 shows that the misfires can be detected by monitoring both amplitude at the engine combustion frequency and amplitude at the half-order frequency (half-order harmonic), whereby the phase of the half-order frequency component shows which cylinder is misfiring. Here and below, an unusual definition is used, and under the term 'amplitude' the difference between maximal and minimal values is understood.

The amplitudes are hypothesis tested for a misfire detection. *One Sample T-test* (the name is carried over from [67]) which compares the average value

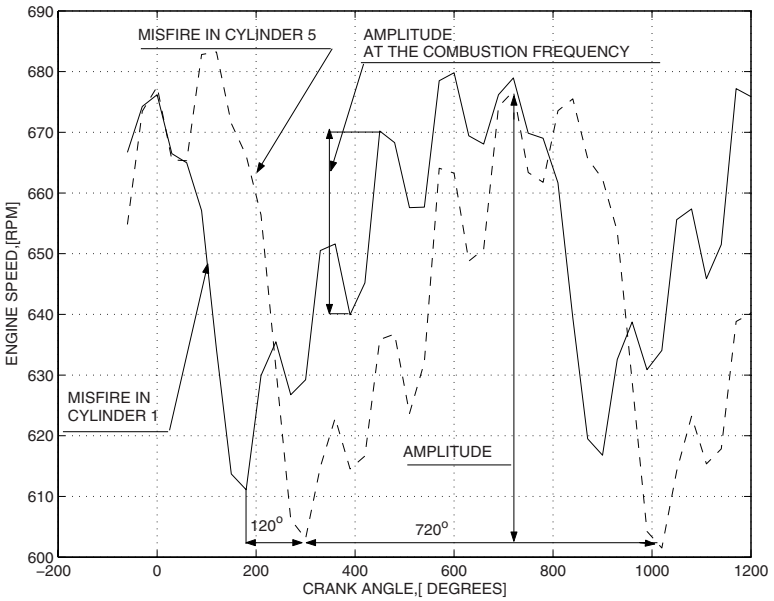

FIG 7.1. Two engine cycles are plotted in the events of a misfire in the fisrt and fifth cylinders. Engine is operating at idle. Engine speed signal in the event of a misfire in the first cylinder is plotted with a solid line. Engine speed signal in the event of a misfire in the fifth cylinder is plotted with a dashed line.

of the amplitude to the target value is used for a misfire detection at the combustion frequency. Hypotheses tests used in this book are also described in Appendix. *Two Sample T-test* which compares the average values of the largest and the next largest amplitudes at the half-order frequency is used for a misfire detection at the half-order frequency. The algorithm is divided into two steps in both cases. In the first step the hypotheses are tested at each step of the moving window of a minimal size, where the value of $t - statistic$ is compared with the value in the Student distribution look-up table for the degrees of freedom corresponding to the minimal size of the window. The window is defined here in terms of a number of engine cycles. If the value of $t - statistic$ is larger than the value in the Student distribution look-up table the null hypotheses are rejected detecting a misfire. If the value of $t - statistic$ is less than the value in the Student distribution look-up table then window size is increased until the value of $t - statistic$ is larger than the value in the Student distribution look-up table or the window size reaches its maximal value. To this end the next step is taken. Since both $t - statistic$ and the values in the Student distribution look-up table depend on the size of the moving window the values in the Student distribution look-up table for a certain significance level are approximated by a polynomial of a certain order. The equation for $t - statistic$ which is equal to the polynomial approximation

of the Student distribution look-up table is solved with respect to the window size, indicating the minimal window size for which the hypotheses can be tested and a misfire can be detected. This approach allows a reliable misfire detection for amplitude signals of different quality (for example for new and aged engine) via a proper selection of the window size (degrees of freedom).

A Volvo passenger car equipped with a six cylinder prototype engine was used in the experiments. Algorithms are implemented in MATLAB and applied to the measured data collected from the experimental vehicle.

The contributions of this Chapter can be summarized as follows: a) new recursive filtering algorithms for misfire detection based on the trigonometric interpolation method, b) new statistical algorithms based on a hypothesis testing for a misfire detection.

7.2 Recursive Trigonometric Interpolation Algorithms

7.2.1 Problem Statement

Suppose that there is a set of the crank angle synchronized measurements of the engine speed ω_k, $k = 1, 2...$, measured at the following points $x_k = k\Delta$, where Δ is a step size. Suppose that the engine speed signal can exactly be approximated by the trigonometric polynomial as follows:

$$\hat{\omega}_k = \varphi_k^T \theta_k, \tag{7.1}$$

$$\theta_k^T = [a_{0k} \quad a_{q1k} \quad b_{q1k} \quad a_{q2k} \quad b_{q2k}, \\ ..., a_{qnk} \quad b_{qnk}], \tag{7.2}$$

$$\varphi_k^T = [1 \quad cos(q_1 x_k) \quad sin(q_1 x_k) \quad cos(q_2 x_k) \\ sin(q_2 x_k), ..., cos(q_n x_k) \quad sin(q_n x_k)] \tag{7.3}$$

where θ_k is the vector of the adjustable parameters and φ_k is the regressor, $q = q_1, ..., q_n$ are the frequencies, a_{0k}, a_{qk} and b_{qk} are the coefficients which should be found, $\hat{\omega}_k$ is the estimate of the engine speed ω_k. Assume that measured engine speed signal can be presented as follows:

$$\omega_k = \varphi_k^T \theta_*, \tag{7.4}$$

where θ_* is the vector of true parameters,

$$\theta_*^T = [a_{0*} \quad a_{q1*} \quad b_{q1*} \quad a_{q2*} \quad b_{q2*}, ..., a_{qn*} \quad b_{qn*}], \tag{7.5}$$

and a_{0*}, a_{q*} and b_{q*} are constant unknown coefficients.

Introducing a moving window of a size w the measured engine speed signal ω_k is approximated by (7.1) in the least squares sense. The idea of the window moving in time is illustrated in Figure 7.2 which shows a single engine cycle

with a misfire in the first cylinder. The window is, in fact, the system of the local coordinates X_L, Y_L which is moving in time. Notice that a set of trigonometric functions defined in (7.3) is not orthogonal in this case since the size of the moving window is $w = 20$.

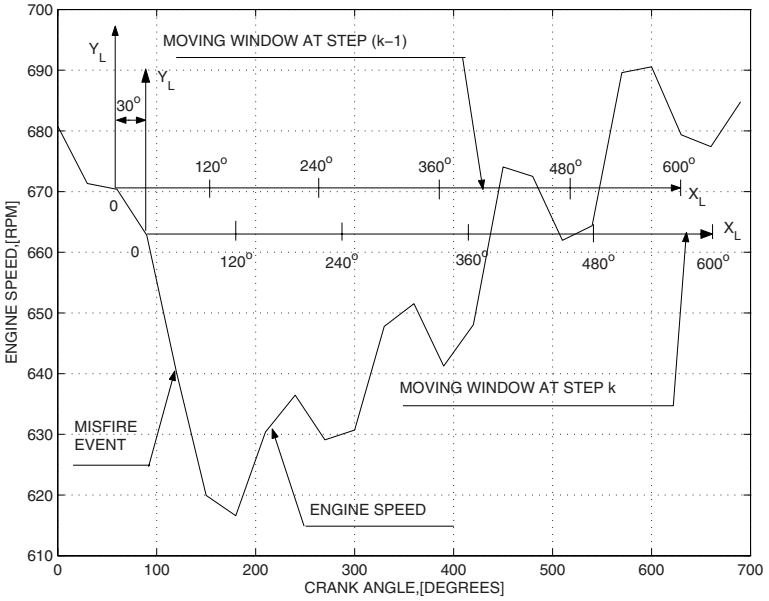

FIG 7.2. Measurements with a step of 30^o on six cylinder prototype engine. Misfire is generated in the first cylinder. The engine speed is plotted with a solid line. The engine is operating at idle. A window of a size $w = 20$ moving in time is defined in the form of local coordinates X_L and Y_L.

The error to be minimized at every step is as follows:

$$E_k = \sum_{i=k-(w-1)}^{i=k} (\omega_i - \hat{\omega}_i)^2, \qquad k \geq w \tag{7.6}$$

7.2.2 Recursive Algorithms for Trigonometric Interpolation

The vector of adjustable parameters θ_k at step k which minimizes the performance index (7.6) can be calculated as follows:

$$\theta_k = [\sum_{i=k-(w-1)}^{i=k} \varphi_i \varphi_i^T]^{-1} \sum_{i=k-(w-1)}^{i=k} \varphi_i \omega_i \tag{7.7}$$

Notice that, if the orthogonality condition for trigonometric polynomials is satisfied for a certain window size the matrix $\sum_{i=k-(w-1)}^{i=k} \varphi_i \varphi_i^T$ becomes a diagonal matrix. This matrix is easily invertable and the vector of adjustable parameters θ_k is the vector of the Fourier coefficients (see Section 4.3). Therefore, the DFT method can be seen as a special case of the trigonometric interpolation method described below.

The vector of adjustable parameters at step $k-1$ of the moving window can be computed as follows:

$$\theta_{k-1} = [\sum_{i=k-w}^{i=k-1} \varphi_i \varphi_i^T]^{-1} \sum_{i=k-w}^{i=k-1} \varphi_i \omega_i \tag{7.8}$$

In step k of the moving window new data ω_k, φ_k enters the window and ω_{k-w}, φ_{k-w} leaves the window.

The vector of adjustable parameters θ_k can be presented as follows:

$$\begin{aligned} \theta_k = &[(\sum_{i=k-w}^{i=k-1} \varphi_i \varphi_i^T) - \varphi_{k-w}\varphi_{k-w}^T + \varphi_k \varphi_k^T]^{-1} \\ &[(\sum_{i=k-w}^{i=k-1} \varphi_i \omega_i) + \varphi_k \omega_k - \varphi_{k-w}\omega_{k-w}] \end{aligned} \tag{7.9}$$

Application of the matrix inversion relation to (7.9) shows that the vector of the adjustable parameters at step k can be computed via the vector of adjustable parameters at step $k-1$ as follows:

$$\begin{aligned} \theta_{rk} = &(I - \frac{A_{k-1}\varphi_k \varphi_k^T}{1 + \varphi_k^T A_{k-1}\varphi_k}) \\ &(\theta_{r(k-1)} + \frac{\Gamma_{k-1}\varphi_{k-w}\varphi_{k-w}^T \theta_{r(k-1)}}{1 - \varphi_{k-w}^T \Gamma_{k-1}\varphi_{k-w}}) \\ &+\Gamma_k(\varphi_k \omega_k - \varphi_{k-w}\omega_{k-w}) \end{aligned} \tag{7.10}$$

where

$$\Gamma_k = A_{k-1}(I - \frac{\varphi_k \varphi_k^T A_{k-1}}{1 + \varphi_k^T A_{k-1}\varphi_k}) \tag{7.11}$$

$$A_{k-1} = \Gamma_{k-1}(I + \frac{\varphi_{k-w}\varphi_{k-w}^T \Gamma_{k-1}}{1 - \varphi_{k-w}^T \Gamma_{k-1}\varphi_{k-w}}) \tag{7.12}$$

where θ_{rk} is a recursive estimate of the parameter vector θ_k, I is the identity matrix and Γ_{k-1} is a recursive estimate of $[\sum_{i=k-w}^{i=k-1} \varphi_i \varphi_i^T]^{-1}$ and Γ_k is a recursive estimate of $[\sum_{i=k-(w-1)}^{i=k} \varphi_i \varphi_i^T]^{-1}$.
The elements of the regressor φ_i, $i \geq 3$ are recursively calculated via the following Chebyshev's three term recurrence relations (see also Section 4.4):

$$\varphi_i = 2d_q \quad * \quad \varphi_{i-1} - \varphi_{i-2} \tag{7.13}$$

$$\varphi_i^T = [1 \quad cos(q_1 i\Delta) \quad sin(q_1 i\Delta) \quad cos(q_2 i\Delta) \quad sin(q_2 i\Delta), ..., cos(q_n i\Delta) \quad sin(q_n i\Delta)] \tag{7.14}$$

$$d_q^T = [1 \quad cos(q_1\Delta) \quad cos(q_1\Delta) \quad cos(q_2\Delta) \quad cos(q_2\Delta), ..., cos(q_n\Delta) \quad cos(q_n\Delta)] \tag{7.15}$$

where Δ is the sampling step, and '$*$' denotes element-wise vector multiplication, and index i is equal to k, $(i = k)$ and index i is equal to $k - w$, $(i = k - w)$, $k \geq (w + 3)$ for the recursive computations of φ_k and φ_{k-w} respectively in (7.10)-(7.12). For the recursive computations of the regressor over the whole window which are required in the first step of the moving window $k = w$ and for calculations of the approximation error (9.7) the index i is defined as follows $i = k - w + p$, where $p = 3, ..., w$.
Notice that in the absence of round-off errors $\theta_{rk} \equiv \theta_k$. Robustness and correction of the recursive algorithms (7.10), (7.11) with respect to the round-off error accumulation is discussed in the next subsection.

7.2.3 Correction of the Recursive Algorithms for Round-Off Errors

On-board implementation of the recursive trigonometric interpolation algorithms is done in ECU (Engine Control Unit) in the finite precision environment, where round-off errors are recursively accumulated. This makes the recursive trigonometric interpolation algorithm unsuitable for continuous use without correction. Correction algorithms proposed in this subsection use Newton's algorithms for correction of the estimates obtained by recursive trigonometric interpolation method. The parameter vector θ_{rk} and the inverse of the 'information matrix' Γ_k obtained by using the recursive least-squares algorithm (7.10), (7.11) are used as the initial states for the correction algorithms.

Correction of θ_{rk}

Suppose that the recursive algorithm for calculation of θ_{rk} (7.10) accumulated rounding errors so that (7.7) (with θ_{rk} substituted instead of θ_k) is not valid. Consider the following algorithm for correction of θ_{rk}.

$$\theta_{cj} = \theta_{c(j-1)} - \Gamma_k e_{j-1} \tag{7.16}$$

where θ_{cj} is the correction of the parameter vector θ_{rk},
$e_{j-1} = \{ \sum_{i=k-(w-1)}^{i=k} \varphi_i \varphi_i^T \} \quad \theta_{c(j-1)} - \sum_{i=k-(w-1)}^{i=k} \varphi_i \omega_i,\ j = 1, 2, 3...$ with the initial value of $\theta_{c0} = \theta_{rk}$ and Γ_k calculated with (7.11). The estimation error $\tilde{\theta}_{cj} = \theta_{cj} - \theta_k$ where θ_k is defined in (7.7) satisfies the following equation:

$$\tilde{\theta}_{cj} = (I - \Gamma_k [\sum_{i=k-(w-1)}^{i=k} \varphi_i \varphi_i^T]) \tilde{\theta}_{cj-1} \tag{7.17}$$

Notice that Γ_k represents a recursive estimate of $[\sum_{i=k-(w-1)}^{i=k} \varphi_i \varphi_i^T]^{-1}$. In the absence of the rounding errors $\Gamma_k \equiv [\sum_{i=k-(w-1)}^{i=k} \varphi_i \varphi_i^T]^{-1}$, $\tilde{\theta}_{cj} \equiv 0$ and $\theta_{cj} \equiv \theta_k$. Since rounding errors also have an impact on the recursive estimate of Γ_k calculated with (7.11), $\Gamma_k \neq [\sum_{i=k-(w-1)}^{i=k} \varphi_i \varphi_i^T]^{-1}$ and $\tilde{\theta}_{cj} \to 0$ as $j \to \infty$ if the eigenvalues of the following matrix $(I - \Gamma_k [\sum_{i=k-(w-1)}^{i=k} \varphi_i \varphi_i^T])$ are located inside of the unit circle.

Correction of Γ_k

As it was mentioned above rounding errors have also impact on the matrix Γ_k calculated with (7.11). The following iterative method similar to the method described above can also be applied for the correction of the elements of the matrix Γ_k.

$$\Gamma_{cj} = \Gamma_{c(j-1)} + \Gamma_{c(j-1)} F_{j-1} \tag{7.18}$$

where Γ_{cj} is the correction of the matrix Γ_k,
$F_{j-1} = I - [\sum_{i=k-(w-1)}^{i=k} \varphi_i \varphi_i^T] \Gamma_{c(j-1)}$ with the initial condition $\Gamma_{c0} = \Gamma_k$, $j = 1, 2, ...$ Straightforward calculations show that $F_j = F_{j-1}^2$ and hence $F_j =$

$F_0^{2^j}$. If $\| F_0 \| \leq c < 1$, where c is a positive constant, then $\| F_j \| \leq c^{2^j}$. Hence $F_j \to 0$ as $j \to \infty$ and $\Gamma_{cj} \to [\sum_{i=k-(w-1)}^{i=k} \varphi_i \varphi_i^T]^{-1}$ as $j \to \infty$. Properties of this algorithm are described in Appendix C.

7.3 Filtering Technique Based on Trigonometric Interpolation Method

Filtering technique based on the trigonometric interpolation method can be divided in two steps. First, the engine speed is approximated via a trigonometric polynomial (7.1) in a window of a certain size moving in time. The performance of the approximation is determined by the error (7.6). Secondly, the filtered engine speed signal is defined by using two frequencies - combustion frequency and half-order frequency, i.e.,

$$\omega_{fk} = \varphi_{fk}^T \theta_{fk}, \tag{7.19}$$

where θ_{fk} is the vector of the adjustable parameters

$$\theta_{fk}^T = [a_{0k} \quad a_{ck} \quad b_{ck} \quad a_{hk} \quad b_{hk}], \tag{7.20}$$

$$\varphi_k^T = [1 \quad cos(q_c x_k) \quad sin(q_c x_k) \quad cos(q_h x_k) \quad sin(q_h x_k)] \tag{7.21}$$

where ω_{fk} is the filtered engine speed signal, q_c and q_h are the combustion and half-order frequencies respectively.

Figure 7.3 shows measured engine speed signal and filtered engine speed signal with filter (7.19).

7.4 Statistical Misfire Detection Technique

7.4.1 Misfire Detection at the Combustion Frequency

The combustion state of a given cylinder is defined via the amplitude which is computed as a difference between maximal and minimal values of the engine speed for a cylinder whose power stroke occurs in the interval at the combustion frequency. Figure 7.4 shows the plots of the amplitudes for the first and the fifth cylinders, which produce two first combustions on the engine cycle (the firing sequence for a six cylinder engine is $1-5-3-6-2-4$). The misfire is generated in the first cylinder. The misfire can be detected by comparing the amplitude signals to a target value of the amplitude (for example to zero). The differences between the target value and the average values of the amplitudes are indicated as distances to target.

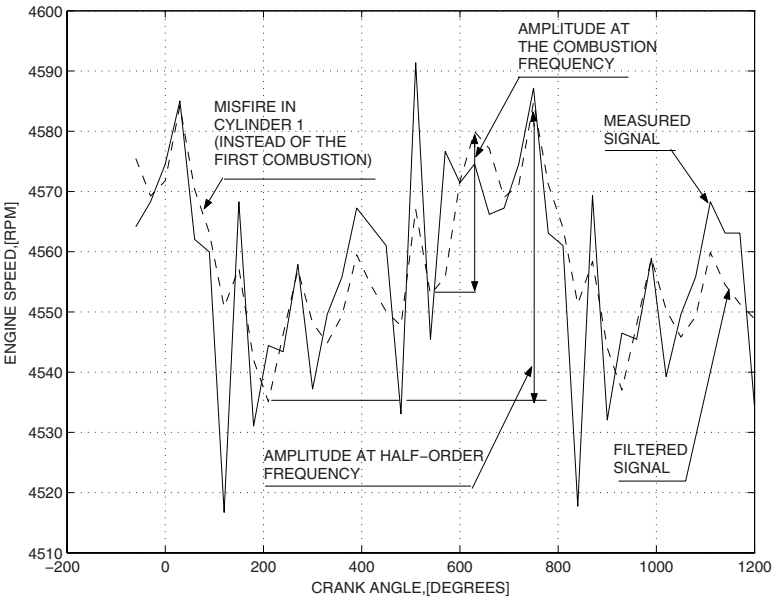

FIG 7.3. Two engine cycles are plotted in the event of a misfire. Engine speed is 4500 [rpm]. Engine is operating at full load. The measurements are made on the experimental vehicle on chassis rolls. The window size is $w = 20$. Measured engine speed signal is plotted with a solid line. Filtered signal with the filter (7.19) is plotted with dashed line.

Figure 7.5 shows the distributions of the amplitude signal for the first cylinder in the event of a misfire in the first cylinder and in the misfire free case. The distributions in both cases are close to normal distributions with good separation between the mean and the target values.

One Sample T-test for Misfire Detection

Suppose that M amplitudes are computed at the combustion frequency as follows $A_i = \omega_{imax} - \omega_{imin}$, where ω_{imax} and ω_{imin} are the maximal and minimal values of the engine speed for cylinder i respectively, $i = 1, ..., M$, where M is the number of engine cylinders (see Figure 7.1).
One Sample T-test is the statistical test for a comparison of a one sample average to a target value. Let A_l be the values of the amplitude to be examined, where l is the cycle number ($l \geq N$), N is the size of a moving window expressed in terms of a number of cycles where the amplitude is examined. Denoting a target value of the amplitude as a_t, (which in fact, is a threshold value) the null hypothesis is $H_0 : \overline{A}_l = a_t$, where $\overline{A}_l$, is the averaged value of the amplitude. Two alternative hypotheses are considered $H_{a1} : \overline{A}_l > a_t$ and $H_{a2} : \overline{A}_l < a_t$. The first alternative hypothesis indicates the misfire free case

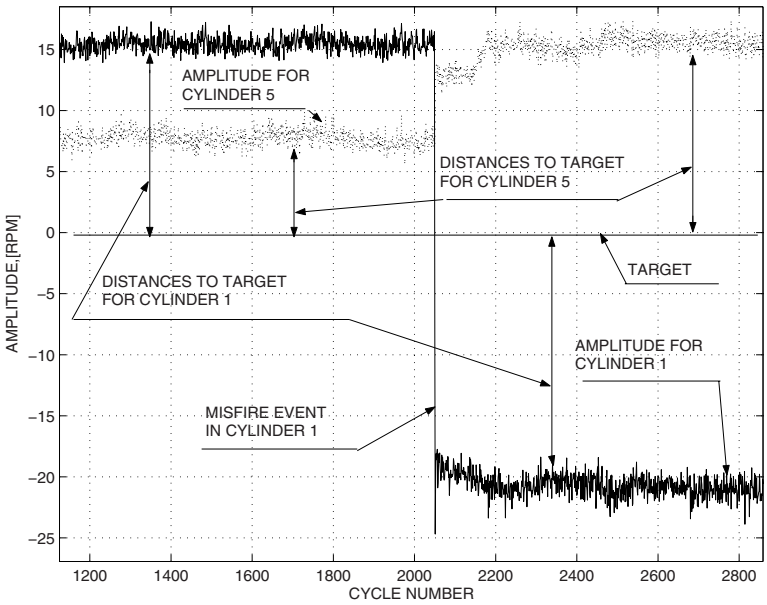

FIG 7.4. Two amplitudes for the first and the fifth cylinders are plotted as a function of cycle number. Engine speed is 4500 [rpm]. The engine is operating at full load. The misfire is generated in the first cylinder. The amplitude for the first cylinder is plotted with a solid line. The amplitude for the fifth cylinder is plotted with dotted line. The differences between the target value and the mean values of the amplitudes are indicated as distances to target.

and the second one indicates a misfire. The algorithm for hypothesis testing can be divided in two steps.

Step 1. First the hypothesis is tested in each step of the moving window of a minimal size N_{min}. The following $t - statistic$ is computed in each step l:

$$t_l = \frac{\mid \overline{A}_l - a_t \mid \sqrt{N-1}}{s_l} \tag{7.22}$$

where $\overline{A}_l = \frac{1}{N} \sum_{i=l-(N-1)}^{i=l} A_i$, is the value of the amplitude averaged over the window of a size $N = N_{min}$, s_l is a standard deviation, $s_l = \sqrt{\frac{1}{N-1} \sum_{i=l-(N-1)}^{i=l} (A_i - \overline{A}_l)^2}$. Notice, that an average amplitude $\overline{A}_l$ and a standard deviation s_l can be computed recursively in each step of the moving window as follows:

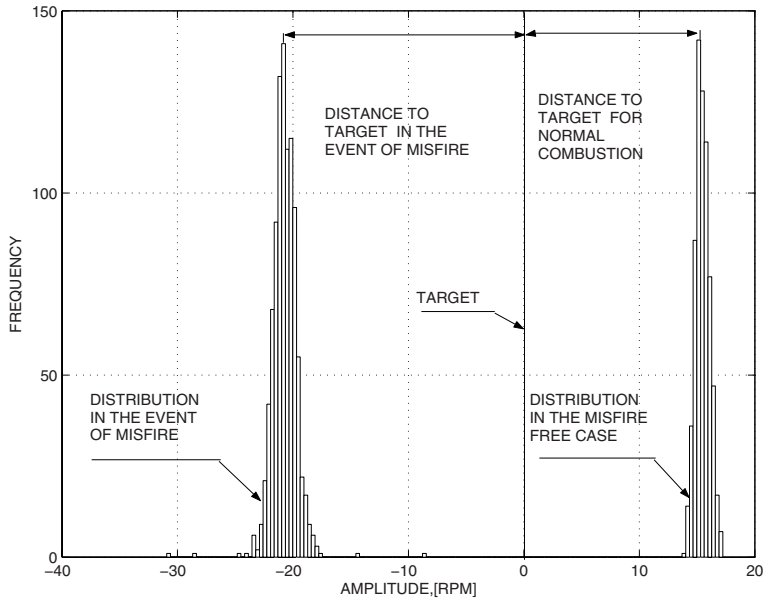

FIG 7.5. istributions of the amplitude signal for the first cylinder in the event of a misfire and in the misfire free case. The misfire is generated in the first cylinder. Engine speed is 4500 [rpm]. The engine is operating at full load. The sample size is 1624. The differences between the target value the mean values of the amplitudes are indicated as distances to target.

$$\overline{A}_l = \overline{A}_{l-1} + \frac{1}{N}(A_l - A_{l-N}) \tag{7.23}$$

$$s_l^2 = s_{l-1}^2 + \frac{1}{N-1}(A_l - \overline{A}_l)^2 - \frac{1}{N-1}(A_{l-N} - \overline{A}_l)^2 \tag{7.24}$$

simply meaning that A_l enters the window and A_{l-N} leaves the window. The value in the Student distribution look-up table for a certain significance level α and degrees of freedom $f = (N_{min} - 1)$ is compared with (7.22) in each step of the moving window. If the value of the statistic (7.22) is larger than the value in the Student distribution look-up table then the null hypothesis is rejected. If the average value of the amplitude is positive the null hypothesis is rejected in favor of H_{a1} that indicates the misfire free case. In all other cases the misfire is indicated. If the value of the statistic calculated with (7.22) is less than the value in the Student distribution look-up table for a certain significance level α and degrees of freedom $f = (N_{min} - 1)$ the misfire can not be detected and hence the value of the statistic should be corrected by adding additional degrees of freedom, i.e., increasing the window size.

Step 2. In this step the size of the moving window is increased until the value of the statistic (7.22) is larger than the value in the Student distribution look-up table. The Student distribution look-up table for a certain significance level is re-scaled so that for a certain sample size N the values correspond to the sample size $(N-1)$. Then the values in the re-scaled table are approximated by the following polynomial:

$$t_t = a_0 + \frac{a_1}{z} + \frac{a_2}{z^2} + \frac{a_3}{z^3} \tag{7.25}$$

where $z = \sqrt{N-1}$, a_i, $i = 0, ...3$ are the coefficients computed by using a least-squares curve fitting algorithm. The window size N_* is defined as a solution for a minimal N of the following equation:

$$\frac{\mid \overline{A}_l - a_t \mid z}{s_l} - (a_0 + \frac{a_1}{z} + \frac{a_2}{z^2} + \frac{a_3}{z^3}) = \delta \tag{7.26}$$

where δ is a small positive number. Equation (7.26) is the fourth order algebraic equation which can be solved by using standard numerical or analytical methods. The window size N_* which satisfies equation (7.26) guarantees that $t_l > t_t$ rejecting the null hypothesis and detecting a misfire, if any. Notice, that the window size N_* is bounded, i.e., $N_{min} < N_* \leq N_{max}$, where N_{max} is the maximal allowable window size (for example one can take $N_{max} = 500$). If a minimal solution of the equation (7.26) is larger than N_{max} the null hypothesis can not be tested and misfire can not be detected. Notice that, N_* is a predicted window size and the mean value and the variance of the amplitude signal might change when new data is coming into the window. Therefore Step 2 should be repeated when the window size reaches the value of N_* and further increasing of the window size should be made, if required. When the window size N_* which guarantees that $t_l > t_t$ is selected the misfire is detected at each step of the moving window. When the detection algorithm is deactivated the window size N_* is saved in the memory of the engine electronic control unit providing the updated value of the minimal window size in the first Step of the algorithm so that the next start of the detection algorithm begins with a renewed value of the minimal window size. If the window size N_* calculated as a solution of the equation (7.26) is larger than the maximal allowable size N_{max} the hypothesis can not be tested and hence the misfire can not be detected. This eventually means a drastic deterioration of the quality of the amplitude signal. The significance level α could be increased in this case reducing the values of t_t in the Student distribution look-up table to guarantee that $t_l > t_t$. Increasing of the significance level increases the probability of rejecting the null hypothesis mistakenly and hence the probability of erroneously detecting a misfire.

Notice that the algorithm described above is related to the statistical sequential analysis [80], [115] where the sample size (the size of a moving win-

dow) is not fixed in advance, and depends on the outcome of the hypothesis test.

The algorithm described above is illustrated by two examples.

Example 1: New Engine. Consider the misfire event shown in Figure 7.4. Step 1 of the algorithm shows that the average value of the amplitude is $\overline{A}_l = -19.15[rpm]$, with a standard deviation $s_l = 0.62[rpm]$ for the window size of ten, $N_{min} = 10$ in one of the steps of the moving window. The value of the statistic is $t_l = 92.67$, with a zero target value $a_t = 0$. This value is larger than the value in the Student distribution look-up table for a significance level $\alpha = 0.0005$ and degrees of freedom 9 (see [67] page 251), $t_t = 4.781$. Therefore, the null hypothesis is rejected and since the average value of the amplitude is negative the misfire in the first cylinder is correctly detected in this step of the moving window.

Example 2: Aged Engine.

The amplitude signal which is used for a misfire detection deteriorates due to the aging of the engine components. Deteriorated amplitude signal as a function of a cycle number for aged engine is shown in Figure 7.6 (compare it with Figure 7.4). The distributions in the event of a misfire and for the misfire free case are shown in Figure 7.7.

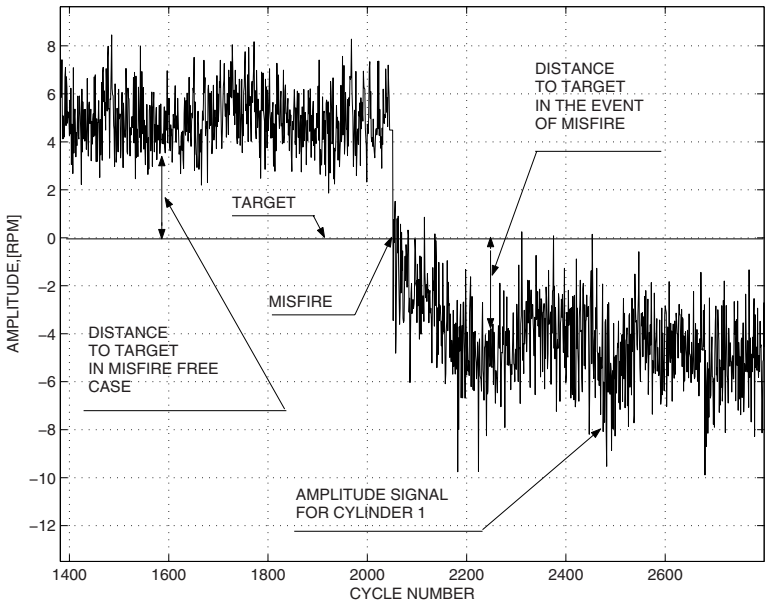

FIG 7.6. The amplitude of the first cylinder is plotted as a function of a cycle number. Engine speed is 4500 [rpm]. The engine is operating at full load. The misfire is generated in the first cylinder. The difference between the target value the mean value of the amplitude is indicated as a distance to target.

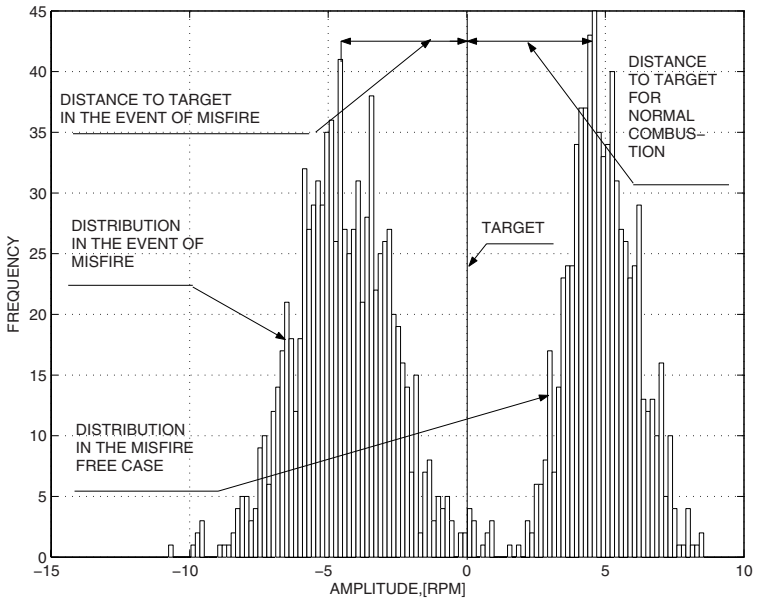

FIG 7.7. Distributions of the amplitude signal for the first cylinder in the event of a misfire and in the misfire free case. The misfire is generated in the first cylinder. Engine speed is 4500 [rpm]. The engine is operating at full load. The sample size is 1624. The differences between the target value the mean values of the amplitudes are indicated as distances to target.

Suppose that Step 1 of the algorithm shows the average amplitude $\overline{A}_l = -0.6519[rpm]$ with a standard deviation $s_l = 0.7436[rpm]$ in one of the steps of the moving window for the window size of ten. The value of the statistic is $t_l = 2.63$, with a zero target value $a_t = 0$. This value is less than the value in the Student distribution look-up table for a significance level $\alpha = 0.0005$ and degrees of freedom 9 (see [67] page 251), $t_t = 4.781$. Therefore the next step is taken.

Step 2. Recursive application of the algorithm described above gives the final value of the window size $N_* = 46$ with $\delta = 0.001$. The window size is increased from 10 to 46. The first step of the moving window after enlarging gives the following average amplitude $\overline{A}_l = -0.6519[rpm]$ and a standard deviation $s_l = 1.24[rpm]$. The value of the statistic is $t_l = 3.5267$ while the value in the Student distribution look-up table for a significance level $\alpha = 0.0005$ and degrees of freedom 45 (see [67] page 251), $t_t = 3.522$. Therefore the null hypothesis is rejected and the misfire is correctly detected in this step of the moving window for aged engine.

These examples show that the misfire detection algorithm based on the *One Sample T-test* provides the same misfire detection performance for both

new and aged engines in terms of the significance level by adjusting the window size, and hence is robust with respect to the signal quality.

7.4.2 Misfire Detection at the Half-Order Frequency

Another technique for a misfire detection is a monitoring of the amplitude at the half-order frequency (see Figure 7.1). The phase of the half-order frequency component shows which cylinder is misfiring. All the amplitudes corresponding to all engine cylinders are calculated at the half-order frequency. In the misfire free case all the amplitude signals should be close to zero. In the event of a misfire the amplitudes deviate from zero and the misfire is suspected in the cylinder with the largest mean value of the amplitude. In the first stage of the detection the amplitude with the largest mean value is compared to the target value which should be chosen relatively large in order to separate the oscillations induced by the misfire event from the oscillations induced by other events. To this end the amplitude signal is statistically tested via *One Sample T-test* described above. In the second stage of the detection a mean value of the largest amplitude is compared to the mean value of the next largest amplitude by hypothesis testing of the equality of two means (*Two Sample T-test*) in order to detect which cylinder is misfiring. The test statistic is the $t - statistic$ where the hypothesis that the mean values of two amplitudes are equal is taken as a null hypothesis which indicates that the misfire is not recognizable. Alternative hypothesis that the mean value of one of the amplitudes is the largest indicates a misfire in the corresponding cylinder. *Two Sample T-test* for a misfire detection can be performed similarly to the *One Sample T-test* described above and therefore is omitted in this Chapter.

7.5 Conclusion

New recursive filtering algorithms for misfire detection based on the trigonometric interpolation method proposed in this Chapter improve the performance of the filtering technique allowing a flexible choice of the size of the moving window, and correction algorithms for trigonometric interpolation method ensure the robustness with respect to round-off errors which are always present in the finite precision implementation environment. The statistical decision making mechanism which is based on a hypothesis testing introduced in this Chapter allows to make a misfire detection with a certain significance level with automatically selected sample size depending on the signal quality that in turn improves the robustness of the misfire detection method.

8

The Cam Profile Switching State Detection Method

A new method for the detection of the CPS (Cam Profile Switching) state of Spark Ignition automotive engines is proposed and implemented. The method is based on the evaluation of the amplitude and the phase of the component of the intake manifold pressure signal with the period of 720^o CA (Crank Angle) degrees. The method allows the detection of the CPS Bank failure even at high rotational speeds.

8.1 Introduction

A new Cam Profile Switching (CPS) technology for Spark Ignition automotive engines has a significant effect on fuel consumption, drivability and exhaust emissions. New legislative requirements for the exhaust emissions demand the ability to conduct a continuous monitoring of the state of CPS. This, in turn, necessitates the development of the diagnostic method for identification of the system failure since the valve lift event can not be directly measured. The CPS mechanism for six cylinder engines has two cylinder groups (Banks) which in turn have two separate oil-driven systems. The cylinder groups are coupled according to the firing sequence. The CPS has two states: low and high cam profiles. The shifting event is controlled by the pressure in the oil Banks.

A couple of methods allow the detection of the CPS state according to the literature. The first one is based on the difference in the air charge inducted in the cylinders for different lifts. The inducted air charge measured by Manifold Air Flow (MAF) sensor is compared with the air charge model based on the measured position of the throttle flap, intake manifold pressure and engine speed. The failure of the CPS mechanism is detected by the error between measured and modeled air charge [31]. The method is based on the difference in the volumetric efficiency for different CPS states. The difference in the volumetric efficiency for different CPS states is due to the air pushback effect at low engine speeds and the difference in valve effective areas at high engine speeds. This difference is also influenced by the IVVT (Intake Variable Valve

A.A. Stotsky, *Automotive Engines*, DOI 10.1007/978-3-642-00164-2_8,

Timing) position. The detection method described above is not able to detect a failure of a single Bank since the difference in the volumetric efficiency is small for this case. This method is also unable to detect an individual cylinder failure.

Another method is based on the combustion state monitoring using fluctuations of the engine speed. The method is based on the fact that the combustion state changes considerably during shifting [79]. The invention uses the technique of the combustion state monitoring via irregularities of the engine speed. Irregularities are associated with the CPS state. The method allows the cylinder individual failure detection. However, the method described in [79] does not allow the detection at high rotational speeds. At high rotational speeds (over 3500 rpm) the high resolution engine speed signal has fluctuations, which occur as a consequence of the combustion events contaminated with the time interval errors, low frequency oscillations from the powertrain and high frequency oscillations due to the crankshaft torsion. The CPS state information can not be recovered at high rotational speeds in the presence of the disturbances described above.

Cylinder groups (Banks) are coupled according to the firing sequence of the engine. The firing sequence for six cylinder prototyping engine is 1-5-3-6-2-4. The Bank "A" includes cylinders 2,4 and 1 while the Bank "B" includes cylinders 5, 3 and 6. As a consequence of the failure of a single oil Bank the component whose period is 720 CA degrees appears in the intake manifold pressure signal. The method proposed in this Chapter associates the CPS state with the amplitude and the phase of this component of the intake manifold pressure signal and allows the CPS failure detection both at low and high rotational speeds. The method is implemented and tested on a Volvo S80 passenger car equipped with six cylinder prototype engine with the CPS mechanism.

8.2 The CPS State Detection Algorithm

A failure of the CPS mechanism in a single cylinder produces oscillations of the period of 720 CA degrees in the intake manifold pressure signal. The amplitude of the oscillations is amplified in the case of the failure of a single Bank due to the ignition synchronized coupling of the CPS cylinder groups. The amplitude of the component of the pressure signal whose period is 720 CA degrees is used in this Chapter for the detection of the CPS Bank failure. The phase of the mentioned above component indicates which Bank is failed. Figure 8.1 and Figure 8.2 show the harmonic contents of the intake manifold pressure signal at 1000 rpm and 4000 rpm for healthy and failed systems. Amplitudes are plotted as a function of a harmonic number of a periodic signal with the period of 720 CA degrees. The harmonic number is defined as an integer which is equal to the ratio of two periods, $n_h = \frac{720^o}{T_h}$, where T_h is the period of the harmonic. Measurements were conducted during normal

driving. It can easily be seen that the CPS Bank failure is recognizable by using the amplitude of the component of the pressure signal whose period is 720 CA degrees.

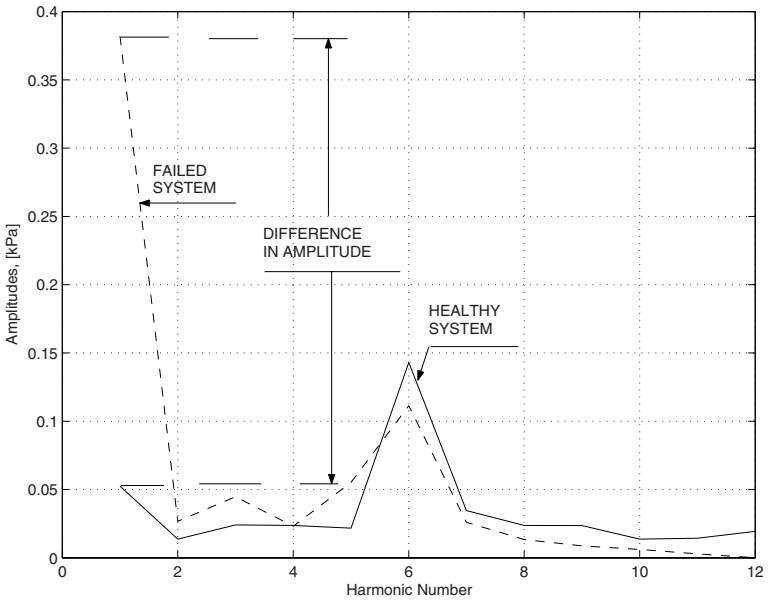

FIG 8.1. Harmonic contents of the intake manifold pressure signal. Amplitudes are plotted as a function of a harmonic number of a periodic signal with the period of 720 CA (Crank Angle) degrees. Engine speed is 1000 rpm. Engine load is 20%. Amplitudes for the healthy system are plotted with solid line. Amplitudes for the failed system are plotted with dashed line.

The behaviour of the intake manifold pressure signal in the presence of the failure of the CPS Bank is characterized, in terms of the pulsations corresponding to the intake events, by three big pulses followed by three small pulses.

The 'peak-to-peak' amplitude of the intake manifold pressure signal, which is sampled Crank Angle synchronized is defined as follows :

$$A_i = p(\theta_{i1}) - p(\theta_{i2}) \tag{8.1}$$

where θ_1 is the angle corresponding to the maximum value of the intake manifold pressure signal $p(\theta_{i1})$, θ_2 is the angle corresponding to the minimum value of the intake manifold pressure signal $p(\theta_{i2})$. Index i indicates different Banks, $i = 1, 2$. To improve the quality of the detection signal the amplitudes are filtered by a lowpass filter. The failure is detected if the filtered amplitude exceeds a threshold value, which in turn, is defined as a function of speed

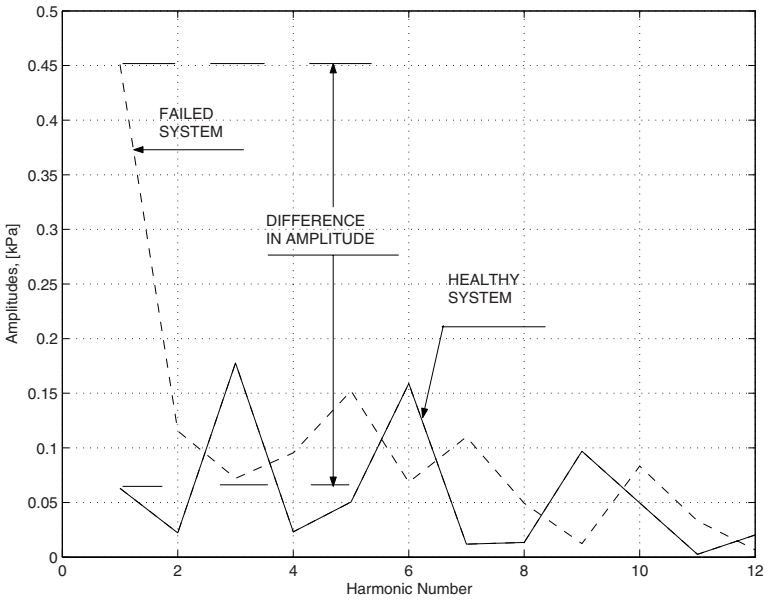

FIG 8.2. Harmonic contents of the intake manifold pressure signal. Amplitudes are plotted as a function of a harmonic number of a periodic signal with the period of 720 CA (Crank Angle) degrees. Engine speed is 4000 rpm. Engine load is 20%. Amplitudes for the healthy system are plotted with solid line. Amplitudes for the failed system are plotted with dashed line.

and load. The algorithm was implemented and extensively tested on a Volvo S80 passenger car equipped with a six cylinder prototyping engine. Implementation results are shown in Figure 8.3,Figure 8.4 and Figure 8.5,Figure 8.6. Figure 8.3,Figure 8.4 show amplitudes of the intake manifold pressure for different failures of the CPS Banks at 1000 rpm. Figure 8.5 and Figure 8.6 shows amplitudes at 4000 rpm.

Experiments showed that the detection of the Bank failure is possible even at extremely high engine speeds, i.e. up to 6000 rpm. The same method can be used for the detection of the failure of a single cylinder or even a single valve.

Other methods for a CPS state detection are described in [101], [103], [104], [106].

8.3 Conclusion

In this Chapter a new diagnostic method for the detection of the CPS state is proposed and implemented. Algorithm allows the detection of the CPS Bank failure at high rotational speeds.

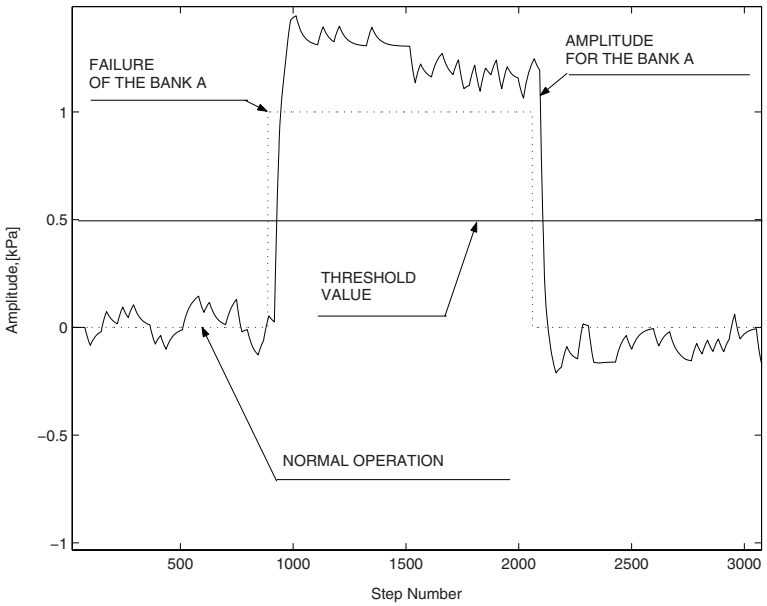

FIG 8.3. Experimental results. Amplitudes of the intake manifold pressure for a failure of the CPS Bank. Engine speed is 1000 rpm. The engine is operating at full load. Amplitude for Bank A is plotted with a solid line. The signal which initiates the CPS failure of Bank "A" is plotted with dotted line.

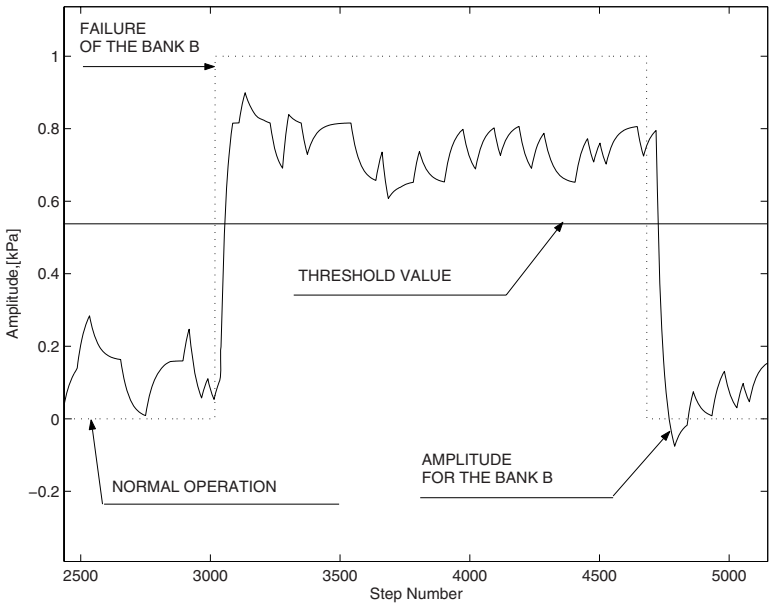

FIG 8.4. Experimental results. Amplitudes of the intake manifold pressure for a failure of the CPS Bank. Engine speed is 1000 rpm. The engine is operating at full load. Amplitude for Bank B is plotted with a solid line. The signal which initiates the CPS failure of Bank "B" is plotted with dotted line.

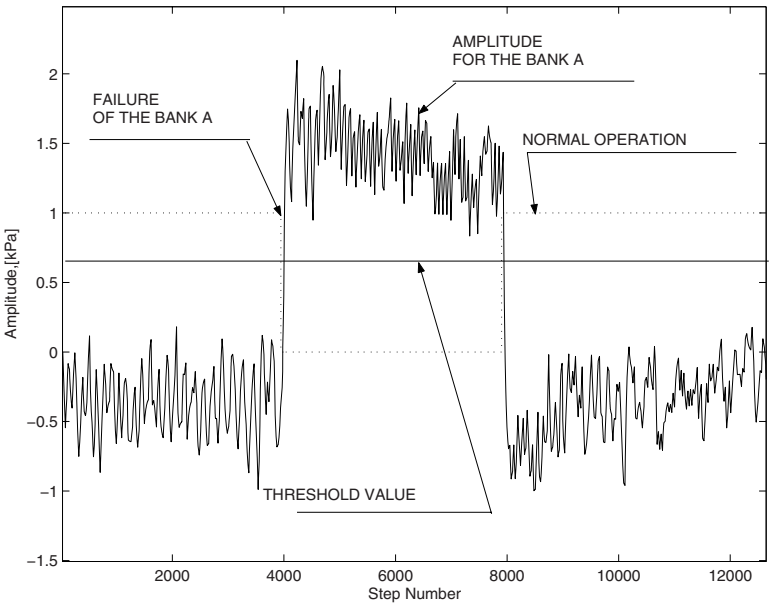

FIG 8.5. Experimental results. Amplitudes of the intake manifold pressure for a failure of the CPS Bank. Engine speed is 4000 rpm. The engine is operating at 50% load. Amplitude for Bank A is plotted with a solid line. The signal which initiates the CPS failure of Bank "A" is plotted with dotted line.

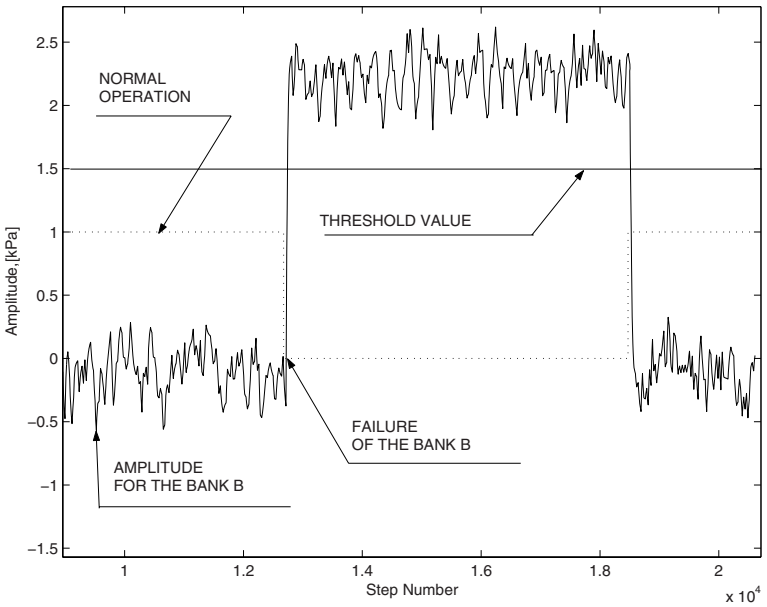

FIG 8.6. Experimental results. Amplitudes of the intake manifold pressure for a failure of the CPS Bank. Engine speed is 4000 rpm. The engine is operating at 50% load. Amplitude for Bank B is plotted with a solid line. The signal which initiates the CPS failure of Bank "B" is plotted with dotted line.

9

Statistical Engine Knock Detection

A knock detection circuit that is based on the signal of an accelerometer installed on the engine block of a spark ignition automotive engine has a band-pass filter with a certain frequency as a parameter to be calibrated. A new statistical method for the determination of the frequency which is the most suitable for the knock detection in real-time applications is proposed. The method uses both the cylinder pressure and block vibration signals. The knock detectability, which is an individual cylinder attribute at a certain frequency, is verified via a statistical hypothesis test for testing the equality of two mean values, i.e. mean values of the amplitudes for knocking and non-knocking cycles. Signal-to-noise ratio is associated in this Chapter with the value of *t - statistic*. The frequency with the largest signal-to-noise ratio (the value of *t - statistic*) is chosen for implementation in the engine knock detection circuit.

9.1 Introduction

Poor knock detectability generates noise and can easily damage the engines. Knock miss-detection, i.e. the state where a knock is mistakenly detected, has a direct impact on engine fuel consumption and drivability performance. Since the engine knock represents one of the major constraints on the engine performance, a large number of papers have been written on the subject of a knock analysis using the cylinder pressure signal and the signal of the accelerometer that is installed on the engine block (knock sensor signal) [8],[62], [75], etc. Very little attention (practically no attention), however, has been paid to the determination of the frequency which is the most suited for engine knock detection since the knock can be detected at a number of frequencies. The knock sensor that measures engine vibrations is combined with the signal processing unit where the band-pass filter is implemented. The knock frequency is an important calibration parameter that should be selected by a calibration engineer. The standard choice of the frequency that is made based on the cylinder geometry often gives poor knock detectability and, as a consequence,

A.A. Stotsky, *Automotive Engines*, DOI 10.1007/978-3-642-00164-2_9,

has an impact on a vehicle drivability performance, noise and fuel consumption. Moreover, possible hardware and knock sensor placement changes during the project development often result in shifts in the frequencies for the engine knock detection. The determination of the most suitable frequency is usually made in a engine test cell. Amplitudes at different frequencies are evaluated using oscilloscope which calculates the frequency contents of the engine block vibration signal. Evaluation is made on a running engine. Engine rig time is expensive, that in turn makes a calibration method expensive. The AVL CONCERTO[1] software tools which also can be used for evaluation of the frequency contents of the engine signals require expensive license which should be annually renewed. The time and cost associated with the calibration of the engine knock detection functionality necessitate the development of computationally efficient algorithms and MATLAB software for the rapid determination of the knock frequency that is the most suitable for the real-time engine knock control applications.

The approach proposed in this Chapter introduces a new statistical decision making technology for knock frequency determination.

A Volvo six cylinder prototype engine equipped with the cylinder pressure and block vibration sensors was used in the experiments. Algorithms are implemented in MATLAB and applied to the measured data collected from the engine.

9.2 Recursive Trigonometric Interpolation Algorithms

Recursive trigonometric interpolation method which allows the calculation of the frequency contents of an oscillating signal is described in this Section. The method is applied to the calculation of the frequency contents of the cylinder pressure and block vibration signals in Section 9.3.

9.2.1 Problem Statement

Suppose that there is a set of measurements of the oscillating signal s_k, $k = 1, 2...$, measured at the following points $x_k = k\Delta$, where Δ is a step size. Two signals are considered in this Chapter: the cylinder pressure signal and the engine block vibration signal. Suppose that the signal can exactly be approximated by the trigonometric polynomial as follows:

$$\hat{s}_k = \varphi_k^T \theta_k, \tag{9.1}$$

$$\theta_k^T = [a_{0k} \quad a_{q1k} \quad b_{q1k} \quad a_{q2k} \quad b_{q2k}, \\ ... \quad a_{qnk} \quad b_{qnk}], \tag{9.2}$$

$$\varphi_k^T = [1 \quad cos(q_1 x_k) \quad sin(q_1 x_k) \quad cos(q_2 x_k) \\ sin(q_2 x_k) \quad ... \quad cos(q_n x_k) \quad sin(q_n x_k)] \tag{9.3}$$

[1] CONCERTO is a sofware tool produced by AVL for engine related post-processing

where θ_k is the vector of the adjustable parameters and φ_k is the regressor, $q = q_1, ..., q_n$ are the frequencies, a_{0k}, a_{qk} and b_{qk} are the coefficients which should be found, $\hat{s}_k$ is the estimate of the signal s_k. The amplitude which plays an important role for the knock detection is defined at a certain frequency as follows:

$$A_{qik} = \sqrt{a_{qik}^2 + b_{qik}^2} \tag{9.4}$$

where $i = 1, ..., n$, where n is the number of the frequencies.

Assume that the signal can be presented as follows:

$$s_k = \varphi_k^T \theta_*, \tag{9.5}$$

where θ_* is the vector of true parameters,

$$\theta_*^T = [a_{0*} \quad a_{q1*} \quad b_{q1*} \quad a_{q2*} \quad b_{q2*} \quad ... \quad a_{qn*} \quad b_{qn*}], \tag{9.6}$$

and a_{0*}, a_{q*} and b_{q*} are constant unknown coefficients.

Notice that an improper choice of the frequencies q might lead to the unreasonably large amplitudes (9.4).

The signal s_k is approximated by (9.1) in the least squares sense in a moving window of a size w. The error to be minimized at every step is as follows:

$$E_k = \sum_{i=k-(w-1)}^{i=k} (s_i - \hat{s}_i)^2, \quad k \geq w \tag{9.7}$$

The problem described above is a well known approximation problem which should be solved in the least-squares sense. The solution is described in Section 7.2. The recursive algorithms are applied to the calculation of the frequency contents of the cylinder pressure and block vibration signal in Section 9.3.

9.3 Knock Detection Algorithms

The knock detection method proposed in this Chapter uses both the cylinder pressure and block vibration signals and is divided in two steps corresponding to two Subsections of this Section.

9.3.1 Step1: Knock Detection by Using the Cylinder Pressure Signal

In the first step the oscillations which occur during the knock event in the cylinder pressure signal are analyzed by means of the trigonometric interpolation method described in Section 7.2. Engine knock was generated by

advancing the spark timing from the nominal spark timing. The knock is detected when at least one absolute value of the maximal amplitudes computed via (9.4) exceeds the threshold value which represents the level of the background noise in the pressure signal. The detection method by using the cylinder pressure signal is in turn, divided in three steps.

Elimination of the Low Frequency Trend

In this Step the cylinder pressure signal is approximated via a low-order polynomial with the purpose of the elimination of the low frequency component of the cylinder pressure signal emphasizing knock induced signal which is the input to the next step of the algorithm. Figure 9.1 shows the cylinder pressure signal and low-order polynomial approximation of the pressure signal. Figure 9.2 shows the difference between the cylinder pressure signal and the low-frequency component of the cylinder pressure signal. This difference between the cylinder pressure signal and its low frequency component that corresponds to the oscillations due to the engine knock is the input to the next step of the algorithm.

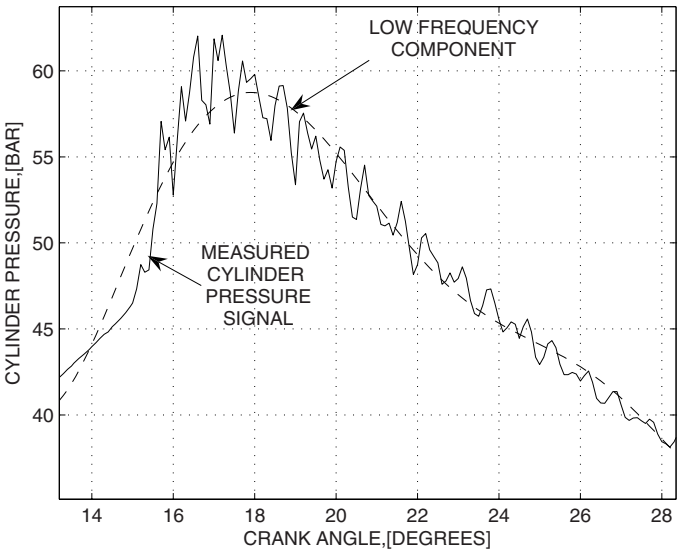

FIG 9.1. The cylinder pressure signal and the low-frequency component of the cylinder pressure signal are plotted as functions of a crank angle in selected crank-angle window during a knocking cycle. Engine is operating at 1000[rpm] at full load. The cylinder pressure signal is plotted with a solid line, and the low frequency component is plotted with a dashed line. The cylinder pressure is measured with the step of 0.1^o.

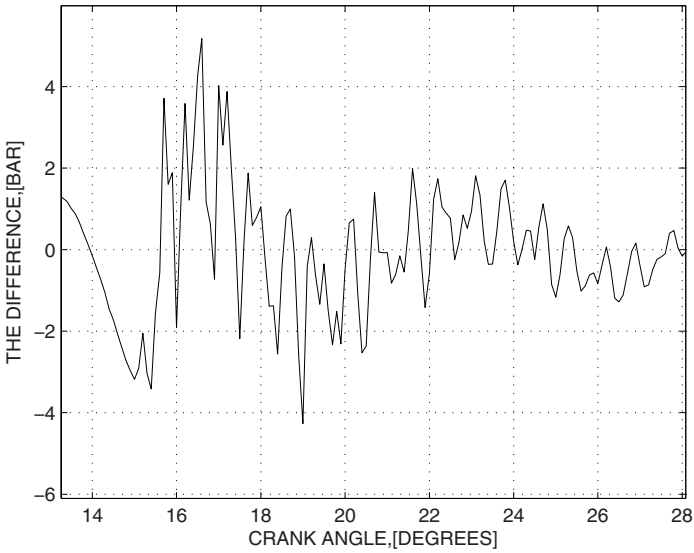

FIG 9.2. The difference between the cylinder pressure signal and the low-frequency component of the cylinder pressure signal is plotted with a solid line as a function of a crank angle in the selected crank-angle window during a knocking cycle. Engine is operating at 1000[rpm] at full load.

Calculation of the Frequency Contents of the Cylinder Pressure Signal

In this step the difference between the cylinder pressure signal and its low frequency component is approximated by the trigonometric polynomial (9.1) aiming to calculation of the frequency contents of the signal. Minimal number of terms (frequencies) should be used for approximation. Initial frequencies can preliminary be estimated from the cylinder geometry. The optimal choice of the number of terms (frequencies) in the approximating polynomial (9.1) could be done as follows. Assume that the cylinder pressure signal can exactly be approximated by the polynomial (9.1) and measured signal has a random measurement noise only. It is assumed that the measurement errors are independent and normally distributed. In this case the errors in the estimated parameters are also normally distributed, and the following ratio $V = \frac{E_k}{(w - 2n - 1)}$ is the estimate of the variance of the measurement noise, where n is the number of frequencies. New frequency is included in the model (9.1), if the ratio V is reduced and this reduction is statistically significant. The significance of the variance reduction is established using the *Test for*

Equal Variances [64], [67], [118]. Hypotheses tests used in this book are also described in Appendix. The choice of the frequencies is optimal if the values of the ratio V and the variance of the measurement noise are approximately the same. Similar algorithm of the automatic term selection for ordinary polynomials is described in Chapter 6.3.

Selection of the Knocking Cycles

The knock does not occur in every cycle of the engine steady-state operation even with a significantly advanced spark timing. A sufficiently large number of the knocking cycles should be selected for further processing of the signal from the knock sensor. The knock event is a non-stationary transient process and the amplitude at the frequencies of interest are time (crank angle) dependent. Maximal amplitudes, where the maximum is taken over the knocking window are used in this Chapter as a measure of the knock intensity (energy). The knock is detected if one of the maximal amplitudes of the pressure signal exceeds the threshold value. Figure 9.3 and Figure 9.4 show maximal amplitudes for non-knocking and knocking cycles as functions of the selected frequencies. If at least one of the maximal amplitudes in a certain cylinder for a certain cycle exceeds the threshold value which is selected by the calibration engineer, this cycle is considered as a knocking cycle and is selected for further knock sensor signal processing. Notice that slight oscillations are present in the pressure signal even during a normal combustion. The intensity of these oscillations is significantly less than the intensity of the oscillations induced by the knock event. Therefore the intensity of the pressure oscillations can be used as an indicator of the true knock intensity.

Notice, that the engine knock does not occur in every cycle even with the significantly advanced ignition timing at the engine steady-state operation. Therefore the cylinder pressure signal, which is the most suitable for the engine knock detection is used for selection of the knocking cycles. Cylinder pressure sensors are not used in the production vehicles and the cylinder pressure signal is only used in this Chapter for the selection of the knocking cycles.

9.3.2 Step2: Knock Detection by Using the Knock Sensor Signal

In this step the frequency analysis is performed with a trigonometric interpolation method on the knock sensor signal for engine cycles selected in the previous step. Simultaneously, the frequency analysis is performed for non-knocking cycles in order to calculate the amplitudes representing a background noise, i.e., vibrations induced by the events which are not related to the engine knock. Figure 9.5 and Figure 9.6 show the engine knock sensor signal for non-knocking and knocking engine cycles. Comparison of the Figures 9.5 and 9.6 show that engine knock is detectable via a block vibration signal.

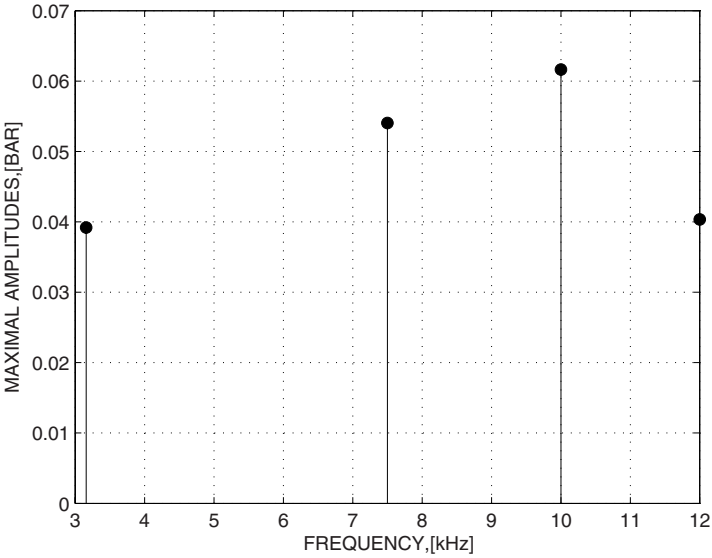

FIG 9.3. Maximal amplitudes for non-knocking cycle as the functions of the frequency. Engine is operating at 1000$[rpm]$ and at full load.

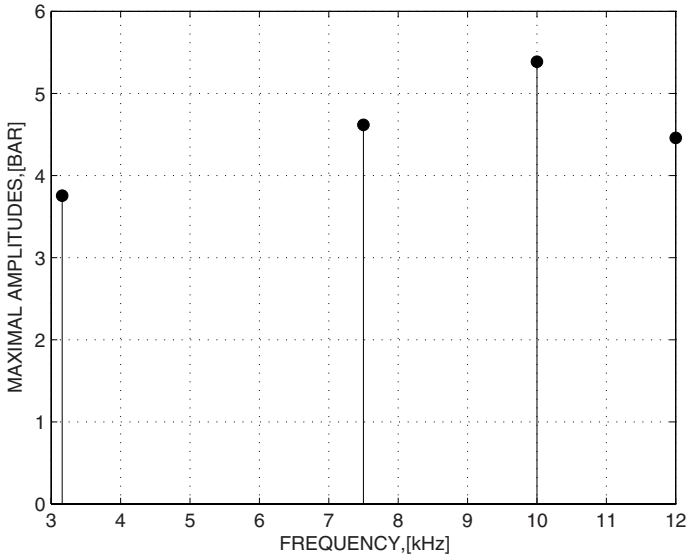

FIG 9.4. Maximal amplitudes for a knocking cycle as the functions of the frequency. Engine is operating at 1000$[rpm]$ and at full load.

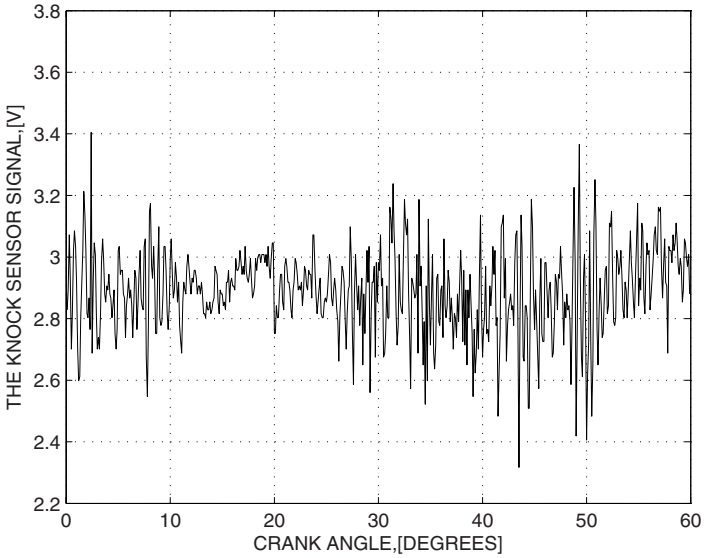

FIG 9.5. The engine knock sensor signal is plotted for a non-knocking cycle. The measurements are made with the step of 0.1^o. Engine is operating at $1000[rpm]$ and at full load.

Frequency contents of two engine cycles: non-knocking and knocking cycles plotted in Figure 9.5 and Figure 9.6 are shown in Figure 9.7.

Figure 9.8 and Figure 9.9 show the distributions of the maximal amplitudes for non-knocking engine cycles and knocking engine cycles at the frequency of 10 $[kHz]$ respectively.

Experimental data acquired from different engines show variability in distribution characteristics of the maximal amplitudes. Two types of models could be used for approximation of the distribution characteristics of the maximal amplitudes: normal and log-normal [66]. Distributions shown in Figure 9.8 and Figure 9.9 are close to the log-normal model. These distributions have longer tails on the right-hand side. The data with log-normal distribution is converted to the normal distribution data using a logarithmic transformation function.

Knock Detectability

The statistical knock detectability introduced in this Chapter is associated with the hypothesis test which compares two mean values of the maximal amplitudes at a certain frequency. The hypothesis that the knock in one of the engine cylinders is not distinguishable from the background noise at a certain frequency is taken as the null hypothesis. The null hypothesis is defined as

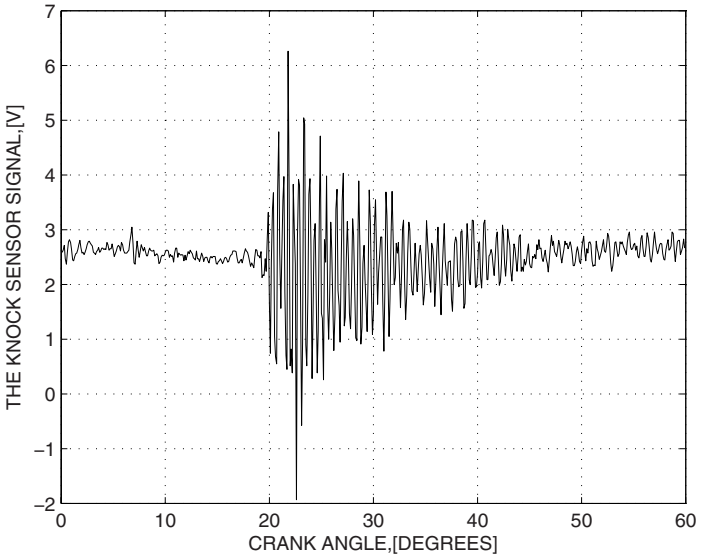

FIG 9.6. The engine knock sensor signal is plotted for a knocking cycle. The measurements are made with the step of 0.1^o. Engine is operating at $1000[rpm]$ and at full load.

follows $H_{0qi} : \overline{A}_{qmaxki} = \overline{A}_{qmaxbi}$, where $\overline{A}_{qmaxki}$ is a maximal amplitude at a frequency q averaged over a certain number of knocking cycles n_{ki}, $\overline{A}_{qmaxbi}$ is a maximal amplitude at the same frequency averaged over a certain number of non-knocking cycles n_{bi}, where i is the cylinder number. Alternative hypothesis that $H_{Aqi} : \overline{A}_{qmaxki} > \overline{A}_{qmaxbi}$ indicates that the knock is recognizable from the background noise. Therefore the knock detectability is defined as follows.

Definition: *The engine knock is detectable at a certain frequency q, in the cylinder i with a certain significance level* α_{qi} *if the null hypothesis* H_{0qi} *is rejected in favor of the alternative hypothesis* $H_{Aqi} : \overline{A}_{qmaxki} > \overline{A}_{qmaxbi}$.

The null hypothesis with a certain significance level is tested using *Two Sample T-test*. Notice that, a probability of rejecting the null hypothesis when it is true is called a level of significance or α risk. Since the variance of a maximal amplitude for knocking cycles is often significantly larger than the variance of the maximal amplitude for non-knocking cycles *Two Sample T-test* is modified in this Chapter for the case of unequal variances (see Appendix D). The test statistic is the t - *statistic* which is calculated as follows:

$$t_{qi} = \frac{\overline{A}_{qmaxki} - \overline{A}_{qmaxbi}}{s_{qi}} \sqrt{\frac{n_{ki} n_{bi}}{(n_{ki} + F_{qi} n_{bi})}} \tag{9.8}$$

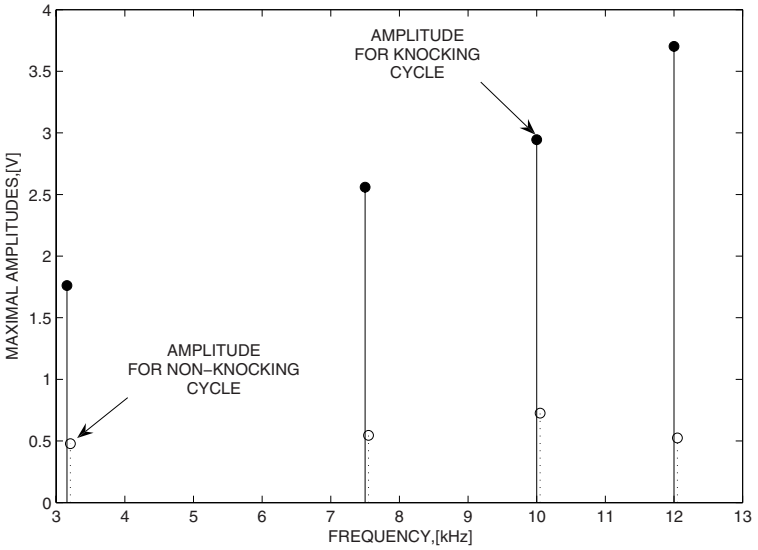

FIG 9.7. Frequency contents of the engine knock sensor signal for knocking and non-knocking cycles. Maximal amplitudes for knocking cycle are plotted with a solid line. Maximal amplitudes for non-knocking cycle are plotted with a dotted line. Engine is operating at 1000[rpm] and at full load.

where s_{qi} is the estimated pooled standard deviation which is defined as follows:

$$s_{qi} = \sqrt{\frac{(n_{ki}-1)s_{qki}^2 + F_{qi}(n_{bi}-1)s_{qbi}^2}{F_{qi}(n_{ki}+n_{bi}-2)}} \tag{9.9}$$

where

$s_{qki} = \sqrt{\frac{1}{(n_{ki}-1)}\sum_{j=1}^{j=n_{ki}}(A_{qmaxki} - \overline{A}_{qmaxki})^2}$,

$s_{qbi} = \sqrt{\frac{1}{(n_{bi}-1)}\sum_{j=1}^{j=n_{bi}}(A_{qmaxbi} - \overline{A}_{qmaxbi})^2}$ are standard deviations for knocking cycles and background noise respectively, $F_{qi} = \frac{s_{qki}^2}{s_{qbi}^2}$ for the case where the difference between variances s_{qki}^2 and s_{qbi}^2 is statistically significant and $F_{qi} = 1$ otherwise. The value of t_{qi} - *statistic* is compared to the value in the Student distribution look-up table $T_{st,(1-2\alpha_{qi})}$ for degrees of freedom $f_{qi} = n_{ki} + n_{bi} - 2$ and a certain significance level α_{qi}. If the value of the statistic t_{qi} is larger than the value in the Student distribution look-up table,

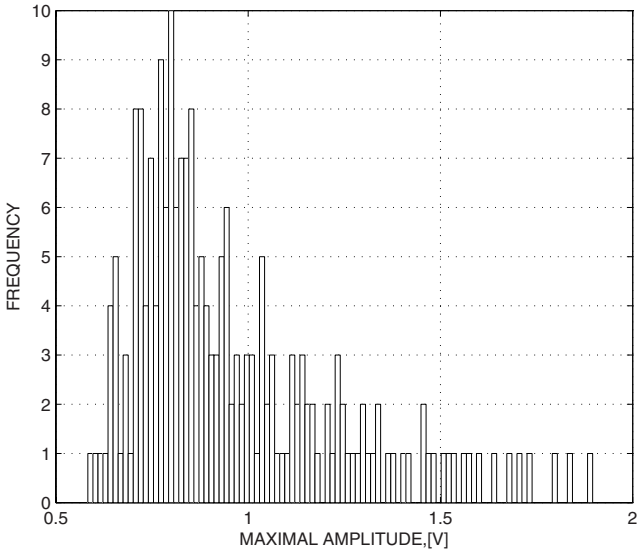

FIG 9.8. Distributions of the maximal amplitudes for non-knocking engine cycles at the frequency of 10 $[kHz]$. Maximal amplitudes are expressed in Voltage, [V] due to the Voltage output of the block vibration sensor. Engine is operating at 1000$[rpm]$ and at full load. The frequency of falling of the random sample of the maximal amplitude into a certain interval is understood under the frequency here.

the null hypothesis H_{0qi} is rejected in favor of H_{Aqi}. This in turn, implies that the engine knock is detectable in the cylinder i at a certain frequency q. If the value of the statistic is less than the value in the Student distribution look-up table, the number of knocking cycles should be increased. Notice, that the number of knocking and non-knocking cycles should be approximately the same for the hypothesis testing. If further increasing of the number of the knocking cycles is impossible due to some constraints (computer memory constraints, for example) then the significance level α_{qi} could be increased reducing the values in the Student distribution look-up table to guarantee that the value of the statistic is larger than the value in the Student distribution look-up table. Increasing of the significance level increases the probability of rejecting the null hypothesis mistakenly and hence the probability of the erroneous knock detection.

The Choice of the Most Suitable Frequency for the Knock Detection

The statistical knock decision making mechanism described above is used for verification of the knock detectability at a certain frequency, but does not allow

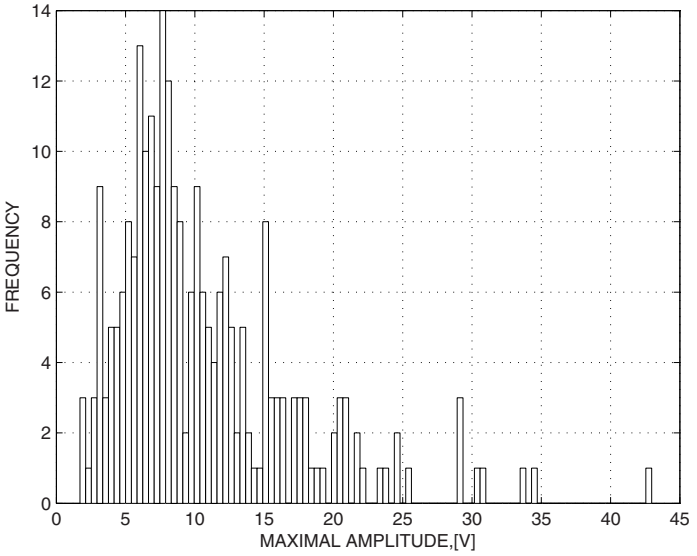

FIG 9.9. Distributions of the maximal amplitudes for knocking engine cycles at the frequency of 10 $[kHz]$. Maximal amplitudes are expressed in Voltage, [V] due to the Voltage output of the block vibration sensor. Engine is operating at 1000$[rpm]$ and at full load. The frequency of falling of the random sample of the maximal amplitude into a certain interval is understood under the frequency here.

the choice of the most suitable frequency for the knock detection. The knock is often detectable at several frequencies and the most suitable frequency have the largest signal-to-noise ratio. The signal-to-noise ratio is evaluated via the comparison of two distributions (see Figure 9.8 and Figure 9.9) representing a background noise and knocking cycles. The better the separation between two distributions at a certain frequency the larger the signal-to-noise ratio. The value of the statistic (9.8) is introduced in this Chapter as a quantitative measure of the separation between two distributions of interest. The larger the difference between mean values of the amplitudes and the larger the number of the knocking cycles and the less the pooled standard deviation the larger the value of the statistic at a certain frequency.

If a single frequency should be chosen for a number of the cylinders, then the cylinder individual values of the statistics are added for a certain number of engine cylinders for which the knock sensor is assigned. The frequency with the largest value of the common statistic is chosen as the best frequency for the knock detection in a certain number of the cylinders for a given sensor. In other words the most suitable frequency q_b for the knock detection in M cylinders at a certain engine speed and engine load has the largest value of the following performance index:

$$p_q = \max_q \sum_{i=1}^{M} t_{qi} \tag{9.10}$$

where t_{qi} is the value of the statistic for a cylinder $i = 1, ..., M$, where M is the number of the cylinders assigned for the knock sensor at the frequency q, engine speed ω and engine load L. The performance index (9.10) allows to choose the best frequency at a certain speed and load. The values of the performance index $\sum_{i=1}^{M} t_{qi}$ can be added for a number of working points with certain weighting factors assigned in every engine speed and load working point, which allows prioritizing certain areas. The frequency which has a maximal value of the performance index is chosen for the knock detection in certain working area.

9.4 Conclusion

New statistical method for determination of the most suitable frequency for the engine knock detection is proposed. The cascaded method uses the cylinder pressure signal for detection of the knock events and block vibration signal for statistical determination of the most suitable frequency for the knock detection in real-time applications. The method is implemented in MATLAB that allows rapid determination of the frequency after the hardware and knock sensor placement changes. This in turn results in significant savings of the calibration time and cost under the project development.

10

Statistical Engine Knock Control

A new statistical concept of the knock control of spark ignition automotive engine is proposed. The control aim is associated with the statistical hypothesis test which compares the threshold value to the average value of the maximal amplitude of the knock sensor signal at a certain frequency. Achievement of the control aim implies the desired separation between the average value of the maximal amplitude and the target value and hence the desired probability of the knock occurrence. This new control concept allows connection of the control algorithm parameters with the probability of the knock occurrence and customer related data. The regulation error is defined as a difference between the actual and the desired values of the statistic. A control algorithm which is used for minimization of the regulation error realizes a simple count-up-count-down logic.

A new adaptation algorithm for the knock detection threshold is developed. Confidence interval method is used as the basis for adaptation. A knock detection threshold is presented using a confidence interval with a certain significance level. The adaptation is performed for aged engine so that the significance level is the same for new and aged engines despite that the detection threshold values are different. This in turn, guarantees the same knock detection performance for new and aged engines.

A simple statistical model which includes generation of the amplitude signals, threshold value determination and a knock sound model is developed for evaluation of the control concept. Statistical knock audibility concept is associated with the outlier detection method and is used in this Chapter for the knock audibility judgement.

A Volvo six cylinder prototype engine equipped with the cylinder pressure and block vibration sensors was used in the experiments. External microphone was used for the knock sound measurements.

A.A. Stotsky, *Automotive Engines*, DOI 10.1007/978-3-642-00164-2_10,

10.1 Introduction

Engine knock in spark ignition automotive engine results in restriction of the ignition advance and is the main limitation to the torque output performance and a fuel economy improvement. Engine knock control system is based on the block vibration (knock) sensor signal filtered via a band-pass filter at a certain frequency which is the most suitable for the knock detection (see Chapter 9). Control system which is driven by the maximal amplitude of the knock sensor signal at a certain frequency reduces the spark timing in the case of a knock event, i.e. when the maximal amplitude exceeds the threshold value, that in turn, increases the fuel consumption and reduces the output power.
A stable statistical nature of a maximal amplitude signal allows using statistical methods for engine knock control, (see [119]) where the controller operates at the borderline knock limit and utilizes such statistical variables as mean value and standard deviation. However, the probability of the knock occurrence was not estimated nor connected to the customer related data such as fuel consumption, for example. The trade-off between the probability of the knock occurrence and the engine fuel consumption allows a proper choice of the controller parameters and hence the performance improvement. Moreover the control method proposed in [119] does not allow the adaptation of the knock detection threshold and judgement of audibility of the knock events.
Notice, that no knock deterministic controller is probably able to operate the engine smoothly at the borderline knock limit without using such statistical variables as the mean value and standard deviation. Therefore a statistical approach only is considered in this Chapter for the engine knock control.

Statistical knock control method proposed in this Chapter introduces a new concept of the engine knock control where the achievement of the control aim is associated with the rejection of the null statistical hypothesis that the average value of the maximal amplitude is equal to the target value. The null hypothesis is asymptotically rejected in favor of the alternative statistical hypothesis that the average value of the amplitude is smaller than the target value. In other words the feedback control loop is used to ensure the desired separation between the average value of the amplitude and the threshold value and hence the desired probability of the knock occurrence. The regulation error is defined in terms of the difference between actual and desired values of the statistic. The statistic which corresponds to *One Sample T-test* (the name is carried over from [64], [67]) converges to the desired value of the statistic taken from the Student distribution look-up table when regulation error converges to zero. This in turn, guarantees that the null hypothesis is asymptotically rejected with a certain significance level which in turn is associated with the probability of the knock occurrence. The statistic which can be seen as a secondary regulation variable is updated in every step of the window which is moving in time and is calculated as a difference between the threshold and averages values divided by the sample standard deviation and multiplied by the window size. Introduction of the statistic as a secondary reg-

ulation variable according to this new control concept allows a connection of the parameters of the algorithm (such as a window size) with the probability of the knock occurrence and such customer related data as a fuel consumption.
The control algorithm which is widely used in industry minimizes the regulation error via a simple count-up-count-down logic.

The performance of the knock sensor signal and hence the average value of the maximal amplitude at a certain frequency and its standard deviation might change with time due to aging of engine components. Erroneous knock detection might occur if the average value of the maximal amplitude and standard deviation increase and the threshold value is not updated. This in turn, results in unnecessary ignition retards which have a direct impact on the fuel consumption. Therefore the engine knock threshold value should be updated if the average value of the maximal amplitude or standard deviation deviate from the pre-calibrated values. Main idea of adaptation is a presentation of the knock detection threshold using a confidence interval (see Appendix D) and holding the same significance level for new and aged engines. To this end, first the value of the pre-calibrated detection threshold is related to such properties of the knock signal at a certain frequency as the average value, standard deviation and a sample size. In other words the knock detection threshold is assigned to the upper confidence limit and presented in terms of the average value, standard deviation, sample size and a significance level. Notice that the endpoints of the confidence interval are defined as confidence limits. Since the average value and standard deviation for the knock sensor signal at a certain frequency are specified at a certain working point the detection threshold is uniquely defined by the significance level, which is the basis for adaptation. The assignment of the knock detection threshold is equivalent to the assignment of the significance level. The confidence limit plays a role of a reference model which should be valid for new and aged engines. Average value and standard deviation of the knock sensor signal might change due to aging of the engine components. New average value and new standard deviation are calculated for a given signal for aged engine. The decision about adaptation of the knock detection threshold is based on the results of *Two Sample T-test* for comparison of the average values (newly estimated and pre-calibrated average values) and the *Test for Equal Variances* which compares newly estimated and pre-calibrated values of the variances. The names of the tests are carried over from [67]. Detection thresholds were presented using confidence intervals in [61]. The detection threshold is adapted provided that *Two Sample T-test* or the *Test for Equal Variances* show the difference between newly estimated and pre-calibrated values of the parameters of the knock sensor signal at a certain frequency (average values and variances). Finally, new values of the detection threshold are calculated using a model for the confidence limit and newly estimated values of the mean and standard deviations.
Engine knock threshold is a function of ignition timing, and new values of the knock detection threshold are available for a certain values of the ignition

timing only. The adaptation however, should be performed for all accessible values of the ignition timing. Therefore a data-driven algorithm described in Section 6.3 which is suitable for adaptation of the look-up tables with a meagre new data representation is chosen for adaptation of the knock detection threshold.

This Chapter also develops a simple statistical model for evaluation of the knock control concept. The model consists of three parts: generation of the amplitude signals, threshold value determination and a knock sound model. Amplitudes for modeled knock sensor and microphone signals are developed using random number generators with average values and standard deviations as input variables. Average values and standard deviations are the functions of the ignition timing. The threshold value is also a function of ignition timing and is assigned using knock occurrence percentage number. Notice, that similar model was developed in [119]. A new part proposed in this Chapter is a knock sound model.

Engine knock produces a 'clanging' or 'pinging' sound coming from the vibrations of the engine block due to the pressure waves generated inside of the cylinder. This sound is detectable by using a signal from the external microphone. The microphone signal has the same knock frequencies as the cylinder pressure and knock sensor signals. This sound could be audible for the driver and passengers. Driver knock audibility is difficult to verify since it depends on many of factors. Statistical knock audibility at a certain frequency is introduced in this Chapter and is associated with the outlier detection method. The sample of the amplitude of the microphone signal at a certain frequency is measured at the knock event. Audibility test is associated with the statistical hypothesis that this sample of the amplitude is drawn from the parent distribution which represents a background noise where the knock, if any, is inaudible. Outlier is detected using *Two Sample T-test* (see Appendix D) which is used for testing the equality of two means, where the first mean is the mean value of the background noise and the second one is a single amplitude sample measured during a knock event with estimated pooled variance which is equal to the variance of the background noise. This concept allows judgement of knock audibility.

A Volvo six cylinder prototype engine equipped with the cylinder pressure and block vibration sensors was used in the experiments. External microphone was used for the knock sound measurements. Algorithms are implemented in MATLAB and applied to the measured data collected from the engine.

10.2 Statistical Models of the Knock Sensor and Microphone Signals

10.2.1 Generation of the Amplitude Signals

Statistical models for the knock sensor and microphone signals are designed via calculation of the frequency contents of the signals using trigonometric

interpolation method described in Section 9.2. Notice that a recursive DFT (Discrete Fourier Transformation) method described in Section 4.3 can also be used for calculation of the frequency contents of the signal. However, the orthogonality condition for the trigonometric polynomials in certain interval is the main restriction to the approximation performance and hence to the application of the DFT method.
Average maximal amplitudes and standard deviations are calculated at all the frequencies as functions of ignition timing. Average maximal amplitudes and standard deviations for the knock sensor signal as functions of the frequency and ignition timing are presented in Figure 10.1 and Figure 10.2 respectively. All the models in this Chapter are designed for 1000 [rpm] and full load.

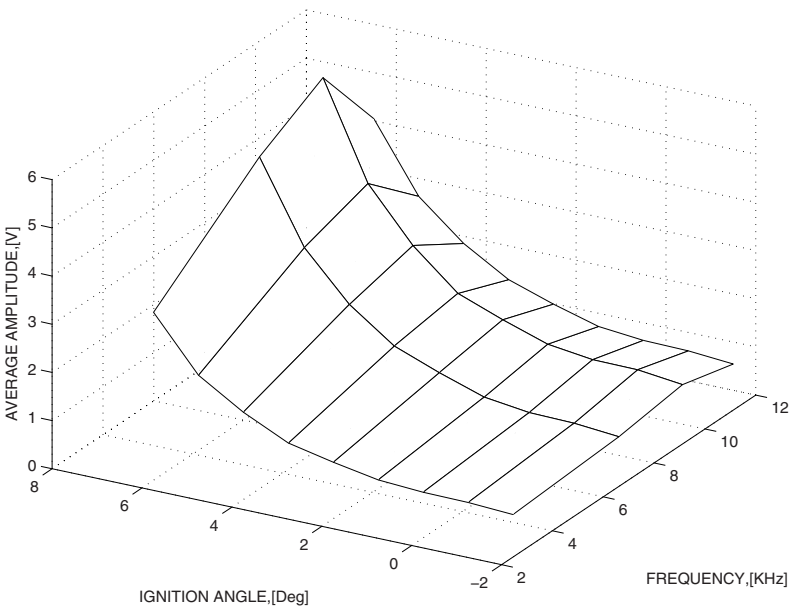

FIG 10.1. Average maximal amplitudes for the knock sensor signal as a function of the frequency and ignition timing. The frequencies are measured in KHz and ignition timing is defined in degrees before TDC (Top Dead Center). Engine is operating at 1000 [rpm] and full load.

Average maximal amplitude and standard deviation of the knock sound pressure as a function of the frequency and ignition timing, measured by the microphone signal are presented in Figure 10.3 and Figure 10.4 respectively.

Engine knock detection circuit has a band-pass filter that filters amplitude signal at a certain frequency. The most suitable frequency (the frequency of 7.5 KHz) for the knock detection is determined according to the method described in Chapter 9. Since the distribution of the maximal amplitudes of

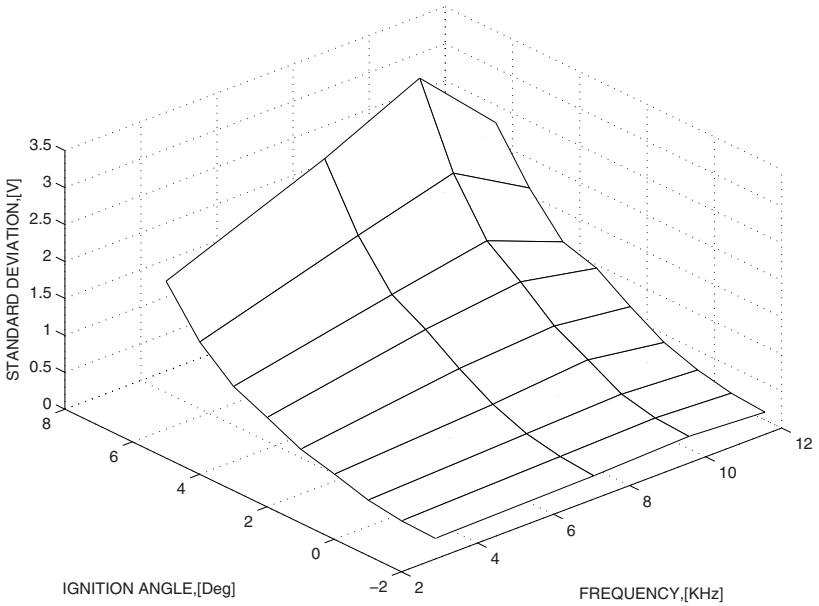

FIG 10.2. Standard deviation for the knock sensor signal as a function of the frequency and ignition angle. Engine is operating at 1000 [rpm] and full load.

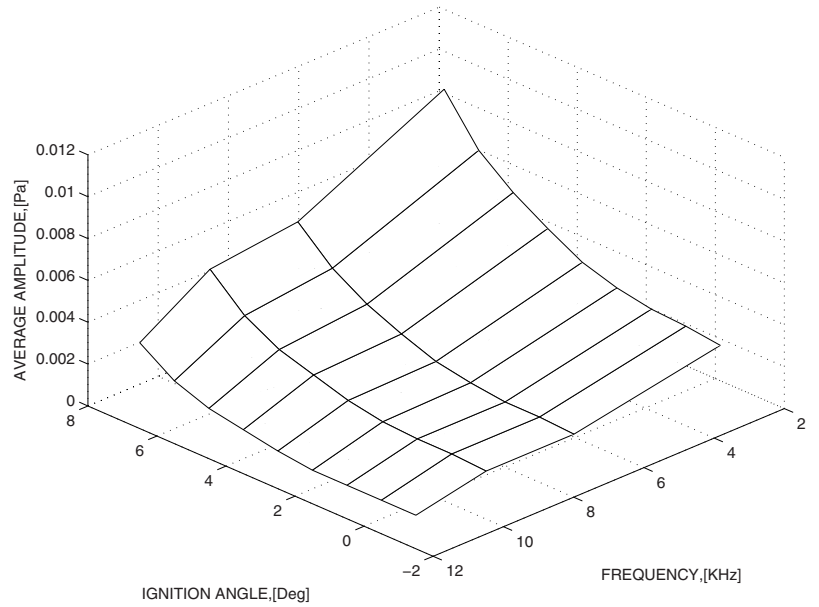

FIG 10.3. Average maximal amplitude of the knock sound pressure signal as a function of the frequency and ignition angle.

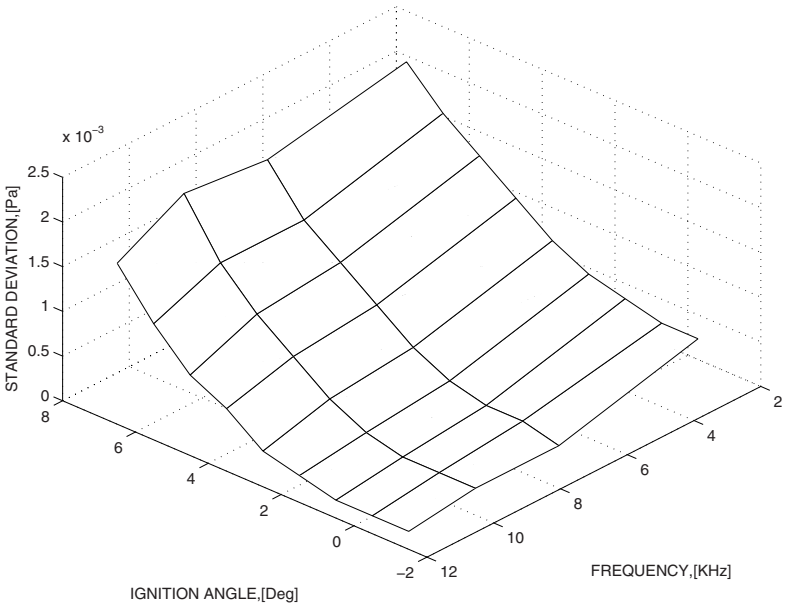

FIG 10.4. Standard deviation of the knock sound pressure signal as a function of the frequency and ignition angle.

the knock sensor signal at this frequency is close to the lognormal distribution (it has a longer tail on the right-hand side), the maximal amplitude signal is generated using lognormal random numbers with the average values and standard deviations presented in Figure 10.1 and Figure 10.2. Distributions for measured and generated maximal amplitudes are plotted in Figure 10.5 and Figure 10.6 respectively. Notice that the agreement between generated and measured distributions is good enough for evaluation of the closed loop knock controller. The closeness of the two distributions can also be evaluated statistically using non-parametric Wilcoxon-Mann-Whitney test [33].

Maximal amplitudes of the microphone signal follow normal distribution at all the frequencies and could be easily generated using normal random numbers. However, generated amplitudes of the microphone signal should be synchronized with the knock signal amplitudes. To this end the difference between the generated value of the maximal amplitude of modeled knock signal and its average value is expressed in terms of standard deviations of this signal. Maximal amplitude of the microphone signal is generated using the same difference between generated and average values expressed in terms of the standard deviations of the microphone signal at a certain frequency.

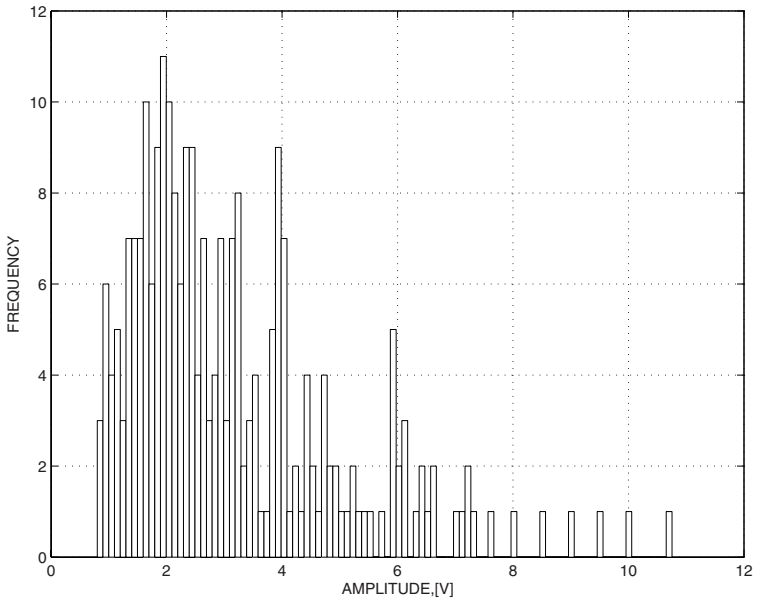

FIG 10.5. Distribution of measured signal of the maximal amplitude at the frequency of 7.5 *KHz*.

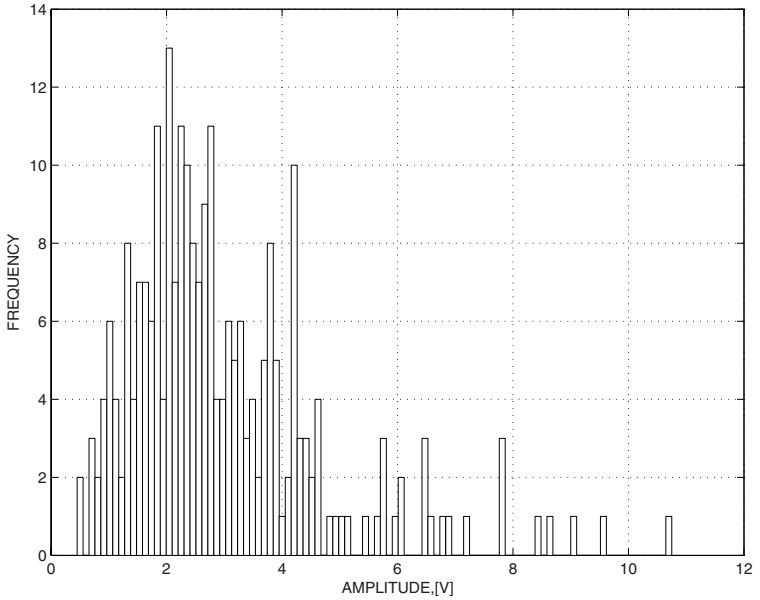

FIG 10.6. Distribution of generated signal of the maximal amplitude at the frequency of 7.5 *KHz*.

10.2.2 Threshold Value Determination

The model is completed by assigning a threshold value for the maximal amplitude signal of the knock sensor at a certain frequency. If the maximal amplitude of the knock sensor signal exceeds this threshold value the knock is judged to occur. This threshold value is the function of ignition timing. The knock occurrence percentage is first determined for a certain number of cycles using the cylinder pressure signal. The threshold value for the maximal amplitude of the knock sensor signal is assigned so that the knock occurrence percentage for the cylinder pressure and knock sensor signals is the same [30].

10.2.3 Knock Sound Model

Statistical knock sound model is developed in this Section for audibility judgement of the knock events. Statistical knock audibility at a certain frequency is associated with the outlier detection method. The sample amplitude of the microphone signal at a certain frequency is measured at the knock event. Audibility test is associated with the statistical hypothesis that this sample amplitude is drawn from the parent distribution which represents a background noise where the knock is inaudible. This background noise normal parent distribution is characterized by the mean value and standard deviation at the ignition angle -1.5^o (see Figure 10.3 and Figure 10.4). Outlier is detected using *Two Sample T-test* which is used for testing the equality of two means, where the first mean is the mean value of the background noise and the second one is a single amplitude sample measured during a knock event with estimated pooled variance which is equal to the variance of the background noise. Outlier detection test which is based on *Two Sample T-test* is illustrated in Figure 10.7. The difference between the value of the statistic calculated in *Two Sample T-test* and the values in the Student distribution look-up table are plotted as a function of the amplitude and significance level for different frequencies. The knock is statistically audible with a certain significance level for those amplitude values where the difference is positive (above zero as is indicated in Figure 10.7), i.e. the value of the statistic is larger than the value in the Student distribution look-up table, that detects those amplitudes as outliers from background noise. Statistical knock audibility depends on the significance level and frequency.

Notice that the statistical models for the knock sensor and microphone signals are based on a data obtained from a given engine. Statistical properties (average value and standard deviation) of the knock sensor and microphone signals might change due to the hardware changes during the project of the engine development. Therefore the model described above should be re-calibrated after changes in the engine hardware.

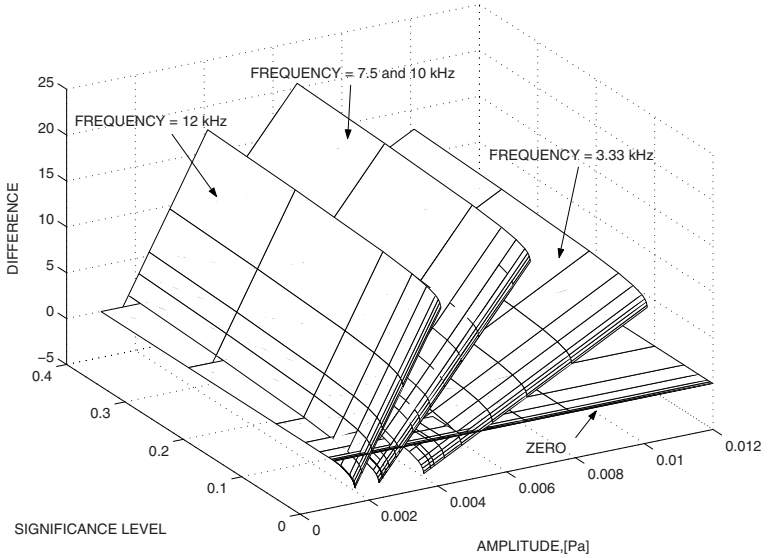

FIG 10.7. The difference between the value of the statistic calculated in *Two Sample T-test* and the values in the Student distribution look-up table are plotted as a function of the amplitude and significance level for different frequencies. The surface with zero values is indicated as 'ZERO'.

10.3 Engine Knock Control with Desired α-risk

10.3.1 Introduction

Suppose that the amplitude of the knock sensor signal is measured at a certain frequency as an output of the band-pass filter and the maximum of this amplitude is calculated over the knock window. Since maximal amplitudes follow lognormal distribution the logarithm of the maximal amplitude signal is taken, converting the data to normally distributed data. Maximal amplitude signal A_k, (k is the cycle number) which is normally distributed is the input for the control algorithm.

Define the following regulation variable

$$T_k = \frac{(A_t - \overline{A}_k)\sqrt{w-1}}{s_k} \tag{10.1}$$

where $\overline{A}_k = \dfrac{1}{w} \displaystyle\sum_{i=k-(w-1)}^{i=k} A_i$, is the value of the maximal amplitude averaged over the window of a size w, s_k is a standard deviation,

$s_k = \sqrt{\frac{1}{w-1}\sum_{i=k-(w-1)}^{i=k}(A_i - \overline{A}_k)^2}$, A_t is a knock threshold value, T_k is a regulation variable, which defines the difference between A_t and $\overline{A}_k$. This difference is expressed in terms of standard deviations multiplied by the size of a moving window. In other words equation (10.1) defines a value of $t-statistic$ used for *One Sample T-test* that compares the average value $\overline{A}_k$ to the target (threshold) value A_t in each step k. Regulation variable (10.1) is controlled via the ignition timing since the average amplitude $\overline{A}_k$, the sample standard deviation s_k and the threshold value A_t are functions of the ignition timing (see Figure 10.1, Figure 10.2 and Figure 10.12).

10.3.2 Control Aims

The achievement of the control aim is associated with the rejection of the null statistical hypothesis H_0 that the average value of the amplitude is equal to the target value. The null hypothesis is tested against the alternative statistical hypothesis H_A that the average value of the amplitude is smaller than the target value, i.e.,

$$H_0 : A_t = \overline{A}_k \tag{10.2}$$
$$H_A : A_t > \overline{A}_k \tag{10.3}$$

In other words the control aim is to regulate the mean value of the amplitude $\overline{A}_k$ so that H_0 is asymptotically rejected in favor of H_A with a certain significance level α. The probability of rejecting the null hypothesis mistakenly is called a significance level or α - risk. The α- risk is associated with the probability of the knock occurrence,i.e., with the probability that the random amplitude A exceeds the threshold value A_t, $P\{A \geq A_t\}$. For estimation of the probability of the knock occurrence the following Markov's inequality is used

$$P\{x \geq \varepsilon\} \leq \frac{E(x)}{\varepsilon} \tag{10.4}$$

where random variable x is positive and has a mathematical expectation $E(x)$, P is a probability sign, ε is any positive constant. Applying inequality (10.4) to the variable $x = (A-a)^2$, where A is a positive random variable (maximal amplitude), and $a = E[A]$ yields

$$P\{(A-a)^2 \geq \varepsilon\} \leq \frac{E[(A-a)^2]}{\varepsilon} \tag{10.5}$$

Taking into account that $E[(A-a)^2] = \sigma^2$ where σ is a standard deviation of the random variable A, and choosing $\varepsilon = (A_t - a)^2 > 0$ in (10.5), the

probability that $A \geq A_t$ for target values which are larger than the average value $A_t > a$, is estimated as follows:

$$\begin{aligned} & P\{A \geq A_t\} \leq P\{[(A-a) \geq (A_t-a)] \\ \cup \quad & [-(A-a) \geq (A_t-a)]\} \\ = \quad & P\{(A-a)^2 \geq (A_t-a)^2\} \\ \overset{\leq}{(10.5)} \quad & \left(\frac{\sigma}{A_t-a}\right)^2 \end{aligned} \tag{10.6}$$

Therefore the probability that the random amplitude A exceeds the threshold value A_t, i.e., the probability of the knock occurrence is bounded by $\left(\frac{\sigma}{A_t-a}\right)^2$. Notice that inequality (10.6) makes sense if $\sigma < (A_t - a)$ otherwise inequality (10.6) is trivial. The upper bound of the probability of the knock occurrence is equal to $\frac{1}{\eta^2}$ provided that the difference $(A_t - a)$ is expressed in terms of the standard deviations $(A_t - a) = \eta\sigma$, $\eta > 0$, showing that the better the separation between the mean value a and the target value A_t the less the probability of the knock occurrence.

The standard deviation σ and $(A_t - a)$ can be expressed in terms of the sample standard deviation s, using confidence intervals for a mean value and standard deviation, and (10.8). It can be shown that the upper bound of the knock occurrence can be reduced via the reduction of the significance level α. Therefore the significance level α can be associated with the upper bound of the probability of the knock occurrence.

The control aim is to find the ignition timing such that

$$T_k \to T_d \quad as \quad k \to \infty \tag{10.7}$$

where T_d is the desired value of the statistic T_k, $T_d = T_t + \Delta$, where T_t is the value in the Student distribution look-up table $T_{1-2\alpha,w-1}$ for degrees of freedom $w-1$, and Δ is a small positive number. If $T_k \to T_d$ as $k \to \infty$ then

$$\frac{(A_t - \overline{A}_k)\sqrt{w-1}}{s_k} > T_t \quad as \quad k \to \infty \tag{10.8}$$

The achievement of the control aim (10.8) guarantees that H_0 is asymptotically rejected in favor of H_A with a certain significance level α (specified by the designer). This in turn guarantees a desired separation between the average value $\overline{A}_k$ and the threshold value A_t, i.e.,

$$A_t > \overline{A}_k + T_t \frac{s_k}{\sqrt{w-1}} \quad as \quad k \to \infty \tag{10.9}$$

Actual value of the statistic T_k which is given by (10.1) is associated with the actual α-risk, $\alpha_{actual,k}$ for a certain degrees of freedom. Actual α-risk, $\alpha_{actual,k}$ is defined as a solution of the following algebraic equation

$$T_k = T_{st}(\alpha_{actual,k}, w-1) \tag{10.10}$$

where $T_{st}(\cdot, w-1)$ is one dimensional look-up table drawn from the Student distribution look-up table for a given degrees of freedom $w-1$, T_k is given by (10.1), $\alpha_{actual,k} = T_{st}^{-1}(T_k, w-1)$. The α-risk can also be defined as a solution of equation (10.10) with $T_k = T_d$, i.e., $\alpha = T_{st}^{-1}(T_d, w-1)$. Taking into account that $T_{st}^{-1}(\cdot)$ satisfies locally Lipshits condition yields

$$\begin{aligned} |\alpha_{actual,k} - \alpha| &= |T_{st}^{-1}(T_k, w-1) - T_{st}^{-1}(T_d, w-1)| \\ &\leq L|T_k - T_d| \end{aligned} \tag{10.11}$$

where $L > 0$ is a local Lipshits constant. Hence the actual α-risk, $\alpha_{actual,k}$ converges to α-risk

$$\alpha_{actual,k} \to \alpha \quad as \quad k \to \infty, \tag{10.12}$$

provided that the control aim (10.7) is reached. Therefore any controller which guarantees the achievement of the control aims (10.8),(10.12) can be called the controller with the desired significance level, which in turn is associated with the probability of the knock occurrence.

10.3.3 Trade-off Between the α-risk and Fuel Consumption

Desired value of the α-risk and hence the statistic T_d should be chosen by taking into account customer related data. Engine fuel consumption can be mapped as a function of ignition angle. Average amplitude $\overline{A}$, the threshold value A_t, and the standard deviation s are also mapped as a function of the ignition angle. Therefore the values of the statistic T can be calculated using (10.1) as a function of two variables: ignition angle and the window size w. Actual α-risk is calculated then via (10.10) and using just calculated value of the statistic. The final step is elimination of the ignition variable by replacing it by the engine fuel consumption table. As a result two dimensional look-up table with two input variables,i.e, the engine fuel consumption and the window size, and one output variable α-risk is produced. Two dimensional look-up table is presented in the form of the surface in three dimensional space in Figure 10.8 where the α-risk is plotted as a function of fuel consumption and the window size. Figure 10.8 shows that the α-risk increases when the window size and the fuel consumption decreases. Specifying a desired fuel consumption and window size, which should be chosen so that to get the best quality of the estimation of the average value, a desired significance level which is related to the probability of the knock occurrence can be calculated using Figure 10.8.

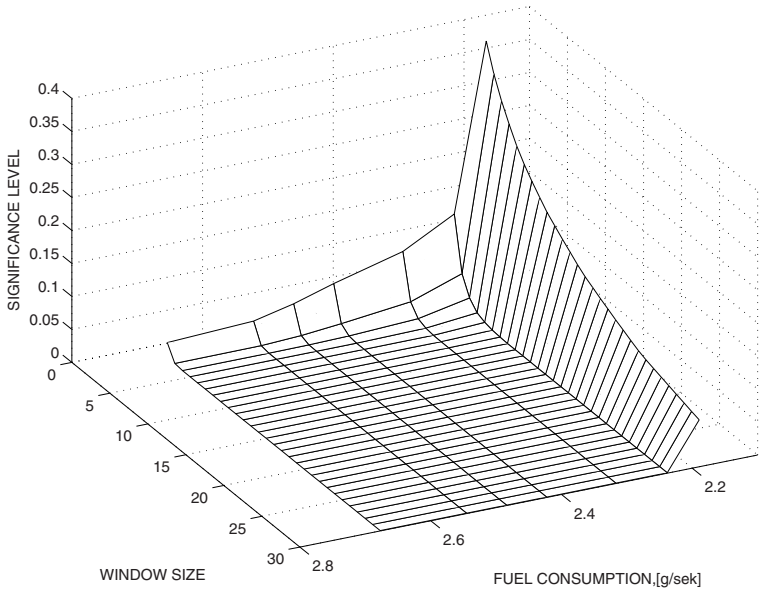

FIG 10.8. The significance level which is proportional to the probability of the knock occurrence is plotted as a function of a window size and engine fuel consumption.

10.3.4 Control Algorithm

The ignition timing is defined according to the conventional knock controller which is widely used in industry and realizes count-up/down logic as follows

$$I_k = \begin{cases} I_{k-1} - \delta_{down} & if \quad e_k < 0 \\ I_{k-1} + \delta_{up} & if \quad e_k > 0 \end{cases}$$

$$e_k = T_k - T_d \tag{10.13}$$

where e_k is the regulation error, I_k is the ignition timing, δ_{down} and δ_{up} are positive constants (count down/count up gains).

In the case of the knock occurrence the amplitude exceeds the threshold value, and therefore the ignition timing should immediately be retarded. To this end a new control aim which is again associated with the statistical hypothesis (10.3) is set up. The ignition retard can be calculated as follows. First, the desired value of the average amplitude $\overline{A}_{des}$ is calculated according to the following reference equation

$$T_{dknock} = \frac{(A_t - \overline{A}_{des})\sqrt{w-1}}{s_k} \tag{10.14}$$

where $\overline{A}_{des}$ is the desired value of the average amplitude, T_{dknock} is the desired value of the statistic (specified by the designer) in the case of knock,

$T_{dknock} = T_{tknock} + \Delta$ where T_{tknock} is the value in the Student distribution look-up table for degrees of freedom $w-1$ and a significance level in case of knock α_{knock}, $T_{tknock} = T_{(1-2\alpha_{knock}),w-1}$, Δ is a small positive number. Notice that the significance level in case of knock α_{knock} is specified by the designer and should be chosen significantly smaller than α, this in turn implies a significant reduction of the probability of the knock occurrence which is achieved by the ignition retard. A desired average amplitude is calculated according to the reference equation (10.14), i.e.,

$$\overline{A}_{des} = A_t - \frac{T_{dknock} s_k}{\sqrt{w-1}} \tag{10.15}$$

Since the average amplitude is a function of ignition timing, i.e., $\overline{A} = f(I)$, the ignition timing in the case of knock is defined as a solution of the following equation $\overline{A}_{des} = f(I_{des})$, where I_{des} is a desired ignition timing, $\overline{A}_{des}$ is calculated with (10.15). Notice that the dependences of the standard deviation and the threshold value from ignition timing are ignored here since the standard deviation decreases and the threshold value increases with the ignition retard. If (10.14) is valid then

$$\frac{(A_t - \overline{A}_k)\sqrt{w-1}}{s_k} > T_{tknock} \tag{10.16}$$

in a certain step k. This in turn implies that the null hypothesis (10.2) is rejected in favor of the alternative hypothesis (10.3) with a significance level α_{knock} which is significantly less than α that results in retard of the ignition timing. The stability analysis of the control system (10.1), (10.13) can be made by means of the Ordinary Differential Equation (ODE) approach [16], [56] (see Appendix E).

10.4 Simulation of the Closed Loop Knock Control System

Engine knock control algorithm (10.13) was simulated in MATLAB using the model described in Section 10.2. Simulation results are presented in Figure 10.9 and Figure 10.10. Figure 10.9 shows ignition angle count-up sequence and ignition retard due to the knock event. The knock event is detected via the comparison of the maximal amplitude signal to the threshold value. Increasing ignition angle reduces a fuel consumption and increases the probability of the knock occurrence (see Figure 10.8). Actual and desired significance levels are plotted in Figure 10.10.

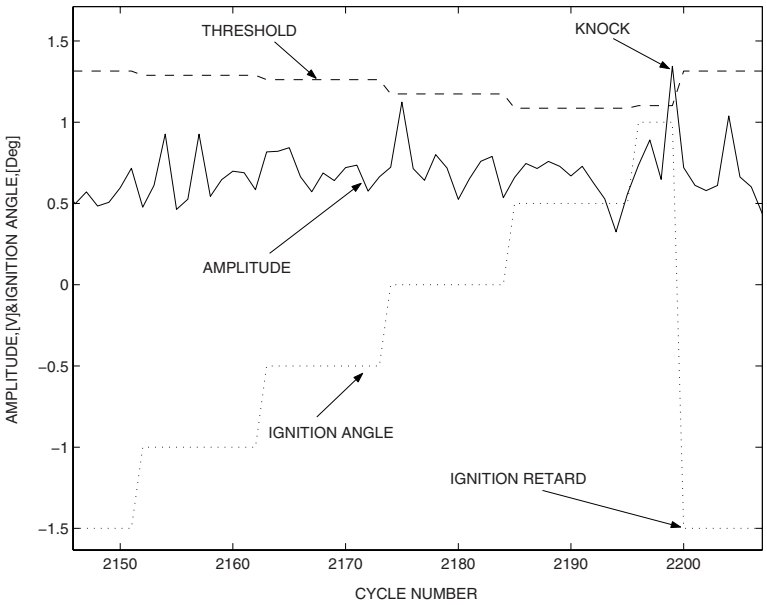

FIG 10.9. Count-up-count-down knock control results. Maximal amplitude, ignition angle and threshold values are plotted as a function of a cycle number. Ignition angle is defined in degrees before TDC. Maximal amplitude is plotted with a solid line. Ignition angle is plotted with a dotted line and threshold is plotted with a dashed line.

10.5 Adaptation of the Threshold Value

The performance deterioration of the knock sensor signal due to aging of the engine components has a direct impact on the average values and standard deviations of the maximal amplitude at a certain frequency. Therefore the knock detection threshold should be updated for aged engines preventing erroneous knock detection. Threshold adaptation algorithm is described in this Section.

First, a pre-calibrated threshold value at a given ignition angle is assigned to the upper confidence limit (see Appendix D) of the amplitude signal as follows:

$$A_t = \overline{A} + t_{\alpha_t/2,n-1} s \sqrt{\frac{n+1}{n}} \tag{10.17}$$

where $\overline{A}$ and s are pre-calibrated values of the average amplitude and standard deviation respectively, n is the sample size, $t_{\alpha_t/2,n-1}$ is the value taken from the Student distribution look-up table for a significance level α_t and degrees of freedom $n-1$, A_t is a pre-calibrated value of the knock detection threshold defined in Section 10.2.2.

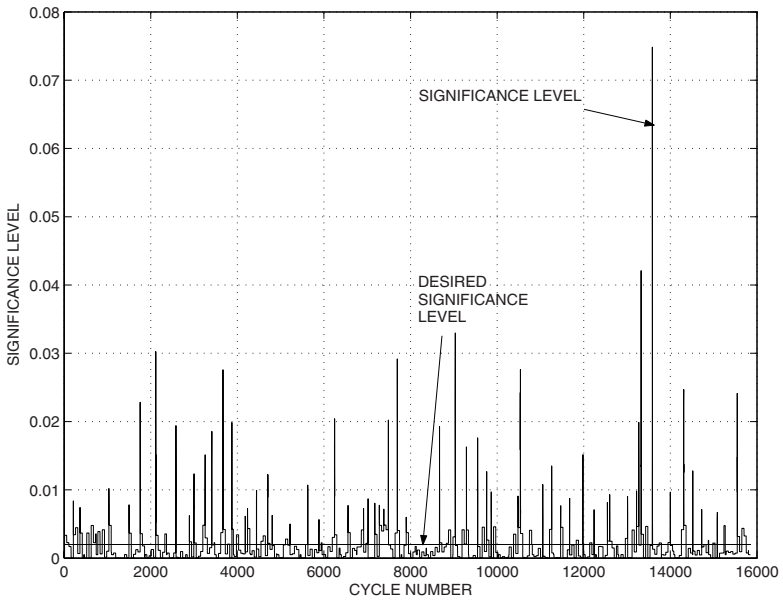

FIG 10.10. Actual and desired significance levels in the closed-loop system. Desired significance level is $\alpha = 0.002$.

Notice, that the confidence interval is usually defined as a stochastic (theoretical) interval [64] where the average value and the standard deviation are random variables. A certain probability of containing a random sample within a confidence interval is associated with this stochastic interval. Therefore the probability of the knock occurrence can be associated to the upper confidence limit provided that the average value and the standard deviation are random variables. When calculating the average value $\overline{A}$ and the standard deviation s for a specific sample of the size n, the upper confidence limit as a fixed number is assigned to the knock detection threshold value. Unfortunately, the probability of the knock occurrence can not be associated with the upper confidence limit for specific (not random) values of $\overline{A}$ and the standard deviation s. However, a certain significance level α_t which is used as a basis for adaptation can be associated with a knock detection threshold. The threshold adaptation is performed for aged engine holding the same significance level which is assigned for a new engine.

Relationship (10.17) is treated as a equation with a significance level α_t as unknown variable. Equation (10.17) is resolved with respect to the significance level α_t for each ignition timing. Significance level as a function of ignition timing is presented in Figure 10.11 and uniquely defines the knock detection threshold value. As soon as the significance level α_t is determined, the relationship (10.17) becomes a function for calculation of the knock detection

threshold with the average value $\overline{A}$, standard deviation s and a sample size n as input variables.

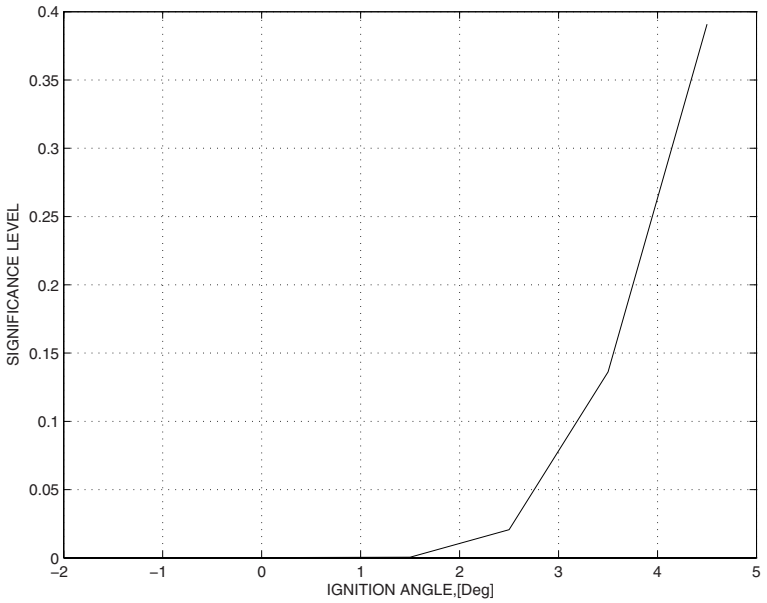

FIG 10.11. Significance level as function of ignition angle. The significance level determines the threshold value for knock detection.

The knock detection threshold is adapted provided that the averaged value $\overline{A}$ and/or the standard deviation s deviate from the pre-calibrated values. New values of the threshold are calculated as a function of ignition timing with newly estimated average value and standard deviation and the significance level α_t presented in Figure 10.11:

$$A_{tim} = \overline{A}_{im} + t_{\alpha_t/2,w-1} s_{im} \sqrt{\frac{w_t + 1}{w_t}} \tag{10.18}$$

where $\overline{A}_{im}$ and s_{im} are the average value and the standard deviation respectively, newly calculated over the window of a size w_t, $i = I_1, I_2, ...$ is the ignition angle, A_{tim} are newly calculated values of the threshold. The difference ε_i between pre-calibrated A_{ti} and new values A_{tim} of the knock detection threshold

$$\varepsilon_i = A_{ti} - A_{tim} \tag{10.19}$$

is approximated as follows:

$$\hat{\varepsilon} = \varphi^T \theta \tag{10.20}$$

$$\varphi = [1 \quad I \quad I^2 \quad I^3 \quad ...]^T \tag{10.21}$$

$$\theta = [\theta_0 \quad \theta_1 \quad \theta_2 \quad \theta_3 \quad ...]^T \tag{10.22}$$

where $\hat{\varepsilon}$ is a polynomial approximation of ε_i, I is the ignition angle, θ_j, $j = 0, 1, ...$ The model is constructed using step-wise regression method (described in Chapter 6), where the contribution of each term θ_0, $\theta_1 I$, $\theta_2 I^2$ is reviewed, to ensure that it remains statistically significant, using the following variance

$$V_j = \frac{1}{(N-j-1)} \sum_{i=1}^{N} (\varepsilon_i - \theta_0 - \theta_1 I_i - \theta_2 I_i^2 - \theta_3 I_i^3 \quad - ... - \quad \theta_j I_i^j)^2 \tag{10.23}$$

where j is the order of the polynomial, N is the number of measured points. The process is stopped if the variance V_{j+1} does not get significantly smaller than the variance V_j. The variances V_{j+1} and V_j are compared using the *Test for Equal Variances* (see Appendix D). The coefficients (10.22) are calculated using a least-squares method. Step-wise regression method is in fact, the method of the selection of the optimal order of the polynomial. Polynomial of a low order which is robust with respect to the measurement noise might give a relatively large approximation error. Polynomial of a high order does not smooth a measurement noise, which in turn has a direct impact on the coefficients of the polynomial.

As soon as the coefficients and the optimal order of the polynomial are found that defines the model $\hat{\varepsilon}$, the values of the compensation term are calculated and added to the values in the nodes of pre-calibrated look-up table of the knock detection threshold.

The result of adaptation is shown in Figure 10.12. Average value $\overline{A}_{im}$ and a standard deviation s_{im} which are larger than pre-calibrated are used for calculation of new values of the threshold with (10.18) and significance level plotted in Figure 10.11. New measured values of the threshold are plotted in Figure 10.12 with plus signs. Notice, that new measured values are available at ignition angles $[-1.5^o \quad -1^o \quad -0.5^o]$ (the angle is measured in degrees before TDC) only since the closed loop knock control system with increased average value and the standard deviation of the amplitude operates mainly at these ignition angles (see Figure 10.9). The adaptation is performed in two steps. In the first step the offset is updated only ($\hat{\varepsilon} = \theta_0$). The result of adaptation is plotted in Figure 10.12 with a dotted line. Figure 10.12 shows that the adaptation can further be improved introducing a term proportional to ignition angle ($\hat{\varepsilon} = \theta_0 + \theta_1 I$). Final result of the threshold adaptation is shown in Figure 10.12 with a dashed line.

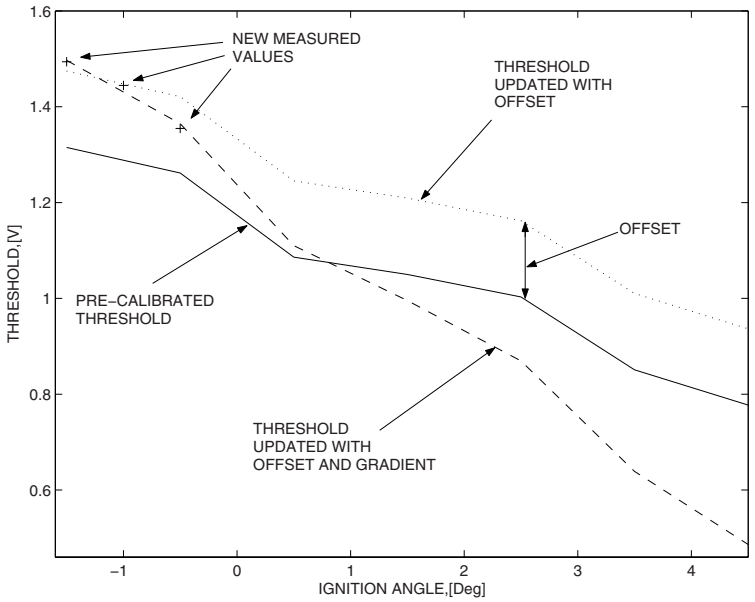

FIG 10.12. Adaptation of the threshold. New measured values of the threshold are plotted with plus signs. Pre-calibrated threshold is plotted with a solid line. Two types of adaptation are shown. The first one is adaptation with the offset only ($\hat{\varepsilon} = \theta_0$) and it is plotted with a dotted line. The second one is adaptation with offset and gradient ($\hat{\varepsilon} = \theta_0 + \theta_1 I$) and it is plotted with a dashed line.

10.6 Conclusion

A novel statistical engine knock control concept that allows the connection of the control algorithm parameters with the probability of the knock occurrence and customer related data is proposed and verified by simulations. New algorithm for adaptation of the knock detection threshold is developed. Adaptation guarantees the same detection performance for new and aged engines, reducing the risk of erroneous knock detection which has a direct impact on the engine fuel economy.

Statistical simulation model which can be used for simulation, calibration and evaluation of different control strategies was also developed. Application of this simulation model to calibration and evaluation of different control strategies reduces the time and cost associated with calibration and algorithm development.

11

Appendix A

Trigonometric Interpolation Method

The trigonometric interpolation algorithm described by (4.3), (4.5), (4.6) and (4.7) is derived in this Appendix.

The coefficients of the polynomial (4.3) which minimize (4.4) satisfy the following equations:

$$wa_0 + \sum_{q=1}^{n}(a_q \sum_{l=1}^{w} cos(qx_l) + b_q \sum_{l=1}^{w} sin(qx_l)) = \sum_{l=1}^{w} y_l \tag{11.1}$$

$$a_0 \sum_{l=1}^{w} cos(px_l) + \sum_{q=1}^{n}(a_q \sum_{l=1}^{w} cos(qx_l)cos(px_l) + b_q \sum_{l=1}^{w} sin(qx_l)cos(px_l)) = \sum_{l=1}^{w} y_l cos(px_l) \tag{11.2}$$

$$a_0 \sum_{l=1}^{w} sin(px_l) + \sum_{q=1}^{n}(a_q \sum_{l=1}^{w} cos(qx_l)sin(px_l) + b_q \sum_{l=1}^{w} sin(qx_l)sin(px_l)) = \sum_{l=1}^{w} y_l sin(px_l), \tag{11.3}$$

where $p = 1, 2, ...n$. Equation (11.1) represents $\frac{\partial E}{\partial a_0} = 0$, whereas equation (11.2) represents $\frac{\partial E}{\partial a_q} = 0$ and, finally, the equation (11.3) represents $\frac{\partial E}{\partial b_q} = 0$.

Let the measurements be crank angle synchronized with a step size of Δ i.e.,

$$x_1 = \Delta, \quad x_2 = 2\Delta, \quad \ldots \quad , \; x_w = w\Delta, \quad \Delta = \frac{2\pi}{w} \tag{11.4}$$

Consider the following sums:

$$\sum_{l=0}^{w} e^{iql\Delta} = 1 + e^{iq\Delta} + e^{iq2\Delta} + \ \ldots \ + e^{iqw\Delta} \tag{11.5}$$

$$e^{iq\Delta} \sum_{l=0}^{w} e^{iql\Delta} = e^{iq\Delta} + e^{iq2\Delta} + \ \ldots \ + e^{iq(w+1)\Delta} \tag{11.6}$$

where $i^2 = -1$.
Subtraction of (11.6) from (11.5) yields

$$(1 - e^{iq\Delta}) \sum_{l=0}^{w} e^{iql\Delta} = 1 - e^{iq(w+1)\Delta} \tag{11.7}$$

Taking into account that

$$\sum_{l=1}^{w} e^{iql\Delta} = \sum_{l=0}^{w} e^{iql\Delta} - 1 \tag{11.8}$$

(11.7) can be written as follows:

$$\sum_{l=1}^{w} e^{iql\Delta} = \frac{e^{iq(w+1)\Delta} - e^{iq\Delta}}{e^{iq\Delta} - 1} \tag{11.9}$$

and

$$\sum_{l=1}^{w} e^{iqx_l} = \sum_{l=1}^{w} e^{iql\Delta} = \frac{e^{iq(w+1)\Delta} - e^{iq\Delta}}{e^{iq\Delta} - 1} = \frac{(e^{i2q\pi} - 1)e^{iq\Delta}}{e^{iq\Delta} - 1}$$
$$= \frac{\{(cos(2\pi q) + isin(2\pi q)) - 1\}e^{iq\Delta}}{(cos(2\pi \frac{q}{w}) + isin(2\pi \frac{q}{w})) - 1} = 0 \tag{11.10}$$

since $\Delta = \frac{2\pi}{w}$, and $cos(2\pi q) + isin(2\pi q) = 1$ where q is any integer, and q is not a multiple of w i.e., $q \neq ws$ where s is any integer. If $q = ws$ then $cos(2\pi \frac{q}{w}) + isin(2\pi \frac{q}{w}) = cos(2\pi s) + isin(2\pi s) = 1$ and the denominator in (11.10) is equal to zero.

Identity

$$\sum_{l=1}^{w} e^{iqx_l} = 0 \tag{11.11}$$

implies in fact, two identities since the real part of (11.11) and imaginary part of (11.11) both have to be satisfied i.e.,

$$\sum_{l=1}^{w} e^{iqx_l} = \underbrace{\sum_{l=1}^{w} cos(qx_l)}_{=0} + i \underbrace{\sum_{l=1}^{w} sin(qx_l)}_{=0} = 0 \tag{11.12}$$

Hence the following identities are true

$$\sum_{l=1}^{w} cos(qx_l) = \sum_{l=1}^{w} sin(qx_l) = 0 \tag{11.13}$$

provided that q is not a multiple of w.

Notice that identities (11.13) follow also from (12.31) and (12.32) with $h = \frac{2\pi q}{w}$ and $n = w$, where $\sin(\frac{n}{2}h) = \sin(\pi q) = 0$ and $\sin(\frac{h}{2}) = \sin(\frac{\pi}{w}q) \neq 0$ for $q = 1, 2, 3, ...$ and not a multiple of w.

Further evaluation gives the following:

$$\sum_{l=1}^{w} cos(qx_l)cos(rx_l) = \frac{1}{2}\sum_{l=1}^{w} cos(q+r)x_l + \frac{1}{2}\sum_{l=1}^{w} cos(q-r)x_l \tag{11.14}$$

$$\sum_{l=1}^{w} sin(qx_l)sin(rx_l) = \frac{1}{2}\sum_{l=1}^{w} cos(q-r)x_l - \frac{1}{2}\sum_{l=1}^{w} cos(q+r)x_l \tag{11.15}$$

The sums in the right hand side of the equations (11.14), (11.15) are equal to zero provided that $q + r$ and $q - r$ are not multiple of w.

Using similar arguments one can show that

$$\sum_{l=1}^{w} cos(qx_l)sin(rx_l) = \frac{1}{2}\sum_{l=1}^{w} sin(q+r)x_l + \frac{1}{2}\sum_{l=1}^{w} sin(q-r)x_l = 0 \tag{11.16}$$

for all q and r, $q \neq r$. Finally one can show that the following is true:

$$\sum_{l=1}^{w} cos^2(qx_l) = \frac{1}{2}\sum_{l=1}^{w}(1 + cos(2qx_l)) = \frac{w}{2} \tag{11.17}$$

$$\sum_{l=1}^{w} sin^2(qx_l) = \frac{1}{2}\sum_{l=1}^{w}(1 - cos(2qx_l)) = \frac{w}{2} \tag{11.18}$$

provided that $2q$ is not a multiple of w.

The system (11.1) - (11.3) can be written by taking into account (11.13) - (11.18) as (4.5), (4.6), (4.7).

Remark 1. The solution of the system (11.1), (11.2) and (11.3) has such a simple form due to the orthogonality which is the property of the trigonometric polynomials.

A set of functions $\{cos(qx_l), sin(qx_l)\}$ is orthogonal on the interval x_l, $l = 1, ..., w$ given by (11.4), i.e

$$\sum_{l=1}^{w} cos(qx_l)cos(rx_l) = \begin{cases} \frac{w}{2} & \text{if } q = r \\ 0 & \text{if } q \neq r, \end{cases}$$

$$\sum_{l=1}^{w} sin(qx_l)sin(rx_l) = \begin{cases} \frac{w}{2} & \text{if } q = r \\ 0 & \text{if } q \neq r, \end{cases}$$

$$\sum_{l=1}^{w} cos(qx_l)sin(rx_l) = 0 \text{ for all } q \text{ and } r,$$

and all non-diagonal terms in the matrix defined by (11.1), (11.2) and (11.3) are equal to zero.

Orthogonality property implies also the following:

$$\sum_{l=1}^{w} e^{i(q-r)x_l} = \sum_{l=1}^{w} e^{iqx_l} e^{-irx_l}$$

$$= \sum_{l=1}^{w} [cos(qx_l) + i\ sin(qx_l)][cos(rx_l) - i\ sin(rx_l)]$$

$$= \underbrace{i \sum_{l=1}^{w} sin(qx_l)cos(rx_l)}_{=0} - \underbrace{i \sum_{l=1}^{w} cos(qx_l)sin(rx_l)}_{=0}$$

$$+ \underbrace{\sum_{l=1}^{w} cos(qx_l)cos(rx_l)}_{=\begin{cases} \frac{w}{2} & \text{if } q = r \\ 0 & \text{if } q \neq r \end{cases}} \underbrace{- i^2 \sum_{l=1}^{w} sin(qx_l)sin(rx_l)}_{=\begin{cases} \frac{w}{2} & \text{if } q = r \\ 0 & \text{if } q \neq r \end{cases}} = \begin{cases} w & \text{if } q = r \\ 0 & \text{if } q \neq r. \end{cases}$$

Remark 2. Interpolating polynomial

$$T(x_l) = a_0 + \sum_{q=1}^{n} a_q cos(qx_l) + b_q sin(qx_l) \tag{11.19}$$

with coefficients (4.5), (4.6) and (4.7) can also be written in a complex compact form. Taking into account that

$$cos(qx_l) = \frac{1}{2}[e^{iqx_l} + e^{-iqx_l}]$$
$$sin(qx_l) = \frac{1}{2i}[e^{iqx_l} - e^{-iqx_l}]$$

(11.19) can be written as follows:

$$\begin{aligned} T(x_l) &= a_0 + \sum_{q=1}^{n} a_q cos(qx_l) + b_q sin(qx_l) \\ &= a_0 + \frac{1}{2}\sum_{q=1}^{n} a_q[e^{iqx_l} + e^{-iqx_l}] \\ &- i\ b_q[e^{iqx_l} - e^{-iqx_l}] \\ &= a_0 + \frac{1}{2}\sum_{q=1}^{n}(a_q - ib_q)e^{iqx_l} + (a_q + ib_q)e^{-iqx_l} \end{aligned}$$

Introducing a coefficient

$$\begin{aligned} c_q &= \frac{1}{2}(a_q - ib_q) = \frac{1}{w}\sum_{l=1}^{w} y_l cos(qx_l) - i\frac{1}{w}\sum_{l=1}^{w} y_l sin(qx_l) \\ &= \frac{1}{w}\sum_{l=1}^{w} y_l[cos(qx_l) - isin(qx_l)] = \frac{1}{w}\sum_{l=1}^{w} y_l e^{-iqx_l} \end{aligned}$$

and taking account that the term $\frac{1}{2}(a_q + ib_q)e^{-iqx_l}$ can be obtained from the term $\frac{1}{2}(a_q - ib_q)e^{iqx_l}$ by substituting $-q$ instead of q, where $q = 1, 2, ..., n$ trigonometric interpolation algorithms (11.19), (4.5), (4.6) and (4.7) are presented in the following complex form:

$$\begin{aligned} T(x_l) &= \sum_{q=-n}^{n} c_q e^{iqx_l} \\ c_q &= \frac{1}{w}\sum_{l=1}^{w} y_l e^{-iqx_l} \end{aligned}$$

where $c_0 = \frac{1}{w}\sum_{l=1}^{w} y_l e^{-i0x_l} = \frac{1}{w}\sum_{l=1}^{w} y_l = a_0$.

Remark 3. The step size Δ can also be chosen as follows $\Delta = \frac{720^0}{w}$. Since the orthogonality property (11.13) also holds in this case, the derivation of the coefficients (4.5) - (4.7) is still valid.

Remark 4. The coefficients (4.5), (4.6) and (4.7) can also be obtained using formulas of the Fourier coefficients where the integrals are approximated using a trapezoidal rule.

Remark 5. A minimal number of terms (frequencies) should be used for trigonometric interpolation. The optimal choice of the number of terms (frequencies) in the approximating polynomial (4.3) could be done as follows.

Assume that the measured data can exactly be approximated by the polynomial (4.3) and a measured signal y_l has a random measurement noise only. It is assumed that the measurement errors are independent and normally distributed. In this case the errors in the estimated parameters are also normally distributed, and the following ratio $V = \dfrac{E}{(w - 2n - 1)}$ is the estimate of the variance of the measurement noise, where n is the number of frequencies and E is given by (4.4). A new frequency is included in the model (4.3), if the ratio V is reduced and this reduction is statistically significant. The significance of the variance reduction is established using the *Test for Equal Variances* [64], [67], [118] (see also Appendix D). The choice of the frequencies is optimal if the values of the ratio V and the variance of the measurement noise are approximately the same.

12

Appendix B

Properties of the Kacmarz Projection Algorithm

Properties of the Kacmarz projection algorithm defined by (4.29), (4.33) and (4.35) are discussed in this Appendix.

Consider the following Lyapunov function candidate

$$V_k = \|\tilde{\theta}_k\|^2 \tag{12.1}$$

where $\tilde{\theta}_k = \theta_k - \theta_*$, where θ_* is the vector of true parameters. Notice that the following is true for the update law (4.35):

$$\tilde{\theta}_k - \tilde{\theta}_{k-1} = -\frac{\varphi_k}{\varphi_k^T \varphi_k} \tilde{\theta}_{k-1}^T \varphi_k \tag{12.2}$$

$$\tilde{\theta}_k^T \varphi_k = 0 \tag{12.3}$$

$$\varphi_k^T \varphi_k = n + 1 \tag{12.4}$$

where (12.2) is derived by subtracting of θ_* from the both sides of (4.35), (12.3) is obtained by multiplication of both sides of (12.2) by φ_k^T, and finally (12.4) follows directly from the definition of φ_k (4.33).
Evaluating $V_k - V_{k-1}$ and taking into account (12.2), (12.3) and (12.4) one gets

$$V_k - V_{k-1} = -\frac{(\tilde{\theta}_{k-1}^T \varphi_k)^2}{(n+1)} \tag{12.5}$$

Thus the boundedness of the parameter error $\tilde{\theta}$ is established. The parameters θ converge to their true values θ_*, if the regressor φ is persistently exciting, i.e., if there exist positive constants α, β and N such that the following inequality holds

$$0 < \alpha I \leq \sum_{k=r}^{r+N} \varphi_k \varphi_k^T \leq \beta I \tag{12.6}$$

where $r = 1, 2, ...$ is the step number, N is the size of the window and I is $(2n+1) \times (2n+1)$ unity matrix, where n is the number of the frequencies involved. Define the following matrix:

$$A = \sum_{k=r}^{r+N} \varphi_k \varphi_k^T = \begin{bmatrix} a_{11} & a_{12} & \dots a_{1m} \\ a_{21} & a_{22} & \dots a_{2m} \\ \vdots & \vdots & \vdots\vdots \\ a_{m1} & a_{m2} & \dots a_{mm} \end{bmatrix}$$

with the terms defined by (4.33)

$$a_{11} = N+1, \quad a_{12} = \sum_{k=r}^{r+N} \cos(kq_1\Delta),$$

$$a_{13} = \sum_{k=r}^{r+N} \sin(kq_1\Delta), \quad a_{1m} = \sum_{k=r}^{r+N} \sin(kq_n\Delta),$$

$$a_{21} = a_{12}, \quad a_{22} = \sum_{k=r}^{r+N} \cos^2(kq_1\Delta), \quad a_{23} = \sum_{k=r}^{r+N} \sin(kq_1\Delta)\cos(kq_1\Delta),$$

$$a_{2m} = \sum_{k=r}^{r+N} \cos(kq_1\Delta)\sin(kq_n\Delta), \quad a_{m1} = a_{1m},$$

$$a_{m2} = a_{2m}, \quad a_{mm} = \sum_{k=r}^{r+N} \sin^2(kq_n\Delta),$$

where $m = (2n+1)$. Notice that the terms in the regressor (4.33) are updated crank angle synchronized with the step Δ, and $x_k = k\Delta$, $k = 1, 2, ...$

The terms in the matrix A can be calculated as follows.

First, the following sums are calculated:

$$\sum_{k=1}^{r+N} \cos(kq_i\Delta) = \frac{\cos(\frac{N+r+1}{2} q_i\Delta)\sin(\frac{N+r}{2} q_i\Delta)}{\sin(\frac{q_i\Delta}{2})} \tag{12.7}$$

$$\sum_{k=1}^{r-1} \cos(kq_i\Delta) = \frac{\cos(\frac{r}{2} q_i\Delta)\sin(\frac{(r-1)}{2} q_i\Delta)}{\sin(\frac{q_i\Delta}{2})} \tag{12.8}$$

where $i = 1, ..., n$, n is the number of the frequencies involved, $r > 1$. The sums are calculated using Lemma presented in the end of this Appendix. The

sum (12.7) follows from (12.32) with $h = q_i\Delta$ and $n = r + N$. The sum (12.8) follows from (12.32) with $h = q_i\Delta$ and $n = r - 1$.

The sum $\sum_{k=r}^{r+N} \cos(kq_i\Delta)$ is calculated using (12.7) and (12.8) as follows

$$\begin{aligned}\sum_{k=r}^{r+N} \cos(kq_i\Delta) &= \sum_{k=1}^{r+N} \cos(kq_i\Delta) - \sum_{k=1}^{r-1} \cos(kq_i\Delta) \\ &= \frac{\cos(\frac{N+r+1}{2} q_i\Delta) \sin(\frac{N+r}{2} q_i\Delta)}{\sin(\frac{q_i\Delta}{2})} \\ &- \frac{\cos(\frac{r}{2} q_i\Delta) \sin(\frac{(r-1)}{2} q_i\Delta)}{\sin(\frac{q_i\Delta}{2})} \end{aligned} \tag{12.9}$$

Using similar arguments one can show that

$$\begin{aligned}\sum_{k=r}^{r+N} \sin(kq_i\Delta) &= \frac{\sin(\frac{N+r}{2} q_i\Delta) \sin(\frac{N+r+1}{2} q_i\Delta)}{\sin(\frac{q_i\Delta}{2})} \\ &- \frac{\sin(\frac{r-1}{2} q_i\Delta) \sin(\frac{r}{2} q_i\Delta)}{\sin(\frac{q_i\Delta}{2})} \end{aligned} \tag{12.10}$$

And

$$\begin{aligned}\sum_{k=r}^{r+N} \cos(kq_i\Delta) \cos(kq_j\Delta) &= \frac{1}{2} \sum_{k=r}^{r+N} \cos(k(q_i + q_j)\Delta) \\ &+ \frac{1}{2} \sum_{k=r}^{r+N} \cos(k(q_i - q_j)\Delta) \end{aligned} \tag{12.11}$$

where

$$\begin{aligned}&\sum_{k=r}^{r+N} \cos(k(q_i + q_j)\Delta) = \\ &\frac{\cos(\frac{N+r+1}{2}(q_i + q_j)\Delta) \sin(\frac{N+r}{2}(q_i + q_j)\Delta)}{\sin(\frac{(q_i + q_j)\Delta}{2})}\end{aligned}$$

$$\frac{-\cos(\frac{r}{2}(q_i+q_j)\Delta)\sin(\frac{(r-1)}{2}(q_i+q_j)\Delta)}{\sin(\frac{(q_i+q_j)\Delta}{2})} \tag{12.12}$$

$$\sum_{k=r}^{r+N}\cos(k(q_i-q_j)\Delta) = \frac{\cos(\frac{N+r+1}{2}(q_i-q_j)\Delta)\sin(\frac{N+r}{2}(q_i-q_j)\Delta)}{\sin(\frac{(q_i-q_j)\Delta}{2})} \frac{-\cos(\frac{r}{2}(q_i-q_j)\Delta)\sin(\frac{(r-1)}{2}(q_i-q_j)\Delta)}{\sin(\frac{(q_i-q_j)\Delta}{2})} \tag{12.13}$$

where $j = 1, ..., n$, $i \neq j$. Further evaluation yields:

$$\sum_{k=r}^{r+N}\sin(kq_i\Delta)\sin(kq_j\Delta) = \frac{1}{2}\sum_{k=r}^{r+N}\cos(k(q_i-q_j)\Delta) -\frac{1}{2}\sum_{k=r}^{r+N}\cos(k(q_i+q_j)\Delta) \tag{12.14}$$

where $\sum_{k=r}^{r+N}\cos(k(q_i+q_j)\Delta)$ and $\sum_{k=r}^{r+N}\cos(k(q_i-q_j)\Delta)$ are calculated using (12.12) and (12.13). One can also show the following:

$$\sum_{k=r}^{r+N}\cos(kq_i\Delta)\sin(kq_j\Delta) = \frac{1}{2}\sum_{k=r}^{r+N}\sin(k(q_i+q_j)\Delta) -\frac{1}{2}\sum_{k=r}^{r+N}\sin(k(q_i-q_j)\Delta) \tag{12.15}$$

where

$$\sum_{k=r}^{r+N}\sin(k(q_i+q_j)\Delta) = \frac{\sin(\frac{r+N}{2}(q_i+q_j)\Delta)\sin(\frac{r+N+1}{2}(q_i+q_j)\Delta)}{\sin(\frac{(q_i+q_j)\Delta}{2})} \frac{-\sin(\frac{r-1}{2}(q_i+q_j)\Delta)\sin(\frac{r}{2}(q_i+q_j)\Delta)}{\sin(\frac{(q_i+q_j)\Delta}{2})} \tag{12.16}$$

$$\sum_{k=r}^{r+N} \sin(k(q_i - q_j)\Delta) =$$
$$\frac{\sin(\frac{r+N}{2}(q_i - q_j)\Delta)\sin(\frac{r+N+1}{2}(q_i - q_j)\Delta)}{\sin(\frac{(q_i - q_j)\Delta}{2})}$$
$$\frac{-\sin(\frac{r-1}{2}(q_i - q_j)\Delta)\sin(\frac{r}{2}(q_i - q_j)\Delta)}{\sin(\frac{(q_i - q_j)\Delta}{2})} \tag{12.17}$$

where $i, j = 1, ..., n$, $i \neq j$.

Finally evaluation of the diagonal terms yields:

$$\sum_{k=r}^{r+N} \sin^2(kq_i\Delta) =$$
$$\frac{N+1}{2} + \frac{\cos(rq_i\Delta)\sin((r-1)q_i\Delta)}{2\sin(q_i\Delta)}$$
$$-\frac{\cos((r+N+1)q_i\Delta)\sin((r+N)q_i\Delta)}{2\sin(q_i\Delta)} \tag{12.18}$$
$$\sum_{k=r}^{r+N} \cos^2(kq_i\Delta) =$$
$$\frac{N+1}{2} - \frac{\cos(rq_i\Delta)\sin((r-1)q_i\Delta)}{2\sin(q_i\Delta)}$$
$$+\frac{\cos((r+N+1)q_i\Delta)\sin((r+N)q_i\Delta)}{2\sin(q_i\Delta)} \tag{12.19}$$

It is easy to see now that all diagonal terms a_{ii}, $i = 2, ..., m$ of the matrix A which are calculated according to (12.18), (12.19) have an average part which depends on the window size N and a periodic part. Non-diagonal terms a_{ij}, $i \neq j$ of the matrix A, can be calculated using formulas (12.9) - (12.17) and have a periodic part only. All diagonal terms are increasing if the size of the window N increases (see (12.18), (12.19)). Non-diagonal terms of the matrix remain bounded if the size of the window N increases (see (12.9) - (12.17)). There exists therefore a sufficiently large N such that the matrix A is strictly diagonally dominant, i.e., the following inequality holds

$$|a_{ii}| > \sum_{j=1 j\neq i}^{m} |a_{ij}| \qquad i = 1, ..., m \tag{12.20}$$

According to the Levy-Desplanques theorem [34], the symmetric diagonally dominant matrix A has positive eigenvalues only and hence (12.6) holds

for $\alpha = \lambda_{min}(A)$, and $\beta = \lambda_{max}(A)$, where $\lambda_{min}(A)$, $\lambda_{max}(A)$ are minimal and maximal eigenvalues of the matrix A. Therefore the adjustable parameters θ converge to their true values θ_* according to the Theorem 6.3 [3].

Lemma. The following relationships are valid:

$$\sum_{k=0}^{n} \cos(a+kh) = \frac{\cos(a+\frac{n}{2}h)\sin(\frac{n+1}{2}h)}{\sin(\frac{h}{2})} \tag{12.21}$$

$$\sum_{k=0}^{n} \sin(a+kh) = \frac{\sin(a+\frac{n}{2}h)\sin(\frac{n+1}{2}h)}{\sin(\frac{h}{2})} \tag{12.22}$$

Proof.
This Lemma can be proved in two ways.

The First Way.

Consider first the following sum:

$$\sum_{k=0}^{n} \cos(a+kh) = \cos(a)+\cos(a+h)+\cos(a+2h)+...+\cos(a+nh) \tag{12.23}$$

which can be presented as follows:

$$\begin{cases} \sin(\frac{h}{2})\cos(a) = \frac{1}{2}[\sin(a+\frac{h}{2}) - \sin(a-\frac{h}{2})] \\ \sin(\frac{h}{2})\cos(a+h) = \frac{1}{2}[\sin(a+\frac{3h}{2}) - \sin(a+\frac{h}{2})] \\ ... \\ \sin(\frac{h}{2})\cos(a+nh) = \frac{1}{2}[\sin(a+\frac{(2n+1)h}{2}) - \sin(a+\frac{(2n-1)h}{2})] \end{cases}$$

Summing up the relations above where the in-between terms vanish and dividing by $\sin(\frac{h}{2})$ yields:

$$\sum_{k=0}^{n} \cos(a+kh) = \frac{1}{2\sin(\frac{h}{2})}[\sin(a+\frac{(2n+1)h}{2}) - \sin(a-\frac{h}{2})] \tag{12.24}$$

Finally, the sum $\sum_{k=0}^{n} \cos(a+kh)$ can be calculated as follows:

$$\sum_{k=0}^{n} \cos(a+kh) = \frac{\cos(a+\frac{n}{2}h)\sin(\frac{n+1}{2}h)}{\sin(\frac{h}{2})} \tag{12.25}$$

The change of variables a to $\frac{\pi}{2} - a$ and h to $-h$ gives

$$\sum_{k=0}^{n} \sin(a+kh) = \frac{\sin(a+\frac{n}{2}h)\sin(\frac{n+1}{2}h)}{\sin(\frac{h}{2})} \tag{12.26}$$

The Second Way.

Calculation of the k-th power of a complex variable $z = \cos(h) + i\sin(h)$, where $i^2 = -1$ and multiplication by $\cos(a) + i\sin(a)$ yields:

$$\begin{aligned}(\cos(a) + i\sin(a))z^k &= (\cos(a) + i\sin(a))(\cos(h) + i\sin(h)) \\ = e^{ia}e^{ikh} &= e^{i(a+kh)} = \cos(a+kh) + isin(a+kh)\end{aligned} \tag{12.27}$$

Relation (12.27) shows that the sums (12.25), (12.26) to be calculated are the real and imaginary parts of the sum of the following geometric series that has $n+1$ terms :

$$\begin{aligned}&(\cos(a) + i\sin(a))(1 + z + z^2 + ... + z^n) \\ &= (\cos(a) + i\sin(a))\frac{z^{n+1}-1}{z-1},\end{aligned} \tag{12.28}$$

where $(1-z)\sum_{k=0}^{n} z^k = (1-z^{n+1})$. Evaluating $\frac{z^{n+1}-1}{z-1}$ yields:

$$\begin{aligned}\frac{z^{n+1}-1}{z-1} &= \frac{\cos((n+1)h) - 1 + i\sin((n+1)h)}{\cos(h) - 1 + i\sin(h)} \\ &= \frac{\sin(\frac{n+1}{2}h)}{\sin(\frac{h}{2})} \quad \frac{-\sin(\frac{n+1}{2}h) + i\cos(\frac{n+1}{2}h)}{-\sin(\frac{h}{2}) + i\cos(\frac{h}{2})} \\ &= \frac{\sin(\frac{n+1}{2}h)}{\sin(\frac{h}{2})}[\sin(\frac{n+1}{2}h) - i\cos(\frac{n+1}{2}h)][\sin(\frac{h}{2}) + i\cos(\frac{h}{2})] \\ &= \frac{\sin(\frac{n+1}{2}h)}{\sin(\frac{h}{2})}(\cos(\frac{n}{2}h) + i\sin(\frac{n}{2}h))\end{aligned}$$

Finally the real part of the following complex variable is the sum (12.25) and imaginary part is the sum (12.26), i.e.,

$$(\cos(a)+i\sin(a))\frac{z^{n+1}-1}{z-1}=\underbrace{\frac{\sin(\frac{n+1}{2}h)}{\sin(\frac{h}{2})}\cos(a+\frac{n}{2}h)}_{=\sum_{k=0}^{n}\cos(a+kh)}$$

$$+\,i\underbrace{\frac{\sin(\frac{n+1}{2}h)}{\sin(\frac{h}{2})}\sin(a+\frac{n}{2}h)}_{=\sum_{k=0}^{n}\sin(a+kh)} \tag{12.29}$$

Corollary.

The following relations follow from (12.25) and (12.26) with $a=0$:

$$\sum_{k=0}^{n}\cos(kh)=\frac{\cos(\frac{n}{2}h)\sin(\frac{n+1}{2}h)}{\sin(\frac{h}{2})} \tag{12.30}$$

$$\sum_{k=0}^{n}\sin(kh)=\frac{\sin(\frac{n}{2}h)\sin(\frac{n+1}{2}h)}{\sin(\frac{h}{2})} \tag{12.31}$$

Moreover, the following relationships are also true:

$$\begin{aligned}\sum_{k=1}^{n}\cos(kh)&=\sum_{k=0}^{n}\cos(kh)-1\\&=\frac{\cos(\frac{n}{2}h)\sin(\frac{n+1}{2}h)}{\sin(\frac{h}{2})}-1\\&=\frac{\cos(\frac{n}{2}h)\sin(\frac{n+1}{2}h)-\sin(\frac{h}{2})}{\sin(\frac{h}{2})}\\&=\frac{\frac{1}{2}\sin(\frac{2n+1}{2}h)-\frac{1}{2}\sin(\frac{h}{2})}{\sin(\frac{h}{2})}\end{aligned}$$

$$= \frac{\cos(\frac{n+1}{2}h)\sin(\frac{n}{2}h)}{\sin(\frac{h}{2})} \tag{12.32}$$

and

$$\sum_{k=0}^{n} \sin^2(a+kh) = \frac{n+1}{2} - \frac{1}{2}\sum_{k=0}^{n} \cos(2a+2kh)$$

$$= \frac{n+1}{2} - \frac{\cos(2a+nh)\sin((n+1)h)}{2\sin(h)} \tag{12.33}$$

$$\sum_{k=0}^{n} \cos^2(a+kh) = \frac{n+1}{2} + \frac{\cos(2a+nh)\sin((n+1)h)}{2\sin(h)} \tag{12.34}$$

$$\sum_{k=0}^{n} \sin^2(a+kh) + \sum_{k=0}^{n} \cos^2(a+kh) = n+1 \tag{12.35}$$

A Lemma similar to Lemma presented above one can also find in Appendix C of [59].

Chebyshev Three Term Recurrence Relations

Two following trigonometric identities

$$\cos[(n+1)\theta] + \cos[(n-1)\theta] = 2\cos[\theta]\cos[n\theta] \tag{12.36}$$

$$\sin[(n+1)\theta] + \sin[(n-1)\theta] = 2\cos[\theta]\sin[n\theta] \tag{12.37}$$

allow recursive calculations of $\cos[(n+1)\theta]$ via $\cos[(n-1)\theta]$, $\cos[n\theta]$ and $\cos[\theta]$; and $\sin[(n+1)\theta]$ via $\sin[(n-1)\theta]$, $\sin[n\theta]$ and $\cos[\theta]$, where θ is the angle and $n = 1, 2, ...$ (see [53] for Chebyshev polynomials).
Relationships (4.40),(4.41) follow from (12.36)and (12.37) with $\theta = k\Delta$ and $n = q - 1$.

13

Appendix C

Recursive Improvement of Inaccurate Inverse Matrix

Consider the problem of calculation of the inverse matrix A^{-1} for the invertible $n \times n$ matrix A for which an inaccurate inverse matrix $D_0 \approx A^{-1}$ is known. The accuracy of the estimate of the inverse matrix A^{-1} can be improved using a recursive method. In the first step the following difference is introduced:

$$F_0 = I - AD_0 \tag{13.1}$$

where I is $n \times n$ unity matrix. Matrix D_0 is equal to A^{-1} provided that $F_0 \equiv 0$. The closeness of the matrices A^{-1} and D_0 implies the smallness of the modules of the terms of F_0. The matrix D_k is updated as follows:

$$D_k = D_{k-1} + D_{k-1}F_{k-1}, \tag{13.2}$$

where $k = 1, 2, ...$, and the estimation error is $F_k = I - AD_k$.

The convergence rate can be estimated as follows:

$$\begin{aligned} F_1 &= I - AD_1 = I - A(D_0 + D_0F_0) \\ &= I - AD_0(I + F_0) = I - (I - F_0)(I + F_0) \\ &= I - (I - F_0^2) = F_0^2, \\ F_2 &= F_1^2 = F_0^4, \\ F_k &= F_0^{2^k} \end{aligned} \tag{13.3}$$

Recursive estimate D_k converges to the matrix A^{-1}, i.e.,

$$\lim_{k \to 0} D_k = A^{-1} \tag{13.4}$$

provided that

$$\|F_0\| \leq c < 1 \tag{13.5}$$

where c is a positive constant.

The upper bound of the estimation error F_k is evaluated using (13.3) as follows:

$$\|F_k\| \leq \|F_0\|^{2^k} \leq c^{2^k} \tag{13.6}$$

and hence

$$\begin{aligned}
&\lim_{k\to 0} \|F_k\| = 0 \\
&\lim_{k\to 0} F_k = \lim_{k\to 0}\{I - AD_k\} = 0 \\
&I - A\lim_{k\to 0} D_k = 0 \\
&\lim_{k\to 0} D_k = A^{-1}I = A^{-1}
\end{aligned}$$

The latter implies the convergence of the estimate D_k to the inverse matrix A^{-1}. The following inequality $\|D_k - D_{k-1}\| \leq \epsilon$, where ϵ is a small positive number can be used in practice as a stopping rule for the algorithm.

This algorithm is described in [15] where the convergence rate of the algorithm is also evaluated.

14

Appendix D

14.1 Hypotheses Tests

A periodic nature and cycle-to-cycle variability of the engine cylinder individual events allows the description of the engine signals as statistical signals. A robust detection of such engine events as misfire events, knock events, engine transients and others in the presence of a stochastic noise needs to be associated with the statistical hypotheses tests. Drastic deterioration of the quality of engine signals for aged engines is an additional motivation for a robust detection of engine events based on hypotheses tests. A number of hypotheses tests is described in this Section: *One Sample t-Test*, *Two Sample t-Test*, *Two Sample t-Test*, *Test on the Variance*, *Test for Equal Variances*, *Transient Detection Test*,*Outlier Detection Test* and *Confidence Intervals*. Hypotheses tests are summarized in Table 14.1. Table 14.2 shows application of the hypotheses tests described in Table 14.1 to the robust detection of engine events.

Hypothesis Test	Purpose	Section	References
One Sample t-Test	Compares One Sample Average to Target	14.1.1	[64]
Two Sample t-Test	Compares Two Sample Averages	14.1.2	[64], [88]
Test on the Variance	Compares One Sample Variance to Target	14.1.3	[64]
Test For Equal Variances	Compares Two Sample Variances	14.1.4	[63], [64]
Transient Detection Test	Compares Variance to the Mean Squared Successive Difference	14.1.5	[29]
Outlier Detection Test	Compares Outlier to a Sample Average	14.1.6	[26], [92]

Table 14.1. Hypotheses Tests

Hypothesis Test	Application	Section
One Sample t-Test	Misfire Detection, Knock Control	7,10
Two Sample t-Test	Knock Detection	9
Test on the Variance		
Test For Equal Variances	Look-up Tables Adaptation	6
Transient Detection Test	Engine Transients Detection	
Outlier Detection Test	Single Misfire Detection, Knock Detection	10

Table 14.2. Applications of the Hypotheses Tests

One Sample t-Test described in Section 14.1.1 is used for a robust detection of misfire events in Section 7, and for robust engine knock control (asymptotical *One Sample t-Test*) in Section 10. The test is applied in the moving-in-time window of a certain size enabling a misfire detection and knock control in every step. *Two Sample t-Test* described and modified in Section 14.1.2 for the case of unequal variances is used in Section 9 for engine knock detection. The *Test for Equal Variances* described Section 14.1.4 is used in data-driven mechanism for adaptation of engine look-up tables described in Section 6. The *Test for Equal Variances* as well the *Test on the Variance* could be applied to the engine knock detection since the variance of the engine knock signal is significantly larger for knocking cycles. A statistical transient detection mechanism described in Section 14.1.5 could be used for a robust detection of engine transients. Finally, an outlier detection method described in Section 14.1.6 could be used for a robust detection of a single misfire event, engine knock events, and a confidence interval method described in the same Section is used in Section 10 for a robust auto-adaptation of engine knock detection threshold. A possibility of application of a Neyman-Pearson Lemma to designing a change in mean test is discussed in the end of this Appendix. This Section provides a useful robust engine event detection tool-kit formulated in terms of statistical hypotheses.

14.1.1 One Sample t-Test

One Sample t-Test compares one sample average to a historical value or to a target. Let x be a normally distributed variable described by a mean value a and a standard deviation σ.

• A null hypothesis is the following: $H_0: \quad a = a_0,$ where a_0 is a target value. The variance σ^2 is unknown. The statistic

$$t = \frac{\overline{x} - a_0}{S/\sqrt{n-1}} \tag{14.1}$$

follows a Student distribution with $n-1$ degrees of freedom, where n is the sample size. Here and below standard definitions of a sample mean $\overline{x}$ and a sample standard deviation S are used.

• Alternative hypotheses and critical regions are the following:

$$\begin{aligned} H_{A1}: &\quad a = a_1 > a_0, &\quad |t| > t_{1-2\alpha,n-1} \\ H_{A2}: &\quad a = a_1 < a_0, &\quad |t| > t_{1-2\alpha,n-1} \\ H_{A3}: &\quad a = a_1 \neq a_0, &\quad |t| > t_{1-\alpha,n-1} \end{aligned}$$

where $t(\alpha, n-1)$ is the value taken from the Student distribution look-up table (see for example [77]) with a significance level α and $n-1$ degrees of freedom.

14.1.2 Two Sample t-Tests

Standard Two Sample t-Test

Two Sample t-Test compares two independent sample averages. Let x and y be two normally distributed variables described by mean values $\overline{x}$ and $\overline{y}$ and sample variances S_x and S_y drawn from the size n sample and size m sample respectively.

• A null hypothesis is: $H_0: \ \overline{x} = \overline{y}$. The variances σ_x^2 and σ_y^2 are assumed to be unknown but equal.

The following statistic

$$t = \frac{\overline{x} - \overline{y}}{S\sqrt{1/n + 1/m}} \ , \tag{14.2}$$

$$S = \sqrt{\frac{(n-1)S_x^2 + (m-1)S_y^2}{(n-1) + (m-1)}} \tag{14.3}$$

follows a Student distribution with $n + m - 2$ degrees of freedom.

• Alternative hypotheses and critical regions are the following:

$$\begin{aligned} H_{A1}: &\quad \overline{x} > \overline{y}, &\quad |t| > t_{1-2\alpha,n+m-2} \\ H_{A2}: &\quad \overline{x} < \overline{y}, &\quad |t| > t_{1-2\alpha,n+m-2} \\ H_{A3}: &\quad \overline{x} \neq \overline{y} &\quad |t| > t_{1-\alpha,n+m-2} \end{aligned}$$

Remark 1. The outlier detection test described in Section 14.1.6 is a special case of this *Two Sample t-Test*.

Remark 2. *A comparison of two sample averages for large sample sizes.* The following statistic

$$N = \frac{\sqrt{mn}(\overline{x} - \overline{y})}{\sqrt{mS_x^2 + nS_y^2}} \tag{14.4}$$

which represents the difference between two mean values divided by the standard deviation of this difference can also be used for comparison of two sample averages. The distribution of statistic (14.4) converges to a standard normal distribution with a zero mean and a unity variance for the sufficiently large sample sizes due to the Central Limit Theorem [13]. The hypothesis that two mean values are equal is taken as a null hypothesis for which a critical region can be defined for large sample sizes using a standard look-up table of a normal distribution.

Testing the Equality of Two Means for the Case of Unequal Variances

Usually *Two Sample T-test* which is used for testing the equality of two means, is performed under the assumption that the variances of two compared variables are equal [64], [67]. The *Two Sample T-test* for the case of unequal variances where the relationship between variances is known, is described below.

Consider two normally distributed variables x and y described by the mean values $\overline{x}$ and $\overline{y}$ and sample variances S_x^2 and S_y^2 calculated from a size n sample and a size m sample respectively. Consider the null hypothesis to be that the mean values of two variables are equal, i.e. $H_0 : \overline{x} = \overline{y}$. Suppose that the variances σ_x^2 and σ_y^2 are different and unknown, but the relationship between variances presented in the form of ratio is known, i.e.,

$$F = \frac{\sigma_y^2}{\sigma_x^2} \tag{14.5}$$

where F is a known number. Denoting the variance of the variable x as σ^2, $(\sigma^2 = \sigma_x^2)$, the variance of the variable y is calculated as $F\sigma^2$. The ratio (14.5) can be estimated for sufficiently large sample sizes by using the sample variances S_x^2 and S_y^2, i.e.,

$$F = \frac{S_y^2}{S_x^2} \tag{14.6}$$

where $S_x^2 = \dfrac{\sum_{i=1}^{n}(x_i - \overline{x})^2}{(n-1)}$, $S_y^2 = \dfrac{\sum_{i=1}^{m}(y_i - \overline{y})^2}{(m-1)}$.

The variance of the difference $(\overline{x} - \overline{y})$ is calculated as follows:

$$\begin{aligned} V(\overline{x} - \overline{y}) &= V\overline{x} + V\overline{y} \\ &= \frac{\sigma_x^2}{n} + \frac{\sigma_y^2}{m} = \frac{(m + Fn)}{nm}\sigma^2 \end{aligned} \tag{14.7}$$

The following variable follows a normal distribution i.e., $\frac{(\overline{x}-\overline{y})}{\sigma}\sqrt{\frac{nm}{m+Fn}} \in N(0,1)$, where $\frac{nm}{m+Fn}$ is the "effective sample size".

The next step is evaluation of the variance σ. To this end the following variables are considered:

$$\frac{(n-1)S_x^2}{\sigma^2} = \frac{\sum_{i=1}^{n}(x_i-\overline{x})^2}{\sigma_x^2}$$
$$\frac{1}{F}\frac{(m-1)S_y^2}{\sigma^2} = \frac{\sum_{i=1}^{m}(y_i-\overline{y})^2}{\sigma_y^2}$$

which follow χ^2 distribution with $(n-1)$ and $(m-1)$ degrees of freedom respectively. Hence the variable

$$\frac{F(n-1)S_x^2+(m-1)S_y^2}{F\sigma^2} \tag{14.8}$$

follows χ^2 distribution with $(n+m-2)$ degrees of freedom. Taking into account that

$$E[S_x^2] = \sigma^2$$
$$E[S_y^2] = F\sigma^2,$$

consider the following mathematical expectation:

$$E[\frac{F(n-1)S_x^2+(m-1)S_y^2}{F(n+m-2)}] = \sigma^2 \tag{14.9}$$

The variable $S^2 = \frac{F(n-1)S_x^2+(m-1)S_y^2}{F(n+m-2)}$ which is often called estimated pooled variance, is in fact an unbiased estimate of the variance σ^2. Consider the following statistic

$$\begin{aligned} t &= \frac{(\overline{x}-\overline{y})}{S}\sqrt{\frac{nm}{(m+Fn)}} \\ &= \frac{(\overline{x}-\overline{y})}{\sigma}\sqrt{\frac{nm(n+m-2)F\sigma^2}{(m+Fn)F(n+m-2)S^2}} \\ &= \frac{(\overline{x}-\overline{y})}{\sigma}\sqrt{\frac{nm(n+m-2)F\sigma^2}{(m+Fn)(F(n-1)S_x^2+(m-1)S_y^2)}} \end{aligned}$$

$$= \frac{(\overline{x}-\overline{y})}{\sigma}\sqrt{\frac{nm}{(m+Fn)}}$$
$$/\ \sqrt{\frac{(F(n-1)S_x^2+(m-1)S_y^2)}{F\sigma^2}\frac{1}{(n+m-2)}}$$

Since $\frac{(\overline{x}-\overline{y})}{\sigma}\sqrt{\frac{nm}{m+Fn}} \in N(0,1)$, and $\frac{F(n-1)S_x^2+(m-1)S_y^2}{F\sigma^2} \in \chi^2_{n+m-2}$ the statistic t follows Student distribution with $(n+m-2)$ degrees of freedom according to the definition ($t \stackrel{def}{=} \frac{N(0,1)}{\sqrt{\frac{\chi^2_{n+m-2}}{n+m-2}}}$). If the value of the statistic t is larger than the value in the Student distribution look-up table the null hypothesis is rejected in favor of alternative hypothesis. Notice that the statistic t can be used for hypothesis testing if the difference in variances σ_x and σ_y is statistically significant. Therefore the hypothesis of the equality of two variances should first be tested by using the *Test for Equal Variances* (see Section 14.1.4 and [64], [67]). If the difference in variances is statistically significant, the statistic t defined above with the ratio $F = \frac{S_y^2}{S_x^2}$ can be used for hypothesis testing. If the difference in variances is not statistically significant, the statistic t with $F = 1$ corresponds to the standard *Two Sample T-test*.

14.1.3 One Sample χ^2-Test (Test on the Variance)

One Sample χ^2-Test is a test on the variance. Let x be a normally distributed variable described by a mean value and a standard deviation σ.

• A null hypothesis is: $H_0: \quad \sigma^2 = \sigma_0^2, \quad$ where σ_0 is a given number. The variance σ^2 and the mean value are unknown.

The statistic

$$\chi^2 = \frac{(n-1)S^2}{\sigma_0^2} \tag{14.10}$$

follows χ^2 distribution with $n-1$ degrees of freedom.

• Alternative hypotheses and critical regions are the following:

$$H_{A1}: \quad \sigma^2 = \sigma_1^2 > \sigma_0^2, \quad \chi^2 > \chi^2_{\alpha,n-1}$$
$$H_{A2}: \quad \sigma^2 = \sigma_1^2 < \sigma_0^2, \quad \chi^2 < \chi^2_{1-\alpha,n-1}$$
$$H_{A3}: \quad \sigma^2 = \sigma_1^2 \neq \sigma_0^2, \quad \begin{cases} \chi^2 > \chi^2_{\alpha/2,n-1} \\ or \\ \chi^2 < \chi^2_{1-\alpha/2,n-1} \end{cases}$$

where $\chi^2(\cdot)$ is the value taken from the χ^2 distribution look-up table.

14.1.4 Test for Equal Variances (F-test)

The *Test for Equal Variances* compares two independent sample variances S_x and S_y drawn from the size n sample and size m sample respectively.

• A null hypothesis is $H_0: \quad \sigma_x = \sigma_y$. The variances σ_x^2 and σ_y^2 are unknown.

Statistic

$$F = \frac{S_x^2}{S_y^2} \tag{14.11}$$

follow a Fisher distribution with $n-1$ and $m-1$ degrees of freedom.

• Alternative hypotheses and critical regions are the following:

$$\begin{aligned}
&H_{A1}: \quad \sigma_x > \sigma_y, \quad && F > F_{\alpha,n-1,m-1} \\
&H_{A2}: \quad \sigma_x < \sigma_y, \quad && F < F_{1-\alpha,n-1,m-1} \\
&H_{A3}: \quad \sigma_x \neq \sigma_y, \quad && \begin{cases} F > F_{\alpha/2,n-1,m-1} \\ or \\ F < F_{1-\alpha/2,n-1,m-1} \end{cases}
\end{aligned}$$

where $F(\cdot)$ is the value taken from the Fisher distribution look-up table (see for example [64]). $F_{1-\alpha}$ for m and n degrees of freedom is reciprocal of F_α for n and m degrees of freedom i.e., $F_{\alpha,n,m} = \dfrac{1}{F_{1-\alpha,m,n}}$.

Remark 1. *Romanovsky's test for equal variances* [63]. In the first step a variable

$$\theta = \frac{df_y - 2}{df_y} \; F, \qquad F = \frac{S_x^2}{S_y^2} \tag{14.12}$$

with a mathematical expectation $E(\theta) = 1$ and a standard deviation $\sigma_\theta = \sqrt{\dfrac{2(df_x + df_y - 2)}{df_x(df_y - 4)}}$ $(df_y > 4)$ with degrees of freedom $df_x = n-1$ and $df_y = m-1$ is introduced. The deviation of θ from one with a relatively high probability does not exceed $3\sigma_\theta$ interval. Therefore the following variable

$$R = \frac{|\theta - 1|}{\sigma_\theta} \tag{14.13}$$

is used for the test for equal variances. The difference in two variances σ_x and σ_y is not significant provided that $R < 3$, and the difference in variances is statistically significant if $R \geq 3$.

Remark 2. *Comparison of several variances.* Bartlett's test [64], [82] is used to test if a number of samples have equal variances. A hypothesis that all the population variances are equal is taken as a null hypothesis, which is tested

against the alternative hypothesis that at least one of the variances is different. Bartlett's test is unfortunately sensitive to departures from normality. The Levene's test [55] (which is an alternative to the Bartlett test) is less sensitive than the Bartlett test to departures from normality and can also be used for comparison of several variances.

14.1.5 A Statistical Transient Detection

A statistical transient detection can be formulated in terms of a statistical hypothesis test where a systematic change in the following sample $x_1, x_2, ..., x_n$ is examined [1], [29]. The hypothesis that

$$E(x_i) = a \tag{14.14}$$

where $E(\cdot)$ is a mathematical expectation and a is a given number is taken as a null hypothesis. This hypothesis is tested against the alternative hypothesis that a systematic change (transient) is present in the mean value of the mentioned above sample. It is assumed that the variance does not change during the transient. For a hypothesis test the sample variance is compared to the mean square successive difference. The following variable

$$r = \frac{q^2}{s^2} \tag{14.15}$$

where

$$q^2 = \frac{1}{2(n-1)} \sum_{i=1}^{n-1} (x_{i+1} - x_i)^2 \tag{14.16}$$

$$s^2 = \frac{1}{n-1} \sum_{i=1}^{n} (x_i - \overline{x})^2 \tag{14.17}$$

with a mathematical expectation $E(r) = 1$ and a standard deviation $\sigma_r = \sqrt{\frac{1}{n+1}(1 - \frac{1}{n-1})}$ is introduced [29]. Variable r is approximately normally distributed variable for a sufficiently large sample size, $n > 20$ provided that x_i is normally distributed. The transient is detected provided that the variance (14.17) is essentially larger than (14.16). Fractiles of the distribution of $r = \frac{q^2}{s^2}$ are given in Table 13.6 of [29].

14.1.6 Outlier Detection and Confidence Intervals as Thresholds

Confidence interval method is presented in this Section as a method for the detection of the signal outlier [26],[74]. It is shown that the outlier can be

detected using standard *Two Sample t-Test* [92]. The confidence limits for the outlier utilize *t-statistic* which in turn is used for *Two Sample t-Test*.

Consider the following principal sample set $y_1, y_2, ..., y_m$ characterized by the mean value $\overline{y} = \frac{1}{m}\sum_{i=1}^{m} y_i$ and a sample standard deviation, $S = \sqrt{\frac{1}{m-1}\sum_{i=1}^{m}(y_i - \overline{y}_i)^2}$, and the extreme observation y^* which is a suspected upper outlier. Here for simplicity an upper outlier detection is considered only. The result is valid for the detection of a lower outlier also.

Consider two normally distributed variables described by the mean values y^* and $\overline{y}$ and the same standard deviation σ, estimated via a sample standard deviation S. Consider the null hypothesis to be that the mean values of two variables are equal, i.e. $H_0 : y^* = \overline{y}$ which is tested against the alternative hypothesis $H_A : y^* > \overline{y}$ detecting y^* as an upper outlier or $H_A : y^* < \overline{y}$ detecting y^* as a lower outlier.

The outlier detection test described above is a special case of *Two Sample t-Test* described in Section 14.1.2. Statistic (14.2) with $\overline{x} = y^*$, $n = 1$ and $S = S_y$ is used for the outlier detection.

Since the test statistic t (14.2) follows the Student distribution a critical value $t_{\alpha/2,m-1}$ can be found using the Student distribution look-up table so that the probability that the statistic $t = \frac{y^* - \overline{y}}{S}\sqrt{\frac{m}{m+1}}$ is smaller than $t_{\alpha/2,m-1}$ is equal to $(1-\alpha)$, i.e.,

$$P\{|\frac{y^* - \overline{y}}{S}|\sqrt{\frac{m}{m+1}} \leq t_{\alpha/2,m-1}\} = (1-\alpha) \tag{14.18}$$

for a certain significance level α and degrees of freedom $m-1$. That gives the basis for estimation of y^* via the confidence interval method and

$$P\ \{\overline{y} - t_{\alpha/2,m-1}S\sqrt{\frac{m+1}{m}} \leq y^* \leq \overline{y} + t_{\alpha/2,m-1}S\sqrt{\frac{m+1}{m}}\} = (1-\alpha)$$

The confidence interval described above has two endpoints which define confidence limits $\overline{y} \pm t_{\alpha/2,m-1}S\sqrt{\frac{m+1}{m}}$. Notice that this confidence interval is defined as a stochastic interval since the average value $\overline{y}$ and the standard deviation S are random variables. Calculating $\overline{y}$ and S for a specific sample, the confidence limits as fixed numbers $\overline{y} \pm t_{\alpha/2,m-1}S\sqrt{\frac{m+1}{m}}$ can be used as detection thresholds. Unfortunately, the probability of containing y^* within the interval $\overline{y} - t_{\alpha/2,m-1}S\sqrt{\frac{m+1}{m}} \leq y^* \leq \overline{y} + t_{\alpha/2,m-1}S\sqrt{\frac{m+1}{m}}$ can not be

associated with the confidence interval for specific (not random) values of $\overline{y}$ and the standard deviation S.

14.1.7 Change in Mean Test Based on Neyman-Pearson Lemma

Assume that a random variable X follows a normal distribution with a mean value a and a variance σ^2, $N(a, \sigma^2)$, where $a = E(X)$, E is a mathematical expectation, is unknown and a variance σ^2 is known.

• The null hypothesis: $H_0 : a = a_0$ is tested against the alternative hypothesis $H_1 : a = a_1 > a_0$.
The likelihood functions are defined as follows:

$$L_0(x_1, ...x_n) = \frac{1}{\sigma^n (2\pi)^{n/2}} \, e^{-\frac{\sum_{i=1}^{n}(x_i - a_0)^2}{2\sigma^2}} \tag{14.19}$$

$$L_1(x_1, ...x_n) = \frac{1}{\sigma^n (2\pi)^{n/2}} \, e^{-\frac{\sum_{i=1}^{n}(x_i - a_1)^2}{2\sigma^2}} \tag{14.20}$$

where (14.19) is a likelihood function if the hypothesis H_0 is true ($X \in N(a_0, \sigma^2)$) , and (14.20) is a likelihood function for H_1 ($X \in N(a_1, \sigma^2)$).

• The Neyman-Pearson Lemma [6], [64] states that the most powerful detection rule is the rule which is based on the likelihood ratio $\frac{L_1}{L_0}$ given by:

$$ln(\frac{L_1}{L_0}) = -\frac{\sum_{i=1}^{n}(x_i - a_1)^2}{2\sigma^2} + \frac{\sum_{i=1}^{n}(x_i - a_0)^2}{2\sigma^2}$$

$$= \frac{1}{2\sigma^2}\sum_{i=1}^{n}[2x_i(a_1 - a_0) - (a_1^2 - a_0^2)] = \frac{1}{2\sigma^2}(a_1 - a_0)\sum_{i=1}^{n}(2x_i - a_1 - a_0)$$

$$= \frac{1}{2\sigma^2}(a_1 - a_0)(2\overline{x} - a_1 - a_0)n \tag{14.21}$$

where $\overline{x} = \frac{1}{n}\sum_{i=1}^{n} x_i$.

The likelihood ratio (14.21) is proportional to the sample mean $\overline{x}$ and the inequality $ln(\frac{L_1}{L_0}) > c$ is equivalent to the inequality $\overline{x} > c_1$, where c and c_1 are constants. Taking into account that $\overline{x}$ is normally distributed with the mean value a_0 and a variance σ^2/n ($\overline{x} \in N(a_0, \sigma^2/n)$) provided that $X \in N(a_0, \sigma^2)$ the critical region is defined as follows:

$$P(\overline{x} > c_1) = 1 - P(\overline{x} \le c_1) = 1 - \left\{ \frac{1}{2} + \frac{1}{2}\Phi(\frac{c_1 - a_0}{\sigma}\sqrt{n}) \right\}$$
$$= \frac{1}{2} - \frac{1}{2}\Phi(\frac{c_1 - a_0}{\sigma}\sqrt{n}) = \alpha$$

where the relationship between a normal distribution and a probability integral Laplace function Φ was used. Denoting u_α as follows $\Phi(u_\alpha) = 1 - 2\alpha$, where α is a significance level, the critical value $c_1 = a_0 + u_\alpha \frac{\sigma}{\sqrt{n}}$ such that $P(\overline{x} > c_1) = \alpha$ is assigned to the detection test, where u_α is the value taken from the look-up table of the Laplace function.

• The most powerful test of the null hypothesis $H_0 : a = a_0$ against the alternative hypothesis $H_1 : a = a_1 > a_0$ is the following:
- the null hypothesis H_0 is rejected provided that $\overline{x} > a_0 + u_\alpha \frac{\sigma}{\sqrt{n}}$
- the null hypothesis H_0 is not rejected if $\overline{x} \le a_0 + u_\alpha \frac{\sigma}{\sqrt{n}}$.

The standard deviation σ can be replaced in practice by its consistent estimate (sample standard deviation S) for a sufficiently large sample size.

Notice that a similar result can directly be obtained from *One Sample t-Test* described in (14.1.1). The attempts of designing the most powerful detection rules based on a Neyman-Pearson Lemma are often reduced (as it is shown above) to the standard hypotheses tests.

15

Appendix E

Stability Analysis of the Engine Knock Control System

The stability analysis of the engine knock control system (10.1), (10.13) is made by means of the Ordinary Differential Equation (ODE) approach [16],[56]. ODE which is associated with the system (10.1), (10.13) can be presented as follows:

$$e(t) = T(t) - T_d = \frac{(A_t - \overline{A})\sqrt{w-1}}{s} - T_d \tag{15.1}$$

$$\overline{A} = f(I) \tag{15.2}$$

$$\dot{I} = \gamma \ \ sign(e) \tag{15.3}$$

where $\overline{A} = \overline{A(t)}$, $s = s(t)$ are continuous time analogs of the average value A_k and a standard deviation s_k, t is the time variable, $I = I(t)$ is the ignition timing, γ is a positive design parameter associated with count up/down gains (it is assumed for simplicity that count up/down gains are the same), $f(\cdot)$ is a smooth function whose derivative is bounded away from zero,i.e., there exist a positive constant c_1 such that the following inequality holds $|\frac{\partial f}{\partial I}| > c_1 > 0$.

Notice that the continuous-time model (15.1) is valid locally only, i.e., in the neighborhood of equilibrium point. The target value A_t which is a function of ignition timing can locally be taken as a constant value.

The control aim in continuous time domain is formulated as follows:

$$e(t) \to 0 \quad as \quad t \to t_* \tag{15.4}$$

where t_* is a given time.

Consider the following Lyapunov function candidate

$$V = e^2 \tag{15.5}$$

Evaluation of the derivative of (15.5) along the solutions of the system (15.1)-(15.3) yields

$$\dot{V} = -e\sqrt{w-1}[\frac{\dot{\overline{A}}}{s} + \frac{(A_t - \overline{A})\dot{s}}{s^2}] \tag{15.6}$$

Taking into account that $\dot{\overline{A}} = \frac{\partial f}{\partial I}\dot{I} = \gamma\frac{\partial f}{\partial I}sign(e)$ and assuming that the standard deviation is bounded, i.e. $s < c_2$, where $c_2 > 0$ yields

$$\dot{V} = [-\gamma\sqrt{w-1}\frac{c_1}{c_2} + \frac{\sqrt{w-1}|A_t - \overline{A}||\dot{s}|}{s^2}]|e| \tag{15.7}$$

It is possible to prove that $\frac{\sqrt{w-1}|A_t - \overline{A}||\dot{s}|}{s^2}$ is bounded, i.e., $\frac{\sqrt{w-1}|A_t - \overline{A}||\dot{s}|}{s^2} < c_3$, where a positive constant c_3 depends on the initial conditions. Then

$$\dot{V} \leq -\gamma_0\sqrt{V} \tag{15.8}$$

where $\gamma_0 = \sqrt{w-1}(\gamma\frac{c_1}{c_2} - c_3)$. The control aim (15.4) is reached with $t_* = \frac{2}{\gamma_0}\sqrt{V(0)}$. According to the ODE approach the trajectories of continuous and discrete time systems are close for sufficiently small discretization step. Thus the stability of the discrete time system (10.1), (10.13) is established.

References

1. Abbe E. (1906) *Ü*ber die Gesetzm*ä*ssigkeit in der Verteilung der Fehler bei Beobachtunsreihen, Werke, Bd 2, Jena, pp. 55-81 (in German).
2. Albers A., Albrecht M., Kruger A., Lux R. (1997) New Methodology for Power Train Development in the Automotive Engineering - Integration of Simulation, Design and Testing , SAE Paper 2001-01-3303.
3. Astrom K. J., Wittenmark B. (1989) Adaptive Control, Addison-Wesley.
4. Bartolini G., Ferrara A. & Stotsky A. (1995) Stability and Exponential Stability of an Adaptive Control Scheme for Plants of any Relative Degree, IEEE Transactions on Automatic Control, vol. 40, N 1, pp.100-104.
5. Bartolini G., Ferrara A. & Stotsky A. (1999) Robustness and performance of an indirect adaptive control scheme in presence of bounded disturbances, IEEE Transactions on Automatic Control, vol. 44, N 4, pp.789-793.
6. Basseville M. and Nikiforov I. (1993) Detection of Abrupt Changes. PTR Prentice-Hall, Inc, 1993.
7. Beechie B., Ohl G., Yip J., Prucka M. (2001) Engine Friction Characterization, US Patent 6,188,951 B1.
8. Brunt M., Pond C., Biundo J. (1998) Gasoline Engine Knock Analysis Using Cylinder Pressure Data, SAE Paper 980896.
9. Chevalier A., Muller M. & Hendricks E. (2000) On the validity of mean value engine models during transient operation, SAE Paper 2000-01-1261.
10. Cho D. and Hedrick K. (1989) Automotive Powertrain Modeling for Control, ASME Journal of Dynamic Systems Measurement and Control, vol. 111, December, pp.568-576.
11. Choi S. and Hedrick K.(1996) Robust Throttle Control of Automotive Engines: Theory and Experiment, ASME Journal of Dynamic Systems Measurement and Control, vol. 118, pp.92-98.
12. Cook J., Grizzle J. & Sun J. (1996) Engine Control. IEEE Control Handbook, 1261-1274, CRC Press, Inc.
13. Cramer H. (1946) Mathematical Methods of Statistics, Uppsala: Almqvist & Wiksells, 575 pages.
14. Dabroom A., Khalil H. (1999) Discrete-Time Implementation of High-Gain Observers for Numerical Differentiation, International Journal of Control, vol. 72 N 17, p.p. 1523-1527.

15. Demidovich B., Maron I., (1963) Numerical Calculations, Moscow, Fizmatgiz, 660 pages (in Russian).
16. Derevitsky D., Fradkov A. (1981) Applied Theory of Discrete Adaptive Systems, Moscow, Nauka, 216 pages, (in Russian).
17. Deur J., Kolmanovsky I., Hrovat D. (2007) An SI Engine Load Torque Observer Based on Combined Input and Parameter Estimation, Proc. on Fifth IFAC Symp. on Advances in Automotive Control, August 20-22, pp.79-86.
18. Diop S., Grizzle J., Moraal P., Stefanopoulou A. (1994) Interpolation and Numerical Differentiation for Observer Design, Proc. American Control Conference, Baltimore, Maryland, pp. 1329 - 1333.
19. Drakunov S. and Utkin V (1995) Sliding Mode Observers. Tutorial, Proc. 34-th CDC, New Orleans, pp.3376-3378.
20. Draper N., Smith H. (1966) Applied Regression Analysis, John Wiley and Sons.
21. Efroymson M. (1960) Multiple Regression Analysis. In A. Ralston and H. Wilf (eds), Mathematical Methods for Digital Computers, pp. 191-203, New York, Wiley.
22. Eun Y., J. Kim, K. Kim and D. Cho (1999) Discrete Time Variable Structure Controller with a Decoupled Disturbance Compensator and its Application to a CNC Servomechanism, IEEE Trans. on Control System Technology, vol.7., N4.
23. Ginoux S., Champoussin J.C. (1997) Engine Torque Determination by Crankangle Measurements: State of the Art, Future Prospects, SAE Paper 970532.
24. Green J. and Hedrick J.K. (1990) Nonlinear Speed Control for Automotive Engines, Proc. of the 1990 ACC, SanDiego, CA, May, pp. 2891-2897.
25. Grizzle J., Cook J. & Milam W. (1994) Improved cylinder air charge estimation for transient air fuel ratio control. Proceedings of the American Control Conference, pp. 1568-1573, Baltimore, MD.
26. Grubbs F. (1950) Sample Criteria for Testing Outlying Observations. Ann. Math. Stat., 21, pp. 27-58.
27. Gustafsson F. (2000) Adaptive Filtering and Change Detection, John Wiley and Sons.
28. Guzzella L., Onder C. (2004) Introduction to Modeling and Control of Internal Combustion Engine Systems, Springer.
29. Hald A. (1952) Statistical Theory with Engineering Applications, John Wiley, New York, USA.
30. Ham Y., Chung K., Lee J., Chang K. (1996) Spark-Ignition Engine Knock Control and Threshold Value Determination, SAE Paper, 960496.
31. Hassdenteufel A. (2001) Method of Checking the Operability of the Variable Valve Control in an Internal Combustion Engine, US Patent 6 213 068, B1, April 10.
32. Heywood J.B. (1988) Internal Combustion Engine Fundamentals, McGraw-Hill.
33. Hollander M., Wolfe D. (1999) Nonparametric Statistical Methods, John Wiley & Sons.
34. Horn R. and Johnson C. (1986) Matrix Analysis, Cambridge University Press, London.
35. Hrovat D. and Sun J. (1997) Models and control methodologies for IC engine idle speed control design, Control Eng. Practice vol. 5, N 8, pp. 1093 - 1100.

36. Hrovat D., Colvin D. and Powell B. (1998) Comments on Applications of Some New Tools to Robust Stability Analysis of Spark Ignition Engine: A case Study, IEEE Trans. on Control System Technology, vol.6., N3.
37. Ioannou P. and J. Sun (1996) Robust Adaptive Control, Prentice Hall.
38. Isermann R. (2005) Fault-Diagnosis Systems: An Introduction from Fault Detection to Fault Tolerance, Springer.
39. Isermann R., Scheerer P. , Nelles O., Schwarz R. (2002) Method for compensating variations of a wheel speed sensor, US Patent 6,446,018, September 3.
40. Kao M. and Moskwa J. (1995) Turbocharged Diesel Engine Modeling for Nonlinear Engine Control and State Estimation, ASME Journal of Dynamic Systems Measurement and Control, vol. 117, pp. 20-30.
41. Kay I. and Lehrach R. (1984) Torque Sensing for Controlled Alternative-Fuel Combustion in Diesel Engines, SAE Paper 841007.
42. Kaynak O. and A. Denker (1993) Discrete Time Sliding Mode Control in the Presence of System Uncertainty, Int J. Contr., vol. 57, N 5, pp. 1177-1189.
43. Kim Y.-W., Rizzoni G. & Utkin V. (1998) Automotive Engine Diagnosis and Control via Nonlinear Estimation, IEEE Control Systems Magazine, pp. 84-99, October.
44. Kolmanovsky I., Jankovic M., van Nieuwstadt M. & Moraal P. (2000) Method of Estimating Mass Airflow in Turbocharged Engines Having Exhaust Gas Recirculation, U.S. Patent 6,035,639, March 11.
45. Kolmanovsky I., Sun J., Druzhinina M. & van Nieuwstadt M (2000) Charge Control for Direct Injection Engines with EGR, Proceedings of 2000 American Control Conference, pp. 34-38, Chicago, Illinois.
46. Kolmanovsky I. & Siverguina I. (2001) Adaptive Identification Schemes in Presence of Bounded Disturbances: An Automotive Case Study, Proceedings of 2001 IEEE Conference on Decision and Control,Orlando, Florida.
47. Kolmanovsky I., Siverguina I., & Sun J. (2006) Simultaneous Input and Parameter Estimation with Input Observers and Set-Membership Parmeter Bounding: Theory and an Automotive Application, International Journal of Adaptive Control and Signal Processing, vol. 20, pp. 225-246.
48. Kolmanovsky I., Stotsky A. (2003) A Method and System for Controlling Partial Pressure of Air in an Intake Manifold of an Engine, US Patent 6,651,492 B2, Nov 25.
49. Kolmanovsky I., Stotsky A. (2003) A Method and System for Engine Air-Charge Estimation, US Patent 6,636,796 B2, Oct 21.
50. Korn G., Korn T. (1961) Mathematical Handbook for Scientists and Engineers, Mgraw-Hill Book Company.
51. Kishimoto Y. , Takahata T, (1998) Device for Diagnosing Misfiring of a Multicylinder Engine, US Patent 5,734,100.
52. Klenk M., Moser W., Muller W., Wimmer W., (1993) Misfire Detection by Evaluating Crankshaft Speed - a Means to Comply with OBD II, SAE Paper 930399.
53. Lanczos C. (1956) Applied Analysis, Prentice Hall, 524 pages.
54. Levant A. (1998) Robust Exact Differentiation via Sliding Mode Technique, Automatica vol. 34, N 3, pp. 379384.
55. Levene H. (1960) In Contributions to Probability and Statistics: Essays in Honor of Harold Hotelling, I. Olkin et al. eds., Stanford University Press, pp. 278-292.

56. Ljung L. (1977) Analysis of Recursive Stochastic Algorithms, IEEE Trans. Aut. Control, AC-22, 551-575.
57. Ljung L.(2006) System Identification: Theory for User, Prentice Hall, Second Edition.
58. Lyons R. (1997) Understanding Digital Signal Processing, Addison Wesley.
59. Madsen H. (2007) Time Series Analysis, Chapman & Hall/CRC.
60. Moskwa J. and Hedrick K. (1989) Sliding Mode Control of Automotive Engines, Proceedings of the 1989 American Control Conference, American Autom. Control Council, Green Valley, AZ, USA, vol.2, pp.1040-5.
61. McDonald D. (2006) An Efficient Alternative for Computing Algorithm Detection Thresholds, SAE Paper, 2006-01-0009.
62. Millo F., Ferraro C. (1998) Knock in S.I. Engines: A Comparision Between Different Techniques for Detection and Control, SAE Paper 982477.
63. Mitropolsky A. (1971) Statistical Calculations, Moscow,Nauka, 576 pages,(in Russian).
64. Montgomery D., Runger G. (2006) Applied Statistics and Probability for Engineers, Fourth Edition, John Wiley & Sons Inc.
65. Muller M. (1997) Mean Value Modeling of Turbocharged Spark Ignition Engines. Master's thesis, The Technical University of Denmark, Institute of Automation and Department of Energy.
66. Naber J., Blough J., Frankowski D., Goble M. and Szpytman J. (2006) Analysis of Combustion Knock Metrics in Spark Ignition Engines, SAE Paper 2006-01-0400.
67. Picard D. Editor (2002) Black Belt Memory Jogger: A Pocket Guide for Six Sigma Success, USA, GOAL/QPC.
68. van Nieuwstadt M., Kolmanovsky I., Moraal P., Stefanopulou A. & Jankovic M. (2000) EGR-VGT Control Schemes: Experimental Comparison for a High Speed Diesel Engine. IEEE Control Systems Magazine, vol. 20, pp. 63-79, June.
69. van Nieuwstadt M., Kolmanovsky I., Haghooie M. & Hammoud M. (2001) Air Charge Estimation in Camless Engines, SAE paper 2001-01-0581.
70. Remboski D., Schumacher D., Lynch M, Chewter A. (1999) Method and Sytem for Misfire Determination Using Synchronous Correction, US Patent 5,906,652.
71. Rizzoni G. (1989) Estimate of Indicated Torque from Crankshaft Speed Fluctuations: A Model for the Dynamics of the IC Engine, IEEE Transactions on Vehicular Technology, vol. 38, N 3, pp. 168-179.
72. Rizzoni G. (1999) Estimation of Instantaneous Indicated Torque in Multicylinder Engines, US Patent 5,771,482.
73. Rizzoni G., Guezennec Y., Soliman A., Lee B. (2005) Engine Control Using Torque Estimation, US Patent 6866024 B2.
74. Rousseeuw P. and Leroy A. (1987) Robust Regression & Outlier Detection, New York: Wiley.
75. Samimy B., Rizzoni G., Leisenring C. (1995) Improved Knock Detection by Advanced Signal Processing, SAE Paper, 950845.
76. Sandoval D., Heywood J. (2003) An Improved Friction Model for Spark-Ignition Engines, SAE Paper, 2003-01-0725.
77. Selby S. (1975) Standart Mathematical Tables, 23-rd Edition, CRC Press.
78. Servati H. & DeLosh R. (1986) A Regression Model for Volumetric Efficiency, SAE Paper 860328.
79. Schwarzental D. (1999) Method and Device for Monitoring the Position of a Variable Valve Control, US Patent 6 006 152, Dec.21.

80. Siegmund D. (1985) Sequential Analysis, Springer Series in Statistics. New York: Springer-Verlag.
81. Slotine J. and Li W. (1991) Applied Nonlinear Control, Prentice Hall, 461 pp.
82. Snedecor G., Cochran W. (1989) Statistical Methods, Eighth Edition, Iowa State University Press.
83. Stone R. (1999) Introduction to Internal Combustion Engines, Third Edition, MACMILLAN PRESS.
84. Storset O., Stefanopoulou A. & Smith R. (2000) Air Charge Estimation for Turbocharged Diesel Engines, Proceedings of 2000 American Control Conference, Chicago, IL, pp. 39-44.
85. Stotsky A. (1995) Performance Improvement in Indirect Adaptive Control Scheme in the Presence of Disturbances, Proc. 34 CDC, New Orleans, Louisiana, USA, Dec.13-15.
86. Stotsky A. (2005) Computationally Efficient Filtering Algorithms for Engine Torque Estimation, Proc. IMechE, vol. 219, Part D: J. Automobile Engineering, pp. 1099-1107.
87. Stotsky A. (2007) Statistical Engine Misfire Detection, Proc. IMechE, vol. 221, Part D: J. Automobile Engineering, pp. 641-649.
88. Stotsky A. (2007) Statistical Algorithms for Engine Knock Detection, International Journal of Automotive Technology, vol.8, No 3, pp. 259-268.
89. Stotsky A. Data-Driven Algorithms for Engine Friction Estimation (2007) Proc. IMechE vol.221, Part D: Journal of Automobile Engineering, pp. 901-909.
90. Stotsky A.(2007) Adaptive Estimation of the Engine Friction Torque, European Journal of Control, vol.13, No 6, pp.618-624.
91. Stotsky A. (2008) Statistical Engine Knock Modeling and Adaptive Control, Proc. IMechE vol.222, Part D: Journal of Automobile Engineering, pp. 429-439.
92. Stotsky A. (2008) Statistical Algorithm for the Adaptation of Detection Thresholds, Proc. IMechE Journal of System and Control Engineering, pp. 633-637.
93. Stotsky A., Forgo A. (2004) Recursive Spline Interpolation Method for Real-Time Engine Control Applications, Control Engineering Practice, vol. 12, pp. 409 - 416.
94. Stotsky A., Hedrick J.K. & Yip P.P. (1997) The Use of Sliding Modes to Simplify the Backstepping Control Method, Proceedings of American Control Conference, pp. 1703-1708, Albuquerque, New Mexico, see also
Applied Mathematics and Computer Sciences, vol. 8, N1, 1998, pp. 123-133.
95. Stotsky A., Egart B. & Eriksson S. (2002) Variable Structure Control of Engine Idle Speed with Estimation of Unmeasurable Disturbances, Journal of Dynamical Systems Mesurement and Control, December, vol.122, pp. 599-603.
96. Stotsky, A. (1994) Combined adaptive and variable structure control, Chapter 15, in the book Variable Structure and Lyapunov Control, Springer-Verlag, London.
97. Stotsky A. (1993) Lyapunov Design for convergence rate improvement in adaptive control, Int.J. Control, vol. 57, N2,501-504.
98. Stotsky A. and Eriksson S. (2002) Composite Adaptive Engine Load Estimation, Proc. of the 10-th Mediterranean Conference on Control and Automation - MED 2002, Lisbon, Portugal, July 9-12.
99. Stotsky A. and Kolmanovsky I. (2002) Application of input estimation techniques to charge estimation in automotive engines, Control Engineering Practice, vol. 10, pp. 1371-1383, see also

Stotsky A. and Kolmanovsky I. (2001) Simple input estimation techniques for automotive applications, Proceedings of 2001 American Control Conference, Arlington, Virginia, December, pp. 3312-3317.
100. Stotsky A. , Kolmanovsky I., Eriksson S. (2004) Composite Adaptive and Input Observer-Based Approaches to the Cylinder Flow Estimation in Spark Ignition Automotive Engines, International Journal Adaptive Control and Signal Processing, vol.18, N2, pp. 125-144.
101. Stotsky A., Eriksson S. (2005) Method and Apparatus for Monitoring the Position of a Variable Valve Control, European Patent EP 1457644 B1, November 23.
102. Stotsky A., Forgo A. (2008) Method and Apparatus for Determining the Variation of an Engine Parameter, European Patent EP 1462638 B1, 7 May.
103. Stotsky A. (2006) Method and Apparatus for Determining Operational Mode in a Cam Profile Switching (CPS) Engine, European Patent EP 1462620 B1, 30 August.
104. Stotsky A., Eriksson S. (2004) Method for Diagnosting an Induction System for an Internal Combustion Engine, European Patent EP 1460254 B1, 29 September.
105. Stotsky A. (2007) Method for Determining the Variation of Engine Epeed, European Patent EP 1559898 B1, October 10.
106. Stotsky A., Eriksson S (2007) Method for Detection Failure in a Cam Profile Switching System, European Patent EP 1580407 B1, 27 December.
107. Stotsky A. (2006) Method for Estimating Engine Friction Torque, US Patent 7,054,738 B1, May 30.
108. Stotsky A. (2008) Computationally Efficient Data-Driven Algorithms for Engine Friction Estimation,US Patent 7,324,888 B1, January 29.
109. Sun J., Kolmanovsky I., Brehob D., Cook J, Buckland J. & Haghgooie M. (1999) Modelling and Control Problems for Gasoline Direct Injection Engines, Proceedings of 1999 IEEE Conference on Control Applications, pp. 471-477, Hawaii.
110. Taylor C. (1985) The Internal Combustion Engine in Theory and Practice, MIT Press, Cambridge, MA, 2-nd edition.
111. Tseng T. & Cheng W. (1999) An Adaptive Air-Fuel Ratio Controller for SI Engine Throttle Transients, SAE paper 1999-01-0552.
112. Utkin V.I. (1978) Sliding Modes and Their Application to Variable Structure Systems, MIR Publishers, Moscow.
113. Unland S., Heinstein A., Gundlach M., Haeming W., Ludwig M. (2004) Method for Adjusting Adaptive Programme Maps of an Adaptive Knock Control in an Internal Combustion Engine and a Method for Adjusting the Knock Control in Said Engine, US Patent 6,745,749 B2.
114. Vahidi, A., Druzhinina, M., Stefanopoulou, A., and Peng, H. (2003) Simultaneous Mass and Time-Varying Grade Estimation for Heavy-Duty Vehicles, Proceedings of 2003 American Control Conference, Denver, Colorado, 4951-4956.
115. Wald A. (1947) Sequential Analysis, New York: John Wiley and Sons.
116. Williams J. (2001) Cylinder Torque Estimation Using Crankshaft Angular Response Measurements, US Patent 6,223,120.
117. Wu G. (2006) A Table Update Method for Adaptive Knock Control, SAE paper 2006-01-0607.

118. Zar J. H. (1974) Biostatistical Analysis, Prentice-Hall, NJ.
119. Zhu G., Haskara I., Winkelman J (2005) Stochastic Limit Control and its Application to Knock Limit Control Using Ionization Feedback, SAE Paper, 2005-01-0018.